NOTE TO USERS

SKELETAL MUSCLE AND WHOLE-BODY REGULATION OF SUBSTRATE PARTITIONING BY NUTRITIONAL AND PHARMACOLOGICAL AMPK ACTIVATION

SERGIU FEDIUC

A DISSERTATION SUBMITTED TO THE FACULTY OF GRADUATE STUDIES IN PARTIAL FULFILMENT OF THE REQUIREMENTS FOR THE DEGREE OF

DOCTOR OF PHILOSOPHY

GRADUATE PROGRAM IN KINESIOLOGY AND HEALTH SCIENCE
YORK UNIVERSITY
TORONTO, ONTARIO

FEBRUARY 2009

Your file Votre référence
ISBN: 978-0-494-51703-1
Our file Notre référence
ISBN: 978-0-494-51703-1

Skeletal muscle and whole-body regulation of substrate partitioning by nutritional and pharmacological AMPK activation

By **Sergiu Fediuc**

a dissertation submitted to the Faculty of Graduate Studies of York University in partial fulfillment of the requirements for the degree of

DOCTOR OF PHILOSOPHY

ABSTRACT

The first three studies outlined in this thesis were intended to enhance our knowledge about the effects of palmitate-, troglitazone-, and AICAR-induced AMPK activation on various aspects of glucose and fatty acid (FA) metabolism in skeletal muscle. Our results provide novel evidence that FAs autoregulate their metabolic fate in skeletal muscle cells by directly promoting the phosphorylation and activation of AMPK and ACC in a dose dependant manner. From these data we hypothesized that by upregulating the AMPK/ACC signaling cascade, high circulating FA levels saturate the ability of this pathway to respond to exogenous AMPK agonists. To overcome this, thiazolidinediones (TZDs) are a class of drugs that reduce circulating FA levels by promoting expression of lipid storage genes in adipose tissue. In addition, they have also been demonstrated to activate the AMPK system. Treatment of L6 cells with the TZD troglitazone reduces FA uptake and increases FA oxidation, effects that are partially mediated by AMPK activation. Additionally, troglitazone also promotes an increase in insulin stimulated glucose uptake, and shifts glucose metabolism away from glycogen synthesis and towards an increase in lactate production. Since skeletal muscle glycogen synthesis is an important process that accounts for the majority of glucose disposal in the body, we wanted to test whether the results obtained in skeletal muscle cells are representative of intact isolated muscles. Indeed, this seems to be the case, as soleus muscles (oxidative) treated with AICAR exhibited a similar shift in glucose metabolism away from glycogen synthesis in favour of increased lactate production. This effect, however, appears to be fiber type specific as isolated epitrochlearis muscles (glycolytic)

do not experience this metabolic shift. The final study was intended to provide an integrated look at the effects of 2-week AICAR injections on whole-body glucose and FA homeostasis in the rat. The results of this investigation confirm that this drug shifts whole-body glucose metabolism in favour of lactate production. We also demonstrate that in week 1 FA utilization is upregulated even though whole-body energy expenditure is reduced by AICAR. In week 2, treated animals adapted to the drug, as any initial disturbances in substrate utilization observed in week 1 returned to normal with the exception of spontaneous physical activity which was increased. Collectively, these effects led to a reduction in whole-body adiposity at the end of the study.

ACKNOWLEDGEMENTS

I would like to thank my supervisor Dr. Rolando Ceddia for giving me the opportunity four years ago to continue my development as a scientist. As one of your first students, I had the opportunity to see this lab grow from the beginning, when we didn't even have a lab space to work in. To see what you have accomplished in just four short years is amazing. I think you are one of the most dedicated and hardest workers I have ever met, and your success is well deserved. You have been an amazing supervisor and a great friend.

Pinky: You have definitely become one of my closest friends in the last few years. I owe you lots of thanks for all the help with the experiments and for making the long days in the lab seem a lot more tolerable. However, most of all, thanks for introducing me to Amanda.

To my parents: Thanks for all the support you have given me throughout my studies. I bet you never thought I would get this far in school when I came to you one day during my first undergraduate year and said: "I wanna drop out".

To my Sister, Lawrence, and Maya: Thank you for all the encouragement and support during this degree.

To my wife and best friend: Amanda, you are one of the most amazing people I have ever met. Without you, I am not sure if this thesis would have ever reached completion. I love you with all my heart.

TABLE OF CONTENTS

LIST OF FIGURES

INTEGRATED SUMMARY

LIST OF ACRONYMS

aa	Amino acids
ACC	Acetyl-coenzyme A carboxylase
ADP	Adenosine diphosphate
AICAR	5-aminoimidazole-4-carboxamide-1-β-D-ribofuranoside
AIS	Autoinhibitory sequence
AMP	Adenosine monophosphate
ara-A	9-β-D-arabinofuranoside
AS160	Akt substrate of 160 kilo daltons
ATP	Adenosine triphosphate
BAT	Brown adipose tissue
CA	Constitutively active
CACT	Carnitine acylcarnitine translocase
CAMKK	Ca2+/calmodulin-dependent protein kinase kinase
CBS	Cystathionine β-synthase
CHO	Carbohydrates
CLAMS	Comprehensive laboratory animal monitoring system
CO_2	Carbon dioxide
CoA	Coenzyme A
Compound C	6-[4-(2-Piperidine-1-yl-ethoxy)]-3-pyridin-4-yl-pyrrazolo[1,5-a]-pyrimidine
CPT-1	Carnitine palmitoyl trasferase-1
DN	Dominant negative
EDL	Extensor digitorum longus
EE	Energy expenditure
Epi	Epididymal
FA	Fatty acids (note: FA/fatty acids are used interchangeably)
FABPpm	Plasma membrane fatty acid binding protein
FAD	Flavin adenine dinucleotide
FAS	Fatty acid synthase
FAT/CD36	Fatty acid translocase
FATP	Fatty acid transport protein
FBS	Fetal bovine serum
FDB	Flexor digitorum brevis
FFA	Free fatty acids
G6P	Glucose 6-phosphate
G6Pase	Glucose 6-phosphatase
GAP	GTPase activating protein
GAPDH	Glyceraldehyde 3-phosphate dehydrogenase
GBD	Glycogen binding domain
Glut	Glucose transporter
GP	Glycogen phosphorylase
GS	Glycogen synthase

GSK-3	Glycogen synthase kinase-3
GTP	Guanosine triphosphate
HMG-CoA reductase	3-hydroxy-3-methyl-glutaryl-CoA reductase
i.c.v.	Intracerebrovascular
i.p.	Intraperitoneal
IRS-1	Insulin receptor substrate-1
KCN	Potassium cyanide
KHB	Krebs-Henseleit bicarbonate
LCFA	Long-chain fatty acids
LDH	Lactate dehydrogenase
MO25	Mouse protein 25
MTT	3[-4,5-dimethylthiazol-2-yl]2,5idiphenyl tetrazolium bromide
NAD	Micotinamide adenine dinuceotide
NEFA	Non-esterified fatty acid
O_2	Oxygen
OAA	Oxaloacetate
PDC	Pyruvate dehydrogenase complex
PDH	Pyruvate dehydrogenase
PDK-1	Phosphoinositide-dependent kinase 1
PEPCK	Phosphoenolpyruvate carboxykinase
PGC-1α	PPAR-γ coactivator-1α
PI(3,4,5)P3	Phosphatidylinositol 3,4,5-triphosphate
PI(4,5)P2	Phosphatidylinositol 4,5-bisphosphate
PI3-K	Phosphatidylinositol 3-kinase
PKA	Protein kinase A
PKB	Protein kinase B (note: used interchangeably with Akt)
PP1	Protein phosphatase 1
PPAR-γ	Peroxisome proliferator activated receptor-γ
PSS	Pseudosubstrate sequence
PVDF	Polyvinylidene difluoride
Retro	Retroperitoneal
RQ	Respiratory quotient
SC	Subcutaneous
Ser	Serine
SNF-1	Sucrose non-fermenting 1
STRAD	Ste20-related adaptor protein
T2DM	Type 2 diabetes mellitus
TG	Triglyceride
Thr	Threonine
TORC2	Transducer of regulated CREB activity 2
TPP	Thiamine pyrophosphate
TZDs	Thiazolidinediones
UDP	Uridine diphosphate

VCO_2	Carbon dioxide production
V_{max}	Maximal velocity
VO_2	Oxygen uptake
ZMP	Zeatin riboside-5-monophosphate
α-MEM	Alpha-minimum Eagle's medium

1. INTRODUCTION

Evolution has allowed many organisms, including mammals, to develop complex mechanisms that enable them to cope with irregular food availability by maintaining energy homoeostasis. When resources are abundant, mammals take in excess fuel substrates which are stored in the form of fat, whereas during times of famine, they reduce energy expenditure and rely on the fat reserves to survive (1). The energy that is constantly taken in, as well as stored within the body, serves as a source for the generation of adenosine triphosphate (ATP) at the cellular level. ATP in turn can be broken down to yield adenosine diphosphate (ADP), P, and energy, the latter of which is utilized to drive various cellular processes (2).

In the last two decades the concept of energy homeostasis has evolved through the discovery of the cytosolic enzyme adenosine monophosphate (AMP)-activated protein kinase (AMPK), which is activated by a rise in the AMP:ATP ratio in the cell. When activated, it shuts down ATP consuming anabolic pathways and promotes catabolism of energy substrates in an attempt to restore the intracellular AMP:ATP ratio back to normal (3). Extensive research has demonstrated that AMPK is a key enzyme involved in the control of carbohydrate and lipid metabolism in many mammalian tissues including: skeletal muscle (4-7), adipose tissue (8-10), liver (11, 12), heart (13), and brain (14, 15). Of these tissues, the effects of AMPK activation on substrate partitioning in skeletal muscle have been most extensively studied due to the implications this tissue has for treating metabolic disorders such as obesity and type 2 diabetes mellitus (T2DM). These disorders are characterized by abnormal metabolism of glucose and fatty acids, due to the

inability of tissues to respond properly to the hormone insulin (insulin resistance) (16). Skeletal muscle accounts for the majority of insulin-stimulated glucose disposal in the body, and is also a major site of the development of insulin resistance (17). Since AMPK has been demonstrated to control glucose disposal via insulin-independent mechanisms (18), it comes as no surprise that that a large part of the AMPK based research has focused on the regulation of this enzyme in skeletal muscle.

Currently, many pharmacological and nutritional based approaches are being utilized to explore the role of AMPK activation on substrate partitioning in muscle. More importantly, drugs that have previously been utilized in the treatment of T2DM have recently been reported to also activate the AMPK pathway; however, their effects on substrate partitioning in muscle are largely unknown and controversial. Therefore, the experiments outlined in this thesis were designed to elucidate the effects of various AMPK activating agents (AICAR, troglitazone) and nutrients (palmitate) on different aspects of glucose and fatty acid metabolism, and insulin signalling in skeletal muscle. In addition, several experiments have been conducted to give a broader understanding of the implication of whole-body AMPK activation and the outcome this has on energy metabolism and body composition in rats.

2. LITERATURE REVIEW

2.1 AMP-activate protein kinase

Although AMPK was not officially discovered until 1987 by Carling et al (19), reports of a nucleotide responsive enzyme involved in lipid metabolism began to surface in 1973. The first of these reports demonstrated that partially purified rat liver acetyl-coenzyme A carboxylase (ACC) activity was modulated by ATP (20), which led the authors to speculate that ACC activity was regulated by an upstream ATP-dependent kinase. In a similar fashion, the second of these reports demonstrated that 3-hydroxy-3-methyl-glutaryl-CoA (HMG-CoA) reductase activity was reduced in the presence of ATP (21). Unknowing of the fact that regulation of ACC and HMG-CoA reductase was in fact achieved by the same enzyme, researchers named these upstream regulators ACC kinase and HMG-CoA reductase kinase, respectively. Subsequent investigations demonstrated that both ACC kinase (22) and HMG-CoA reductase kinase (23) were stimulated by 5'-AMP, which later gave rise to the name AMP-activated protein kinase (AMPK) (24). When AMPK was eventually sequenced, it was found to be a homolog of the budding yeast (Saccharomyces cerevisiae) protein kinase sucrose non-fermenting-1 (SNF-1) (25).

Similar to SNF-1 in yeast, AMPK is a heterotrimeric enzyme that has been proposed to function as a sensor of cellular energy status (2). It is comprised of a catalytic subunit (α) and two regulatory subunits (β and γ), which are widely distributed in a variety of tissues in the body including skeletal muscle, heart, brain, adipose tissue, pancreas, and liver (26). There are 2 or 3 genes that encode each subunit which can

result in 12 different combinations, with splice variants adding even more diversity (2, 18).

The α subunit can be found in two isoforms, namely α1 and α2, both of which are encoded by two distinct genes (PRKAA1 and PRKAA2, respectively) with the enzyme kinase domain being located in the N-terminal region (2) (Figure 1). In addition, this region of the α-subunit also contains a threonine residue (Thr-172) which is phosphorylated by upstream kinases and is an important regulatory site for activation of AMPK. On the other hand, The C-terminal region of the α subunit contains an autoinhibitory sequence (AIS) that represses kinase activity (Figure 1). This is evident from bacterial constructs that exhibit greater than 10-fold reduction in activity when the AIS is expressed (27). The C-terminal region of the α-subunit is also important for forming an active complex with the β and γ subunits. Even though the two α isoforms appear to have similar substrate specificity, the α1 is primarily found in the cytoplasm, whereas the α2 isoform is enriched in the nucleus of different cell lines including skeletal muscle (28), pancreatic β cells (29), and neurones (30).

Similar to the α subunits, the β subunits (β1 and β2) are also encoded by two separate genes (PRKAB1 and PRKAB2) (2, 18). These subunits contain two conserved regions in the C-terminal domain which are required to form a functional αβγ complex regulated by AMP and are therefore regarded as protein 'scaffolds' on which the AMPK complex is assembled (2). The central region of the β subunits contains a glycogen binding domain (GBD) that allows the AMPK complex to associate with glycogen in intact cells (18) (Figure 1). This domain is related to non-catalytic domains found in

enzymes that metabolize the α1-6 linkages found in starch and glycogen. While the current physiological function for this domain remains unclear, it is believed that it may be important to localize the AMPK complex close to glycogen synthase (GS) which is a substrate of AMPK (2, 18). Bringing these two enzymes in close proximity to each other may be a way to accelerate the deactivation of GS and promote glycogenolysis thereby increasing cellular ATP levels (2). In support of this, recent evidence has shown that the β-subunit interacts with glycogen debranching enzyme, which may be an additional level of control that helps increase the rate of glycogen breakdown under conditions of cellular energy depravation (31).

Similar to the α and β subunits, the γ subunits (γ1, γ2, and γ3) are also encoded by three distinct genes (PRKAG1, PRKAG2 and PRKAG3) (2) (Figure 1). The γ2 and γ3 isoforms contain N-terminal extensions (γ2 and γ3 long isoforms) which can be truncated by RNA splicing to form γ2 and γ3 short isoforms. The current function of the latter two isoforms has not been established and requires future investigation. Immediately adjacent to the N-terminal extension on the C-terminal side are short, conserved regions that serve as the site of interaction with the β-subunit (Figure 1). This region is followed by 4 tandem repeat domains that were first discovered by Bateman in the enzyme cystathionine β-synthase (CBS) and are accordingly called CBS sequences (2, 18, 32). Collectively these 4 sequences form a pair of Bateman domains responsible for nucleotide binding and allosteric activation of AMPK (2, 18, 25). It has previously been demonstrated that each of these domains is capable of binding either AMP or ATP, although the former binds with a higher affinity than the latter (18). However, recent

investigations have revealed that site B of the Bateman domains is also capable of binding ADP, although the importance of this still remains to be revealed (33).

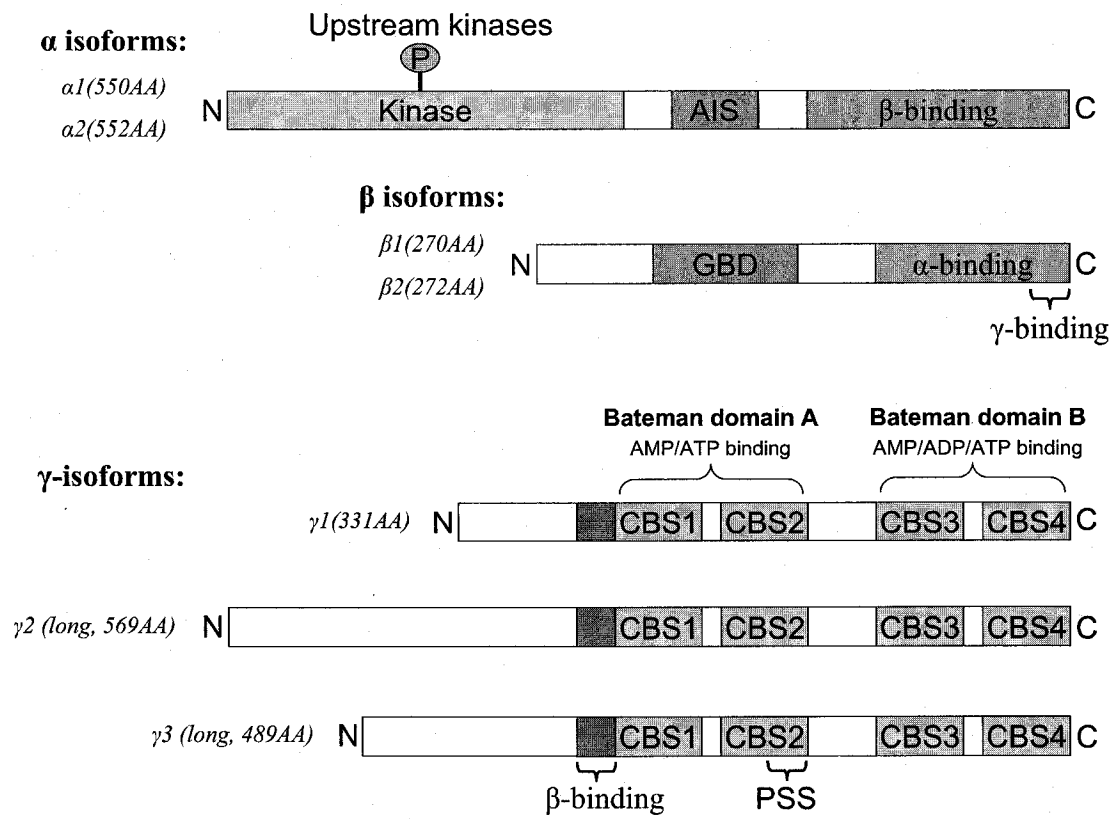

Figure 1. AMPK subunits and various domains. The mammalian α1/α2 and β1/β2 are similar in size (indicated by the number of amino acids (AA) in brackets) and sequence and therefore, a generalized example is shown for each. The α subunits contain the N-terminal kinase domain which can be phosphorylated on Thr-172 by upstream kinases. The phosphorylation is critical for enzyme activity. The C-terminal contains an AIS that is important in repressing kinase domain activity and a β-binding domain that forms a complex with the β-subunit. The β-subunits are considerably smaller in size than α-subunits and contain an N-terminal GBD and a C-terminal α/γ binding domain. The γ-subunits contain a small region on the C-terminal side immediately adjacent to the N-terminal side which is important for β binding. This region is flanked by 4 tandem CBS domain repeats which form a pair of Bateman domains. Bateman domain A binds AMP and ATP, while domain B also binds ADP. The CBS2 domain also contains a pseudosubstrate sequence (PSS) which plays a role in inhibiting kinase activity in the absence of AMP (2, 18).

2.2 Regulation of AMPK by AMP and Calcium

The binding of AMP to the γ subunit of AMPK leads to allosteric activation of the enzyme by up to 5-fold (19). Until recently, the mechanisms by which activation of the AMPK complex by AMP took place were unclear; however, work by Scott et al (34) established the presence of a pseudosubstrate sequence (PSS) within the CBS2 domain of the γ-subunit, which resembles the recognition motif for AMPK substrates (Figure 1). It was later proposed by Hardie et al (2) that in the absence of AMP, the PSS interacts with the substrate binding region on the kinase domain, which inhibits kinase activity. In turn, the binding of AMP to the γ-subunit prevents the interaction of the kinase domain with the PSS and leads to activation of the enzyme (2).

Aside from allosterically activating AMPK, AMP also promotes its phosphorylation by upstream kinases on Thr-172 of the α subunit. One of these upstream kinases has been identified as the tumor suppressor protein LKB1, which forms a complex with two accessory subunits termed Sterile 20-related adaptor protein (STRAD) and mouse protein 25 (MO25) (35). The LKB1 complex is thought to be constitutively active, therefore, AMP does not activate it, but instead makes AMPK a better substrate for phosphorylation (Figure 2). In addition, AMP also makes AMPK a worse substrate for protein phosphatases that dephosphorylate AMPK on Thr-172 (36). In contrast to allosteric activation, phosphorylation of AMPK increases its activity by up to 100-fold (37). However, even though AMP induces AMPK activation on a number of different levels, these effects are antagonized by high concentrations of ATP (18). Therefore, one of the most important factors that regulates AMPK activity is the AMP:ATP ratio in the

cell. In skeletal muscle, ATP concentrations in the basal state are approximately 5mM, whereas AMP levels are approximately 0.2mM (38). During exercise, ATP is broken down to ADP, and subsequently the adenylate kinase reaction catalyses the conversion of 2ADP molecules to one ATP and one AMP molecule (39). As a result the ATP levels are reduced by approximately 20% and the AMP levels increase by as much as 300% (38), making the AMP:ATP ratio a very sensitive indicator of cellular energy status. In this context, any metabolic stress that either inhibits ATP production or stimulates ATP consumption is, in theory, capable of inducing AMPK activation. For example, 2-deoxyglucose, a nonmetabolizable glucose analog depletes cellular ATP stores, and has therefore, the capacity to activate AMPK (40). Other agents that activate AMPK by depleting ATP levels include poisons that inhibit oxidative phosphorylation and consist of potassium cyanide (KCN), arsenite, and azide (18). Ischemia and hypoxia are also two stressors that can alter the AMP:ATP ratio and can, therefore activate AMPK (41). However, activation of AMPK is not always dependent on LKB1 as other upstream enzymes have also been identified to play a role in this process.

In HeLa cells, a cell line that lacks LKB1, as well as embryonic fibroblasts isolated from LKB1 knockout animals, there is still some level of basal AMPK phosphorylation (35, 42). Interestingly, the addition of the calcium ionophore, inomycin, to these cells increases phosphorylation of AMPK on Thr-172 and also its activity (42). The enzyme responsible for performing this action has been identified as Ca^{2+}/calmodulin-dependent protein kinase kinase (CaMKK) (43, 44). This protein is primarily expressed in the brain but can also be found in the testis, thymus, and T cells

(18, 45). Any treatment that increases Ca^{2+} influx in these cell types creates an immediate demand for ATP, as these ions are pumped out of the cytoplasm by ATP-dependant pumps in the plasma membrane and endoplasmic reticulum (18). Towler et al (18) speculate that activation of AMPK under these conditions is a way for the cell to anticipate the need for ATP created by Ca^{2+} entry into the cell. However, due to the limited tissue distribution of CaMKKs, it is unlikely that this mechanism for AMPK activation is present in skeletal muscle (18).

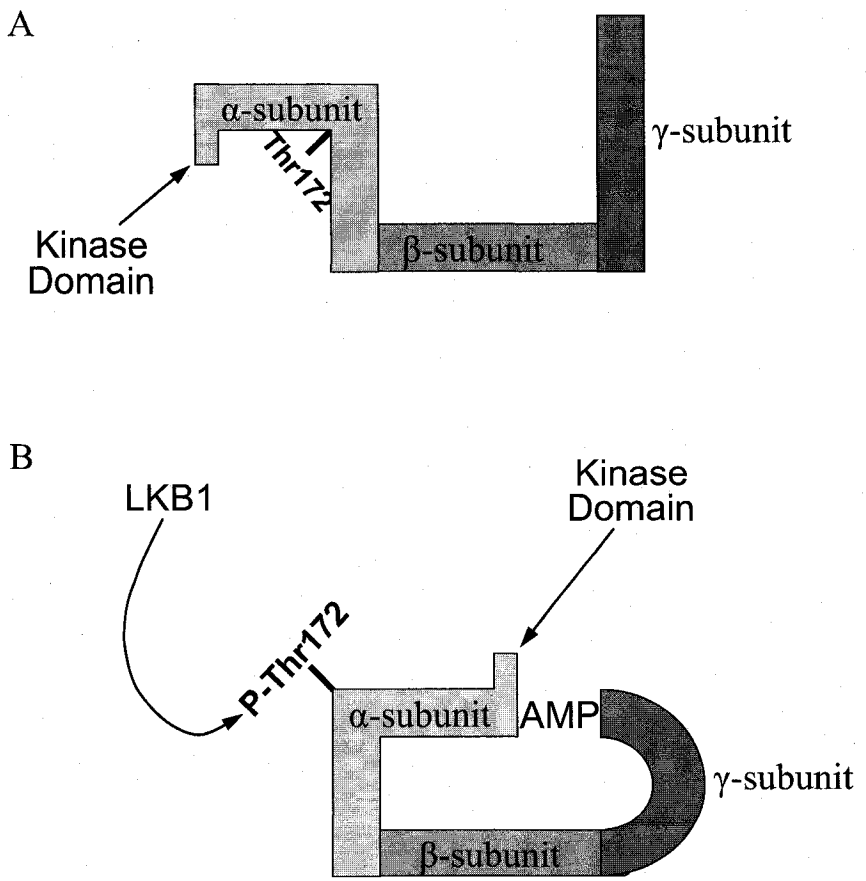

Figure 2. Depiction of AMPK activation by AMP. *Panel A:* Normal ATP levels in the cell maintain AMPK in its inactive state making it difficult for upstream kinases to phosphorylate the α-subunit. *Panel B:* Various cellular stresses that deplete ATP levels

and promote the formation of AMP lead to the activation of AMPK. As the AMP:ATP ratio increases, AMP molecules bind to the γ-subunit, allosterically activating the enzyme and allowing AMPK to change conformation in such a way that it becomes a better substrate for upstream kinases like LKB1 (46).

2.3 Pharmacological activation of AMPK

2.3.1 Activation of AMPK by AICAR

The compound 5-**a**mino**i**midazole-4-**ca**rboxamide-1-β-$_D$-**r**ibofuranoside (AICAR) is perhaps one of the most frequently utilized pharmacological agents to induce AMPK activation. This adenosine analog is rapidly taken up by adenosine transporters located on the plasma membrane and is phosphorylated by adenosine kinase to form the nucleotide 5-aminoimidazole-4-carboxamide-1-β-$_D$-ribofuranosil-5'-monophosphate, also known as **z**eatin riboside-5-**m**ono**p**hosphate (ZMP) (47, 48). Originally, this drug was first utilized nearly 30 years ago to improve the recovery following myocardial ischemia and heart attacks (49, 50). At the time, researchers were not aware of the presence of AMPK and therefore, alternate mechanisms by which AICAR elicited its beneficial effects were proposed. The principles as to why AICAR improved recovery following myocardial ischemia were centred on the fact that adenine nucleotide depletion takes place during reperfusion (51-53). ATP is converted to ADP and AMP when high energy phosphates are utilized for myocardial contraction. Oxygen deprivation impairs mitochondrial rephosphorylation of AMP resulting in a rise in tissue AMP levels (52). Plasma membrane nondiffusable AMP is further degraded to adenosine, inosine, and hypoxanthine, all of which diffuse easily through cell membranes. During reperfusion, these extracellular adenine metabolites are, to a large degree, washed away resulting in

depleted tissue adenine nucleotide levels leading to AMP values that are far below preischemia levels (52). The reduced AMP levels were believed to be responsible for impaired ATP recovery, even following prolonged reperfusion after ischemia. Since ZMP is an intermediate in the synthesis of ATP and guanosine triphosphate (GTP), it was proposed that AICAR might have beneficial effects by replacing, via *de novo* synthesis, the depleted levels of these nucleotides caused by ischemia and reperfusion (54) (Figure 3). However, at the time it was not realized that ZMP also mimics the effects of AMP on the yet unknown AMPK pathway (46).

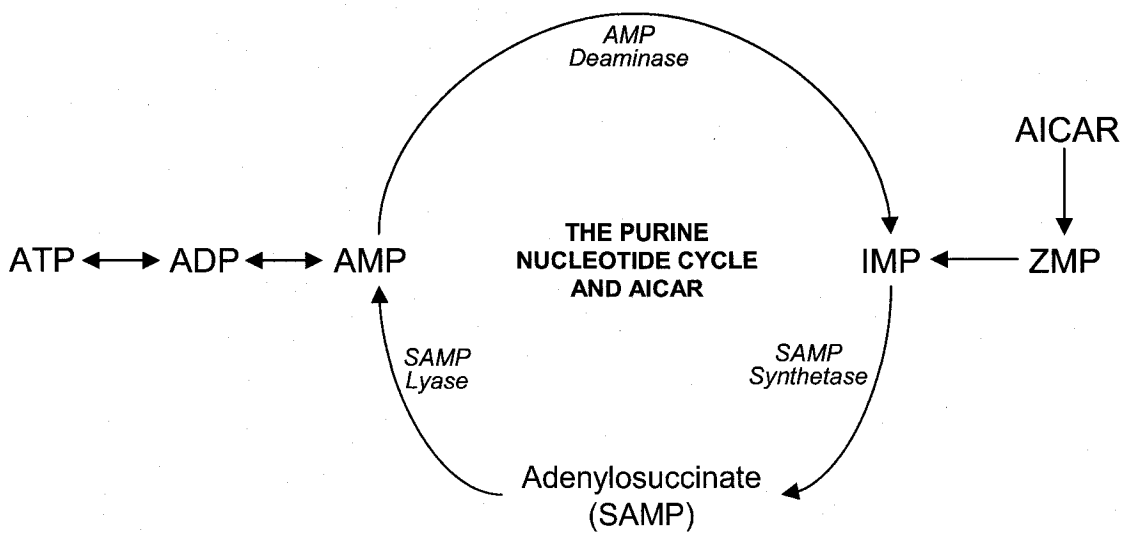

Figure 3. Previously believed theory regarding the effects of AICAR on nucleotide replenishment in ischemic and reperfused cardiac muscle. Under ischemic conditions the breakdown of AMP into adenosine, inosine, and hypoxanthine accounts for a large part of AMP loss, which limits ATP recovery during reperfusion. It was believed that AICAR elicits its beneficial effects in ischemic heart muscle by replenishing the AMP pool, and by doing so was preventing nucleotide loss. Currently, we know this not to be the case, but instead AICAR delivers its beneficial effects by activating the AMPK pathway (51).

2.3.2 Activation of AMPK by Thiazolidinediones (TZDs)

Thiazolidinediones (TZDs) are a common class of drugs used for treatment of T2DM. These oral antidiabetic agents, such as troglitazone, pioglitazone, and rosiglitazone, improve insulin sensitivity and glucose homeostasis in both humans (55) and animals (56-58). It is widely accepted that the molecular target of TZDs is the peroxisome proliferator activated receptor-γ (PPAR-γ), a transcription factor that belongs to the nuclear receptor family and is predominantly expressed in adipose tissue (59). Activation of PPAR-γ by TZDs increases the transcription of genes involved in fatty acid synthesis and storage causing a reduction of plasma non-esterified fatty acid (NEFA) levels (60, 61).

Although a large body of evidence supports the importance of TZD-mediated PPAR-γ activation on the improvement of insulin sensitivity, it appears that TZDs also exert metabolic effects that are independent of the activation of this transcription factor. In fact, it has been reported that after 10 to 20min of infusing troglitazone in rats *in vivo*, blood glucose levels were significantly reduced (62). However, it was not clear whether this acute *in vivo* glucose lowering effect was primarily due to actions of troglitazone on fat tissue or by also affecting other tissues that may contribute to glucose disposal. Interestingly, lipoatrophic (fatless) mice treated with TZDs had improved insulin sensitivity, suggesting non-adipocyte targets for these drugs (63). More recently, it was observed that incubating rat extensor digitorum longus (EDL) muscles with either troglitazone or rosiglitazone for 30min increased glucose uptake and fatty acid oxidation in this tissue (64). Due to the short exposure to TZDs and also because muscle expresses

very low levels of PPAR-γ (59), these acute effects of TZDs were unlikely dependent on activation of this transcription factor. In fact, the authors of the study presented evidence that TZDs exert direct effects on glucose and lipid metabolism in skeletal muscle, an effect that was attributed to phosphorylation/activation of AMPK (64). Along these lines, several studies have reported that TZDs cause rapid activation of AMPK in L6 (65), H-2K^b muscle cells (66), and in isolated rat EDL muscles (64). However, the metabolic implications of TZD-induced AMPK activation in skeletal muscle, especially regarding long-chain fatty acid (LCFA) oxidation and substrate partitioning, have been controversial and not clearly established. Previous short (90min) and long-term (up to 25h) studies have reported that TZDs inhibit complex I respiration and suppress glucose and palmitate oxidation in isolated rat skeletal muscles (67). This scenario seems clearly at odds with the hypothesis that AMPK activation by TZDs would increase LCFA oxidation and exert an anti-lipotoxic effect in skeletal muscles. It could be argued that the effects of TZDs on AMPK activation leading to oxidation of LCFAs are overridden by other more powerful direct inhibitory effects of these drugs on crucial steps of the respiratory chain. However, in opposition to this idea are the recent findings that troglitazone and pioglitazone rapidly induce phosphorylation/activation of AMPK and cause a significant increase in palmitate oxidation in isolated rat EDL muscles (64). Currently, there is no consensus regarding the regulation of the AMPK/ACC system by TZDs and its effects on lipid metabolism and substrate partitioning in skeletal muscles. Furthermore, it may be possible that by promoting AMPK activity and acutely altering glucose and lipid partitioning in muscle cells, TZDs may also affect other metabolic

pathways such as fatty acid uptake and lipogenesis in muscle cells. These alterations could mediate potential insulin sensitizing effects of TZDs in skeletal muscle cells. In fact, evidence has been provided that in isolated muscle incubations ranging from 30min to 25h (64, 65, 67), TZDs improve glucose uptake in this tissue. Some of these studies indicate that AMPK activation seems to be responsible for these acute effects of TZDs in skeletal muscle (64, 65). However, it still remains to be determined whether TZDs exert acute insulin sensitizing effects exclusively by activating AMPK or by also independently affecting crucial steps of the insulin signaling pathway. In this context, a recent investigation has reported that acute treatment of L6 muscle cells with troglitazone does not alter basal phosphatidylinositol 3-kinase (PI3-K) activity or Akt/protein kinase B (PKB) phosphorylation in the insulin signaling pathway (65). Surprisingly, this study did not provide data regarding the effect of combining insulin and troglitazone on insulin signaling and on glucose uptake and metabolism. This is particularly important since in *in vivo* conditions TZDs and insulin are simultaneously present. Therefore, analysis of potential interactions between glucose and lipid metabolism under conditions where insulin and TZDs are combined is of great physiological relevance and require further clarification. A series of experiments in this thesis have been designed to clarify these issues.

2.4 Pharmacological inhibition of AMPK

Since the discovery of AMPK in 1987 by Carling et al (19), a number of pharmacological inhibitors have been utilized to investigate the effects of this enzyme in various cells. Idotubercidin and adenine 9-β-D-arabinofuranoside (ara-A) are two

compounds that have been demonstrated to inhibit AMPK activity (68). However, neither of these compounds were specifically designed to inhibit activity of AMPK, but instead have been utilized to investigate activity of other enzymes as well. In this respect, ara-A is an inhibitor of DNA synthesis and has been utilized for many years in the treatment of chronic hepatitis B (69). It reduces the serum levels of virus DNA-polymerase leading to a loss of infectivity and an overall improvement in liver disease (70). In addition, ara-A has also been utilized as an adenylate cyclase inhibitor (71). In a similar fashion, idotubercidin was utilized for other purposes prior to being employed in studies necessitating inhibition of AMPK. In this context, this chemical compound is an adenosine kinase inhibitor (72), an enzyme that catalyses the phosphorylation of adenosine to AMP, utilizing ATP in the process. Since such a reaction amplifies an increase in the AMP:ATP ratio leading to AMPK activation, then inhibition of adenosine kinase would prevent this from occurring. Taken as a whole, these data demonstrate that both idotubercidin and ara-A are non-specific inhibitors of AMPK and have the capability of influencing various other cellular processes as well. To address this problem in 2001, Zhou et al (12) created a small molecule specifically designed to inhibit AMPK in a more selective manner. The authors demonstrated that the agent 6-[4-(2-Piperidin-1-yl-ethoxy)-phenyl)]-3-pyridin-4-yl-pyrrazolo[1,5-a]-pyrimidine (compound C) is competitive with ATP for ATP binding sites on AMPK. In addition, in *in vitro* assays, compound C did not show significant inhibition of several kinases, including zeta-associated protein kinase, spleen tyrosine kinase, protein kinase C θ, protein kinase A (PKA), and janus kinase 3. Zhou et al (12) also established that compound C is able to

block AICAR-induced AMPK activation in hepatocytes. The conclusions that can be drawn from these experiments are that compound C is a better suited pharmacological agent to inhibit AMPK as opposed to idotubercidin and ara-A.

2.5 Control of different metabolic pathways by AMPK in muscle

2.5.1 Fatty Acid Metabolism

2.5.1.1 Regulation of fatty acid uptake (general overview)

Since intramuscular lipids are limited energy sources, skeletal muscle has to rely on a steady fatty acid (FA) supply from adipose tissue. Prior to lipid oxidation taking place inside the muscle, FAs first have to gain access to the oxidative machinery by crossing the plasma membrane. This is a process that happens in one of two ways: 1) free fatty acids (FFAs) freely diffuse across the plasma membrane, and 2) they are taken up by proteins present on the membrane. Generally, it is believed that LCFA transport into the mitochondria by the mitochondrial membrane enzyme carnitine pamitoyl transferase (CPT)-1 is the rate-limiting step in the oxidation process. However, in recent years evidence has been accumulating suggesting that plasma membrane protein-mediated FA uptake into the cell is also a highly regulated process.

An important component of FA uptake into any cell is the level of FFA available for transport. In the plasma, the majority of circulating FAs are bound to the carrier protein albumin, with only a very small fraction circulating in a completely free, unbound form. It is only the albumin unbound form of fatty acids that can be taken up by cells and metabolized. Most manuscripts refer to the levels FFAs in serum to range between 200 and 600μM under normal conditions (73). However, these values include the

albumin bound form as well as the unbound form of FA. In reality the levels of FFA that are not bound to albumin, and therefore available for transport into cells are in a much lower range of approximately 7.5 ± 2.5nM in healthy humans (74). These levels of albumin unbound FA are determined by the FA:albumin molar ratio in the plasma, which in healthy humans is approximately 1 (73, 74). Interestingly, this ratio is a crucial determinant of FA availability for transport as an increase in it from 1 to 4 results in a 19-fold increase in the unbound FFAs from approximately 8 to 151nM (74).

It was believed that entry of the unbound FFAs into cells occurs via diffusion across the plasma membrane; however, several proteins have been identified in the past century, which have now been implicated to participate in this process (75, 76). Of the different proteins involved in this process, the 88kDa fatty acid translocase (FAT/CD36) has received the most attention. Its involvement in LCFA uptake was first discovered in 1993 in studies utilizing reactive sulpho-N-succinimidyl FA esters, a compound that inhibits FA uptake in isolated adipocytes (77). Unlike other fatty acid transporters, one of the most interesting characteristics of FAT/CD36 is that it can be found both on the plasma membrane and in intracellular compartments (78). The role of these intracellular pools was clarified in studies that used both exercise and insulin as treatment protocols and found that both increase the recruitment of this transporter from intracellular compartments to the plasma membrane (79). In this context, it has been demonstrated that exercise-induced translocation of FAT/CD36 involves activation of AMPK (80). On the other hand, in the case of insulin it has been established by the use of the selective PI3-K inhibitors wortmannin and LY-294002 that PI3-K activation is necessary for

insulin-stimulated translocation of FAT/CD36 (80-82). Currently, it is not clear which downstream targets to PI3-K and AMPK are involved in FAT/CD36 translocation. However, it is believed that similar mechanisms leading to Glut-4 translocation to the membrane may also be responsible for FAT/CD36 recruitment (75, 80).

In addition to its role in FA uptake into the cell, FAT/CD36 has been implicated in the control on FA uptake into the mitochondria (83). The first indication that FAT/CD36 may be involved in regulating FA uptake into the mitochondria came from immunopricipitation studies, which established the co-localization of these transporters with CPT-1 (83) (Figure 4). Interestingly, the addition of the FAT/CD36 inhibitor sulfo-N-succinimidyl oleate to isolated muscle mitochondria reduced palmitate oxidation by approximately 85%, a finding that implies an important role for these proteins in mitochondrial FA metabolism (83). Recent experiments conducted in isolated mitochondria from human skeletal muscle have suggested that the role of these transporters is to shuttle acylcarnitine formed by CPT-1 from the outer to the inner mitochondrial membrane where it is translocated into the matrix by carnitine acylcarnitine translocase (CACT) (84) (Figure 4). The conclusions that can be drawn from these investigations are that FAT/CD36 is a crucial player in the control of FA uptake into skeletal muscle and also mitochondria for oxidation. Currently, it still remains to be determined whether these proteins have additional functions in skeletal muscle.

A second integral membrane protein with an apparent role in fatty acid uptake into skeletal muscle is the 63 kDa FA transport protein (FATP). Thus far, six isoforms of

this protein have been identified with tissue specific dirstribution (76). While FATP1 is predominantly expressed in adipose tissue, heart and skeletal muscle, it is absent in the liver, a tissue that almost exclusively expresses the FATP5 isoform. FATP4 on the other hand is the only FATP transporter expressed in enterocytes, and is therefore believed to play a crucial role in intestinal fatty acid transport (76). Interestingly, it has been demonstrated that insulin, similar to FAT/CD36 translocation, also induces FATP1 translocation to the plasma membrane from perinuclear compartments in adipocytes (85). However, more work is necessary to determine if the other members of this family follow a similar pattern in other tissues.

The third candidate FA transporter that has been implicated in FA transport into cells is the 40 kDa protein termed plasma membrane FA binding protein ($FABP_{pm}$), which is bound to the outer surface of the plasma membrane (86). Evidence for its involvement in FA uptake stems from observations that $FABP_{pm}$ is induced during differentiation of 3T3-L1 fibroblasts into adipocytes (87). Additional studies have also shown that application of an antibody raised against $FABP_{pm}$ inhibits FA uptake in different cell lines including hepatocytes, cardiomyocytes and adipocytes (86).

An important area of study that has evolved from the discovery of these different FA transports is the roles they play in different physiological and pathological conditions. In this context, it has been demonstrated that endurance training increases the cellular content of both FAT/CD36 (88) and $FABP_{pm}$ (89). In addition, short-term fasting also results in increased abundance of $FABP_{pm}$ (90). These adaptations most likely take place due to an increased reliance on FAs as an energy substrate during either endurance

exercise or fasting. Interestingly, findings in pathological states like obesity indicate that this process is also upregulated in individuals and animal models affected by this condition (91, 92). It has been reported that skeletal muscle of obese subjects has higher levels of $FABP_{pm}$ (93). In line with these findings, Bonen et al (94) reported that LCFA transport is upregulated by approximately 4-fold in muscle of obese individuals, a finding which coincided with increased levels of FAT/CD36. As a result of the increase in FA uptake and reduced capacity to oxidize these FAs in these individuals, lipid metabolism byproducts such as diacylglycerol and ceramides accumulate in muscle and can lead to insulin resistance. Taken together, these findings represent an area of therapeutic intervention in obesity which could potentially be geared towards reducing FA uptake and storage in skeletal muscle, thus aiding in the improvement of whole-body metabolism.

2.5.1.2 Effect of AMPK activation on fatty acid uptake in muscle

The first reports that AMPK may be involved in skeletal muscle FA uptake began surfacing in the year 2000. Bonen et al (95) demonstrated that *in vitro* electrical stimulation of skeletal muscle giant sarcolemmal vesicles induces translocation of FAT/CD36 to the plasma membrane from intracellular pools. In addition, the authors of this study also demonstrated a rapid increase in palmitate uptake into these vesicles which was blocked by sulpho-N-succinimidyl oleate, a specific inhibitor of FAT/CD36 (95). Subsequent studies demonstrated that AICAR stimulates LCFA uptake in a non-additive manner to electrical stimulation in cardiac myocytes (80). Furthermore, in the presence of idotubercidin, the AICAR-induced increase in LCFA uptake was abolished,

indicating that the formation of ZMP by adenosine kinase is necessary for these effects to occur (80). From an energy balance perspective, it makes perfect sense that since AMPK activation induces an increase in FA oxidation in skeletal muscle, it should simultaneously also increase availability of this substrate by promoting its uptake.

2.5.1.3 Mitochondrial uptake and oxidation of fatty acids (general overview)

Once LCFAs translocate across the plasma membrane, they have to be activated by the addition of a CoA-SH group to the molecule. This reaction is catalyzed by the enzyme fatty acyl-CoA synthetase and requires ATP (39). The activation process allows FAs to be utilized in various cellular reactions including esterification into TG pools, or oxidation by the mitochondria. The importance of FA activation prior to utilization in various cellular processes is highlighted by the association of fatty acyl-CoA synthetase with a number of different organelles including: the plasma membrane, outer mitochondrial membrane, endoplasmic reticulum, and lipid droplets in adipocytes (73). FAs taken up from the extracellular fluid are activated in this way by the plasma membrane bound form of fatty acyl-CoA synthetase, whereas FAs released from the intracellular TG pool are activated either by the lipid droplet or the mitochondrial membrane-bound form of this enzyme (73) (Figure 4). In skeletal muscle, activated FAs are primarily utilized by the mitochondria for oxidation, as the lipid storage capacity of these cells is limited.

One of the highly regulated processes in skeletal muscle fatty acid metabolism is the translocation of LCFA-CoA molecules across the outer mitochondrial membrane by the rate-limiting enzyme CPT-1. This enzyme imports LCFA-CoA into the

mitochondrial intermembrane space and in the process it also catalyses the reversible esterification of carnitine with LCFA-CoA to form long-chain acylcarnitine (96) (Figure 4). Recent evidence suggests that acylcarnitine is shuttled from the outer mitochondrial membrane to the inner membrane by FAT/CD36 (84). Subsequently, acylcarnitine is transported from the intermembrane space into the mitochondrial matrix in a simultaneous 1:1 exchange ratio with matrix-derived free carnitine via CACT, located within the inner mitochondrial membrane (Figure 4). Inside the matrix, CPT-2 located on the matrix side of the inner mitochondrial membrane transesterifies acylcarnitine back to free carnitine and LCFA-CoA (96). The intramitochondrial LCFA-CoA is now ready to enter the β-oxidation pathway where it is broken down into two-carbon acetyl-CoA molecules to be utilized in the Krebs cycle. In this system, it is important to note that CPT-1 is the rate-limiting enzyme for LCFA entry into the mitochondria. However, inhibition of CPT-1 only prevents the oxidation of FAs with a carbon chain length greater than eight (97). Octanoate, a medium chain FA composed of eight carbons bypasses the site of CPT-1 inhibition by diffusing directly into the matrix where medium-chain fatty acyl-CoA synthetase forms octanoyl-CoA which can then be oxidized (97). Nevertheless, the metabolism of LCFAs by the CPT system is an important pathway by which lipids gain access to the oxidative machinery in the mitochondria. Interestingly, data from obese individuals demonstrating an elevated respiratory quotient (RQ) suggests that this process is impaired in this population (98). In this context, Simoneau et al (93) demonstrated that indeed, CPT-1 activity is significantly depressed in skeletal muscle obtained from obese individuals compared to lean subjects. Therefore, understanding the

factors that control this pathway may represent an important therapeutic aspect towards improving the metabolic phenotype in obese populations.

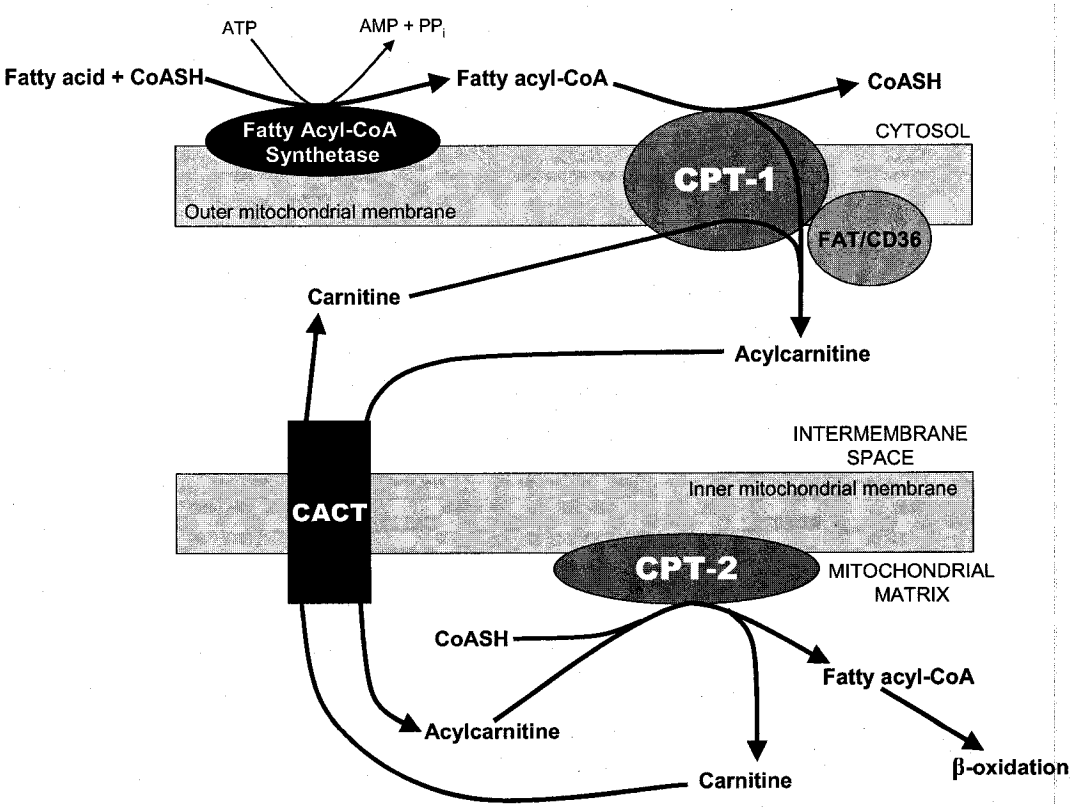

Figure 4. Import of LCFA into the mitochondria for β-oxidation by the CPT system. LCFA are activated by fatty acyl-CoA synthetase located on the outer mitochondrial membrane. The product of the reaction, fatty acyl-CoA is esterified with carnitine by CPT-1 and simultaneously translocated to the intermembrane space. CoASH is liberated in the reaction to be reused in other reactions. Acylcarnitine is shutteled across the intermembrane space by FAT/CD36 which is associated with CPT-1 on the inner surface of the outer mitochondrial membrane. Once it reaches the inner mitochondrial membrane, acylcarnitine is transported into the matrix in a simultaneous 1:1 exchange ration with free carnitine from the matrix. Inside the matrix acylcarnitine is transesterified back to free carnitine and fatty acyl-CoA in a reaction catalyzed by CPT-2, which is situated on the matrix side of the inner mitochondrial membrane (96, 97).

2.5.1.4 Effects of AMPK activation on fatty acid oxidation

One of the well established pathways controlled by AMPK is the import of FAs into the mitochondria. In its active state, AMPK phosphorylates and deactivates its direct substrate ACC. When ACC is inactive, it fails to convert acetyl-CoA to malonyl-CoA, thus resulting in a fall in intracellular malonyl-CoA levels (Figure 5). This disinhibits CPT-1 and increases mitochondrial import and oxidation of LCFAs in skeletal (99, 100) and heart muscle (101-103). Therefore, the AMPK/ACC pathway is thought to play a central role in the regulation of cellular lipid homeostasis (Figure 5).

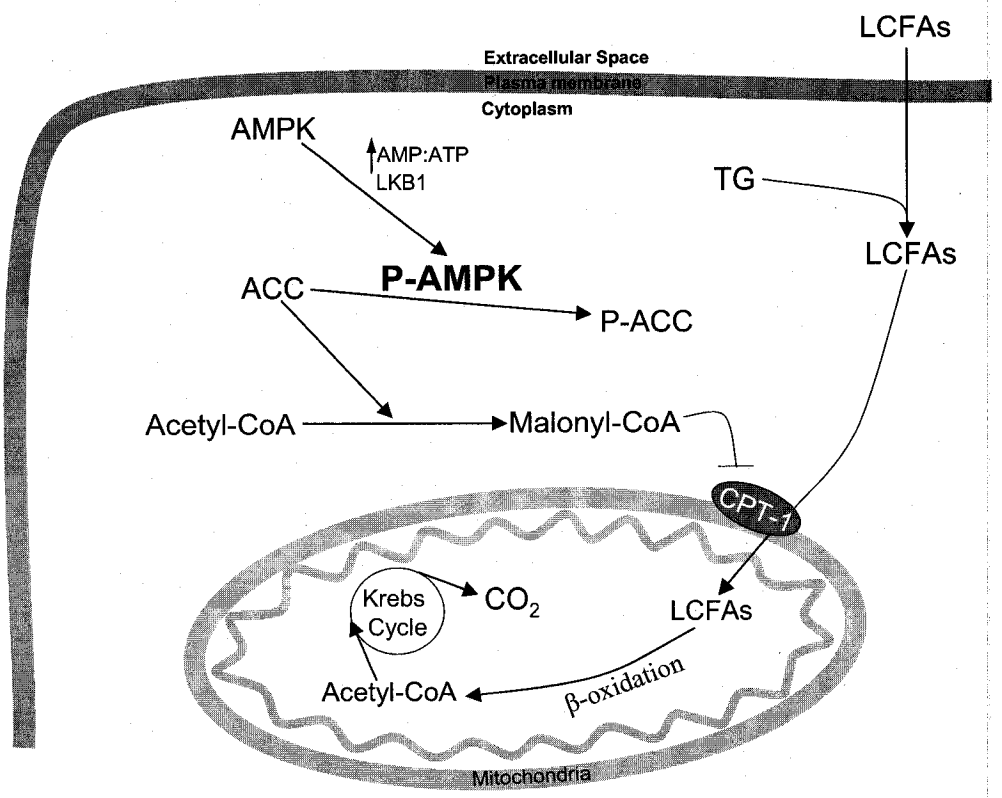

Figure 5. Effect of AMPK activation on LCFA import into the mitochondria. When AMPK is activated either allosterically or by phosphorylation by upstream kinases, it phosphorylates and inactivates ACC. Under these conditions, the malonyl-CoA levels in

the cytoplasm begin to drop leading to increased activation of CPT-1 and the import of LCFAs into the mitochondria for oxidation.

2.5.1.5 Regulation of AMPK by fatty acids

In skeletal muscle, the activity of AMPK has been reported to be regulated by the intracellular creatine:phosphocreatine ratio (104, 105) and glycogen content (106, 107), both directly related to the energy charge of muscle cells. Fatty acids, another major cellular energy source may also regulate AMPK activity in skeletal muscle; however, no data for this have been published. It has been reported that in perfused rat cardiac muscle, palmitate (250 and 500μM) and oleate (500μM) significantly increased AMPK activity without causing any significant alterations in the AMP/ATP ratio (108). Another study has reported that exposure to 150μM acetate, octanoate, or palmitate caused a significant increase in the AMP/ATP ratio followed by a significant increase in AMPK activity in primary rat hepatocytes (109). In contrast to these observations are reports that long-chain acyl-CoA esters inhibit activity and phosphorylation of AMPK by the upstream LKB1/STRAD/MO25 complex (110). Currently, there is no consensus regarding the regulation of the AMPK/ACC system by FAs. However, it is hypothesized that LCFAs could increase AMPK and ACC phosphorylation by 1) ATP utilization for LCFA activation (109) and 2) directly regulating ACC phosphorylation, because in the presence of exogenous FAs the *de novo* lipid synthesis pathway would be suppressed (111). In rat skeletal muscle, refeeding after a fast increases malonyl-CoA and decreases FA oxidation, which has been attributed to a decrease in FAs releasing the allosteric inhibition of ACC (112). In order to clarify these issues some experiments in this thesis

have been designed to shed some light on the role that FAs play on activation of the AMPK/ACC system in muscle cells.

2.5.2 Glucose Metabolism

Once glucose enters the muscle cell via the glucose transporter (Glut)-4 or Glut-1 transporters it can be diverted to a number of different metabolic pathways including glycogen synthesis, glycolysis, lactate production, oxidation, or conversion into lipids (Figure 6).

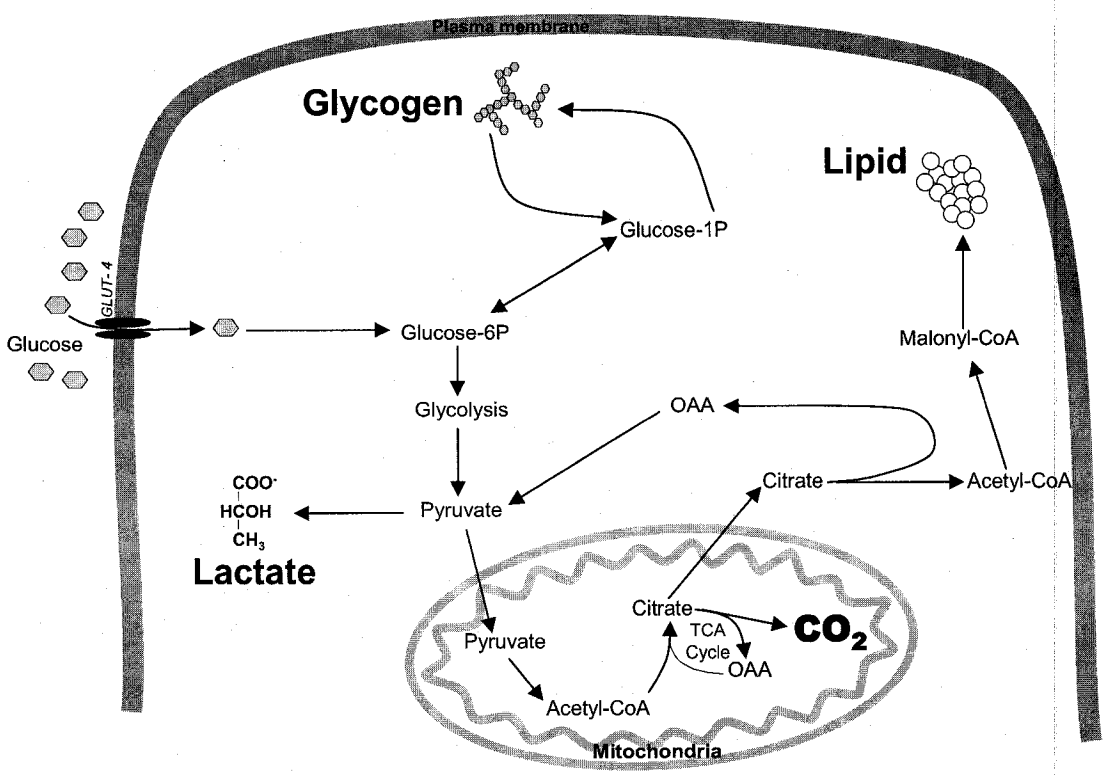

Figure 6. Pathways of glucose metabolism. Glucose enters the muscle cell via Glut-4 transporters. Upon entry, it is rapidly converted into glucose-6P, a molecule that serves as a precursor for glycolysis and glycogen synthesis. In post-prandial or post-exercise conditions, glucose-6P is almost exclusively diverted towards glycogen synthesis with

only a small quantity committed towards the glycolytic pathway. Under conditions of stress, such as exercise, glucose-6P generated by the breakdown of glycogen and the entry of glucose from the extracellular space is diverted towards glycolysis where it is processed to form pyruvate. Pyruvate can then undergo one of two fates: 1) It can be converted to lactate under conditions where the production of pyruvate exceeds its removal by the mitochondria (i.e. intense exercise), or 2) it is taken up by the mitochondria where it is oxidized to form acetyl-CoA. Acetyl-CoA condenses with oxaloacetate (OAA) to form citrate, which can either be processed in the TCA or Krebs cycle or it can exit the mitochondria. In the cytoplasm citrate can be cleaved back into OAA and acetyl-CoA. Of the two molecules, the latter is an important precursor for the formation of malonyl-CoA. In lipogenic tissues such as the liver and adipose tissue, malonyl-CoA serves as the building block for the formation of long-chain fatty acids.

2.5.2.1 Insulin signalling and glucose transport in muscle (general overview)

Insulin initiates its actions by binding to the insulin receptor which belongs to a family of growth factor receptors, all with protein tyrosine kinase activity (113). This receptor is widely distributed and can be found in virtually all mammalian tissues at different concentrations ranging, from as few as 40 receptors in erythrocytes to as many as 200,000 in adipocytes and hepatocytes (114). The insulin receptor is a heterotetrameric glycoprotein structure consisting of two α-subunits and two β-subunits bound together by disulfide bonds (114). The α-subunits are entirely extracellular and contain the insulin binding site, whereas the β-subunits are transmembrane proteins and are responsible for intracellular signalling (114) (Figure 7). The binding of insulin to the α-subunit of the receptor leads to its auto-phosphorylation on multiple tyrosine sites, which creates a recognition motif for insulin receptor substrate-1 (IRS-1). As a result, the insulin receptor phosphorylates IRS-1 on multiple tyrosine residues which recruits and catalyzes the interaction with the regulatory (p85) subunit of PI3-K (115). In its activated state, the p85 subunit of PI3-K activates the catalytic (p110) subunit of the enzyme and

targets it towards the plasma membrane localized substrate phosphatidylinositol 4,5-bisphosphate ($PI(4,5)P_2$). The p110 subunit then phosphorylates $PI(4,5)P_2$ at position 3 of the inositol ring and produces the membrane bound lipid product PI 3,4,5-triphosphate ($PI(3,4,5,)P_3$) which binds both Akt/PKB and phosphoinositide-dependent kinase 1 (PDK-1) (39). The binding of both of these proteins by $PI(3,4,5)P_3$ enables PDK-1, which is constitutively active to phosphorylate Akt/PKB on Thr308 thereby activating the enzyme (Figure 7). However, full activation of Akt/PKB is not achieved until the Ser473 residue is phosphorylated by what is believed to be PDK2 (115, 116). Until recently, the events that occurred between Akt/PKB activation and Glut-4 translocation to the plasma membrane were not fully clear. It was speculated that Akt/PKB phosphorylated and activated one or several proteins which ultimately led to Glut-4 translocation. Recently, a new Akt substrate has been identified and shown to participate in Glut-4 vesicle movement towards the plasma membrane (117). This novel protein was termed Akt substrate of 160 kilo Daltons (AS160), and contains six consensus Akt phosphorylation sites as well as a Rab GTPase activating protein (GAP) domain (115). Rab proteins are small G-proteins which cycle between a GDP-bound and GTP-bound state and regulate several processes associated with membrane vesicle transport and trafficking in cells (118). Interestingly, the Rab proteins 2A, 8A, 10 and 14 appear to be substrates of AS160 and are also associated with insulin-responsive Glut-4 vesicles (119). Under basal, non-insulin stimulated conditions AS160 associates with Glut-4 vesicles and maintains Rab proteins in their GDP-complexed inactive form. Upon insulin stimulation, AS160 is phosphorylated by Akt, which inhibits its GAP activity towards Rab proteins

leading to an active Rab-GTP complex. This results in increased Glut-4 vesicle translocation to the plasma membrane (119). Interestingly, muscle contraction also increases AS160 phosphorylation and Glut-4 translocation, a finding that now shows a convergence of signals derived by two different stimuli onto the same protein (115, 120).

While Glut-4 is one of 13 sugar transporters encoded by the human genome (Glut 1-12, and myo-inositol transporter (HMIT)), it has the unique characteristics of being located mostly in the intracellular compartments with only a very limited number of transporters located on the cell surface in non-insulin stimulated conditions (121). Its K_m is approximately 5mM for glucose; however as the density of plasma membrane transporters increases in the presence of insulin, the maximal velocity (V_{max}) for glucose uptake increases (122). Under low circulating insulin conditions it is mainly the Glut-1 transporters that are responsible for glucose transport across the plasma membrane (122). This transporter is constitutively located on the plasma membrane and does not need to be translocated from intracellular pools like Glut-4s.

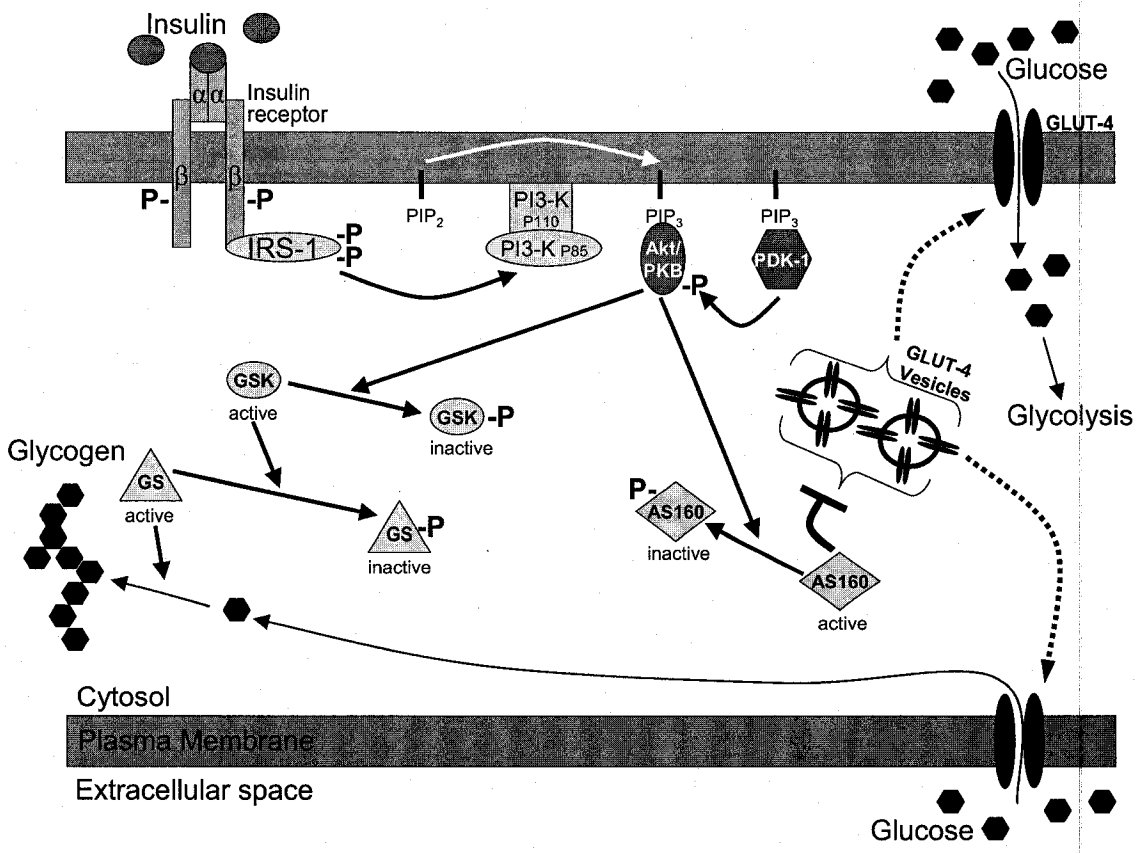

Figure 7: The insulin signalling pathway and the control of glucose uptake and glycogen synthesis. Insulin binds to the insulin receptor on the plasma membrane resulting in autophosphorylation of tyrosine residues. Subsequently, IRS-1 is phosphorylated by the insulin receptor leading to the activation of PI3-kinase, which phosphorylates PIP_2 and converts it to PIP_3 in the plasma membrane. PIP_3 attracts both Akt/PKB and PDK-1 to the surface bringing them in close proximity to each other, thus allowing for the phosphorylation/activation of Akt/PKB by PDK-1. In its active state, Akt/PKB phosphorylates AS160, inactivating the enzyme in the process. This lifts the inhibitory effects of this enzyme on Glut-4 translocation from intracellular pools to the plasma membrane ultimately resulting in an increase in glucose uptake. The glucose that has now entered is diverted either to glycolysis or glycogen synthesis. Akt/PKB also plays an important role in activating the glycogen synthesis pathway. When activated, Akt/PKB phosphorylates/inactivates GSK-3, which then fails to phosphorylate/inactivate GS thus maintaining it in an active state. The glucose that has now entered the cell via Glut-4 transporters is synthesized by GS into glycogen.

2.5.2.2 Effect of AMPK activation on glucose uptake in skeletal muscle

Besides playing a crucial role in lipid metabolism, AMPK has also been shown to promote carbohydrate metabolism in skeletal muscle. Since this tissue accounts for the majority of glucose disposal in the body, it is only natural that a large amount of research has been conducted to better understand the underlying mechanisms that regulate this process in this tissue. Studies performed by Hutber et al (123) provided evidence that glucose uptake was increased in isolated skeletal muscle in response to contraction. This suggested that the intracellular energy deficiency caused by contraction was partly accountable for an increase in glucose uptake in order to provide metabolic fuel for ATP generation (123). In addition, the fact that AMPK is activated by a change in the AMP:ATP ratio, was making this enzyme a potential candidate for the contraction induced increases in glucose uptake. Subsequent investigations demonstrated that AICAR also increases glucose uptake in skeletal muscle (124). In addition, it was observed that the addition of wortmanin, a PI3-K inhibitor, completely blocked the effects of insulin on glucose uptake but did not affect either the AICAR or contraction induced increase in this variable (124). In this context, several studies have demonstrated that either exercise or AICAR-induced AMPK activation increases glucose uptake by increasing Glut-4 translocation to the plasma membrane in an insulin-independent manner (125, 126). These data prove that AMPK-induced glucose uptake is not reliant on the insulin-induced signalling cascade but instead represents an alternate pathway that culminates in Glut-4 recruitment to the membrane (Figure 8).

One of the candidate enzymes that has been hypothesized to be responsible for the AMPK-induce increase in glucose uptake is AS160. Recent experiments revealed that wortmanin was able to completely block insulin mediated phosphorylation of AS160 by Akt/PKB, but it did not effect contraction induced phosphorylation of this enzyme (120). Taken as a whole, these experiments demonstrate that both AMPK and insulin signalling converge onto the same target enzyme (AS160) to stimulate glucose uptake in skeletal muscle via Glut-4 translocation (Figure 8). However, due to the fact that AMPK heterotrimeric subunit combinations vary in different skeletal muscle fiber types (127), the effects of AMPK activation on glucose uptake in this tissue are not as simple as they may appear. Several investigations provided evidence of an apparent difference in glucose uptake between skeletal muscles composed of different fiber types (28, 128, 129). Interestingly, when these muscles were incubated with AICAR ranging from 0 to 4mM, the soleus, a primarily oxidative muscle was the only one that did not increase glucose uptake at any of the AICAR concentrations (28). On the other hand, the epitrochlearis and flexor digitorum brevis (FDB) muscles (primarily glycolytic) increased glucose uptake at AICAR concentrations as low as 0.5mM (28). These results are not surprising given the fact that AICAR did not increase AMPK activity in the soleus muscle similar to the way it did in the epitrochlearis and FDB in this study. However, while AICAR did not affect glucose uptake in the soleus, contractions led to an approximately 3-fold increase in this variable under both fed and fasted conditions similar to the effects observed in epitrochlearis and FDB muscles (28). This great degree of variability with respect to the response to AICAR may be due to the different fiber

type expression patterns of AMPK α subunits. In this context, Ai et al (28) showed that the soleus muscle expresses a higher amount of AMPK α2 versus α1, epitrochlearis muscles expresses a similar amount of α1 and α2, and the FDB expresses a higher amount of α1 than α2. It may be possible that these different AMPKα subunit expression patterns are important in determining the response to AICAR but may not be crucial in the contraction induced response as that does not appear to be affected in the soleus. The introduction of transgenic and genetic knockout mouse models to study AMPK action has enhanced our understanding of AMPK signalling and has helped to shed more light on both contraction and AICAR induced glucose uptake. It has been demonstrated that ablation of skeletal muscle α2 subunit impairs the AICAR-induced glucose uptake response, but not the contraction mediated response on this variable (130, 131). Similarly, overexpression of an α2 kinase-dead subunit abolished AICAR, but not contraction-stimulated glucose uptake (126). From these data it is clear that differential AMPK subunit expression in skeletal muscle plays an important role in the AICAR induced glucose uptake response.

In addition to increasing glucose uptake, AMPK also promotes activation of the glycolytic pathway (132). From a physiological perspective, it would be expected that if the availability of glucose is increased, at least some of this glucose would be diverted towards the glycolytic pathway. In the heart, hypoxia leads to impaired mitochondrial ATP production via oxidative phosphorylation and as a result ATP levels have to be maintained by other pathways (132). In this respect, Marsin et al (132) demonstrated that hypoxia-induced AMPK activation led to phosphorylation and activation of

phosphofructokinase-2 (PFK-2) and subsequent activation of the glycolytic pathway in perfused hearts. In these circumstances, the increased activity of the glycolytic pathway is a mechanism for cardiac cells to compensate for reduced mitochondrial ATP production. More importantly, this effect occurs concomitantly with an increase in glucose uptake, therefore providing the necessary substrate for this pathway.

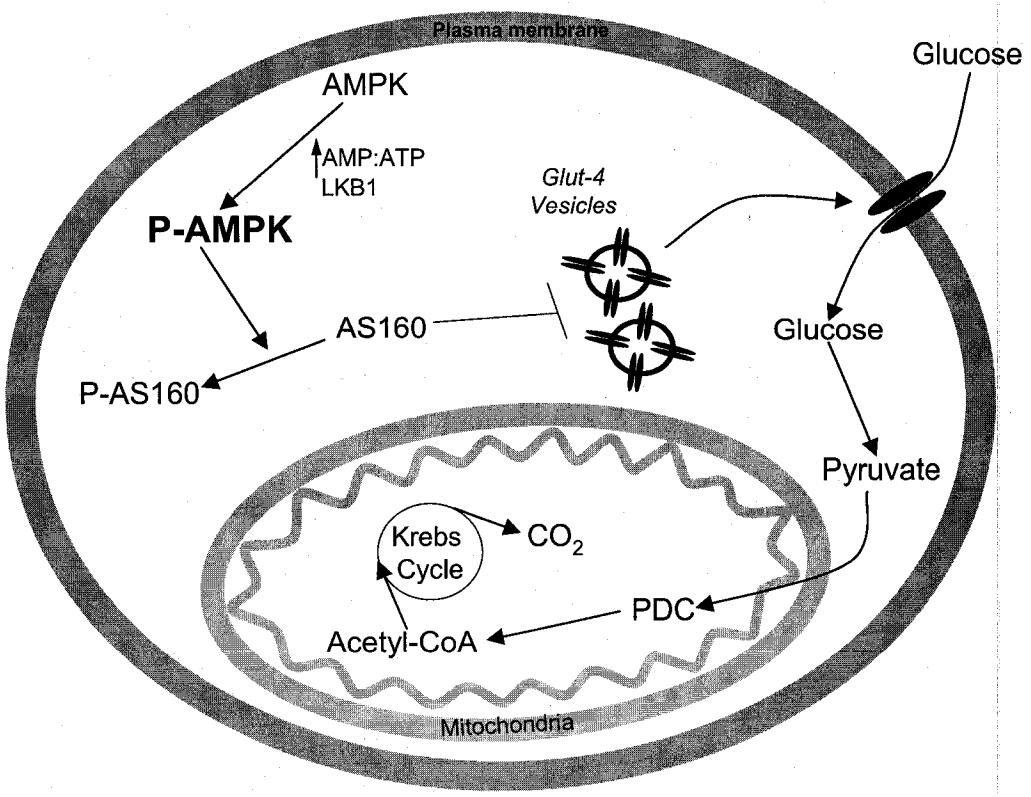

Figure 8. Effects of AMPK activation on glucose uptake in skeletal muscle. An increase in the AMP:ATP ratio allosterically activates AMPK and changes its conformation in such a way that it becomes a better substrate for phosphorylation by the upstream enzyme LKB1. In its active state, AMPK increases glucose uptake by directly phosphorylating and inactivating AS160. This promotes GLUT-4 vesicle translocation to the plasma membrane thereby increasing glucose uptake. PDC = Pyruvate dehydrogenase complex.

2.5.2.3 Glycogen synthesis in skeletal muscle (general overview)

The process of glycogen synthesis involves the conversion of individual glucose molecules into a highly branched polysaccharide structure bound together by α1-4 and α1-6 linkages in the glucose carbon ring (39). The purpose of this process in skeletal muscle is to store readily available energy that can be quickly mobilized during high intensity physical activity or during periods of stress such as the fight-or-flight response. On average, a 70-kg person stores approximately 400g of muscle glycogen under basal, non-fasted and non-stressed conditions which has an energy potential of 1600 kcal (133). Even though the role of glycogen is to provide readily available energy for muscle cells, the process of glycogen synthesis has a crucial function in maintaining whole-body glucose homeostasis. It has been demonstrated that synthesis of muscle glycogen accounts for most of the whole-body glucose uptake, and virtually the entire nonoxidative glucose metabolism in both normal and diabetic subjects (134). More importantly, the incorporation of glucose into glycogen is approximately 50% lower in type 2 diabetic subjects compared to normal individuals (134), and therefore, understanding this process may provide critical insights into improving glycemic control in these diseased populations.

In the postprandial state when blood glucose levels are increased, circulating insulin binds to the insulin receptor on the muscle cell plasma membrane and triggers a cascade of events that simultaneously promote Glut-4 translocation to the membrane and activation of key enzymes involved in glycogen synthesis (Figure 7). Upon entry into the cell, glucose is phosphorylated by hexokinase to form glucose 6-phosphate (G6P). This

product, if it is not processed rapidly enough either by the glycogen synthesis pathway or the glycolytic pathway, can exert negative feedback inhibition on hexokinase activity, thereby reducing glucose uptake (135). G6P also acts as an allosteric activator for glycogen synthase (GS), which determines the rate of glucose incorporation into glycogen and is the rate-limiting enzymes in this process (136). GS activity can also be regulated covalently by phosphorylation and dephosphorylation leading to inactivation and activation of the enzyme, respectively (136), a process that is regulated by insulin. Briefly, insulin increases Akt activation, which in turn phosphorylates, and inactivates the downstream enzyme glycogen synthase kinase-3 (GSK-3) (136, 137) (Figure 7). GSK-3 exists in two isoforms, namely GSK-3α and GSK-3β, both of which are phosphorylated by Akt on Ser21 and Ser9, respectively (138). In its inactive state, GSK-3 fails to phosphorylate GS, thereby allowing it to remain in an active form that promotes the incorporation of uridine diphosphate (UDP) glucose into glycogen (39). GS can be phosphorylated on nine or more sites (137). Of these sites, phosphorylation of sites 2 and 2a, which correspond to Ser7 and 10 and sites 3a and 3b which correspond to Ser640 and Ser644, respectively, decrease activity of GS more than phosphorylation on the other sites (139). Phosphorylation on site 2 is catalyzed by PKA and AMPK, whereas phosphorylation of site 3a and 3b is achieved by GSK-3 (137).

Besides regulation by upstream enzymes, GS activity is also inversely regulated by skeletal muscle glycogen content. It has been demonstrated that depletion of muscle glycogen during exercise activates GS (136, 137), and this activation becomes greater as muscle glycogen stores become lower (140). This adaptation results in a faster rate of

glycogen resynthesis in the early post-exercise period. Further support that glycogen levels control GS activation comes from patients with McArdle's disease, a condition in which glycogen can not be broken down due to a deficiency in glycogen phosphorylase (GP), the key enzyme involved in glycogen breakdown. In these patients, GS is not activated after exercise in contrast to a control group that experienced significant activation of this enzyme (141). The mechanisms by which this occurs are currently not known; however, it is hypothesized that changes in the glycogen levels alter the localization of GS within the cell and lead to its activation by protein phosphatase 1 (PP1) (136, 137). It is speculated that both GS and PP1 are bound to glycogen, and when glycogen content is decreased, both enzymes are released and PP1 can now dephosphorylate GS and activate it (136, 142, 143).

2.5.2.4 Effect of AMPK activation on glycogen metabolism

Although the involvement of AMPK in glucose metabolism has been well documented, its role in glycogen metabolism is a lot less clear. Because AMPK is activated under conditions of cellular stress to promote ATP synthesis and restore the AMP:ATP ratio, it is expected that energy consuming processes, such as glycogen synthesis, would be shut down by activation of AMPK in skeletal muscle (144). In support of this hypothesis, Carling et al (145) provided evidence that AMPK phosphorylates isolated and purified GS, therefore decreasing its activity. However, subsequent *in vitro* and *in vivo* studies provide conflicting results regarding the role of AMPK activation in skeletal muscle glycogen metabolism. It has been demonstrated that incubation of isolated FDB and epitrochlearis muscles (fast twitch muscles) with AICAR

does not alter either GS or glycogen phosphorylase activity (146). Glycogen phosphorylase, which catalyses the degradation of glycogen to glucose-1-phosphate, is an important determinant of the rate of glycogenolysis. Activation of glycogen phosphorylase by AMPK is expected to lead to a reduction in glycogen content in skeletal muscle. In this context, Young *et al* (147) demonstrated that either basal or insulin-stimulated glycogen synthesis was unaffected by AICAR treatment in soleus muscles (primarily slow twitch), even though glycogen phosphorylase activity and lactate production were increased. However, in this previous *in vitro* study reporting that acute AICAR treatment induced an increase in glycogen phosphorylase activity, glycogen content in skeletal muscle was not measured (147). To complicate this matter further, it has been demonstrated that rats chronically treated (5-28 days) with AICAR have increased (up to 2-fold) muscle glycogen content (5, 6, 148). Interestingly, white fast twitch muscles elicit the most pronounced increases in glycogen content after chronic AICAR treatment (6, 148), suggesting important fiber type differences regarding the role of AMPK activation in muscle glycogen metabolism. Even though these *in vivo* studies provide relevant information regarding the metabolic responses to AICAR-induced AMPK activation, they do not allow for separation of direct from systemic effects of AICAR on skeletal muscle glycogen metabolism.

Another aspect that remains poorly explored is the role of AMPK activation in insulin-stimulated skeletal muscle glycogen synthesis and the impact on whole-body insulin-stimulated glucose homeostasis. This is particularly important given the fact that insulin-stimulated muscle glycogen synthesis has been demonstrated to account for the

majority of whole-body glucose uptake, and virtually the entire non-oxidative glucose metabolism in both normal and diabetic subjects (17). In this context, it has been demonstrated that AICAR-induced AMPK activation causes phosphorylation of IRS-1 on Ser-789 residues in C_2C_{12} myotubes, suggesting crosstalk between AMPK and early steps of insulin signaling that could have important implications for glycogen metabolism (149). Importantly, there is evidence that serine-phosphorylated forms of IRS-1 fail to associate with an active PI3-K, resulting in decreased translocation of glucose transporters and other associated downstream events related to glucose metabolism (150). From a glycogen synthesis perspective, it is hypothesized that AMPK activation could cause IRS-1 phosphorylation on serine residues, impair downstream insulin signaling events that depend on PI3-K activation, reduce phosphorylation and inactivation of glycogen synthase kinase-3 (GSK-3), and cause inactivation of GS in skeletal muscle. However, no data supporting this hypothesis have been published thus far and therefore, this will be addressed by experiments outlined in this thesis.

2.5.2.5 Metabolism of glucose and glycogen to lactate

Under conditions that demand a high energy output by skeletal muscles such as intense exercise, glycogen is rapidly broken down to yield G6P molecules. These, together with G6P molecules generated by the phosphorylation of glucose, enter the glycolytic pathway (38, 39). Subsequently, the G6P molecules are converted to fructose 6-phosphate, an intermediary product that acts as a substrate for the rate limiting glycolytic enzyme PFK-1. PFK-1 is an allosterically regulated enzyme and possesses binding sites for ATP, citrate and AMP. Under basal conditions, when cellular energy

stores are high, ATP binds to the PFK-1 allosteric site and inhibits the enzyme, limiting the flux of glucose through this pathway (38). Under conditions where the levels of fatty acid oxidation are increased, high cytoplasmic citrate levels also inhibit PFK-1 by binding to the allosteric citrate site. On the other hand, as the ATP stores are depleted newly formed AMP molecules bind to the AMP allosteric site of PFK-1 and increase affinity of the enzyme for fructose 6-phosphate (38). The formation fructose 1,6-bisphosphate by PFK-1 consumes one ATP molecule and is generally considered to be the first committed step in glycolysis due to its kinetically irreversible nature (38). Subsequently, fructose 1,6-bisphosphate is broken apart into two 3 carbon molecules that get processed through a series of reactions in the glycolytic pathway to yield 4 ATP molecules, 2 NADH + H^+ molecules, and 2 pyruvate molecules (39). During intense exercise, when the rapid activation of this pathway produces pyruvate at a faster rate than it can be taken up by the mitochondria for oxidation, it is rapidly converted to lactic acid by lactate dehydrogenase (LDH) (151). The lactate ions which are formed this way can then exit the muscle cell and can be metabolized by different tissues.

2.5.2.6 Effects of AMPK activation on lactate production

A number of different investigations have provided evidence that the AMPK activating drug AICAR increases systemic lactate concentrations in animals (5, 146) and humans (152). In these investigations, however, it is difficult to determine where this lactate is being produced, since most tissues in the body are affected by this drug. Additional studies have shown that isolated soleus muscles are one of the tissues that respond to AICAR by increasing lactate production (147). Currently, the mechanisms by

which this takes place in muscle are not fully clear. The possibility that LDH activity may be augmented by AICAR was ruled out in a study conducted by Winder et al (148). This investigation demonstrated that four weeks of AICAR injections does not alter LDH activity in white and red quadriceps, and soleus muscles (148). Therefore, it may be possible that AICAR is increasing lactate production by promoting an acceleration of the glycolytic pathway driven by changes in the activity of enzymes located upstream of LDH. This would lead to the production of pyruvate at a higher rate than the ability of mitochondria to oxidize this substrate, thus favouring its conversion to lactate. In support of this, an investigation conducted by Bergeron et al (153) showed that 75 minutes of AICAR treatment in rats increases calf muscle pyruvate concentrations by approximately 30%, whereas lactate concentrations were increased by approximately 3-fold. Taken as a whole, these data suggest that AICAR accelerates the glycolytic pathway and promotes lactate formation in skeletal muscle, effects that are independent of the activity of lactate dehydrogenase.

2.5.2.7 Metabolism of lactate by different tissues

Lactate production in skeletal muscle is determined by the balance between the activities of glycogen phosphorylase/PFK-1 and the activity of the pyruvate dehydrogenase complex (PDC) in the mitochondria (151, 154). The PDC determines the rate of pyruvate oxidation and conversion to acetyl-CoA, which is then further processed in the Krebs cycle. If glycogen phosphorylase/PFK-1 are operating at a higher rate than the PDC, then pyruvate accumulates and shifts the overall equilibrium in favour of lactate production (151, 154). As the intramuscular lactate concentrations increase, some of the

lactate ions are released into the circulation where they are utilized by different tissues as a metabolic carbon source, whereas some are utilized by adjacent muscle fibers (151). In the liver, the process of gluconeogenesis can convert lactate back into glucose to be released into the circulation, or it can be used to restore liver glycogen stores following exercise-induced depletion. In the heart, adipose tissue, and even neural tissue lactate released by skeletal muscles can be converted back to pyruvate and oxidized in the Krebs cycle (39, 151). Lactate can also be oxidized by skeletal muscles or it can be used to restore muscle glycogen levels during the recovery from exercise (154, 155). In fact, it is believed that due to its large mass and metabolic capacity, skeletal muscle, aside from being the largest producer of lactate, is probably also the major tissue in the body that uptakes and utilizes this ion (156). It has been demonstrated that during recovery from short term exercise, or even during continued prolonged exercise there is a net lactate uptake from the blood by resting muscles or by other muscles that are exercising at a low intensity (155, 157, 158). During moderate to high intensity exercise, glycolytic muscle fibres are likely producing lactate, whereas neighbouring oxidative fibres are oxidizing it (157, 159, 160).

In addition to lactate representing a carbon source for metabolic breakdown in different tissues, its accumulation in skeletal muscle has also been implicated in the development of insulin resistance (161). In this context, Choi et al (161) demonstrated that infusion of lactate in rats led to a reduction in glucose disposal during a hyperinsulinemic-euglycemic clamp, an effect that was associated to a reduction in PI3-K and Akt/PKB activation. Interestingly, anti-diabetic drugs such as troglitazone,

rosiglitazone, pioglitazone, metformin, and AICAR all improve skeletal muscle insulin sensitivity, while at the same time increasing lactate production (146, 162-164). Clearly, in these cases, the increase in lactate production is not enough to overpower the insulin sensitizing effects of these drugs; however, inhibition of lactate production in the presence of these pharmacological agents may be a method to further improve insulin sensitivity in skeletal muscle.

2.5.2.8 The pyruvate dehydrogenase complex (PDC) and glucose oxidation

Pyruvate, the end product of glycolysis is a rather important molecule with a number of different fates in skeletal muscle. As discussed above, it can be converted into lactate, or it can enter the mitochondria where the PDC catalyses the irreversible oxidative decarboxylation of pyruvate to acetyl-CoA (165). The PDC thereby provides the link between the glycoglytic pathway and the oxidative machinery in the mitochondria, and in doing so it also generates acetyl-CoA, the necessary precursor molecule for lipid biosynthesis (165).

The PDC is comprised of three different enzymes (pyruvate dehydrogenase (PDH), dihydrolipoyl transacetylase, and dihydrolipoyl dehydrogenase) and requires five different coenzymes (thiamine pyrophosphate (TPP), flavin adenine dinucleotide (FAD), coenzyme A (CoA), nicotinamide adenine dinucleotide (NAD), and lipoate) (166). In the first reaction of the PDC, pyruvate reacts with TPP bound to pyruvate dehydrogenase undergoing decarboxylation to form CO_2 (Figure 9). Next, dihidrolipoyl transacetylase catalyzes the formation of acetyl-CoA, which is now ready to enter the Kerbs cycle. The

third group of reactions involves the utilization of FAD and NAD leading to the formation of NADH + H^+ by the enzyme dihidrolipoyl dehydrogenase (166).

The regulation of the PDC is determined by various nutritional and hormonal states and for the most part, is regulated by the enzymes PDH kinase and PDH phospahtase. These proteins regulate the PDC either by phosphorylation or dephosphorylation of PDH, a process that deactivates and activates the complex, respectively (167) (Figure 9). For example, inactivation of PDC by PDH kinase is important for glucose conservation during times of starvation (168). Under these circumstances, PDH kinase is activated by increases in the mitochondrial acetyl-CoA/CoA and NADH/NAD^+ ratios that result due to the increased rates of fatty acid oxidation (167). Furthermore, in conditions of prolonged caloric restriction circulating insulin concentrations are low, thus failing to stimulate PDH phosphatase and maintaining the PDC in a less active state. PDH phosphatase is important for the reactivation of the PDC after starvation, and also for increasing PDC activity under conditions where the acetyl-CoA requirement is increased, such as during periods of exercise (168). In this context, it has been demonstrated that muscle contraction induced-Ca^{2+} release stimulates PDH phospatase and in doing so, activates the PDC (169) (Figure 9). PDH phosphatase is also activated in lipogenic tissues under conditions of carbohydrate surplus and promotes the formation of acetyl-CoA which is utilized in TG synthesis. Under these conditions, it has been shown that pyruvate inhibits PDH kinase, therefore promoting PDC activity and its own entry into the mitochondria (170) (Figure 9).

The formation of acetyl-CoA from pyruvate by the PDC is the first major step in the glucose oxidation process. Subsequently, citrate synthase catalyzes the formation of citrate from acetyl-CoA and oxaloacetate. The product of this reaction can then undergo two different fates: 1) It will be utilized in the Krebs cycle to form the electron transport chain substrates NADH and $FADH_2$ releasing CO_2 in the process (39); and 2) It can exit the mitochondria via a tricarboxylate carrier and can be converted back to acetyl-CoA which is utilized for lipid synthesis in the cytoplasm (39).

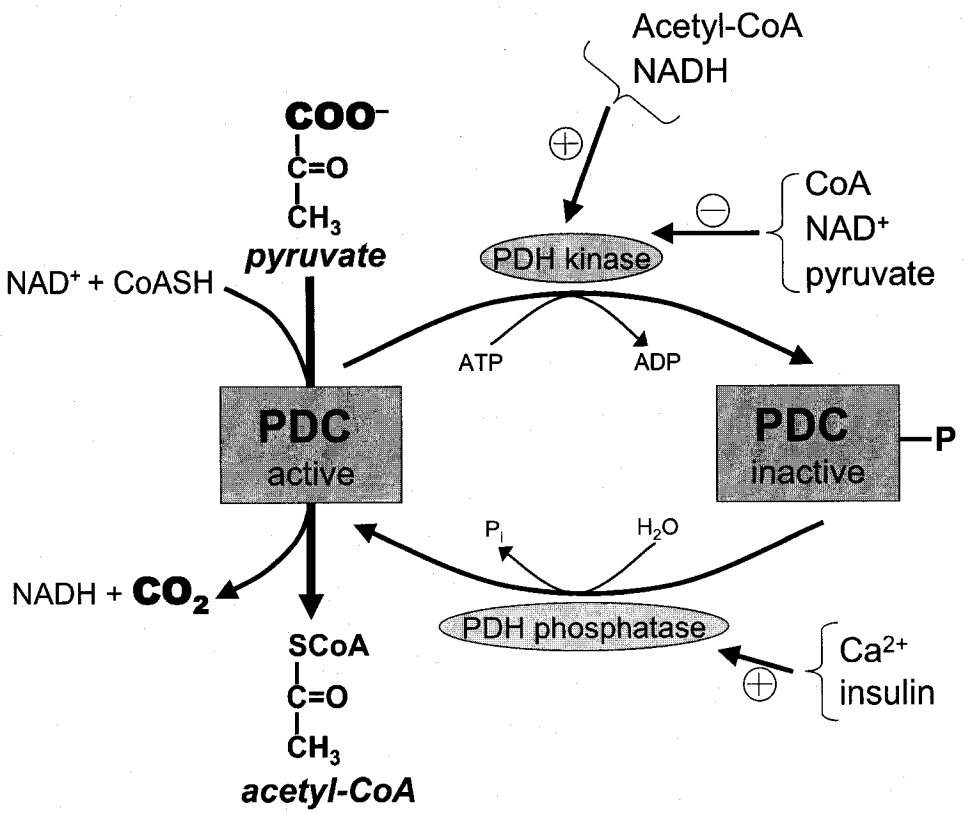

Figure 9. Regulation of pyruvate dehydrogenase complex (PDC) by PDH kinase and PDH phosphatase. In the first reaction, the PDC catalyzes the decarboxylation of pyruvate on carbon 1 producing CO_2 in the process. In the second reaction, the PDC promotes the transesterification of the decarboxylated pyruvate molecule with CoASH to form acetyl-CoA. In the third group of reactions, the PDC converts NAD^+ to NADH + H^+. Within the PDC, PDH is the ratelimiting enzyme. It is deactivated by phosphorylation by PDH kinase. In turn, PDH kinase is activated by an increase in the

acetyl-CoA/CoA and $NADH/NAD^+$ ratio and conversely is inactivated by a reduction in these ratios as well as pyruvate. On the other hand, PDH is activated by dephosphorylation by PDH phosphatase which is activated by Ca^{2+} and insulin (167, 168).

2.5.2.9 The PDC and AMPK

Although the PDC and AMPK never come in direct contact with one another as they are compartmentally separated by the mitochondrial membranes, a recent investigation conducted by Smith et al (7) demonstrated that acute (60 minute) incubation of isolated soleus muscle with AICAR does increase PDC activation. In an attempt to explain the mechanisms responsible for this, the authors measured pyruvate concentrations in the muscles, since this molecule can inhibit PDH kinase and increase PDC activity. They were not able to find any difference in the concentrations of this molecule between muscles treated with and without AICAR, which led them to speculate that PDC may be a direct target of AMPK. In support of this, a subsequent investigation showed that PDC activity of AMPKα2-knockout mice is elevated under resting and exercise conditions compared to wild-type littermates (171). This indicates that AMPKα2 may act as cellular break, to keep the activity of the PDC in check. However, more work is necessary to fully establish a strong link between AMPK and the PDC.

2.5.2.10 Glucose incorporation into lipids

The lipid storage capacity of skeletal muscle is limited in nature, and therefore only a small fraction of glucose contributes to lipid product formation in this tissue. As described above, pyruvate enters the mitochondria where it is converted to citrate in a series of reactions involving the PDC and citrate synthase. Citrate then exits the mitochondria via a tricarboxylate carrier and is cleaved in the cytoplasm by ATP-citrate

lyase to form oxaloacetate and acetyl-CoA (96). The latter of the two molecules is considered to be a short-chain fatty acid, and can be transferred into the mitochondria for oxidation by the CPT-1 isozyme acetylcarnitine transferase (38). In the cytosol, the enzyme ACC converts the two carbon acetyl-CoA molecule into a three carbon malonyl-CoA product, which acts as a building block for lipids in lipogenic tissues such as the liver and adipose tissue. In addition, malonyl-CoA also promotes lipid storage by inhibiting LCFA entry into the mitochondria where oxidation takes place (172). The next step in lipid synthesis is catalyzed by the enzyme fatty acid synthase (FAS), and is a process that is primarily operating in liver and adipose tissue, since skeletal muscle does not express this enzyme. In those tissues, FAS initiates the elongation of the fatty acid by the condensation of a malonyl-CoA molecule with an acetyl-CoA molecule, a reaction that releases CO_2 in the process (39). The resulting four carbon molecule can now be continuously elongated by the addition of other malonyl-CoA molecules to form fatty acids of different carbon chain lengths, which can now be esterified with glycerol-3 phosphate to form a TG (39). However, it is important to note that the majority of TGs present in skeletal muscle are not a result of the *de novo* lipid synthesis pathway, but rather due to increased circulating fatty acid levels in the plasma (173).

2.5.2.11 The glucose-fatty acid cycle

In 1963 Randle et al (174) published data describing a glucose-fatty acid cycle which has traditionally been used to explain the mechanisms behind FA-induced skeletal muscle insulin resistance. The basis of the model proposed by Randle et al (174) is centred on the fact that in conditions like obesity an increase in FA delivery to muscle

leads to increased FA oxidation resulting in elevated acetyl-CoA/CoA and NADH/NAD ratios that inhibit PDC activity. Because the PDC is an important site controlling substrate entry into the mitochondria, its inhibition results in reduced pyruvate conversion into acetyl-CoA. In addition, high levels of lipid oxidation also lead to increased ATP and citrate production which inhibit PFK-1 in the glycolytic pathway. As a result, G6P accumulates and inhibits hexokinase activity ultimately reducing the rate of glucose uptake into the cell. To date, a considerable amount of evidence has been gathered to support the involvement of the Randle cycle in the impairment of glucose utilization in individuals with T2DM (175, 176). However, it is important to note that this is not the only mechanism that impairs glucose uptake in muscle of individuals afflicted by this disease. Recent evidence has revealed that a significant amount of impairment exists in the insulin signalling pathway of individuals with T2DM, an outcome that has been, at least in part, attributed to the accumulation of lipid metabolism by-products within the cell (17, 116). In fact, it is hypothesized that the defects in insulin signalling are the primary causes of insulin resistance rather than a competition between oxidative fuels proposed by Randle et al (134, 174).

2.6 Effect of AMPK activation in different tissues

2.6.1 Effect of AMPK activation in the Liver

The liver is an important organ that plays a crucial role in glucose homeostasis in the body. Plasma glucose is maintained by a balance between hepatic glucose production and glucose disposal in other peripheral tissues. Its inability to regulate glucose output adequately is exemplified in pathological states such as T2DM in which an elevated

glucose production by the liver is one of the major causes of fasting hyperglycemia (177). Insulin is one of the primary hormons that suppresses hepatic glucose production by inhibiting the expression of the gluconeogenic enzymes, phosphoenolpyruvate carboxykinase (PEPCK) and glucose-6 phosphatase (G6Pase) (11). PEPCK is a cytosolic enzyme that regulates the conversion of oxaloacetate to phosphoenolpyruvate utilizing GTP and releasing CO_2 in the process. G6Pase is an enzyme in the gluconeogenic pathway located downstream of PEPCK and is associated with the endoplasmic reticulum (39). This enzyme catalyses the conversion of glucose 6-phosphate to glucose, which is then released into the circulation via the insulin independent Glut-2 transporter. Interestingly, activation of AMPK mimics the effects of insulin by repressing PEPCK and G6Pase gene transcription in hepatoma cells (11). These findings are supported by results demonstrating that systemic infusion of AICAR in normal and insulin-resistant obese rats leads to inhibition of hepatic glucose production (178). Furthermore, the antidiabetic drug metformin, which also activates AMPK in liver, reduces glucose production in primary cultured hepatocytes similar to the effects of AICAR (12). The mechanism by which AMPK induces these effects has been linked to the transcriptional coactivator, transducer of regulated CREB activity 2 (TORC2) (179). In response to fasting TORC2 translocates to the nucleus and associates with CREB transcription factor increasing PPAR-γ coactivator-1α (PGC-1α) expression. PGC-1α in turn promotes the transcription of the gluconeogenic enzymes PEPCK and G6Pase, thereby increasing glucose output by the liver. AMPK activation by either AICAR or metformin prevents TORC2 from translocating to the nucleus and inducing PGC-1α expression thereby

inhibiting activation of the gluconeogenic pathway (179). However, a study conducted by Pencek et al (180) provided conflicting results with respect to the AICAR induced suppression of gluconeogenesis. The infusion of AICAR into the portal vein of dogs suppressed net hepatic glucose uptake in the presence of elevated insulin and glucose levels. In fact, under these conditions, AICAR not only suppressed hepatic glucose uptake, but actually increased glucose output. Interestingly, the authors of this study did not establish whether the increase in glucose output by the liver was mediated by AMPK or was an AMPK independent effect of AICAR. In this context, a subsequent study by Guigas et al (181) demonstrated that both AICAR and metformin inhibit glucose phosphorylation by glucokinase in rat hepatocytes independently of AMPK activation. Since the liver only expresses the high K_m Glut-2 transporter and lacks Glut-4 transporters, glucose uptake is regulated by the activity of glucokinase (Hexokinase IV) rather than by Glut recruitment to the plasma membrane. It has been proposed that glucokinase activators may be important tools to stimulate glucose uptake by the liver and reduce hyperglycemia in T2DM patients (182). Despite these conflicting findings, the implication of AMPK in the suppression of gluconeogenesis has been firmly established as a primary mechanism for the plasma glucose lowering effects of metformin.

In addition to gluconeogenesis, AMPK activation in the liver also controls several pathways associated to lipid metabolism including: lipogenesis, lipid oxidation, and cholesterol synthesis. AMPK activation suppresses lipogenesis associated genes such as fatty acid synthase (183), ACC, and pyruvate kinase (184), which are all important

regulators of the *de novo* lipid synthesis pathway. Similar to the effects in muscle, in rat primary hepatocytes, activation of AMPK by AICAR or metformin increases FA oxidation by inhibition of ACC (12). Furthermore, rats treated with metformin experience reduced blood TG levels indicating that AMPK activation in the liver has an important lipid lowering property. Taken together, these investigations provide crucial evidence that highlights the importance of AMPK activation in the control of glucose and lipid metabolism by the liver.

2.6.2 Effect of AMPK activation in adipose tissue

Traditionally it was thought that the only role of adipose tissue was to store excess calories in the form of TGs in times of energy surplus and to release FAs in times of energy deficit for use by other tissues. Work over the past decade has revealed that adipose tissue plays an important role in controlling whole-body glucose homeostasis in both normal and diseased states (185). In T2DM, which is often associated with obesity, high circulating lipid levels released by adipose tissue have been linked to ectopic fat accumulation in skeletal muscle and liver leading to lipotoxicity and ultimately impaired glucose metabolism (185). Since AMPK is an enzyme associated with increased energy dissipation, interests have been sparked to investigate the role of this enzyme in adipose tissue in hopes of transforming the fat cell from an energy storage to an energy burning compartment. Salt et al (10) demonstrated that AICAR-induced AMPK activation led to an ~40% reduction in insulin stimulated glucose uptake in 3T3-L1 cultured adipocytes. A subsequent investigation conducted in isolated primary adipocytes confirmed the findings that acute (1 hour) AICAR treatment does indeed inhibit insulin-stimulated glucose

uptake (8). In addition, it also demonstrated that several other pathways related to glucose metabolism including, glucose oxidation, lactate production, and glucose incorporation into lipids (lipogenesis) are also inhibited by acute AICAR-induced AMPK activation (8, 186). Furthermore, it was observed that both palmitate and oleate oxidation and uptake were reduced in the presence of AICAR. However, a more recent study demonstrated that incubation of primary adipocytes for 15 hours with AICAR increases palmitate oxidation by ~2-fold, an effect that was attributed to increased expression of oxidative genes and enzymes (9). From these data it is clear that the effects of AICAR-induced AMPK activation on fatty acid oxidation in adipose tissue depend on the time of exposure to the drug.

2.6.3 Effect of AMPK activation in the brain

The control of food intake is a tightly regulated process that is controlled by the communication of signals originating in the periphery to the feeding centre in the hypothalamus. Since AMPK functions as a "fuel gauge", it is logical to assume that activation of this enzyme in the hypothalamic region of the brain by different hormonal and nutrient signals may affect food intake. A link between various hormonal and nutrient signals and hypothalamic AMPK was established by Minokoshi et al (14) in 2004. It was shown that both intraperitoneal (i.p.) leptin and intracerebrovascular (i.c.v.) leptin or insulin administration had potent effects on inhibiting AMPK activity. In addition, the authors demonstrated that either i.p or i.c.v. glucose administration also leads to a reduction in AMPK activity in the hypothalamus. In opposition to these effects, the orexigenic peptides ghrelin and agouti related protein increase AMPK activity

in the hypothalamus (14, 187). To determine the significance of AMPK inhibition in this region of the brain, Minokoshi et al (14) expressed either a constitutively active (CA) or dominant negative (DN) form of AMPK via adenovirus injection in the hypothalamus of mice. Indeed, the DN-AMPK mice showed a reduction in 24 hour food intake, as well as a reduction in body weight shortly after adenovirus administration. On the other hand, the CA-AMPK mice displayed a sustained increase in food intake which led to a significant difference in body weight. Additional support that AMPK activation in the hypothalamus causes an increase in food intake comes from studies utilizing AICAR in their experiments. It was demonstrated that i.c.v. administration of this drug to mice causes an increase in AMPK (188) and ACC (189) phosphorylation which was associated with an increase in food intake. Interestingly, C75, a pharmacological agent utilized to inhibit the lipogenic enzyme fatty acid synthase also inhibits AMPK phosphorylation in the hypothalamus and reduces food intake whereas AICAR reverses these effects (188). The conclusions that can be drawn from these investigations are that hypothalamic AMPK activity may be a key factor involved in translating peripheral hormonal and nutritional signals into either increased or decreased food intake.

Aside from its role in controlling food intake, hypothalamic AMPK has also been demonstrated to exert significant control over AMPK activity in peripheral tissues. Studies in mice showed that intrahypothalamic injections of leptin increased the activity of AMPK in soleus muscles only one hour after administration (15). More importantly, this effect was sustained for up to 6 hours following leptin administration in these animals. In support of these findings a more recent investigation demonstrated that i.c.v.

infusion of C75 led to an increase in skeletal muscle ACC phosphorylation, which accordingly was accompanied by a reduction in malonyl-CoA concentrations and an increase in FA oxidation in this tissue (190). These peripheral effects appear to be mediated, at least in part by activation of sympathetic pathways in the body. In this respect, administration of α blocker phenotolamine 1 hour before C75 i.c.v. infusion significantly reduced the capacity of skeletal muscle to oxidize FAs (190). While these data indicate that the sympathetic nervous system is involved in communicating signals originating in the hypothalamus to effects observed in skeletal muscle, it is important to note that other, yet unknown factors may also be involved in this process.

2.7 Effects of whole-body AMPK activation: What is the end result?

It has been well documented that AMPK activation can affect several pathways of substrate utilization including glucose and FA metabolism in a number of different tissues. In skeletal muscle AICAR has been shown to increase glucose uptake (28, 124, 153, 191), glucose oxidation (7), lactate production (147), and FA uptake and oxidation (164). In addition, several *in vivo* studies have demonstrated that either acute or chronic AICAR administration leads to an increase in skeletal muscle glucose disposal in healthy men (4) and normal and ZDF rats (192). Data from isolated primary adipocytes, 3T3L1 cultured adipocytes and liver shows that acute AICAR-induced AMPK activation can antagonize the effects observed in skeletal muscle. One-hour AICAR treatment in adipocytes leads to a reduction in glucose uptake, glucose oxidation, lactate production, palmitate and oleate uptake, and palmitate oxidation (8, 10). Similarly, in liver data obtained from dogs shows that acute portal venous AICAR infusion potently suppresses

net hepatic glucose uptake, and acutely causes insulin resistance (180). To complicate the matter further, in addition to its peripheral effects, AMPK activation in the brain has been shown to regulate food intake and whole-body energy dissipation (14). In this context, it has been demonstrated that leptin has potent anorectic properties by inhibiting AMPK activation in the hypothalamus (14). Interestingly, intrahypothalamic injection of leptin increases skeletal muscle AMPK activity, only 60 minutes after administration (15). In opposition to the effects of leptin, AICAR-induced AMPK activation in the hypothalamus also modulates energy expenditure by increasing food drive (188, 189). From these data it is clear that AMPK activation can regulate energy balance in the body by acting either through the central nervous system or directly in peripheral tissues to modulate substrate partitioning and energy expenditure. However, since AMPK activation in different tissues has the potential to yield opposing results, and in light of the fact that its activation in the hypothalamus can also influence peripheral AMPK activity (Figure 10), it is difficult to speculate which of these effects would prevail in a whole-body, *in-vivo* setting.

Due to the recent technological advances in small laboratory animal monitoring systems it is possible to answer these questions with relative ease. At any given time, various tissues in the body utilize a combination of carbon sources for ATP production, which are provided in terms of FAs, carbohydrates (CHO), and to a lesser extent, protein. The energy supplied by the oxidative system is relatively easy to determine. The techniques of indirect calorimetry with measurements of oxygen uptake (VO_2) and carbon dioxide production (VCO_2) have been standard practice in humans for many

years. The combination of VO_2 and RQ provides a relatively accurate measure of whole body aerobic production of ATP. By utilizing a comprehensive laboratory animal monitoring system (CLAMS) it is possible to treat animals with AMPK activating agents and assess the effects on whole-body substrate metabolism in a non-invasive manner. Several experiments in this thesis have been carried out using the CLAMS in an attempt to resolve unanswered questions with respect to the effects of whole-body AMPK activation.

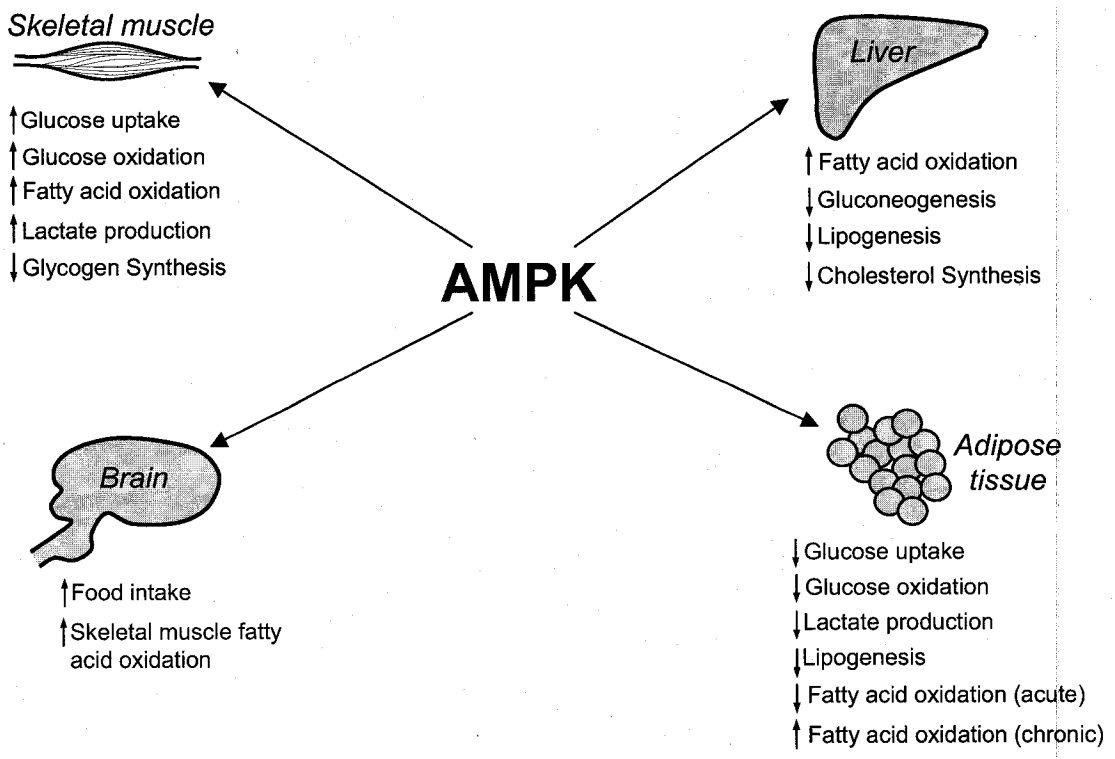

Figure 10. Effect of AMPK activation in skeletal muscle, liver, adipose tissue, and brain on substrate metabolism.

3. OBJECTIVES AND HYPOTHESES

AMPK has been demonstrated to play a major role in skeletal muscle energy homeostasis by controlling various aspects of glucose and fatty acid metabolism. Although a large body of research has been centered on understanding the mechanisms that regulate AMPK in this tissue, there are still experimental gaps that require understanding. Therefore, the general aims of the first three investigations undertaken in this thesis were to elucidate the effects of nutrient (palmitate)- and pharmacological (AICAR and troglitazone)-induced AMPK activation on various aspects of glucose and fatty acid metabolism in skeletal muscle.

3.1 Specific objectives and hypotheses

3.1.1 Study 1: Regulation of AMPK and ACC phosphorylation by palmitate in skeletal muscle cells

Objectives:

1) To determine if physiological concentrations of LCFAs can acutely regulate AMPK and ACC phosphorylation in skeletal muscle cells.

2) To establish if LCFAs can stimulate their own oxidation by activating the AMPK/ACC pathway.

3) To determine if the mechanisms for increasing FA oxidation in the presence of LCFAs are solely dependent on AMPK activation.

Hypotheses:

1) Exposure of L6 muscle cells to various concentrations of fatty acids will increase AMPK and ACC phosphorylation.

2) This will lead to an increase in the rate of LCFA oxidation.

3) Exposure to LCFAs will regulate ACC phosphorylation by AMPK dependent and independent mechanisms.

3.1.2 Study 2: Acute effects of troglitazone in muscle cells

Objectives:

1) To characterize the acute effects of troglitazone-induced AMPK activation on various aspects of glucose and fatty acid metabolism including: glucose uptake, glycogen synthesis, glucose oxidation, lactate production, fatty acid oxidation and uptake, and CPT-1 activity in L6 muscle cells.

2) To determine the acute effects of troglitazone on the phosphorylation of major enzymes in the insulin signalling cascade.

Hypotheses:

1) Troglitazone will have antilipotoxic effects by promoting an increase in CPT-1 activity and fatty acid oxidation.

2) This will augment various aspects of glucose metabolism including: glucose uptake and oxidation, and glycogen synthesis.

3) The improvements in glucose metabolism will be linked to the troglitazone-induced increase in AMPK activation.

3.1.3 Study 3: Effects of AICAR-induced AMPK activation on glycogen synthesis in isolated skeletal muscle

Objectives:

1) To determine the effects of acute AICAR-induced AMPK activation on the rate of insulin-stimulated glycogen synthesis in isolated soleus and epitrochlearis muscles.

2) To elucidate the effects of AICAR-induced AMPK activation on major intracellular insulin-signalling events relevant to the regulation of glycogen synthesis in these muscles.

Hypotheses:

1) AICAR will impair the rate of insulin-stimulated glycogen synthesis in isolated soleus and epitrochlearis muscles.

2) AICAR will reduce the activation of key enzymes involved in the synthesis of glycogen in these muscles.

3.1.4 Study 4: Effects of 2-week AICAR injections on whole-body energy homeostasis

To date, many investigations have studied the effects of chronic AMPK activation in various animal models, and the effect this has on glucose or fatty acid metabolism in select tissues. However, no investigations have provided data related to the effects of chronic AMPK activation on whole-body substrate homeostasis and energy balance.

Objectives:

1) The main objective on this investigation was to determine the effects of 2-week AICAR injections on whole-body energy homeostasis in the rat, by measuring VO_2, RQ,

energy expenditure, the relative contribution of carbohydrates and fatty acids to total energy expenditure, and activity patterns in rats.

2) To determine the effects of 2-week AICAR injections on whole-body adiposity.

3) To determine the effects of 2-week AICAR injections on the phosphorylation of AMPK in various tissues including: skeletal muscle, liver, adipose tissue, and heart tissue.

Hypotheses:

1) AICAR will reduce the RQ, and promote a shift in metabolism towards increased fatty acid oxidation, which will reduce whole-body adiposity in animals receiving this drug.

2) These effects will be driven by increased activation of AMPK in skeletal muscle, liver, adipose tissue and heart tissue.

4. MATERIALS AND METHODS

4.1 Study 1: Regulation of AMPK and ACC phosphorylation by palmitate in skeletal muscle cells

4.1.1 Reagents

Alpha-minimum Eagle's medium (α-MEM) and fetal bovine serum (FBS) were purchased from Wisent (Quebec, Canada). AICAR was purchased from Toronto Research Chemicals, Inc. (Toronto, Ontario, Canada). "Compound C", a selective AMPK inhibitor, was provided by MERCK Research Laboratories. Fatty-acid-free albumin, palmitic acid, and phenylethylamine were from Sigma (St Louis, MO, USA). [1-^{14}C]Palmitic acid was purchased from American Radiolabeled Chemicals, Inc. (St. Louis, MO). Specific antibodies against *P*-AMPK and *P*-ACC were from Cell Signaling Technology (Beverly, MA) and Upstate Biotechnology (Charlottesville, VA), respectively. All other chemicals were of the highest grade available.

4.1.2 Cell Culture and Treatment

Stock cultures of rat L6 skeletal muscle cells were obtained from the American Type Culture Collection and grown in α-MEM medium containing 10% (v/v) FBS, 100 U/ml penicillin, 100 μg/ml streptomycin (growth medium), and antimycotic in a humidified atmosphere of 95% air and 5% CO_2 at 37°C. For experimental procedures, stocks were trypsinized and reseeded in 6-well plates or 35 x 10 mm Petri dishes at a density of 4000 cells/cm^2. After 24 h (~80% confluence) the medium was changed to α-MEM containing 2% (v/v) FBS and antibiotic/antimycotic as described above (differentiation medium) that was replaced after 2, 4, and 6 days of culture. After 7 days,

myotube differentiation was complete, and experimental procedures were initiated. In all experiments, L6 myotubes were serum-starved for 4h prior to the exposure to fatty acids, AICAR and/or Compound C. All controls were incubated with equal amounts of the vehicles used for AICAR, Compound C, and the respective concentrations of fat-free albumin as present in palmitate-treated cells.

4.1.3 Cell viability testing, trypan blue exclusion

Cells were treated with AICAR (2mM), palmitate (1 – 800μM), and Compound C (10 and 40μM). Subsequently, cells were rinsed with PBS, trypsinized, washed with medium, centrifuged, and resuspended in PBS. Next, cells were mixed with the same volume of 0.25% trypan blue and transferred to a slide for 3 min. A total of 300 cells were microscopically counted using a hemocytometer to determine the dead cell (stained blue) rate. The experiments were performed in triplicate. Compared to control (cells not exposed to either AICAR, palmitate or Compound C), no significant differences were detected for cell viability after exposing the cells for 1h to all different treatment conditions.

4.1.4 Production of $^{14}CO_2$ from [1-^{14}C]palmitic acid

Palmitate was conjugated with essentially fatty acid-free BSA to generate a stock solution of 25% (w/v) BSA and 6mM fatty acid in serum-free medium as previously described (193). After conjugation with albumin, the concentration of fatty acids in the solution was measured by using a NEFA kit (Wako Chemicals Inc., Richmond, USA). The stock solution was diluted into the final culture medium to obtain concentrations of 1, 10, 50, 100, 200, 400, 600, and 800μM fatty acid. Palmitate oxidation was measured

by the production of $^{14}CO_2$ from [1-^{14}C]palmitic acid as previously described (105) with a few modifications. Briefly, cells were incubated for 1h in 35 x 15 mm Petri dishes with medium containing 0.2 μCi/ml of [1-^{14}C]palmitic acid and non-labeled Palmitate (1, 10, 50, 100, 200, 400, 600, and 800μM) in the presence or absence of Compound C as indicated. Each Petri dish was sealed with parafilm which had a piece of Whatman paper taped facing the inside of the Petri dish. After 1h of incubation, the Whatman paper was wetted with 100μl of phenylethylamine–methanol (1:1) to trap the CO_2 produced during the incubation period. Subsequently, 200μl of H_2SO_4 (4M) was added to the cells, which were then incubated for one additional hour at 37°C (105). Finally, the pieces of Whatman paper were carefully removed and transferred to scintillation vials for radioactivity counting.

4.1.5 Western blot determination of P-AMPK and P-ACC

Cells were grown in 6-well plates and incubated for 60 min in the presence or absence of palmitic acid (1, 10, 50, 100, 200, 400, 600, and 800μM) and Compound C (40μM) as indicated. Experiments conducted using variable concentrations of ATP revealed that Compound C is a potent reversible small-molecule AMPK inhibitor that is competitive with ATP (12). In *in vitro* assays, Compound C did not exhibit significant inhibition of several kinases including Zeta-associated Protein Kinase, Spleen Tyrosine Kinase, Protein Kinase C θ, Protein Kinase A, and Janus Kinase 3 (12). AICAR (2mM, 60 min) was used as a positive control for AMPK and ACC phosphorylation and also to test the effectiveness of Compound C to inhibit AMPK phosphorylation and activation in L6 myotubes. Since ACC is a substrate for AMPK (111, 194), the determination of ACC

phosphorylation also served as an indicator of AMPK activity. Immediately after all treatments, cells were lysed in buffer containing 135mM NaCl, 1mM $MgCl_2$, 2.7mM KCl, 20mM Tris pH 8.0, Triton 1%, glycerol 10%, and protease and phosphatase inhibitors (0.5mM Na_3VO_4, 10mM NaF, 1μM leupeptin, 1μM pepstatin, 1μM okadaic acid, and 0.2mM PMSF), heated (65°C, 5min), and passed through a 25-gauge syringe five times. An aliquot of the cell lysates was used to determine the protein concentration in each sample by the Bradford method. Prior to loading onto SDS-PAGE gels the samples were diluted 1:1 (v/v) with 2x Laemmli sample buffer (62.5mM Tris-HCl pH 6.8, 2% w/v SDS, 50mM DTT, 0.01% w/v bromophenol blue). Aliquots of cell lysates containing 30μg of protein were then subjected to SDS-PAGE (12% and 7.5% resolving gels for *P*-AMPK and *P*-ACC, respectively), and then transferred to polyvinylidene difluoride membranes (PVDF) membranes (Bio-Rad Laboratories, Burlington, ON). The phosphorylation of AMPK was determined by using phospho-AMPK(Thr172) antibody (1:1000 dilution), which detects AMPK-α only when activated by phosphorylation at Thr-172 (Cell Signaling Technologies, Beverly, MA). ACC phosphorylation was detected using a phospho-ACC-specific antibody (1:500 dilution, Upstate Biotechnology, Charlottesville, VA) which recognizes ACC when phosphorylated at serine 79 (Ser-79). Equal loading of samples was confirmed by Coomassie blue staining of all gels.

4.2 Study 2: Acute effects of troglitazone in muscle cells

4.2.1 Reagents

α-MEM and FBS were purchased from Wisent (Quebec, Canada). The NEFA and lactate kits were obtained from Wako Chemicals, Inc. (Richmond, USA) and Trinity Biotech (Berkeley Heights, NJ), respectively. Troglitazone, etomoxir, defatted albumin, palmitic acid, phenylethylamine and the MTT (3[-4,5-dimethylthiazol-2-yl]2,5idiphenyl tetrazolium bromide) assay kit were purchased from Sigma (St. Louis, MO). [1-^{14}C]palmitic acid, D-[U-^{14}C]glucose, 2-deoxy-D-[^{3}H]glucose, and [1-^{14}C]pyruvic acid were purchased from Amersham Biosciences (Piscataway, NJ). Compound C was kindly provided by Merck Research Laboratories. Antibodies against *P*-AMPK, *P*-Akt and *P*-GSK-3α/β were purchased from Cell Signaling Technology Inc. (Beverly, MA). *P*-ACC was obtained from Upstate Biotechnology (Charlottesville, VA), and GAPDH was obtained from Abcam, Inc. (Cambridge, MA). All other reagents used in these experiments were of the highest grade available.

4.2.2 Cell culture and assessment of viability

L6 skeletal muscle cells were grown in α-MEM and differentiated as previously described in study 1. Cells were serum-starved (α-MEM without FBS) for 4h prior to exposure to troglitazone (5, 50 and 100μM), insulin (100nM), compound C (10 and 20μM), etomoxir (2.5μM), and various combinations of these drugs. All controls were incubated with equal amounts of vehicle used for the previously mentioned conditions. Cell viability was tested by using the MTT (3[-4,5-dimethylthiazol-2-yl]2,5idiphenyl tetrazolium bromide) assay kit after myotubes were exposed to all treatment conditions.

No significant differences were observed in cell viability after myotubes were exposed for 1h to all troglitazone, compound C, and etomoxir concentrations mentioned above.

4.2.3 Determination of P-AMPK, P-ACC, P-Akt (Thr308 and Ser473), and P-GSK-3α/β

Cells were grown in 6-well plates and incubated for 60min in the absence or presence of either troglitazone (50μM), insulin (100nM), compound C (10 and 20μM), troglitazone plus insulin, and troglitazone plus compound C. Determination of P-Akt and P-GSK were performed after cells had been exposed to insulin in the last 5, 10, and 20 minutes of the 60min incubation period. Immediately after all treatments, cell lysates were prepared as described in study 1. Aliquots (30μg of protein) were loaded onto the gels and subjected to SDS-PAGE and then transferred to PVDF membranes (Bio-Rad, Hercules, CA). Membranes used for P-AMPK and P-ACC blotting were derived from the same samples, therefore, the same GAPDH blots are representative of loading for both proteins. The phosphorylation of AMPK and ACC was determined as described in study 1. The phosphorylation of Akt was determined using *P*-Akt (Thr308, dilution 1:1000) and *P*-Akt (Ser473, dilution 1:1000) antibodies which detect Akt only when phosphorylated at Thr-308 or Ser-473. The phosphorylation of GSK was determined using a *P*-GSK-3α/β (Ser21/9, dilution 1:1000) antibody, which detects GSK only when phosphorylated at Ser-21 and Ser-9. Equal loading of all gels was confirmed by Coomassie staining of all gels and/or by the use of GAPDH (dilution 1:5000) as a loading control.

4.2.4 Production of $^{14}CO_2$ from [1-^{14}C]palmitic acid, D-[U-^{14}C]glucose, and [1-^{14}C]pyruvic acid

Palmitate, glucose, and pyruvate oxidation were measured by the production of $^{14}CO_2$ from [1-^{14}C]palmitic acid, D-[U-^{14}C]glucose, and [1-^{14}C]pyruvic acid, respectively. Production of acetyl-CoA by the PDC depends on decarboxylation of pyruvate that occurs at the site of carbon 1 of the molecule; therefore determination of $^{14}CO_2$ from [1-^{14}C]pyruvic acid allows us to trace the activity of the PDC (105, 195, 196). All determinations were performed as previously described in study 1 (105). Briefly, cells were incubated for 1h in 35 x 10mm Petri dishes with α-MEM containing each specific isotope in the following concentrations: [1-^{14}C]palmitic acid (0.2μCi/ml) plus non-labeled palmitate (20μM), D-[U-^{14}C]glucose (0.2 μCi/ml) or [1-^{14}C]pyruvic acid (0.1μCi/ml) plus 2mM non-labled pyruvic acid either in the absence or presence of troglitazone (50μM), insulin (100nM), compound C (10 and 20μM), troglitazone plus insulin, troglitazone plus compound C, and troglitazone plus insulin plus compound C. The rates of $^{14}CO_2$ production from [1-^{14}C]palmitic acid, D-[U-^{14}C]glucose, and [1-^{14}C]pyruvic acid were determined in the presence of 5.5mM non-labeled D-glucose. After 1h of incubation, produced $^{14}CO_2$ was collected for radioactivity counting (105, 196).

4.2.5 CPT-1 activity

L6 myotubes were exposed to insulin (100nM), etomoxir (2.5μM), troglitazone (50μM), and troglitazone plus insulin for 1h and then the activity of CPT-1 was determined by using a radiometric assay (197). Briefly, the assay buffer contained 50mM

imidazole, 70mM KCl, 1mM KCN, 80mM sucrose, 1mM EGTA, 2mM $MgCl_2$, 1mM dithiothreitol (DTT), 1mM ATP, 70μM Palmitoyl-CoA, 0.1% fat-free BSA, 40μM digitonin, and 0.5μCi/ml L-[^{3}H]carnitine. Cells were exposed to the assay buffer for 5min and the reaction was terminated by aspirating the assay buffer and adding ice-cold perchloric acid (4M) to each well. Cells were then collected, lipid was extracted using butanol, and used for scintillation counting. Etomoxir was used as a negative control (97).

4.2.6 Palmitate and Glucose Uptake

For palmitate uptake, L6 myotubes were exposed to insulin (100nM), troglitazone (5, 50, and 100μM), and troglitazone plus insulin for 1h and then incubated for 4min in starve medium containing 0.2μCi/ml [1-^{14}C]palmitic acid and non-labeled palmitate (20μM) (8). For glucose uptake, cells were incubated in the absence or presence of insulin (100nM), troglitazone (50μM), troglitazone plus insulin, compound C (20μM), insulin plus compound C, troglitazone plus compound C, and troglitazone plus insulin plus compound C. Cells were exposed to compound C 30min prior to receiving troglitazone while insulin was added to the medium in the last 20min of the 1h incubation period. Subsequently cells were washed and incubated with Hepes-buffered saline solution containing 10μM 2-deoxy-D-glucose (0.5μCi/ml 2-deoxy-D-[^{3}H]glucose) for 5 min as previously described (105). Both assays were terminated by adding ice-cold PBS and the cells were then lysed in 0.1M KOH. An aliquot of the lysate was used for radioactivity counting and the remainder was used for protein determination by the Bradford method (8).

4.2.7 Glycogen Synthesis, glucose incorporation into lipids, and lactate production

The rate of glycogen synthesis was assessed by the incorporation of D-[U-^{14}C]glucose into glycogen (198). Briefly, myotubes were incubated for 1h in starve medium (α-MEM without FBS) containing 5.5mM D-glucose and 0.2μCi/ml D-[U-^{14}C]glucose either in the absence or presence of: Insulin (100nM), troglitazone (50μM), or troglitazone plus insulin. The reaction was terminated by adding ice-cold PBS and the cells were lysed in KOH. Glycogen was precipitated overnight and transferred to scintillation vials for radioactivity counting. Incorporation of glucose into total lipids was determined after myotubes were exposed to 0.4μCi/ml D-[U-^{14}C]glucose for 2h. Subsequently, the total fraction of glucose incorporated into lipids was extracted with 1.25ml of Dole's reagent (Isopropanol/Heptane/Sulfuric acid (0.5M), 40:10:1). The lipid fraction was then counted for readioactivity (8). Lactate released into the medium was measured by a colorimetric assay using a commercially available kit.

4.3 Study 3: Effects of AICAR-induced AMPK activation on glycogen synthesis in isolated skeletal muscle

4.3.1 Animals

Male albino rats from the Wistar strain (Charles River Laboratories, Montreal, QC., Canada) weighing 40-60g were used in all experiments. The animals were housed in cages with free access to water and standard rat chow, except for the night before the experiments during which they were not allowed to eat. The animals were maintained in a constant-temperature (22°C), with a fixed 12h light/12h dark cycle (07:00-19:00h). All

animal procedures were approved and performed in accordance with the York University Animal Care Committee guidelines.

4.3.2 Reagents

AICAR was purchased from Toronto Research Chemicals (Toronto, ON, Canada). Glycogen, fatty-acid-free albumin, amyloglucosidase, hexokinase, and glucose-6-phosphate dehydrogenase were obtained from Sigma (St. Louis, MO, USA). Human Insulin (Humulin® R) was purchased from Eli Lilly Inc. (Toronto, ON, Canada). D-[U-^{14}C]glucose was purchased from GE Healthcare Radiochemicals (Quebec City, QC, Canada). 2-[1,2-^{3}H]-Deoxy-D-glucose and D-[1-^{14}C]Mannitol were purchased from American Radiolabeled Chemicals, Inc. (St. Louis, MO, USA). Lactate reagent and standards were purchased from Trinity Biotech (Berkeley Heights, NJ, USA). ATP, nicotinamide adenine dinucleotide phosphate (NADP), mannitol, and 2-deoxy-D-glucose were obtained from BioShop Canada Inc. (Burlington, ON, Canada). All other reagents used for the experiments were of the highest grade available.

4.3.3 Muscle extraction and incubation

Before muscle extraction, all animals were anesthetised with a single i.p. injection of Ketamine/Xylazine (0.2ml/100g of body weight). Subsequently, the soleus (15 – 20mg) and epitrochlearis (10 – 15mg) muscles were quickly extracted and mounted onto thin, stainless steel wire clips to maintain optimal resting length. The incubation procedures were performed as previously described (196). Briefly, immediately following extraction the muscles were placed in plastic scintillation vials containing 2ml of gassed [30min with O_2:CO_2/95:5% (vol/vol)] Krebs-Hanseleit bicarbonate (KHB) buffer with 4% fat-

free BSA and 6mM glucose. The scintillation vials were then sealed with rubber stoppers and gasification was continued for the entire 1h pre-incubation period. After pre-incubation, the muscles were transferred to a second set of vials with 1.5ml of KHB buffer containing D-[U-^{14}C]glucose (0.2μCi/ml). All muscles were maintained either in the absence or presence of the following conditions: insulin (100nM), AICAR (2mM), and AICAR plus insulin for the entire 1h incubation. For the AICAR plus insulin conditions, all muscles were exposed to AICAR for 30min prior to the addition of insulin.

4.3.4 Measurement of glycogen synthesis in isolated muscle

Glycogen synthesis was assessed by measuring the incorporation of D-[U-^{14}C]glucose into glycogen as previously described (196). Briefly, upon termination of the incubation experiment as outline above, muscles were quickly washed in ice-cold PBS, blotted on filter paper, frozen (N_2), and digested in 0.5ml of 1M KOH at 70°C for 1h. Of the digested muscle solution, aliquots were taken for protein determination (Bradford method), determination of glycogen content, and glycogen synthesis. Formation of glycogen from labeled glucose was estimated by adding 10mg of carrier glycogen to the hydrolysates. Subsequently, glycogen was precipitated overnight with 100% ethanol. The precipitate was re-suspended in 0.5ml of water and its radioactivity was determined using a scintillation counter (196).

4.3.5 Measurement of glycogen content and lactate production

After incubation of muscles in the presence of the various conditions outlined above, the muscles were digested in 0.5ml of 1M KOH. For analysis of glycogen content, the pH of muscle digest was titrated to 4.8 prior to the addition acetate of buffer (pH=4.8)

and 0.5mg/ml of amyloglucosidase. Subsequently, glycogen was hydrolyzed at 40°C for 2h and glucose was analyzed enzymatically (199) and the absorbance read in a spectrophotometer (Ultraspec 2100 pro; Biochrom Ltd., Cambridge, UK) at 340nm wavelength. Lactate concentration was measured in deproteinized and neutralized muscle incubation medium using a commercially available kit.

4.3.6 Measurement of glucose transport into muscle

Soleus and epitrochlearis muscles were extracted as described above. Subsequently, they were pre-incubated for 1h in KHB buffer containing 8mM glucose, 32mM Mannitol, and 0.1% BSA. After the pre-incubation, all muscles were exposed for 1h to the following conditions: Insulin (100nM), AICAR (2mM), and AICAR plus insulin. All AICAR plus insulin conditions received AICAR for 30min prior to the 1h incubation period. Following the incubation, all muscles were washed for 10min in KHB buffer containing 40mM mannitol at 29°C, and if present during the previous incubation period, insulin (100nM) and AICAR (2mM). For measurement of glucose transport, the muscles were transferred to new flasks and incubated for 20min at 29°C in 1.5ml of KHB containing 0.5μCi/ml 2-[1,2-^{3}H]deoxy-D-glucose (2-DG, and 8mM non-labeled 2-DG) and 0.1μCi/ml [U-^{14}C]mannitol as an extracellular space marker (200). To terminate the experiment, immediately after the 20min glucose uptake period muscles were blotted (4°C) and quickly frozen in liquid N_2. Muscles were then digested in 0.5ml of 1M KOH at 70°C and centrifuged (1000g). Aliquots (450μl) of the muscle extract supernatant and of the incubation medium were counted for radioactivity using a scintillation counter with channels preset for simultaneous ^{3}H and ^{14}C counting. The amounts of D-[U-

^{14}C]mannitol and 2-[1,2-^{3}H]deoxy-D-glucose present in the samples were used to calculate extracellular space and glucose transport, respectively, as previously described (201). The intracellular water content of the muscles was calculated subtracting the measured extracellular space water from total muscle water. Total water content was assumed to be 77%, which is the average value for soleus and epitrochlearis muscles after drying the tissues to a constant weight in our laboratory.

4.3.7 Western blot determination of p-AMPK, p-ACC, p-Akt (Thr308, Ser473), p-GSK-3α/β, p-GS, AMPKα1, AMPKα2, and GAPDH

Soleus muscles were incubated in the absence or presence of insulin (100nM), AICAR (2mM), and AICAR plus insulin. All muscles were pre-incubated in KHB buffer as described above. To investigate time-dependent alterations in phosphorylation levels of Akt (Thr308 and Ser473), GSK-3α/β, and GS, we exposed the muscles to insulin for 15, 30, and 45min. AICAR was added to the incubation medium 30min prior to adding insulin and remained in the medium thereafter. Control muscles received neither AICAR nor insulin. In order to test the effectiveness of AICAR to induce AMPK activation, we measured the phosphorylation state of ACC, a downstream target of AMPK. In addition, we also examined the distribution of AMPKα1 and AMPKα2 in soleus and epitrochlearis muscles to determine the fiber type specific distribution of the two AMPK catalytic isoform subunits. Immediately following all treatments, muscles were frozen in liquid N_2 and stored at -80°C until analysis. For preparation of muscle lysates, the solei and epitrochlearis muscles were homogenized in buffer containing 135 mM NaCl, 1 mM $MgCl_2$, 2.7 mM KCl, 20 mM Tris, pH 8.0, 1% Triton, 10% glycerol and protease and

phosphatase inhibitors (0.5 mM Na_3VO_4, 10 mM NaF, 1 μM leupeptin, 1 μM pepstatin, 1 μM okadaic acid, and 0.2 mM PMSF), and heated (65°C, 5min). An aliquot of the homogenate was used to determine the protein concentration in each sample by the Bradford method. Before loading onto SDS-PAGE gels, the samples were diluted 1:1 (v/v) with 2 × Laemmli sample buffer (62.5 mM Tris-HCl, pH 6.8, 2% (w/v) SDS, 50 mM DTT, and 0.01% (w/v) bromophenol blue). Aliquots of muscle homogenates containing 75 μg of protein were run through SDS-PAGE gels (12% for p-AMPK, 7.5% for *P*-ACC, and 10% for *P*-Akt (Thr308 and Ser473), *P*-GSK-3α/β, *P*-GS, and GAPDH) and then transferred to PVDF membranes (Bio-Rad Laboratories, Burlington, ON, Canada). The phosphorylation of AMPK, ACC, Akt, and GSK-3α/β was determined as described in study 2. GS phosphorylation was detected using a *P*-GS specific antibody, which recognizes GS when phosphorylated at serine 641 (Ser641). Equal loading of all gels was confirmed by Coomassie staining of all gels and by the use of GAPDH as a loading control. Specific antibodies against *P*-Akt, *P*-GSK-3α/β, *P*-GS and *P*-AMPK were purchased Cell Signaling Technology Inc. (Beverley, MA, USA). Specific antibodies against the α-1 and α-2 subunits of AMPK were purchased from Santa Cruz Biotechnology, Inc. (Santa Cruz, CA, USA). *P*-ACC was obtained from Upstate Biotechnology (Charlottesville, VA, USA) and GAPDH was from Abcam, Inc. (Cambridge, MA, USA). All antibodies were applied in a 1:1000 dilution, except GAPDH, which was used in a 1:5000 dilution.

4.4 Study 4: Effects of 2-week AICAR injections on whole-body energy homeostasis

4.4.1 Chronic Experiments

Upon arrival, male, Wistar rats weighing 110-115g were randomly assigned to two groups (Control and AICAR), and allowed to acclimatize for 4 days prior to beginning the treatment protocol (Figure 11). Beginning on day 5, animals in the AICAR group received an injection of AICAR (0.7g/kg of body weight, i.p.) prepared in sterile saline (0.9% NaCl). Similarly, all animals in the Control group received an equal volume of saline without AICAR. Body weight and food intake of the animals was determined every morning prior to AICAR administration. All animals were injected for two consecutive weeks (days 5-9, and days 12-16) at 10am (Figure 11). Blood samples were collected via the saphenous vein in heparinized tubes (Sarstedt, Montreal, Quebec, Canada) on days 5, 9, 12, and 16 prior to AICAR injection. The plasma was then separated by centrifugation and used for the determination of various hormone and metabolite concentrations. Upon completion of the two week injection protocol (day 17), all animals were anaesthetized and euthanized by cervical dislocation 24 hours after the last AICAR injection.

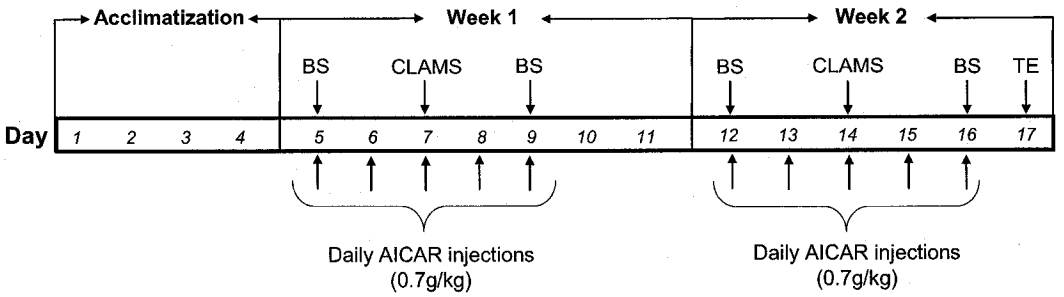

Figure 11. Schematic representation of the *in vivo* AICAR experiments. The animals were allowed to acclimatize for 4 days prior to beginning the injection protocol. On day 5 of week 1 AICAR animals received daily AICAR injections (0.7g/kg body weight, i.p.) until day 9 of the study. Control animals were injected with an equal amount of saline. Blood samples (BS) for all animals were collected prior to AICAR injection on days 5 and 9, and days 12 and 16 of week 1 and 2, respectively. On days 7 and 14 in the mornings, immediately following injections, animals were placed in the CLAMS until the following days (day 8 and 15). On day 17 of week 2 all animals were anaesthetized, euthanized, and tissues were extracted (TE).

4.4.2 Tissue Extractions

Immediately following euthanization at the end of the 2 week study, the following tissues were extracted and frozen at -84°C for future analysis: soleus, epitrochlearis, and EDL muscles, liver, brain, and heart. The following fat pads were extracted and immediately weighed: Retroperitoneal (Retro), epididymal (Epi), subcutaneous (SC), and brown adipose tissue (BAT). The weight was expressed relative to the body weight of the animal prior to euthanization. The fat pads were subsequently frozen at -84°C for future analysis.

4.4.3 Western blot determination of P-AMPK, P-ACC, and GAPDH

In order to test the effectiveness of AICAR to induce AMPK activation, we measured the phosphorylation state of AMPK and its downstream target ACC in various tissues including: EDL muscle, liver, heart, and adipose tissue at the end of the

investigation. Tissue lysates and western blot analyses for P-AMPK, P-ACC, and GAPDH were performed as described in study 3.

4.4.4 Metabolic Cage Experiments

Oxygen consumption (VO_2), CO_2 production (VCO_2), accumulated O_2 consumption, energy expenditure (EE), respiratory quotient (RQ), food intake, and activity were measured using the automated Comprehensive Laboratory Animal Monitoring System (CLAMS, Columbus Instruments, Columbus, OH) on the third day of AICAR injections (Day 7 and 14) in both week 1 and week 2 of the treatment protocol (Figure 11). This eight chamber open-circuit system allowed the animals to be housed individually in plexiglass cages with free access to food and water, while the above measurements were collected by the automated CLAMS. Prior to placing the animals in the cages, the CLAMS gas sensors were calibrated with primary gas standards of high purity (20.40% O_2 and 0.50% CO_2). Subsequently, the system was operated on ambient air. The gas sensors measured the CO_2 and O_2 concentrations from a sample drawn from the selected cage to generate VCO_2 and VO_2 values. The VCO_2 value was calculated by taking the difference between the output and input CO_2 flow rates. Similarly, the VO_2 value was calculated by taking the difference between the input and output O_2 flow rates. Accordingly, the equations used by the computer software to measure these variables were as follows:

$$VCO_2 = V_oCO_{2o} - V_iCO_{2i}$$

$$VO_2 = V_iO_{2i} - V_oO_{2o},$$

where V_i and V_o are the input and output ventilation rates (LPM), CO_{2i} and CO_{2o} are the carbon dioxide fractions at the input and output, and O_{2i} and O_{2o} are the oxygen fractions at the input and output, respectively. The air flow rate to each individual cage (V_i) was maintained at 1.85 litres/minute in week 1, and 2.0 litres/minute in week 2 of the protocol. The V_o rate on the other hand, was not known and had to be estimated using the Haldane transformation.

$$\text{Haldane transformation:} \quad V_o = V_i \times (N_i/N_o) ,$$

where N_i is nitrogen fraction in the air supplied to the chamber, and N_o is the nitrogen fraction of the sample.

An additional measurement that was derived by the CLAMS from the VO_2 reading is accumulated O_2 consumption. This measurement represents the cumulative O_2 consumed by the animals during the entire time they are maintained in the cages, and is expressed in liters. From the VCO_2 and VO_2 values RQ was calculated by the following equation:

$$RQ = VCO_2/VO_2$$

The RQ is a measure of substrate oxidation and ranges from 0.7 to 1.0. Values near 0.7 indicate an increased rate of fatty acid oxidation whereas values near 1.0 indicate increased rates of carbohydrate oxidation. In addition, the software also calculated EE by the following equations:

$$EE = CV \times VO_2$$

$$CV = 3.815 + 1.232 \times RQ$$

The program obtained a calorific value (CV) by utilizing the RQ. This value was then used together with the VO_2 to obtain the EE expressed in kcal/hr. The RQ together with EE were also utilized to calculate the relative contribution that carbohydrates and fatty acids made towards EE. This was accomplished by determining, from the RQ, the percent of fatty acids and carbohydrates that were being utilized at every time point for each animal. Those percentages were then multiplied by the observed EE at the same time point to obtain two separate values. This procedure was performed for both weeks of the investigation.

Activity measurements were obtained using a series of infrared beams that are passed from one side of the cage/chamber to the other. Each time a successive beam is broken by the rat it is recorded as an activity count. Therefore, this measure does not provide an indication of distance but instead generates arbitrary units of spontaneous physical activity by the rat. In our experiments activity in the x-plane (the length of the cage) and the z-plane (the height of the cage) were measured (Figure 12). Activity in these two planes was summed (x + z) to give a better indication of the total spontaneous physical activity for the animals.

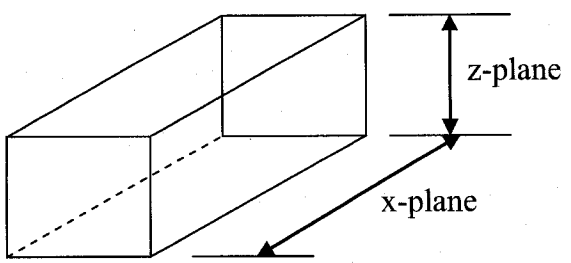

Figure 12: Activity measurements in the x and z-planes

Animals were placed in the cages at approximately 10am immediately following AICAR injection. As a result of the injection, all animals experienced significant excitation within the first hour in the CLAMS. The data obtained within that timeframe is not an accurate representation of values typically obtained at that particular time point in the day. Therefore, data acquired in the first hour following saline and AICAR injections are not presented in the figures and were not utilized for statistical analyses. All measurements collected via the CLAMS and presented in the figures to follow were obtained at the start of the second hour following AICAR injections, when animal behaviour appeared to be a more accurate representation of basal values. The data presented in the figures were recorded from 11am to 8am the following morning. At 8am, all experiments were terminated and animals were weighed, and returned back to the original cages prior to injecting with either AICAR or saline at 10am.

Measurements from each cage were taken approximately every 4 minutes. For each animal, data for VO_2, EE, accumulated O_2 consumption, RQ, and activity (x + z axis) were analyzed by generating an average for all measurements taken every hour. These averages were subsequently used to generate the figures as well as the statistical analyses. All CLAMS data presented in the figures to follow were compiled from three independent experiments with an N=3 animals/group/experiment.

4.4.5 Blood sampling for the determination of plasma AICAR, glucose, lactate, and NEFAs

Although the main purpose of the *in vivo* AICAR experiments was to examine the chronic effects of this drug on whole-body substrate homeostasis, additional data regarding the plasma concentrations of various metabolites following injection would be useful to support the findings obtained via the CLAMS. In this context, a separate group of experiments were conducted in which plasma AICAR, glucose, lactate, and NEFA concentrations were measured at different time points, for up to 8 hours following a single AICAR injection. For these experiments, a separate set of animals were used, which were not utilized in CLAMS experiments. These short term analyses were intended to provide additional support for the metabolic alterations observed in week 1 and week 2 of the CLAMS experiments. Animals were injected i.p. with AICAR or saline at 9am (0.7g/kg of body weight) and blood samples were collected from the saphenous vein into heparin coated tubes at the following time points: 0 (basal sample), 5 min, 10 min, 15 min, 30 min, 1 h, 2 h, 4 h, 8 h. Plasma was separated by centrifugation, stored at -84°C, and used for the determination of AICAR, glucose, lactate, and FFA levels. Following the last time point, the animals were euthanized and sacrificed via cervical dislocation and the tissues were extracted for future analysis as described above.

4.4.6 Plasma AICAR determination assay

AICAR was measured in the plasma using a colorimetric assay as previously described with slight modifications (202). Briefly, a 1% w/v solution of sodium nitrite, a 3% w/v solution of ammonium sulfamate, and a 0.75% w/v solution of N-(1-

naphthyl)ethylenediamine were freshly prepared. AICAR standards ranging from 0.125 to 64 μg/ml were made by dissolving AICAR in deionized water. Prior to use, the plasma was spun down to remove particulates and buffered by mixing plasma with phosphate-buffered saline (pH=7.4) in a ratio of 1:12. Subsequently, 500μl of diluted plasma was mixed with 150μl of 1N HCl and 50μl of sodium nitrite solution and incubated at room temperature for 5 minutes. Next, 50μl of ammonium sulfamate solution was added, vortexed and incubated for 10 minutes at room temperature. For the final step, 100μl of N-(1-naphthyl)ethylenediamine solution was added to the mixture. The samples were then allowed to react for 10 additional minutes at room temperature and read in a spectrophotometer at 540nm wavelength.

4.4.7 Plasma Glucose, Lactate, NEFA and leptin assays

To better understand the metabolic alterations measured using the CLAMS in week 1 and week 2 of the investigation, plasma glucose, lactate, and NEFAs were measured in blood samples collected after a single AICAR injection. Leptin levels were measured in plasma samples collected at the beginning and end of week 1 (days 5 and 9, respectively) and 2 (days 12 and 16, respectively) prior to AICAR injection. All plasma metabolite and hormone concentrations were assessed by colorimetric assays using commercially available kits from Trinity Biotech (lactate, Berkeley Heights, NJ), Sigma (glucose, St. Louis, MO), Wako Chemicals, Inc. (NEFAs, Richmond, VA), and Medicorp (leptin, Montreal, Quebec).

4.5 Statistical analysis

4.5.1 Study 1: Regulation of AMPK and ACC phosphorylation by palmitate in skeletal muscle cells

Statistical analyses were performed by one-way or two-way ANOVAs with the Tukey-Kraemer multiple comparison test or Bonferroni posttest. The level of significance was set at $P < 0.05$. All data are presented as means ± SEM.

4.5.2 Study 2: Acute effects of troglitazone in muscle cells

Statistical analyses were performed by one-way ANOVAs with Tukey-Kraemer multiple comparison post-hoc tests. The level of significance was set at $P < 0.05$. All data are presented as means ± SEM and expressed relative to control.

4.5.3 Study 3: Effects of AICAR-induced AMPK activation on glycogen synthesis in isolated skeletal muscle

Statistical analyses were performed by one-way ANOVAs followed by Fisher multiple comparison post hoc tests. The level of significance was set at $P < 0.05$. All data are presented as means ± SEM.

4.5.4 Study 4: Effects of 2-week AICAR injections on whole-body energy homeostasis

Statistical analyses were performed by one or two-way ANOVAs with Tukey-Kraemer multiple comparison post-hoc tests or contrasts. The level of significance was set at $P < 0.05$. All data are presented as means ± SEM.

5. RESULTS

5.1 Study 1: Regulation of AMPK and ACC phosphorylation by palmitate in skeletal muscle cells

5.1.1 AMPKα and ACC phosphorylation by AICAR and Palmitate

As expected, AICAR elicited a 2.5- to 3.5-fold increase in AMPK and ACC phosphorylation as compared to control (Figure 13). Interestingly, the incubation of myotubes with palmitate also caused a significant increase in AMPK and ACC phosphorylation. A significant effect (~1.9-fold) on both AMPK and ACC phosphorylation was observed in the presence of palmitate concentrations as low as 10μM (Figure 13A and 13C). A dose-response effect was found as the concentration of palmitate in the incubation medium was increased (1 to 800μM). However, maximum increases of 3.5-fold for AMPK (Figure 13B) and 4.5-fold for ACC phosphorylation (Figure 13D) were obtained at 400μM compared to control (Figure 13C and D). Higher palmitate concentrations of 600 and 800μM also induced phosphorylation of AMPK (2.7- and 2.6-fold, respectively) and ACC (3.7- and 3.4-fold, respectively) compared to control; however, the values obtained were lower than in the presence of 400μM palmitate (Figure 13A-D). These results indicate that either low (10μM) or high (800μM) fatty acid concentrations increase both AMPK and ACC phosphorylation in L6 skeletal muscle cells.

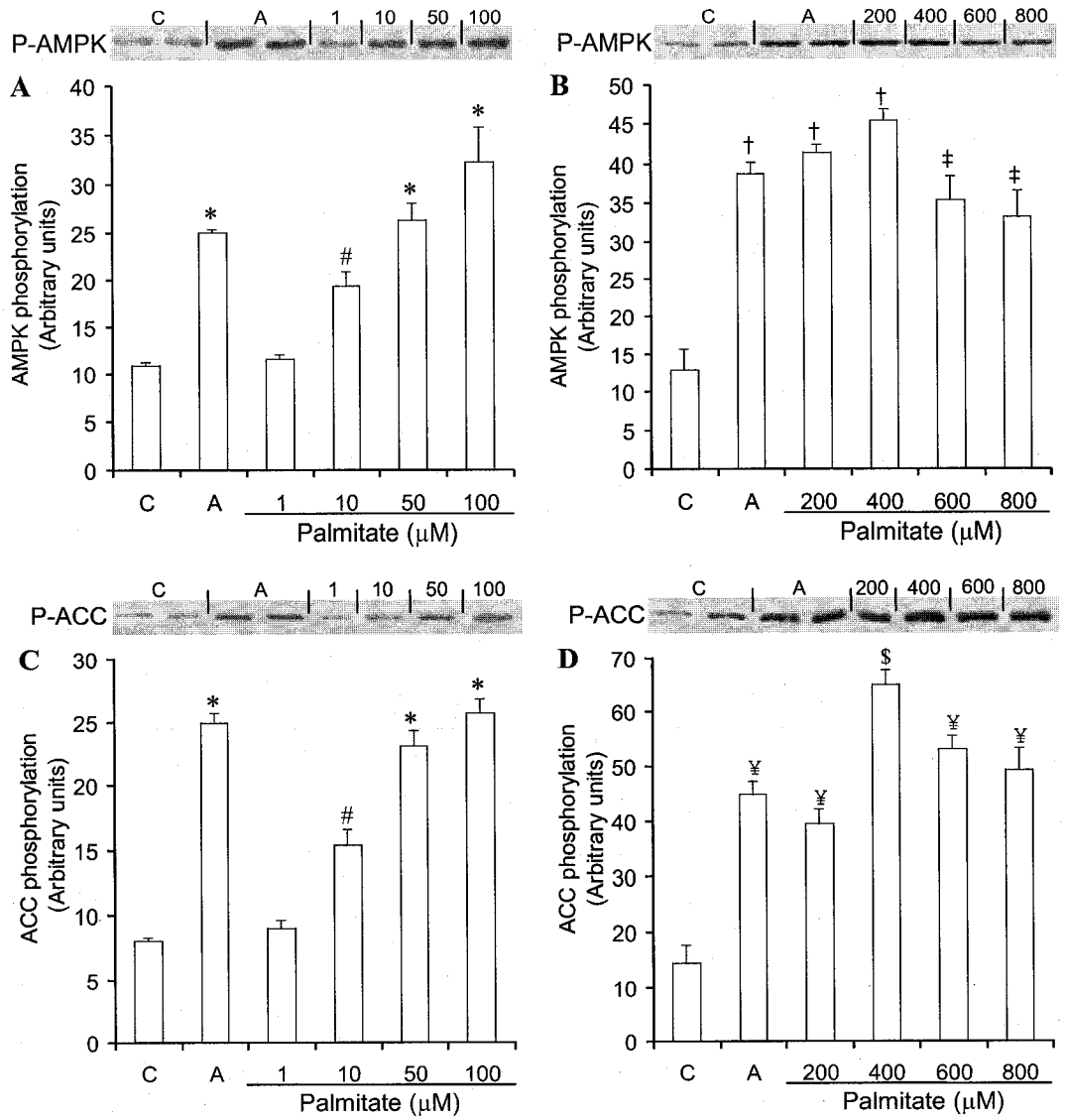

Figure 13. Dose-response effect of palmitate on AMPK (A and B) and ACC (C and D) phosphorylation in L6 myotubes. Densitometric analysis (graphs) and respective representative blots (upper panels) for each experimental condition. Cells were exposed to different concentrations of palmitate (from 1 to 800μM) for 1h and then lysed as described in methods. Control cells (C) were neither exposed to AICAR (A) nor to palmitate. AICAR was used as a positive control for AMPK and ACC phosphorylation. Data presented as average ± SEM. *P<0.05 vs. control and palmitate 1μM. #P<0.05 vs. control, AICAR, and palmitate 1, 50, and 100μM. †P<0.05 vs. control and palmitate 600 and 800μM. ‡P<0.05 vs. control and palmitate 400μM. ¥P<0.05 vs. control and palmitate 400μM. $P<0.05 vs. all other conditions. Data compiled from four independent experiments with duplicates in each experiment.

5.1.2 Inhibition of AICAR-induced AMPK and ACC phosphorylation by Compound C

In order to determine if the effects on ACC phosphorylation and fatty acid oxidation were solely due to the activation of AMPK by palmitate, we applied the AMPK inhibitor (Compound C) in our experiments. To establish the efficacy of Compound C to inhibit AMPK phosphorylation and activity, we treated L6 myotubes with either 10μM or 40μM of the inhibitor 30 min prior to exposing the cells to AICAR (2mM). The inhibitor did not affect basal AMPK (Figure 14A) and ACC phosphorylation (Figure 14B) levels but significantly blocked AICAR-induced phosphorylation of AMPK and ACC. The utilization of 10μM of Compound C significantly reduced (35% and 50%, respectively) AICAR-induced AMPK and ACC phosphorylation, whereas in the presence of 40μM of Compound C phosphorylation of both AMPK and ACC was completely abolished reducing it to basal values (Figure 14A and B). Therefore, 40μM of Compound C was chosen to be used in all subsequent experiments.

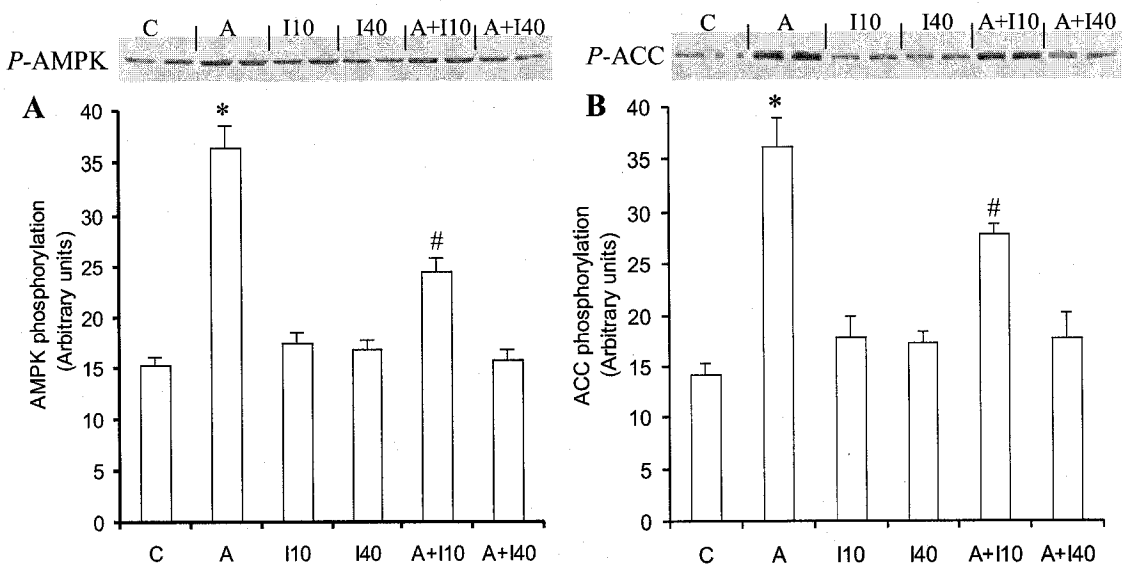

Figure 14. Effect of Compound C on basal (C, control) and AICAR-induced AMPK (panel A) and ACC (panel B) phosphorylation in L6 myotubes. Densitometric analysis (graphs) and respective representative blots (upper panels) for each experimental condition. Thirty minutes prior to AICAR (A) treatment, cells were exposed to either 10 μM (I10) or 40 μM (I40) of Compound C. Subsequently, cells were incubated for 60 min in the presence of AICAR (2mM) as indicated. Data presented as average ± SEM. *P<0.05 vs. control (C), AICAR, AICAR + inhibitor 10 (A + I10), and AICAR + inhibitor 40 (A + I40). #P<0.05 vs. control, AICAR, and AICAR + I40. Data compiled from four independent experiments with duplicates in each experiment.

5.1.3 Effect of Compound C on palmitate-induced AMPK and ACC phosphorylation

Palmitate-induced AMPK phosphorylation was blocked by Compound C for all fatty acid concentrations ranging from 1 to 800μM (Figure 15A and 15B). Interestingly, palmitate-induced ACC phosphorylation was also prevented by Compound C in the presence of palmitate concentrations ranging from 1μM to 100μM; however, this AMPK inhibitor did not prevent palmitate-induced phosphorylation of ACC in the presence of higher concentrations (200 to 800μM) of this fatty acid (Figure 15C and 15D). In

previous experiments, we exposed cells to various concentrations of palmitate in the presence of Compound C; AICAR was used as a positive control for AMPK phosphorylation (Figure 15). However, in those experiments, we did not have data from cells exposed to palmitate alone to serve as a control for those treated with Compound C and palmitate in the same experiment. In order to fulfill this experimental gap, we exposed muscle cells to either 10μM or 400μM of palmitate in the absence and presence of Compound C. These palmitate concentrations were chosen because in previous experiments both elicited significant increases in phosphorylation of AMPK and ACC (Figure 13), but were differently affected by the presence of Compound C (Figure 15). As expected, AMPK phosphorylation was significantly increased in the presence of either 10μM (1.7-fold) or 400μM (2.4-fold) of palmitate, and it was completely blocked by Compound C (figure not shown). Also, palmitate 10μM induced a significant increase (~1.6-fold) in ACC phosphorylation, which was completely prevented by Compound C (Figure 16A). Interestingly, in the presence of 400μM ACC phosphorylation increased by ~2.7-fold and remained equally phosphorylated despite the presence of Compound C in the incubation medium (Figure 16B). These results confirm and strengthen the observations that elevated concentrations of palmitate exert a regulatory effect on ACC phosphorylation/ activity independently of AMPK.

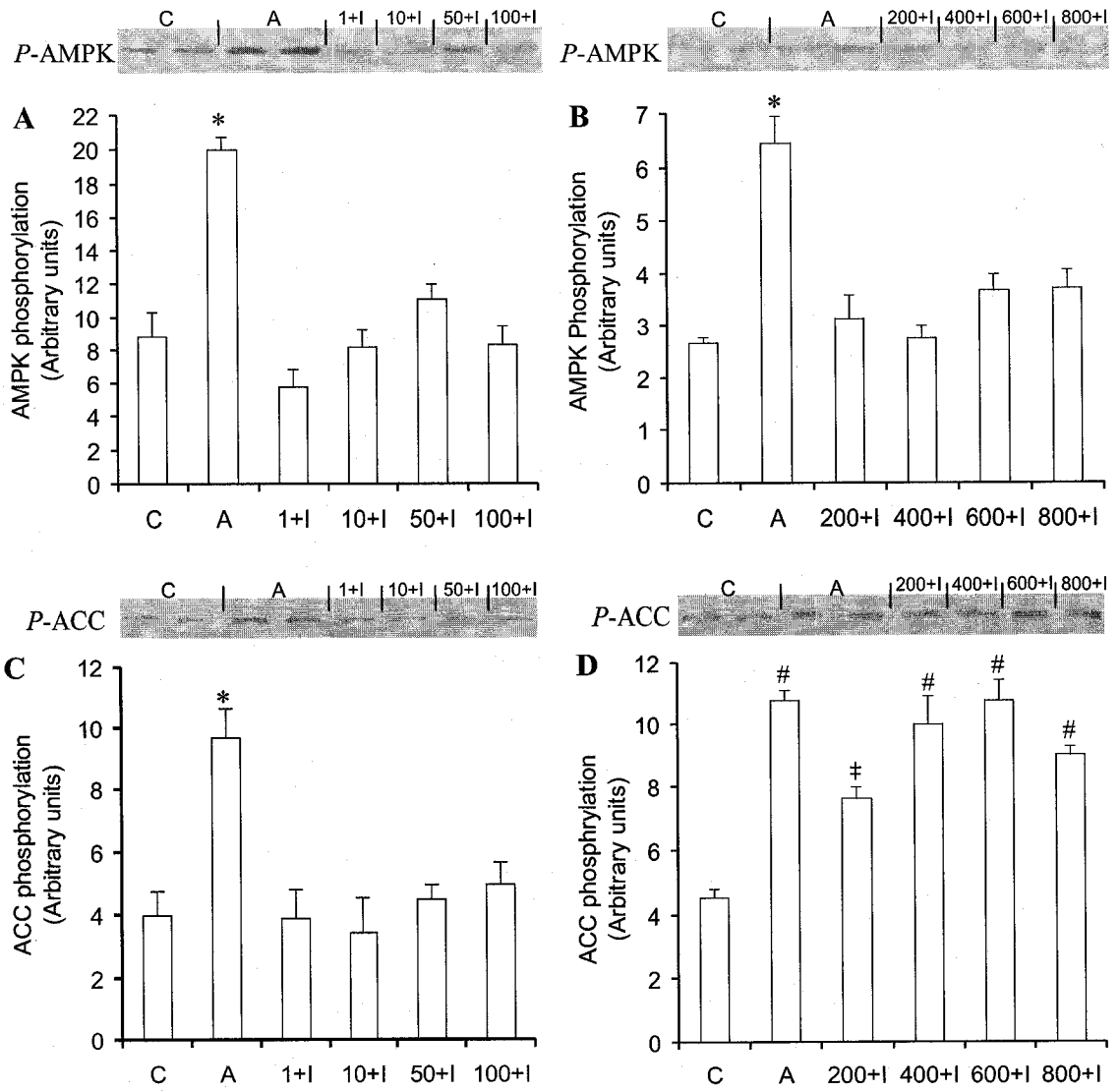

Figure 15. Effect of Compound C (40μM) on palmitate (1 to 800μM)-induced AMPK (A and B) and ACC (C and D) phosphorylation in L6 myotubes. Densitometric analysis (graphs) and respective representative blots (upper panels) for each experimental condition. Compound C (I, inhibitor of AMPK) was added to the incubation medium 30 minutes prior to palmitate treatment and was also present during the entire 1h-palmitate-incubation-period. AICAR (A, 2mM) was used as a positive control for AMPK and ACC phosphorylation. Data presented as average ± SEM.*$P<0.05$ vs. all conditions. $^{\#}P<0.05$ vs. control and palmitate 200+I. $^{\ddagger}P<0.05$ vs. control, AICAR, palmitate 400+I and 600+I. Data compiled from four independent experiments with duplicates in each experiment.

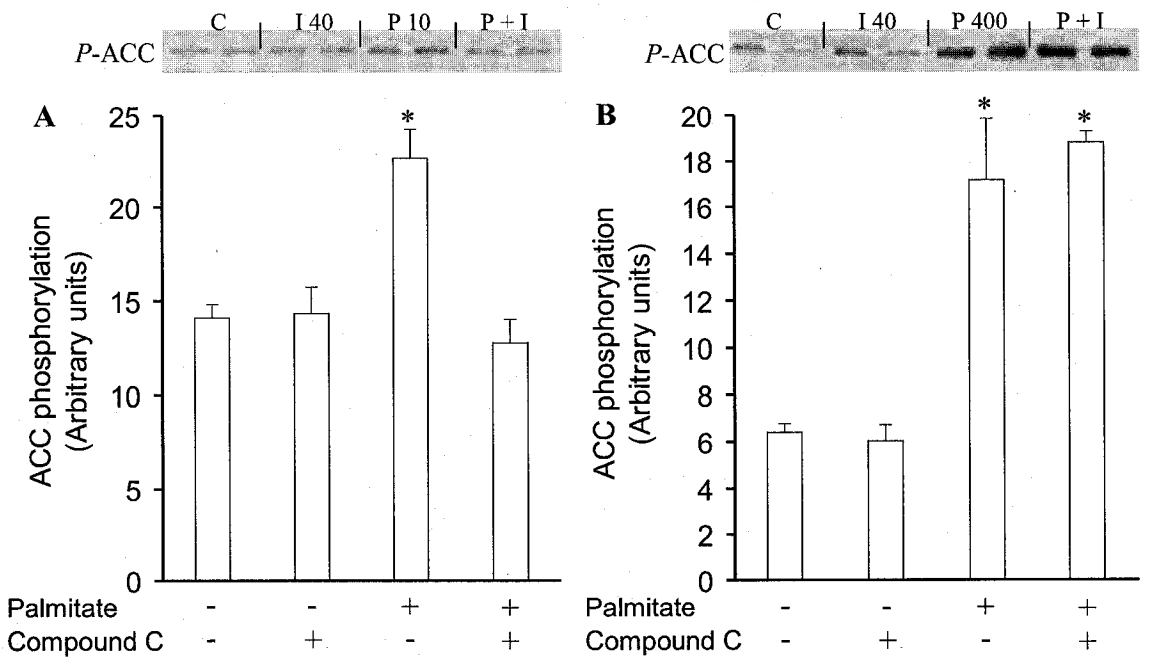

Figure 16. Effect of Compound C (40μM) on basal (C, Control – cells neither exposed to palmitate nor to Compound C) and palmitate-induced ACC phosphorylation in L6 myotubes. Densitometric analysis (graphs) and respective representative blots (upper panels) for each experimental condition. Compound C (I, inhibitor of AMPK) was added to the cells 30 minutes prior to palmitate treatment and was also present during the entire 1h-palmitate-incubation-period. Cells were exposed to either 10μM (A) or 400μM (B) of palmitate and then lysed for western blotting. Data presented as average ± SEM. *P<0.05 vs. control and Compound C. Data compiled from four independent experiments with duplicates in each experiment.

5.1.4 Effect of palmitate, AICAR, and Compound C on AMPK/ACC phosphorylation and $^{14}CO_2$ production from [1-^{14}C]- palmitate

AICAR and palmitate (10μM and 400μM) induced AMPK phosphorylation and this was again prevented by Compound C. Although ACC phosphorylation was also induced by AICAR and Palmitate, Compound C only prevented its phosphorylation at the lower concentration (10μM) of palmitate (Figure 17A). We also determined the

phosphorylation state of AMPK and ACC after the cells had been exposed to a combination of AICAR and palmitate. The phosphorylation induced by AICAR and palmitate in this experiment was similar to what was observed for either AICAR or palmitate alone, with no additive effect on AMPK and ACC phosphorylation (Figure 17A). ACC phosphorylation serves as a good indicator of AMPK activation while LCFA oxidation provides an indication of ACC activity. Since AMPK and ACC phosphorylation play an important role regulating the rate of fatty acid oxidation in skeletal muscle, we investigated the rates of $^{14}CO_2$ production from [1-^{14}C]palmitate in L6 myotubes. As palmitate concentration in the incubation medium was increased from 1 to 800μM, the rate of oxidation of this fatty acid also rose significantly from 12.4 pmols/h (basal, Figure 17B inset) to 676.86 nmols/h (800μM, Figure 17B). The basal condition had only labeled palmitate (0.2 μCi/ml of [1-^{14}C]palmitic acid) in the incubation medium. Even though this does not reflect physiological circulating non-esterified fatty acids levels, it was technically the correct control to give us an idea of the magnitude of the increase in fatty acid oxidation by skeletal muscle cells in the presence of very low to high concentrations of palmitate. The most accentuated increase in oxidation took place in the presence of palmitate concentrations ranging from 1 to 200μM (from 3.9 nmols/h to 487.38 nmols/h). However, as the concentration of palmitate was increased from 400μM to 800μM, the oxidation rate of this fatty acid still rose but at a much lower rate (from 559.98 nmols/h to 676.86 nmols/h, respectively) (Figure 17B). Here, we also tested the effect of AICAR-induced AMPK activation on palmitate oxidation. As expected, in the presence of AICAR (2mM) we observed a

significant increase in $^{14}CO_2$ production either under basal (~1.4 fold, Figure 17B inset) or in the presence of up to 100μM of palmitate (1.7-fold, 2-fold, 1.6-fold, and 1.7-fold versus palmitate alone for 1, 10, 50, and 100μM of palmitate, respectively) (Figure 17B). However, as palmitate concentration was increased from 200μM to 800μM the AICAR-induced effect on $^{14}CO_2$ production from [1-^{14}C]palmitic acid was significantly attenuated (1.07-fold, 1.09-fold, 1.09-fold, and 1.03-fold for 200, 400, 600, and 800μM of palmitate, respectively) when compared to palmitate alone (Figure 17B). Interestingly, the addition of Compound C significantly blocked the oxidative effect of palmitate alone and of AICAR in the presence of palmitate concentrations ranging from 1 to 100μM. However, in the presence of higher palmitate concentrations (200, 400, 600, and 800μM) Compound C was not effective in blocking the oxidative responses induced by palmitate alone or in combination with AICAR (Figure 17B). These results are compatible with the effects of palmitate on AMPK and ACC phosphorylation previously reported (Figures 15 and 16). This suggests that under elevated concentrations of fatty acids (above 200μM) an AMPK-independent pathway was responsible for inducing fatty acid oxidation in skeletal muscle cells.

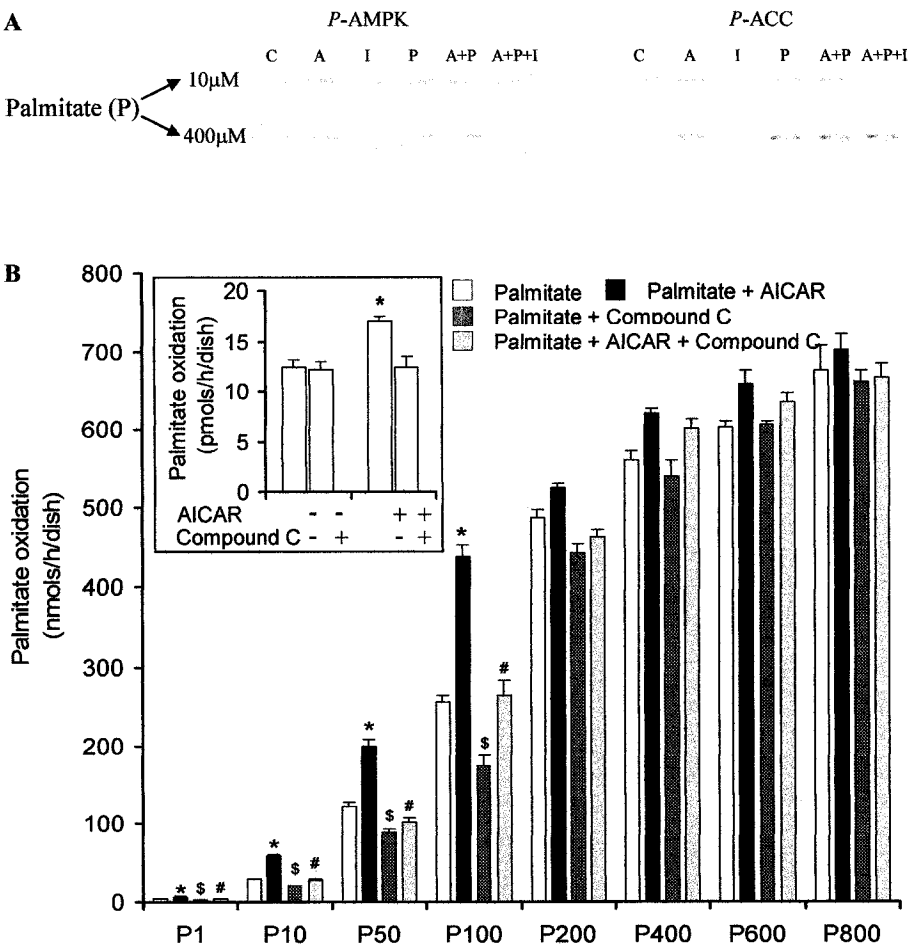

Figure 17. A: Representative blots of the effects of Palmitate (P, 10μM and 400μM), AICAR (A), Compound C (I), AICAR plus Palmitate (A+P), and AICAR plus Palmitate plus Compound C (A+P+I) on AMPK and ACC phosphorylation. **B**: Effect of various palmitate concentrations (ranging from 1 to 800μM, P1 to P800), palmitate plus AICAR (2mM), palmitate plus Compound C (40μM), and Palmitate plus AICAR plus Compound C on $^{14}CO_2$ production from [1-^{14}C]palmitate (palmitate oxidation, nmols/dish/h) in L6 myotubes. The inset refers to the effect of Compound C on basal (in the absence of AICAR and compound C) and AICAR (2mM)-induced $^{14}CO_2$ production from [1-^{14}C]palmitate (palmitate oxidation, pmols/dish/h). Basal was determined in the presence of only radiolabeled palmitate (0.2μCi/ml). Data presented as average ± SEM. *P<0.05 vs. palmitate, palmitate + Compound C, and palmitate + AICAR + Compound C. $^{\$}$P<0.05 vs. palmitate and palmitate + AICAR. $^{\#}$P<0.05 vs. palmitate + AICAR. Data compiled from four independent experiments with triplicates in each experiment.

5.2 Study 2: Acute effects of troglitazone in muscle cells

5.2.1 AMPK and ACC phosphorylation

Troglitazone significantly increased AMPK phosphorylation by ~2.5-fold (Figure 18A) and insulin did not affect the phosphorylation state of this enzyme. However, the troglitazone-induced AMPK phosphorylation effect was completely suppressed by insulin (Figure 18A). Troglitazone also significantly increased (~3.5-fold) phosphorylation of ACC (Figure 18B), indicating that the activity of AMPK was indeed elevated by this drug. Treatment of myotubes with insulin suppressed troglitazone-induced ACC phosphorylation (Figure 18B), which is in line with the inhibitory effect of this hormone on AMPK phosphorylation/activation.

5.2.2 Palmitate Oxidation and CPT-1 activity

Treatment of myotubes with troglitazone led to an ~30% increase in palmitate oxidation while insulin elicited an ~40% reduction in this variable (Figure 19A). Interestingly, even though troglitazone alone increased palmitate oxidation, exposure of myotubes to a combination of troglitazone and insulin did not fully reverse the suppressive effects of insulin on fatty acid oxidation. In fact, the insulin plus troglitazone group elicited rates of palmitate oxidation that were ~29% lower than control but only ~14% higher than insulin alone conditions (Figure 19A). As expected, etomoxir almost completely suppressed CPT-1 activity, which clearly demonstrates that our *in vitro* system was responsive to metabolic stimuli (Figure 19B). The activity of CPT-1 in permeabilized myotubes was not affected by insulin treatment; however, troglitazone significantly increased (~60%) the activity of this enzyme (Figure 19B). Interestingly,

CPT-1 activity was also elevated (~55%) in cells exposed to both insulin and troglitazone (Figure 19B).

5.2.3 Effect of compound C on troglitazone-stimulated fatty acid oxidation

Western blot analysis of AMPK and ACC revealed that AMPK phosphorylation/activation was effectively inhibited by compound C. As previously described, treatment of cells with troglitazone resulted in a ~2- and 2.3-fold increase in AMPK and ACC phosphorylation, respectively (Figure 18C and D). Compound C did not affect the basal phosphorylation state of either enzyme, but completely prevented the troglitazone-induced increase in AMPK and ACC phosphorylation (Figure 18C and D). Troglitazone increased basal fatty acid oxidation by approximately 30% relative to control (Figure 19C). Interestingly, treatment with 10 and 20μM of compound C led to ~15 and 30% reductions in basal palmitate oxidation relative to control, respectively (Figure 19C). Strikingly, both concentrations (10 and 20μM) of compound C completely prevented troglitazone-induced increases in fatty acid oxidation by skeletal muscle cells. In fact, the rates of troglitazone-induced palmitate oxidation in cells exposed to either 10 or 20μM of compound C were ~20% and ~40% lower than control values, respectively (Figure 19C).

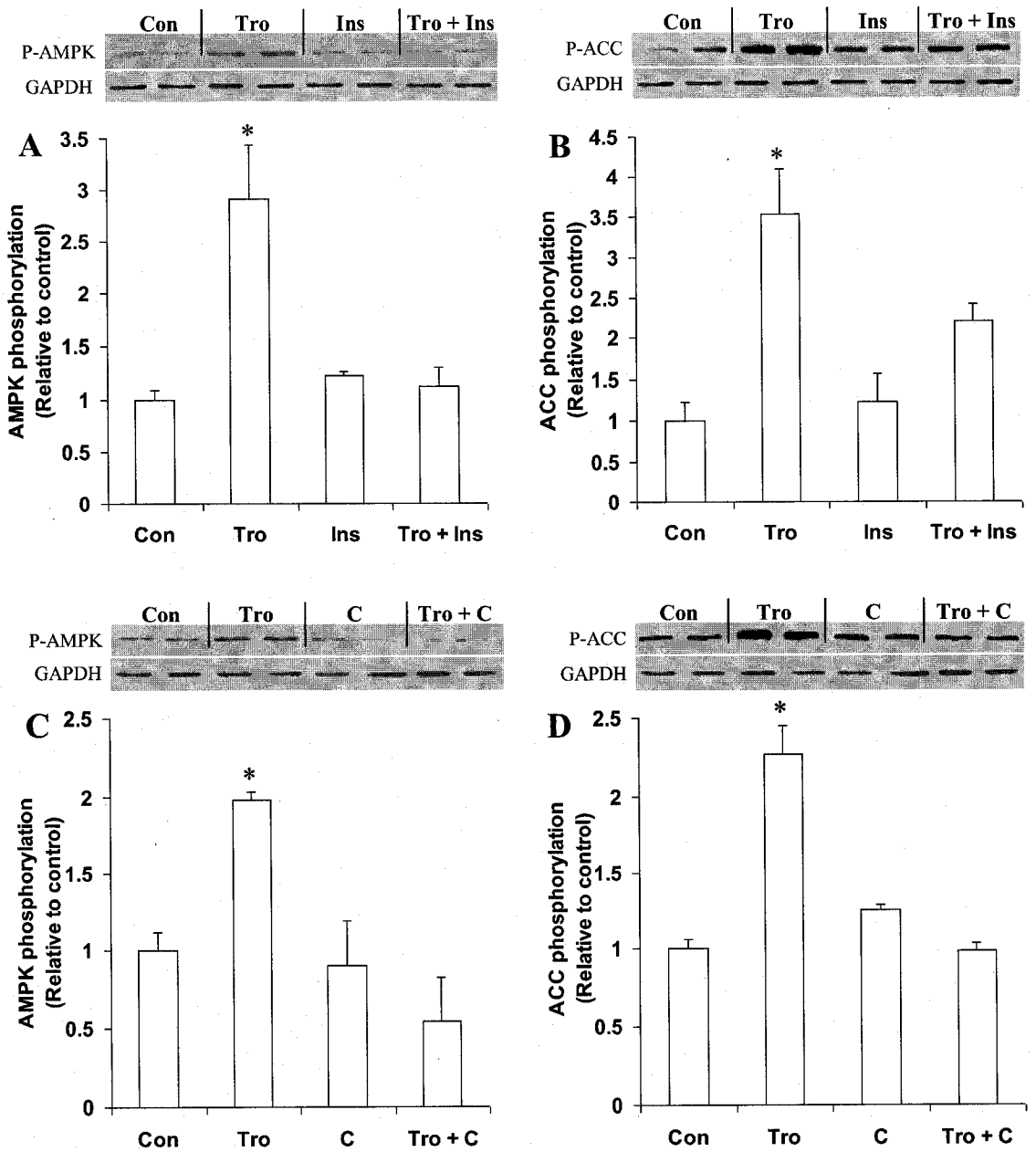

Figure 18. Effects of troglitazone (Tro, 50μM), insulin (Ins, 100nM), troglitazone plus insulin (Tro + Ins), compound C (C, 10 and 20μM), and troglitazone plus compound C (Tro + C) on AMPK (Panels A and C) and ACC (Panels B and D) phosphorylation in L6 myotubes. Control (Con) cells were not exposed to insulin, troglitazone, or compound C. Densitometric analysis and respective representative blots are shown for each experimental condition for AMPK (Panels A and C) and ACC (Panels B and D). GAPDH was used as loading control. Data were compiled from three independent experiments with duplicates in each condition and presented as means ± SEM. *P<0.05 *vs.* all groups.

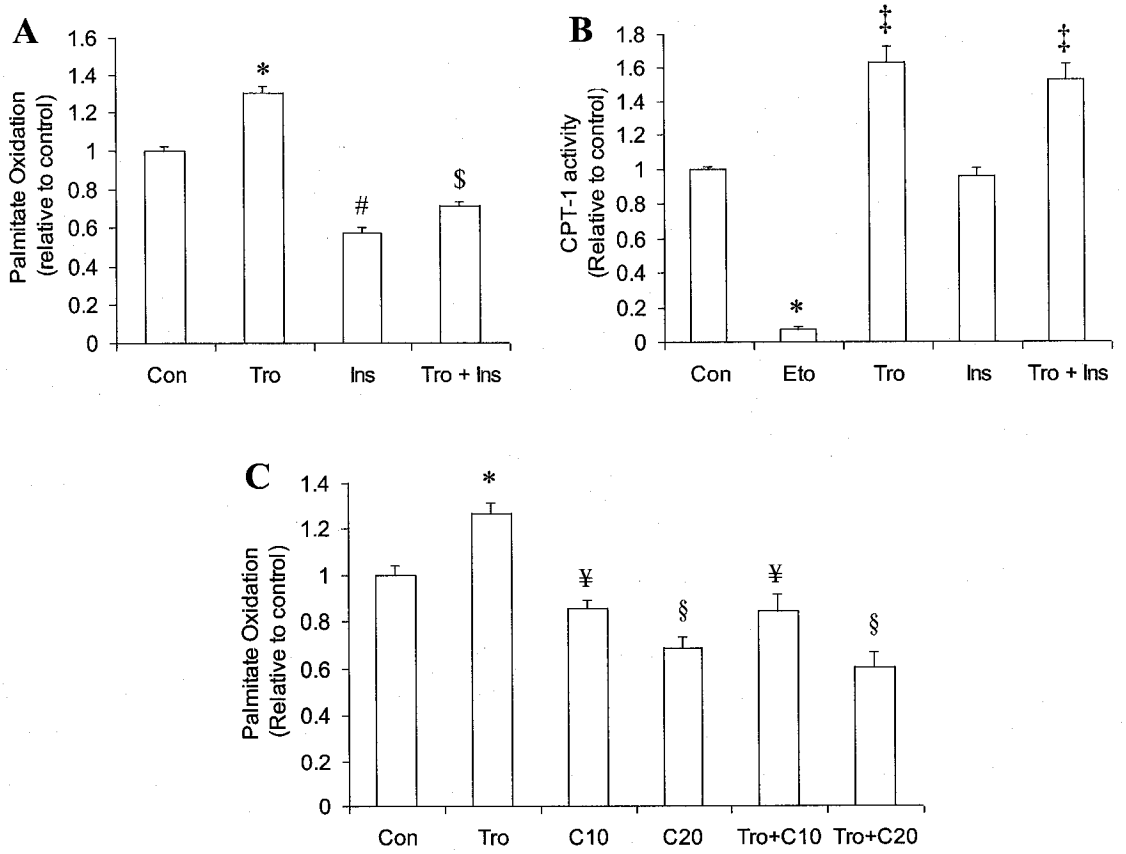

Figure 19. Effects of troglitazone (Tro, 50μM), insulin (Ins, 100nM), etomoxir (Eto, 2.5μM), troglitazone plus insulin (Tro + Ins), compound C (C, 10 and 20μM) and troglitazone plus compound C (Tro + C) on palmitate oxidation (Panels A and C) and CPT-1 activity (Panel B) in L6 myotubes. Control (Con) cells were not exposed to Ins, Tro, Eto or compound C. Palmitate oxidation was measure by the rate of production of $^{14}CO_2$ from [1-^{14}C]palmitic acid during 1h of incubation. CPT-1 activity was assessed by the conversion L-[^{3}H]carnitine to palmitoyl-[^{3}H]carnitine during a 5min assay following 1h exposure to the respective conditions mentioned above. Data were compiled from three independent experiments with triplicates in each condition and presented as means ± SEM. *P<0.05 *vs.* all groups; $^{\#}$P<0.05 *vs.* Con, Tro, and Tro + Ins; $^{\$}$P<0.05 *vs.* Con, Tro, and Ins; ‡P<0.05 *vs.* Con, Eto, and Ins; $^{¥}$ P<0.05 *vs.* Con, Tro, C20, and Tro + C20; § P<0.05 *vs.* Con, Tro, C10, and Tro + C10.

5.2.4 Palmitate Uptake

Insulin elicited a ~20% increase in palmitate uptake compared to control (Figure 20A). The incubation of myotubes with low concentrations (5μM) of troglitazone did not affect basal palmitate uptake; however, it completely abolished the insulin-stimulated increase in this variable. Interestingly, a higher concentration (50μM) of troglitazone reduced both basal and insulin-stimulated palmitate uptake by ~23% compared to control conditions (Figure 20A). Further increases in troglitazone concentration from 50 to 100μM did not affect basal palmitate uptake but the insulin-stimulated uptake was reduced by an additional ~13% (Figure 20A).

5.2.5 Effect of troglitazone on basal and insulin-stimulated glucose uptake, glycogen synthesis, lactate production, glucose oxidation, and glucose incorporation into lipids

As expected, insulin elicited an ~1.7-fold increase in glucose uptake compared to control, while treatment of L6 myotubes with troglitazone resulted in ~2-fold increase in this variable (Figure 20B). Interestingly, the combination of troglitazone and insulin elicited an additive effect leading to a ~2.8-fold increase in glucose uptake (Figure 20B). Treatment of muscle cells with compound C did not affect basal or insulin-stimulated rates of glucose uptake; however it reduced troglitazone-induced glucose uptake by ~30% compared to control (Figure 20B). Compound C also completely prevented the additive effect of combining troglitazone and insulin on glucose uptake. In fact, myotubes receiving insulin, troglitazone, and compound C elicited glucose uptake values that were also ~30% lower than control (Figure 20B). Further analysis of several pathways of

glucose metabolism revealed that, as expected, insulin significantly increased glucose oxidation (~1.5-fold), glycogen synthesis (~2-fold), incorporation of glucose into lipids (~1.4-fold), and lactate production (~2.5-fold) as compared to control (Figure 21A-D). Interestingly, troglitazone reduced basal and insulin-stimulated rates of glucose oxidation (Figure 21A), glycogen synthesis (Figure 21B), and incorporation of glucose into lipids (Figure 21C) to values corresponding to ~30%, ~30%, and ~60%, of the controls, respectively. The inhibitory effect of troglitazone on glycogen synthesis was observed either when insulin and troglitazone were added simultaneously (Figure 21B) or when cells were pre-treated with troglitazone for 1h and then subsequently exposed to insulin (data not shown). On the other hand, troglitazone significantly increased basal (~3.5-fold) and insulin-stimulated (~5.5-fold) rates of lactate production (Figure 21D). These data indicate that troglitazone promotes an insulin-sensitizing effect by increasing glucose uptake and shifting glucose metabolism towards lactate production in skeletal muscle cells.

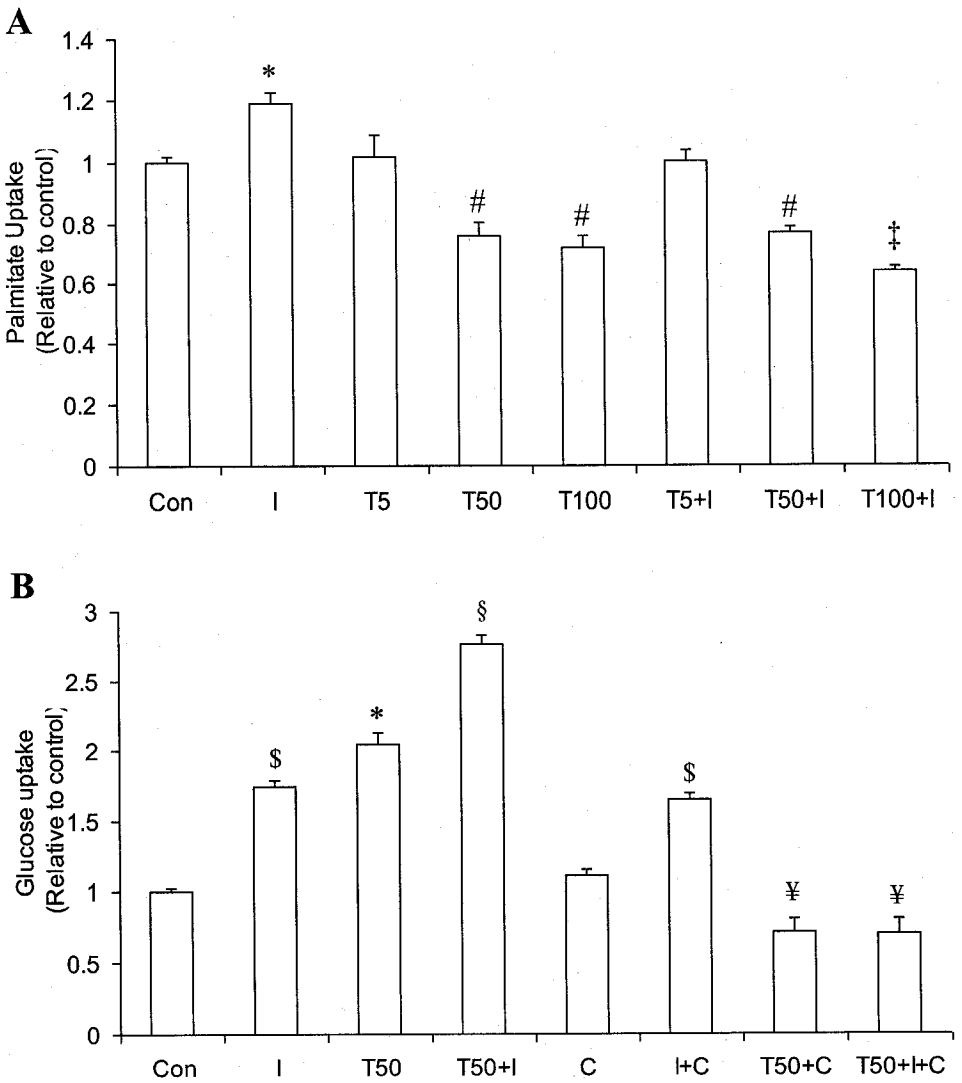

Figure 20. Effects of insulin (I, 100nM), troglitazone (T, 5, 50 and 100μM), troglitazone plus insulin (T5 + I, T50 + I, and T100 + I), compound C (C, 20μM), insulin plus compound C (I + C), troglitazone plus compound C (T50 + C), and troglitazone plus insulin plus compound C (T50 + I + C) on palmitate (Panel A) and glucose (Panel B) uptake in L6 myotubes. Control (Con) cells were not exposed to troglitazone, insulin, or compound C. All cells were exposed to the treatment conditions for a period of 1h. The rates of palmitate and glucose uptake were assessed by the uptake of [1-^{14}C]palmitic acid and 2-deoxy-D-[^{3}H]glucose during a 4min and 5min assay, respectively, after the 1h incubation, as described in the methods. Data were compiled from three to four independent experiments with triplicates for each condition and presented as means ± SEM. *P<0.05 *vs.* all conditions; $^{\#}$P<0.05 *vs.* Con, I, T5, T5 + I, and T100 + I; ‡P<0.05 *vs.* Con, I, T5, T50, T100, T5 + I, and T50 + I; $^{\$}$P<0.05 *vs.* Con, T50, T50 + I, C, T50 + C, and T50 + I + C; §P<0.05 *vs.* all conditions; $^{¥}$P<0.05 *vs.* Con, I, T50, T50 + I, C, and I + C.

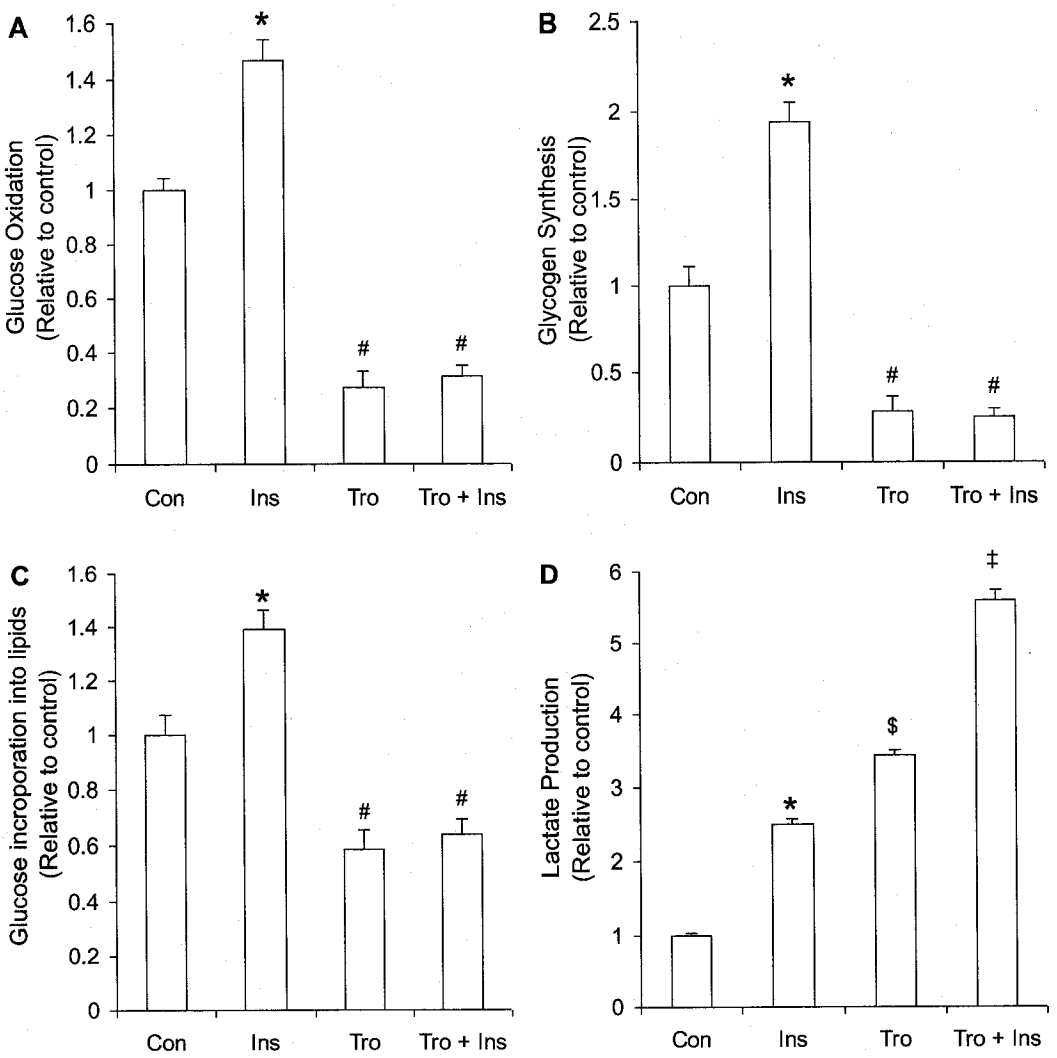

Figure 21. Effects of insulin (Ins, 100nM), troglitazone (Tro, 50μM), and troglitazone plus insulin (Tro + Ins) on glucose oxidation (Panel A), glycogen synthesis (Panel B), glucose incorporation into lipids (Panel C), and lactate production (Panel D) in L6 myotubes. Control (Con) cells were treated with neither Ins nor Tro. The rates of glucose oxidation was measured by the production of $^{14}CO_2$ from D-[U-^{14}C]glucose during 1h. The rates of glycogen synthesis, and glucose incorporation into lipids were measured by the incorporation of D-[U-^{14}C]glucose into glycogen and lipids for 1 and 2h, respectively. Data were compiled from three independent experiments with quadruplicates in each condition and presented as means ± SEM. *$P<0.05$ *vs.* all conditions; $^{\#}P<0.05$ *vs.* Con and Ins; $^{\$}P<0.05$ *vs.* all conditions; $^{\ddagger}P<0.05$ *vs.* all conditions.

5.2.6 Effect of troglitazone and compound C on [1-^{14}C]-pyruvate decarboxylation

Muscle cells exposed to troglitazone elicited a significant reduction (~97%) in the rate of $^{14}CO_2$ production form [1-^{14}C]-pyruvate in comparison to control (Figure 22). The addition of compound C alone to the incubation medium neither affected basal pyruvate oxidation nor reversed the potent suppressive effect of troglitazone on this variable.

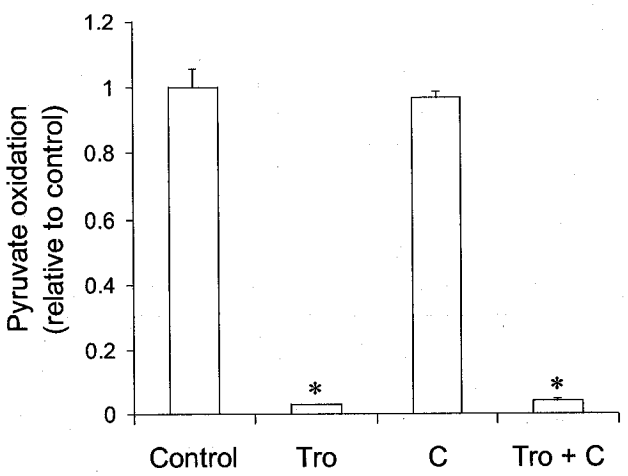

Figure 22. Effects of troglitazone (Tro), compound C (C), and troglitazone plus compound C (Tro + C) on pyruvate decarboxylation in L6 myotubes. The rate of pyruvate decarboxylation was measured by the production of $^{14}CO_2$ from [1-^{14}C]-pyruvic acid during 1h. Data were compiled from three independent experiments with quadruplicates in each condition and presented as means ± SEM. * $P<0.05$ vs. control and C.

5.2.7 Effect of troglitazone on basal and insulin-stimulated phosphorylation of $Akt_{Thr-308}$, $Akt_{Ser-473}$, and GSK-3α/β

Cells exposed to insulin for 5min elicited a marked (~60-fold) increase in Akt_{Thr308} phosphorylation (Figure 23) compared to control. Troglitazone on its own led to ~4-fold increase in Akt_{Thr308} phosphorylation and when combined with insulin produced an increase in this variable that was ~50% higher than the effect of insulin alone. Also, insulin increased Akt_{Ser473} phosphorylation by approximately 7-fold, while troglitazone increased it by ~2.7-fold relative to control. Again, the combination of troglitazone and insulin elicited an increase in Akt_{Ser473} phosphorylation that was ~50% higher than the effect of these agents alone (Figure 23). Under control and troglitazone treated conditions GSK-3α/β phosphorylation was undetectable; however, exposure of muscle cells to insulin for 5, 10, and 20min resulted in ~6-, ~21-, and ~20-fold increases in GSK-3α and 1.5-, 13-, 14-fold increases in GSK-3β phosphorylation, respectively. Interestingly, exposure of muscle cells to both troglitazone and insulin led to an increase in phosphorylation of GSK-3α/β that was higher than insulin alone (Figure 23). In fact, after 5 and 10min of insulin exposure, troglitazone-treated cells elicited more than 2-fold increase in GSK-3α/β phosphorylation when compared to insulin alone. The effect of troglitazone on insulin-stimulated GSK-3α/β phosphorylation was even more pronounced (~4-fold) after 20min of insulin exposure (Figure 23). All together, our data indicate that troglitazone potentiates the effects of insulin on major intracellular signalling pathways involved in glucose uptake and metabolism in L6 myotubes.

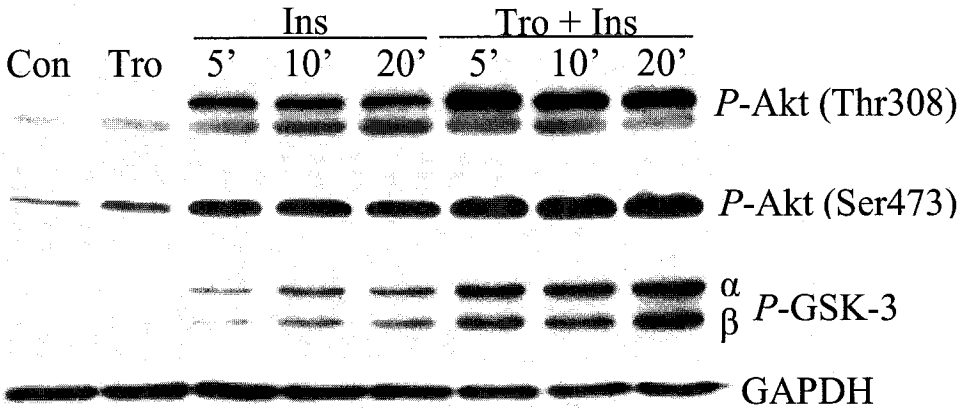

Figure 23. Time course effects (5, 10, and 20min) of insulin (Ins, 100nM), troglitazone (Tro, 50μM), and troglitazone plus insulin (Tro + Ins) on the phosphorylation of Akt-Thr308 (*P*-Akt308), Akt-Ser473 (*P*-Akt473), GSK-3α (*P*-GSK-3α), and GSK-3β (*P*-GSK-3β) in L6 myotubes. Cells were exposed to insulin for the last 5, 10 and 20min of a 1h incubation period. Troglitazone was added to the medium at the beginning of the 1h incubation period and remained in the medium after insulin was added. Control (Con) cells were exposed to neither insulin nor troglitazone.

5.3 Study 3: Effects of AICAR-induced AMPK activation on glycogen synthesis in isolated skeletal muscle

5.3.1 Effect of AICAR on glycogen synthesis in soleus and epitrochlearis muscles

As expected, in soleus muscle, insulin elicited a 6.4-fold increase in glycogen synthesis compared with the control condition (Figure 24A). Interestingly, while treatment with AICAR alone did not alter the basal rate of glycogen synthesis, it resulted in a ~60% reduction of glycogen synthesis in the presence of insulin. Treatment of epitrochlearis muscles with insulin resulted in a 1.8-fold increase in glycogen synthesis relative to control (Figure 24B). AICAR treatment did not affect either basal or insulin-stimulated conditions in epitrochlearis muscles.

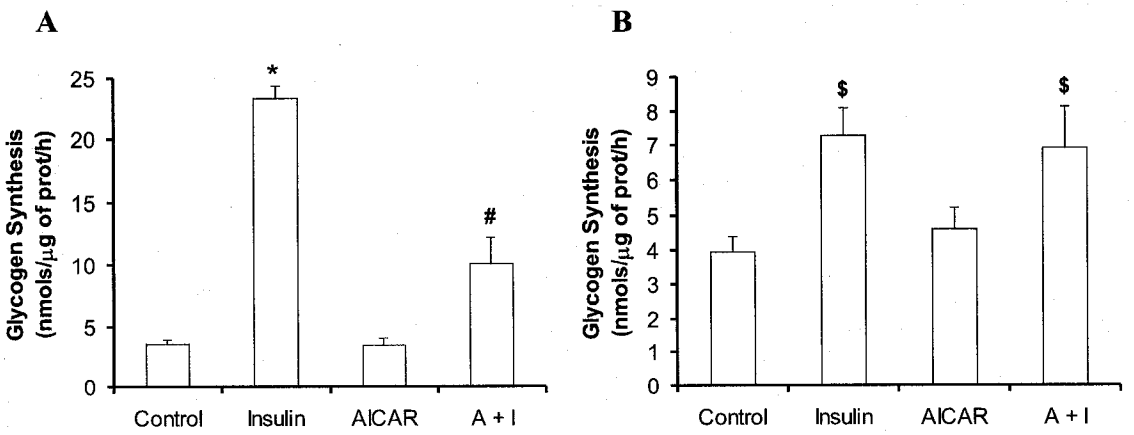

Figure 24. Effect of insulin (100nM), AICAR (2mM) and AICAR plus insulin (A + I) on glycogen synthesis in isolated soleus (panel A) and epitrochlearis (panel B) muscles. Glycogen synthesis was estimated from the incorporation of D-[U-^{14}C]glucose into glycogen for 1h in the presence of the various conditions as indicated. Control muscles were exposed neither to AICAR nor to insulin. Muscles in the A + I condition were pre-incubated with AICAR for 30min before insulin and D-[U-^{14}C]glucose were added to the medium. Data were compiled from three independent experiments with triplicates in each experiment and presented as means ± SEM. *P<0.05 versus control, AICAR, and A + I. $^{\#}P$<0.05 versus Control, insulin, and AICAR. $^{\$}P$<0.05 versus Control and AICAR.

5.3.2 Effect of AICAR on glycogen content in soleus and epitrochlearis muscles

To further characterize the effects of AICAR treatment on glycogen metabolism, glycogen content was assessed. In soleus, 1h treatment with insulin resulted in a significant increase (~27%) in glycogen content relative to control (Figure 25A). Interestingly, AICAR completely reversed the increase in glycogen content induced by insulin in soleus muscles. Incubation of epitrochlearis muscles (Figure 25B) with insulin, AICAR and AICAR plus insulin, did not have any effect on glycogen content.

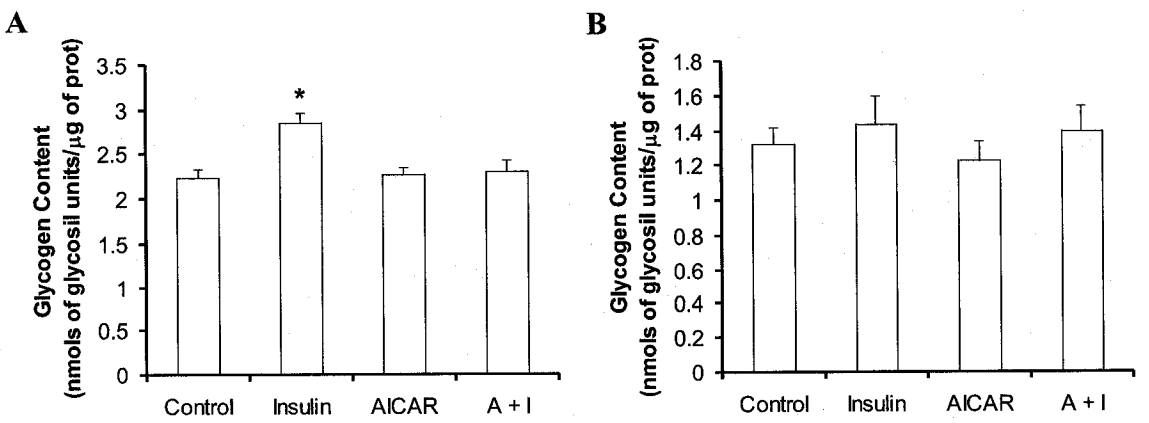

Figure 25. Effect of insulin (100nM), AICAR (2mM) and AICAR plus insulin (A + I) on glycogen content in isolated soleus (panel A) and epitrochlearis (panel B) muscles. Control muscles were exposed neither to AICAR nor to insulin. Muscles in the A + I condition were pre-incubated with AICAR for 30min before insulin was added to the medium. Data were compiled from three independent experiments with triplicates in each experiment and presented as means ± SEM. *$P<0.05$ versus Control, AICAR, and A + I.

5.3.3 Effect of AICAR on lactate production in soleus and epitrochlearis muscles

To determine whether the effects of AICAR on glycogen synthesis would also cause other metabolic changes in soleus and epitrochlearis muscles, lactate production was assessed. In soleus (Figure 26A), incubation with insulin resulted in a significant ~1.6-fold increase in lactate production relative to control. The effect of AICAR on the basal condition showed a trend towards increased lactate production, but did not reach statistical significance (Figure 26A). However, incubation of the soleus with AICAR and insulin caused a 2-fold increase in lactate production relative to control, which was ~21% higher than that of insulin alone (Figure 26A). The epitrochlearis muscles (Figure 26B) also showed a similar increase in lactate production (~1.7-fold) when treated with insulin. However, AICAR did not affect insulin-stimulated lactate production in these muscles (Figure 26B).

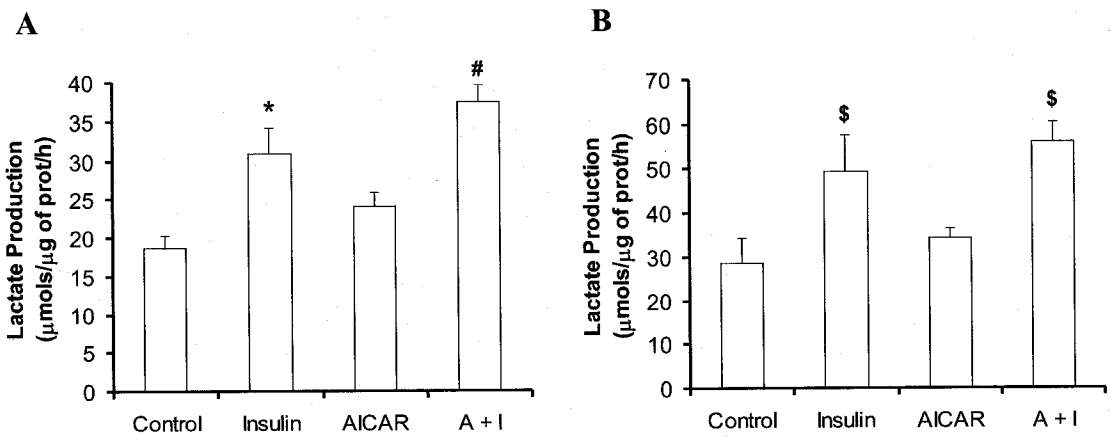

Figure 26. Effect of insulin (100nM), AICAR (2mM) and AICAR plus insulin (A + I) on lactate production in isolated soleus (panel A) and epitrochlearis (panel B) muscles. Control muscles were exposed neither to AICAR nor to insulin. Muscles in the A + I condition were pre-incubated with AICAR for 30min before insulin and D-[U-^{14}C]glucose were added to the medium. Data were compiled from three independent

experiments with triplicates in each experiment and presented as means ± SEM. *P<0.05 versus Control, AICAR, and A + I. #P<0.05 versus Control, insulin, and AICAR. $$P$<0.05 versus Control and AICAR.

5.3.4 Effect of AICAR on glucose uptake in soleus and epitrochlearis muscles

In soleus muscles, treatment with insulin resulted in a ~3.3-fold increase in glucose uptake relative to control (Figure 27A). The addition of AICAR to the medium did not affect either the basal or the insulin-stimulated rate of glucose transport in the soleus (Figure 27A). As expected, epitrochlearis muscles elicited an increase in glucose uptake (~1.7-fold) in the presence of insulin. AICAR treatment also caused a significant increase (~1.4-fold) in glucose uptake in epitrochlearis muscles (Figure 27B). The addition of AICAR to the insulin-stimulated epitrochlearis muscles resulted in ~2.0-fold increase in glucose uptake. However, this increase was not statistically different from the insulin or AICAR only conditions.

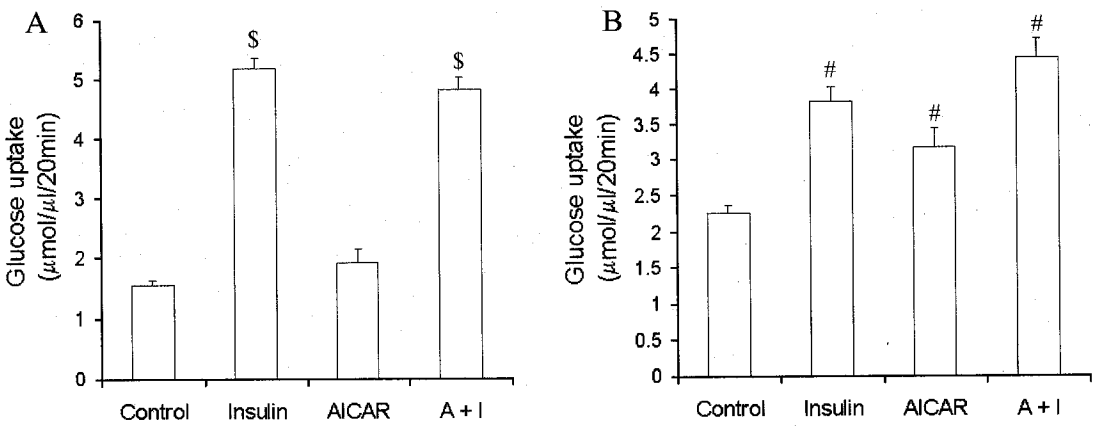

Figure 27. Effect of insulin (100nM), AICAR (2mM), and AICAR plus insulin on 2-deoxy-D-glucose uptake in isolated soleus (panel A) and epitrochlearis (panel B) muscles. Control muscles were exposed neither to AICAR or to insulin. Data were compiled from three independent experiments with triplicates in each experiment and presented as means ± SEM. $P<0.05 vs. control and AICAR. #P<0.05 vs. Control.

5.3.5 Effect of AICAR on the phosphorylation of AMPK, ACC, Akt, GSK-3α/β, and GS in soleus muscles

The effectiveness of AICAR treatment to increased AMPK phosphorylation/ activation was determined by Western blot. As expected, AICAR treatment led to a marked increase in AMPK and ACC phosphorylation, respectively (Figure 28A). In addition, we also examined the differential expression of the AMPKα1 and AMPKα2 catalytic subunits in both, soleus and epitrochlearis muscles. The AMPKα1 content was markedly higher (~1.6-fold) in epitrochlearis than soleus muscles while AMPKα2 appeared similar in both muscles (Figure 28B). In order to determine if the effects of AICAR-induced AMPK activation affected major intracellular pathways of insulin signalling, we examined the phosphorylation states of Akt Thr308, Akt Ser473, GSK-3α/β and GS. As anticipated, exposure of the soleus muscle to insulin for 15min resulted in a ~9-fold increase in Akt Thr308 phosphorylation compared to control. Even though this effect decreased as exposure time to insulin increased, Akt Thr308 phosphorylation remained markedly elevated after 45min of insulin exposure compared to control (Figure 28C). AICAR on its own did not cause any changes in the phosphorylation state of Akt Thr308. However, pre-treatment of soleus muscles with AICAR resulted in ~33% and 55% reductions in Akt Thr308 phosphorylation after 15 and 30min of insulin exposure, respectively (Figure 28C). Insulin also increased Akt Ser473 phosphorylation (~1.6-fold) but this was unaffected by AICAR. To further investigate the effects of AICAR on enzymes involved in glycogen metabolism, we examined the phosphorylation state of GSK-3α/β (Figure 28C). This enzyme is a downstream target of Akt and is active when

in its de-phosphorylated state. Under control conditions, GSK-3α/β phosphorylation was virtually undetectable. A pronounced increase in the phosphorylation state of GSK-3α was observed in the presence of insulin (Figure 28C). Interestingly, AICAR markedly reduced the 15, 30, and 45min insulin-stimulated phosphorylation of GSK-3α. The phosphorylation of GSK-3β under insulin stimulation was not as high as GSK-3α, however, the effect of AICAR on the insulin-stimulated condition followed a similar pattern to that of GSK-3α (Figure 28C). These data indicate that AICAR prevented the insulin-induced suppression of GSK-3α/β activity in soleus muscles.

Analysis of GS phosphorylation revealed that this enzyme was highly phosphorylated under basal conditions, and AICAR alone did not affect basal GS phosphorylation. As expected, treatment of soleus muscles with insulin elicited a time-dependent reduction in GS phosphorylation, reaching its lowest after 45min exposure to insulin (Figure 28C). Interestingly, AICAR treatment initially decreased the GS phosphorylation after 15 and 30min of insulin exposure. However, GS phosphorylation markedly increased after 45min of exposure to insulin (Figure 28C).

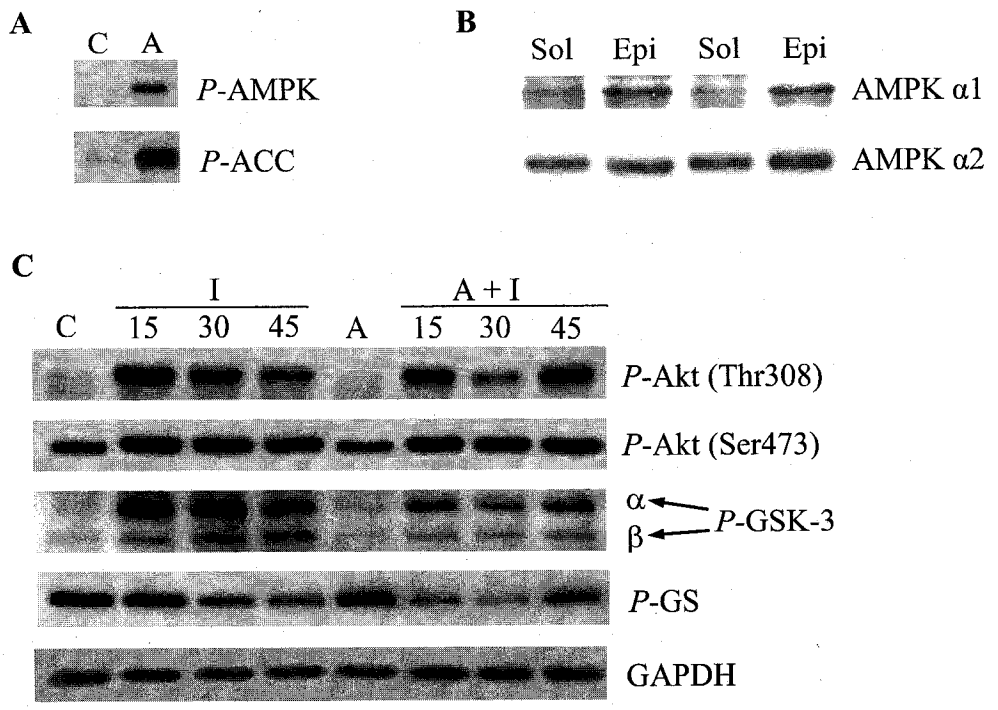

Figure 28. Panel A: Induction of AMPK and ACC phosphorylation by AICAR in soleus muscles. Panel B: Expression of AMPKα1 and AMPKα2 catalytic subunits in soleus (Sol) and epitrochlearis (Epi) muscles. Panel C: Time course effects (15, 30, and 45min) of insulin (I, 100nM), AICAR (A, 2mM), and AICAR plus insulin (A + I) on the phosphorylation of AktThr 308 (*P*-Akt308), AktSer473 (*P*-Akt473), glycogen synthase kinase-3α (*P*-GSK-3α), glycogen synthase kinase-3β (*P*-GSK-3β), and glycogen synthase (*P*-GS) in isolated soleus muscles. Muscles were exposed to insulin for 15, 30, and 45 min. AICAR was added to the incubation medium 30min prior to adding insulin and remained in the medium thereafter. Controls (C) represent soleus muscles not subjected to any treatment.

5.4 Study 4: Effects of 2-week AICAR injections on whole-body energy homeostasis

5.4.1 Body Weight and Food intake

To accurately characterize the effects of chronic AICAR administration, body weight and food intake were measured on a daily basis. Saline and AICAR injected animals elicited a similar increase in body weight (Figure 29A). AICAR did not alter food intake significantly over the course of the study (Figure 29B).

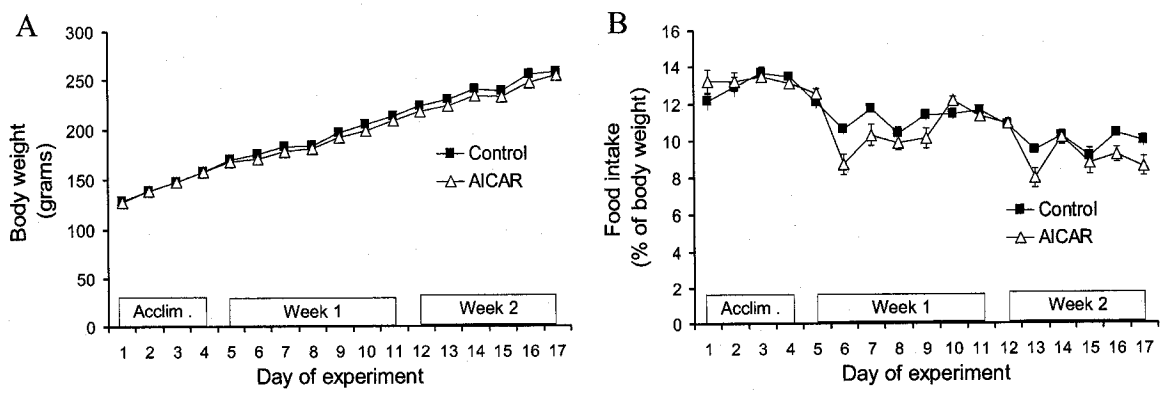

Figure 29. Body weight (A) and food intake (B) of rats injected with AICAR for 2 weeks. All animals were allowed to acclimatize (Acclim.) for 4 days prior to the start of the injection protocol. Food intake is presented as a percentage of the body weight for each respective day. Data are compiled from four independent experiments with an N=3 animals/group/experiment and presented as means ± SEM.

5.4.2 VO_2 and energy expenditure

After 3 days of injections in week 1 of the treatment protocol, VO_2 (Figure 30A) and EE (Figure 30B) were significantly lower (between ~6-15% for VO_2, and ~8-17% for EE) in AICAR versus Control animals. These differences were apparent at 1200 and 1300h for both variables and between 2000 and 0300h, and 1900 and 0400h for VO_2 and

energy expenditure, respectively. In week 2, no differences were found for either variable between the two groups of animals (Figures 30C and D).

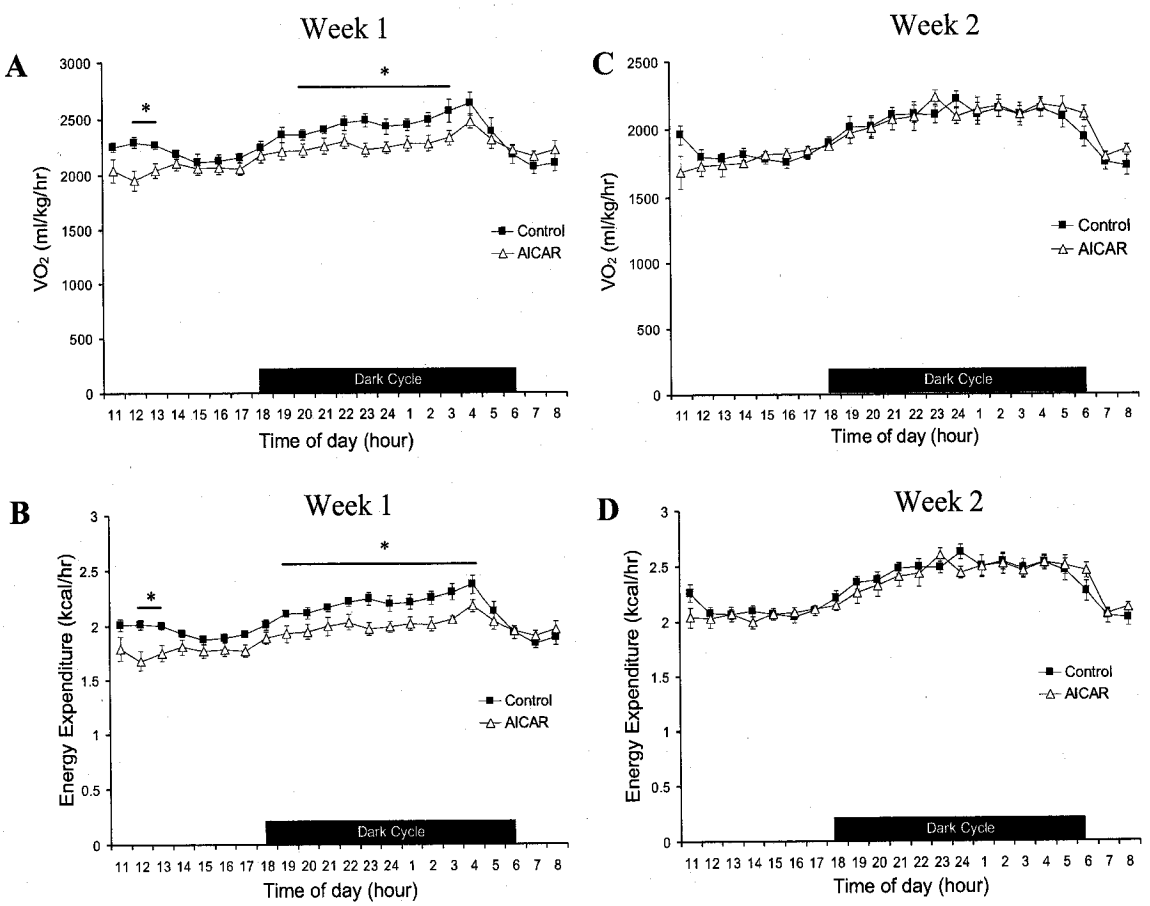

Figure 30. Effect of AICAR on VO_2 and energy expenditure in week 1 (A and B) and week 2 (C and D) of the treatment protocol, respectively. The dark cycle is depicted in each individual panel and took place from 1800h to 0600h. Data are compiled from three independent experiments with an N=3 animals/group/experiment and presented as means ± SEM. *, $P < 0.05$ vs. control.

5.4.3 Accumulated O_2 consumption

To confirm that the differences observed in VO_2 were in fact accompanied by a lower O_2 utilization in AICAR treated animals, the accumulated O_2 utilized was assessed. In week 1 AICAR treated animals were consistently utilizing less O_2 than Controls at every time point following AICAR injection (Figure 31A). This trend reached statistical significance at 1700h and resulted in an ~10% lower accumulated O_2 utilization at the end of the measurement period (Figures 31A and B). This difference disappeared in week 2 of the treatment protocol (Figure 31C and D).

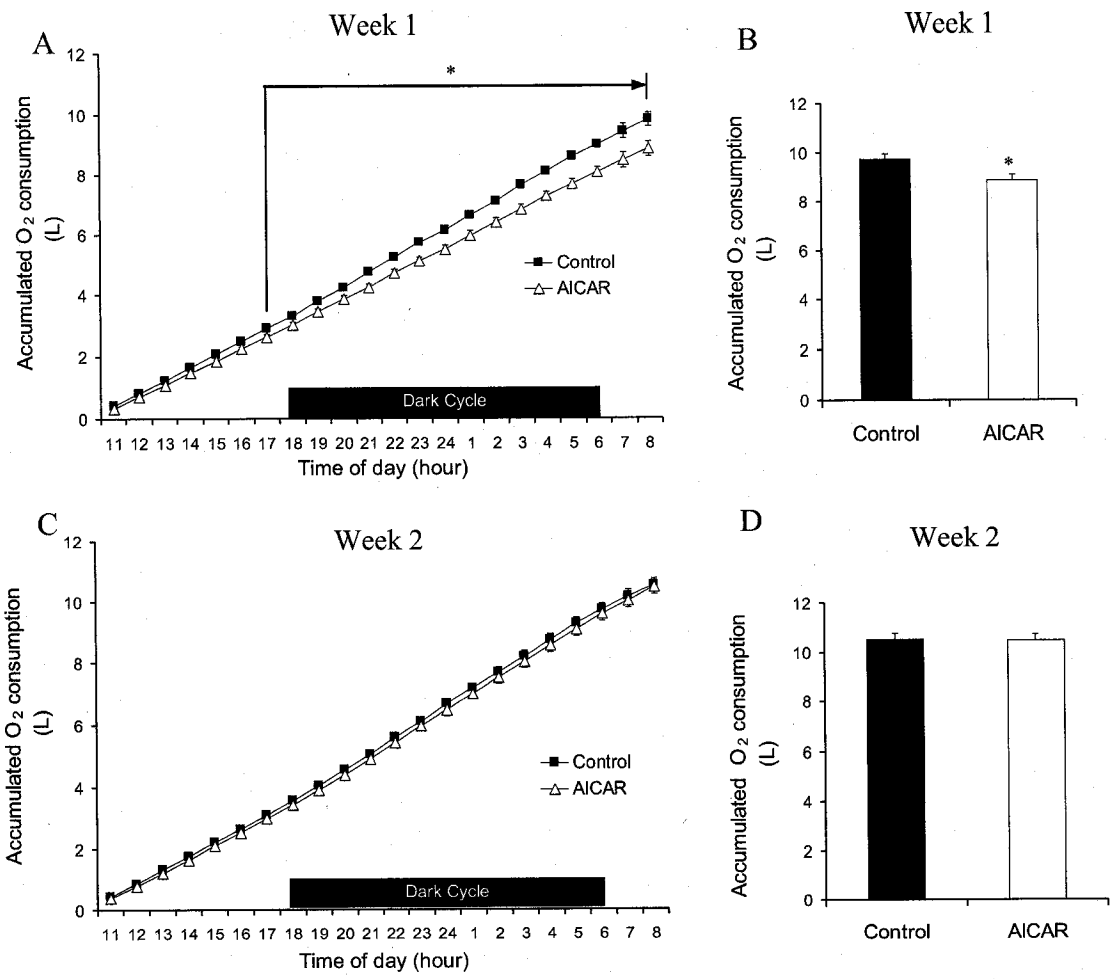

Figure 31. Effect of AICAR on accumulated O_2 utilized in week 1 (A and B) and week 2 (C and D). Panels B and D represent the total amount of O_2 utilized during the 22 hours following AICAR injection. The dark cycle is depicted in panels A and C and took place from 1800h to 0600h. Data are compiled from three independent experiments with an N=3 animals/group/experiment and presented as means ± SEM. *, $P < 0.05$ vs. control.

5.4.4 Respiratory Quotient

In order to determine if AICAR treatment would affect substrate utilization, respiratory quotient (RQ) was measured. In week 1 of the investigation this variable rapidly decreased in the AICAR group only two hours following drug administration, and remained significantly lower than Control animals for the following 8 hours (Figure 32A). The largest difference in RQ between the two groups was recorded at 1300h with values corresponding to ~0.77 vs. 0.87 for AICAR and Control animals, respectively. However, the reduction in RQ observed in week 1 of treatment did not take place in week 2, as both groups showed similar values (Figure 32B).

5.4.5 Relative contribution of carbohydrate and fatty acid oxidation towards total energy expenditure

The RQ in conjunction with EE were used to calculate the relative contribution of either carbohydrates or fatty acids towards total energy expenditure. In week 1, the rate of carbohydrate oxidation was significantly reduced in AICAR treated animals for 15 hours following drug administration (Figure 32C). On the other hand, fatty acid oxidation was increased between 1300 and 1900h in week 1 (Figure 32E). No differences were observed in week 2 of the investigation (Figure 32D and F).

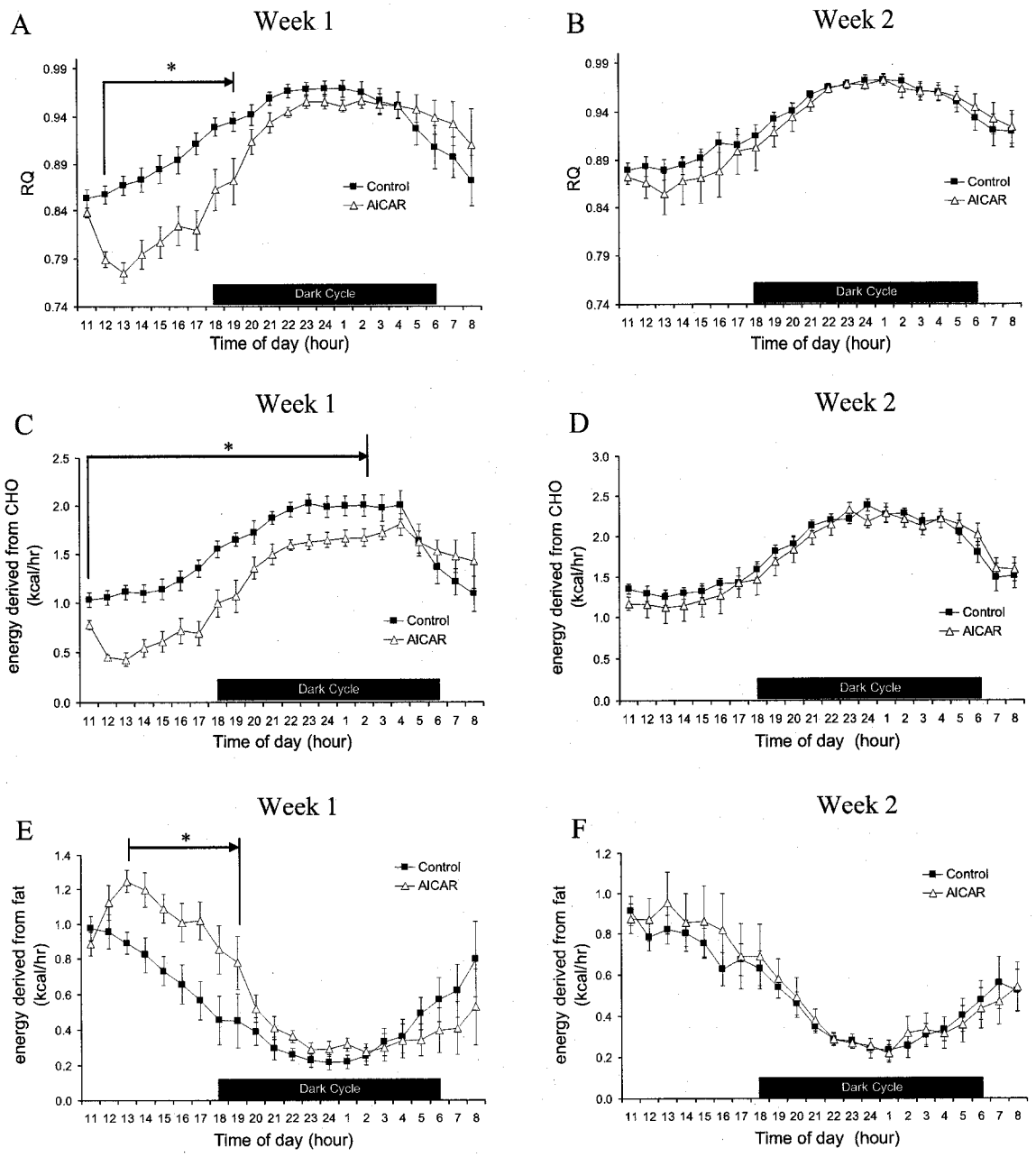

Figure 32. Respiratory Quotient and relative contribution of carbohydrates (CHO) and fatty acids to energy expenditure in week 1 (A, C, E) and week 2 (B, D, F) of the treatment protocol, respectively. The dark cycle is depicted in each individual panel and took place from 1800h to 0600h. Data are compiled from three independent experiments with an N=3 animals/group/experiment and presented as means ± SEM. *, $P < 0.05$ vs. control.

5.4.6 Fat pad masses

Fat-pad weights were measured once the animals were sacrificed at the end of the investigation. The epididymal (Epi), subcutaneous (SC), and retroperitoneal (Retro) fat pads were approximately 17, 18 and 40% smaller in AICAR treated animals versus control, respectively, after body weight was taken into account (Figure 33A). Brown adipose tissue (Bat) was not significantly different ($p = 0.09$).

5.4.7 Plasma Leptin concentrations

Since the amount of body fat is positively correlated with circulating leptin levels, and leptin is an important hormone involved in the regulation of food intake and energy expenditure, circulating leptin concentrations were measured in these animals at the beginning (days 5 and 12) and end (days 9 and 16) of each week of injection (Figure 33B). On day 5 of week 1, both control and AICAR animals had similar circulating leptin levels; however, at the end of week 1 (day 9), after five days of AICAR injection, animals in the AICAR group demonstrated an ~25% reduction in circulating leptin levels. This difference continued to increase in week 2 of the study to values that were ~27 and 31% lower in the AICAR versus control animals on days 12 and 16, respectively (Figure 33B). In addition, the leptin levels in control animals increased in week 2 of the investigation by ~17 and 24% (days 12 and 16, respectively) relative to the starting values in week 1.

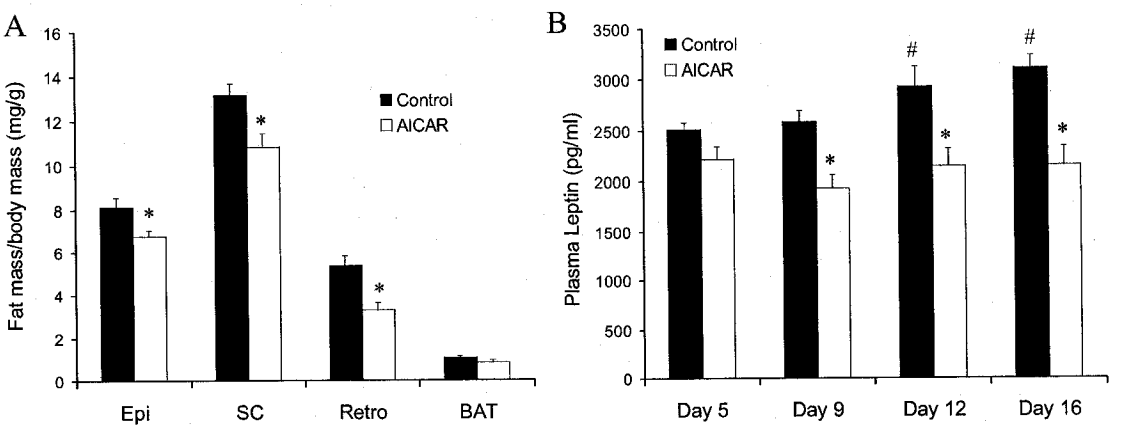

Figure 33. Effect of 2-week AICAR injections on fat pad mass (A), and weekly plasma leptin concentrations (B). Fat pad mass was measured at the end of the 2 week treatment protocol for epididymal (Epi), subcutaneous (SC), retroperitoneal (Retro), and brown adipose tissue (BAT) fat pads. Plasma leptin measurements were performed on samples collected at the beginning (Day 5 and 12) and end (Day 9 and 12) of each week of treatment. N=7-9 animals/group for fat pad and plasma leptin measurements. All data are presented as means ± SEM. *, $P < 0.05$ vs. control, #, $P < 0.05$ vs. control (Day 5).

5.4.8 Activity

Activity in the X + Z plane was measured to help explain possible differences in metabolic parameters as well as body composition alterations. There was no significant difference in the 22 hour activity pattern of either AICAR or Control animals in week 1 (Figure 34A). When the activity performed in each hour of measurement was summed to obtain a cumulative total, the two groups showed virtually identical total activity counts (Figure 34B). On the other hand, the week 2 data showed a consistently elevated level of activity in AICAR versus Control animals (Figure 34C). In fact, when activity for each hour was summed in week 2, AICAR animals were ~25% more active than Control animals (Figure 34D).

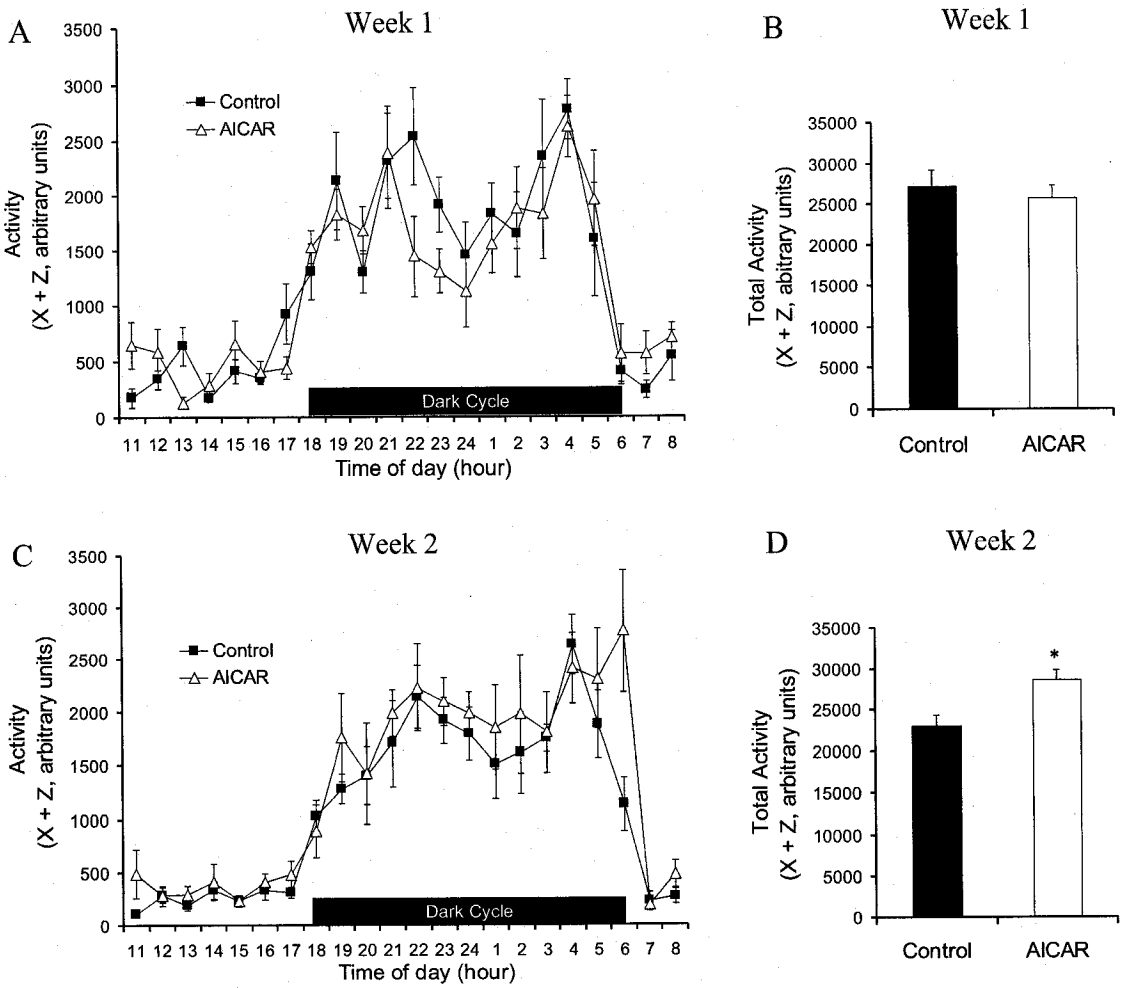

Figure 34. Effect of AICAR on activity (A and C, x + z axis) and total activity (B and D) in week 1 and 2 of the treatment protocol. The dark cycle is depicted in panels A and C and took place from 1800h to 0600h. The data are compiled from three independent experiments with an N=3 animals/group/experiment and presented as means ± SEM. *, $P < 0.05$ vs. control.

5.4.9 Plasma AICAR concentrations following i.p. AICAR injection

Due to the fact that AICAR elicited acute alterations in RQ, VO_2 and EE in week 1, it was important to determine the time-course of AICAR appearance in the circulation. AICAR plasma concentrations peaked 10 minutes following injection, reaching approximately 600mM (Figure 35A). Subsequently, the plasma concentrations dropped

to ~412 and 270mM at 15 and 30 minutes post injection, respectively. One hour following injection the plasma AICAR values continued to decrease to ~170mM. By the 2 hour time point only trace amounts of AICAR remained (~25mM), and by 4 hours it was not detectable (Figure 35A).

5.4.10 FFAs, glucose, and lactate concentrations following i.p. AICAR injection

The following time-course measurements of plasma FFAs, glucose, and lactate levels following a single AICAR injection were obtained to provide additional insight into the results collected in week 1 and week 2 using the CLAMS.

Plasma FFAs were significantly lower (~50%) in AICAR animals compared to saline injected controls 30 minutes after injection (~0.19 vs. 0.37 mM, respectively). At the 1h and 2h time points AICAR animals had similar values to saline injected controls. FFAs increased by ~100% at the 4 and 8h time points relative to control, to values corresponding to 1.08 and 1.04mM, respectively (Figure 35B).

Plasma glucose levels decreased rapidly in AICAR animals at the 15 minute time point by ~30% to values of 5.43mM (Figure 35C). Plasma glucose continued to decrease at the 30 minute time point by ~45% (Control = 7.5 vs. AICAR = 4.1mM). For the remaining time points (1, 2, 4, and 8h) glucose values remained significantly lower in AICAR animals compared to saline injected Controls (Figure 35C).

Both, AICAR and Control animals had similar basal lactate levels (~2mM). At the 15 minute time point, lactate concentrations in the AICAR animals increased by approximately 2.5-fold to 4.3mM (Figure 35D). At the 30 minute and 1 hour time points lactate levels continued to increase in AICAR animals by ~3- and 4.2-fold to values

corresponding to ~5 and 5.4mM, respectively. At the 2 h time point lactate levels began to decrease in AICAR animals, but still remained ~3.5-fold higher than Controls. No significant differences were detected at the 4 and 8h time points between the two groups (Figure 35D).

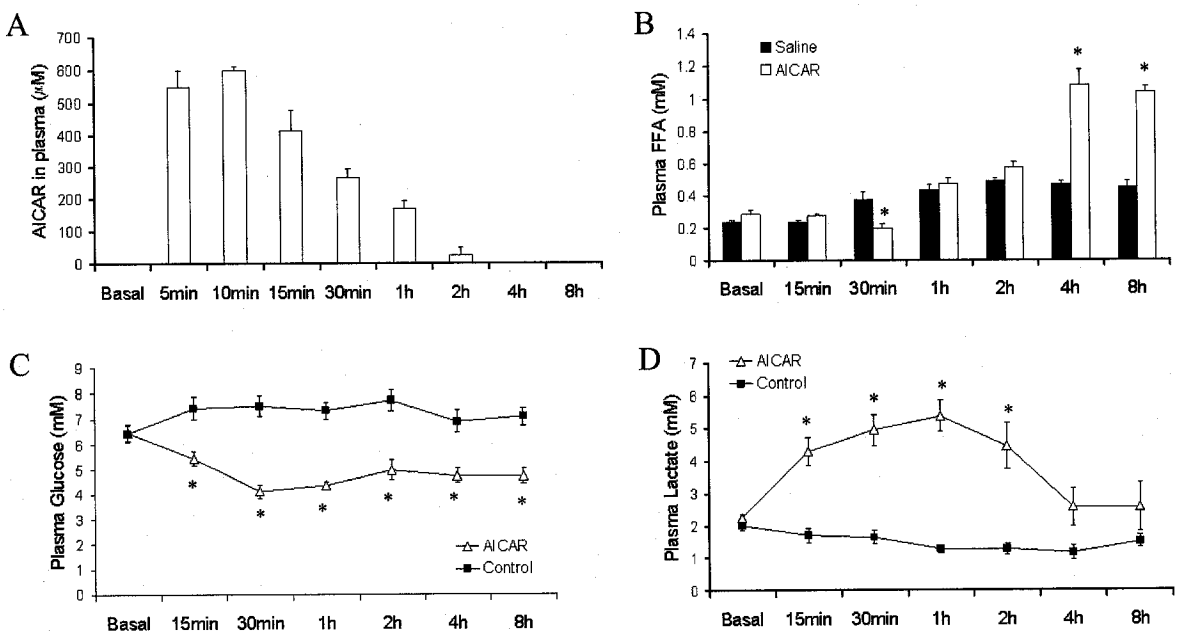

Figure 35. Effects of intraperitoneal AICAR injection (0.7g/kg) on plasma AICAR (A), FFAs (B), glucose (C), and lactate (D) concentrations in rats. Basal plasma samples for all measurements were collected immediately prior to AICAR injection. Data are presented as means ± SEM. N=5-9 animals/time point. * $P < 0.05$ vs. saline at the same time point.

5.4.11 Effects of AICAR on AMPK and ACC phosphorylation in skeletal muscle, liver, adipose tissue, and heart

AMPK and ACC phosphorylation was assessed in various tissues 24 hours following the last AICAR injection. EDL muscles (Figure 36A) showed an ~7- and 2.2-fold increase in AMPK and ACC phosphorylation relative to control, respectively. Liver

AMPK and ACC phosphorylation (Figure 36B) increased by ~23- and 40-fold, respectively. An increase in the phosphorylation of these two enzymes was also seen in the epididymal fat pad (Figure 36C, ~40-fold for AMPK and 60-fold for ACC) and the heart (Figure 36D, ~33-fold for AMPK and 60-fold for ACC).

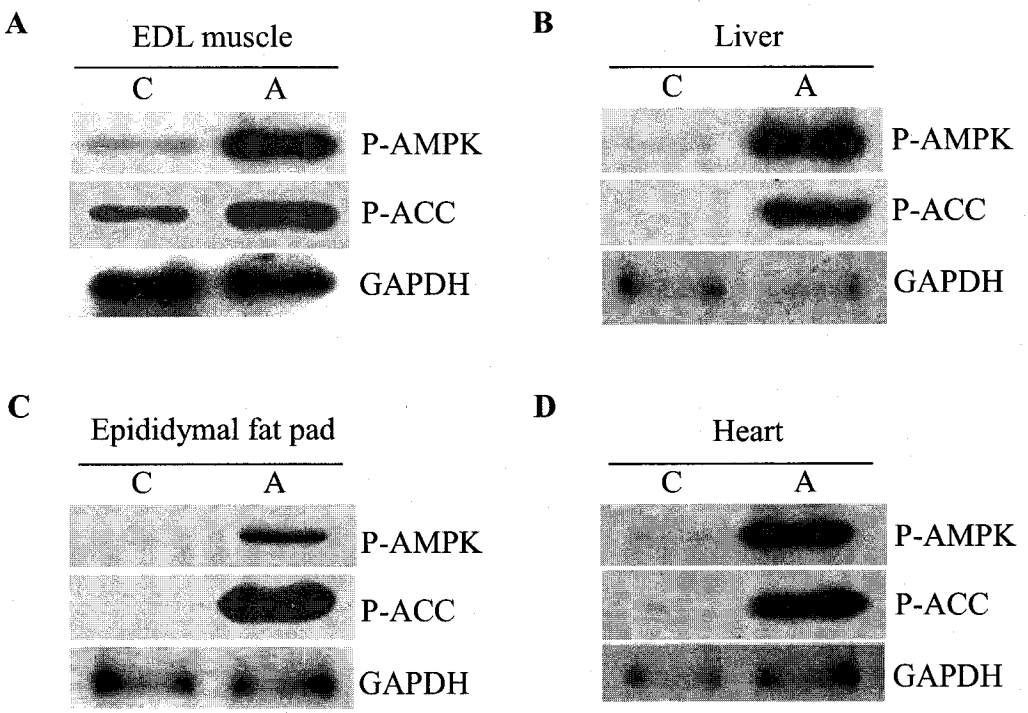

Figure 36. Effects of 2-week AICAR (A) injections on AMPK and ACC phosphorylation in the EDL muscle (A), liver (B), epididymal fat pad (C), and heart (D). Western blots were performed on tissues extracted 24 hours after the last AICAR injection. Control (C) animals were injected with an equal volume of saline as described in Methods.

6. DISCUSSION

6.1 Study 1: Regulation of AMPK and ACC phosphorylation by palmitate in skeletal muscle cells

Here we describe the novel finding that AMPK and ACC activity are regulated by palmitate in skeletal muscle cells in a dose-dependent manner. The concentrations of palmitate applied ranged from 1 to 800μM, which are within values observed either in physiological conditions such as overnight fast (~100 – 500μM) and prolonged exercise (~500 – 1000μM) or pathological conditions such as obesity (~600 – 800μM) and type 2 diabetes mellitus (~700 – 900μM) (203). However, although plasma fatty acids can reach 800μM, this is unlikely the case for the extracellular fluid to which skeletal muscle is exposed to *in vivo*. This raises the question whether the treatment of L6 muscle cells with high palmitate concentrations (400 – 800μM) could be toxic to the cells and affect cell viability. High levels of palmitate did not alter cell viability when measured by the trypan blue exclusion method as reported in Methods. Additionally, even though in our system the maximum phosphorylation response of AMPK and ACC was obtained in the presence of 400μM, the effect on oxidation was significantly increased and remained elevated as palmitate concentrations were raised up to 800μM in the incubation medium. This sustained functional response to high levels of palmitate (400 – 800μM) indicates that the muscle cells were viable and well responsive under all experimental conditions.

ACC phosphorylation was coupled to AMPK phosphorylation and activation in the presence palmitate concentrations raging from 1 to 100μM. However, at

concentrations above 200μM, ACC phosphorylation remained high, despite the total inhibition of AMPK phosphorylation by Compound C, a selective AMPK inhibitor. These results indicated that palmitate regulates ACC phosphorylation/activity by AMPK-dependent and -independent mechanisms, based on its abundance in skeletal muscle cells.

It has been previously demonstrated that the cytoplasmic process of fatty acid activation (formation of fatty acyl-CoA) consumes ATP and increases cytosolic AMP by ~30-fold leading to AMPK activation in isolated hepatocytes (109). Also, activation of heart AMPK in response to physiological concentrations of LCFA has been reported (108). These are in agreement with our results in skeletal muscle cells showing that palmitate increases AMPK phosphorylation and also phosphorylation of its direct substrate ACC, which are also compatible with the observed increase in fatty acid oxidation. In fact, the rate of palmitate oxidation by skeletal muscle cells rose as the concentration of this fatty acid in the medium was increased up to 400μM, and practically reached a plateau thereafter. Interestingly, inhibition of AMPK phosphorylation by Compound C significantly reduced (30%) basal (containing only labeled palmitate - 0.2 μCi/ml of [1-^{14}C]palmitic acid) and AICAR-induced (~45%) palmitate oxidation for concentrations of this fatty acid ranging from 0 to 100μM. However, Compound C exerted no significant effect on either basal or AICAR-induced palmitate oxidation as the concentration of this fatty acid was increased from 200 to 800μM, even though AMPK phosphorylation was prevented by Compound C. Additionally, the combination of AICAR and palmitate elicited a significant additive effect on oxidation (~75%) up to 100μM of palmitate but this effect was practically abolished (~7.5%) when palmitate

concentration ranged from 200 to 800μM. Importantly, no additive effect on AMPK and ACC phosphorylation was observed when cells were exposed to a combination of AICAR and palmitate (either 10μM or 400μM).

These findings indicate that LCFAs autoregulate their metabolism by two separate pathways: one that depends on AMPK activation and another that directly modulates ACC phosphorylation/activity and overrides the effects of AMPK activation. The concentration of LCFAs in the cell is the major factor determining which of these pathways will prevail in the regulation of fatty acid metabolism in skeletal muscle cells. Previous studies performed in perfused heart muscle (108) and in isolated rat hepatocytes (109) have shown that not only palmitate, but also acetate, octanoate, and oleate increase AMPK activity (108, 109) and fatty acid oxidation (108). In our experiments we used only palmitate and further studies need to be performed to test whether other fatty acids also regulate phosphorylation/activity of the AMPK/ACC pathway and β-oxidation in skeletal muscle.

The fact that ACC remained phosphorylated even after Compound C prevented palmitate-induced AMPK phosphorylation, suggests that fatty acids may also regulate ACC activity by inducing phosphorylation of this enzyme by an alternative kinase. Additionally, it may be possible that fatty acids inhibit phosphatases that might otherwise dephosphorylate and activate ACC. The inhibition by palmitate of phosphatases that target ACC would divert metabolism of LCFAs towards oxidation instead of lipid synthesis in the presence of high levels of fatty acids. In fact, in the present study we also observed that ACC phosphorylation was accompanied by up-regulation of palmitate

oxidation in skeletal muscles cells. Further studies are necessary to precisely identify the mechanisms by which fatty acids regulate ACC phosphorylation/activity in skeletal muscle cells and, therefore, autoregulate their metabolic fate.

The AMPK-independent effect of high levels of palmitate on fatty acid oxidation may also have derived from a potent feedback inhibition of ACC by long-chain fatty acyl-CoA esters (111, 204, 205). There is compelling evidence that citrate and acetyl-CoA function as allosteric activators of ACC, whereas LCFA-CoA acts as an allosteric inhibitor opposing the action of citrate on purified rat-hindlimb-muscle ACC (206). Suppression of lipogenesis by fatty acids has also been previously demonstrated in extracts of rat epididymal fat pads (207) and in rat perfused livers (208), even though there is little evidence that these were through allosteric inhibition of ACC. In rat skeletal muscle, refeeding after a fast rapidly decreased fatty acid oxidation *in vivo*, and this has been attributed to a decrease in circulating fatty acid levels releasing allosteric inhibition of ACC in muscle (112). All these observations are in agreement with our findings, which indicate that fatty acid abundance leads to ACC inhibition and suppression of lipogenesis. From a functional perspective this seems logical, because it would be unnecessary and counterproductive to maintain the *de novo* lipid synthesis pathway active under conditions of high cellular fatty acid levels. However, it has recently been reported that long-chain acyl-CoA esters inhibit *in vitro* phosphorylation and activation of recombinant AMPK by liver purified LKB1/STRAD/MO25, suggesting that in the presence of LCFAs the activation of the AMPK pathway may actually be impaired (110). Even though AMPK activity was directly measured by Taylor *et al* (110), the *in vitro*

analysis performed with purified enzymes did not allow for complex cellular metabolic interactions of AMPK with its allosteric regulators to take place. This is particularly important because in our experiments using muscle cells, palmitate consistently increased phosphorylation of AMPK in a dose dependent manner, whereas palmitate-induced ACC phosphorylation was regulated by AMPK-dependent and -independent mechanisms. From a metabolic perspective, the activity of ACC is what ultimately determines malonyl-CoA production and whether fatty acids will be produced or oxidized in the cell (111, 194). Because ACC activation does not depend exclusively on AMPK phosphorylation, the implications of AMPK regulation by fatty acids have to be analyzed in a more complex and interactive system.

The implications of our findings are that the fatty acid oxidative response that is normally triggered via AMPK activation by endogenous hormones, nutrients, and other pharmacological agonists (26, 209) may be impaired in the presence of high fatty acid concentrations in skeletal muscle. In the presence of fatty acids the AMPK/ACC system becomes activated and the oxidative response of the muscle cell may reach its maximum capacity preventing any potential additional effect that could be triggered by other AMPK agonists. In fact, we found that AICAR (a well known inducer of AMPK activity) did not elicit any additive oxidative effect in L6 muscle cells when in the presence of palmitate concentrations above 200μM. This is particularly important because certain metabolic disorders, such as obesity and type 2 diabetes, are accompanied by chronically elevated levels of circulating fatty acids (~600 – 900 μM) (203), which may limit the response of the AMPK/ACC pathway to endogenous and exogenous AMPK agonists.

Recently, it has been reported that adipokines such as leptin (26, 209) and adiponectin (210) exert direct antilipotoxic effects on skeletal muscle by activating the AMPK/ACC pathway. Resistance to these adipokines could be partially due to high levels of fatty acids maximally activating the AMPK/ACC pathway and impairing further activation of the AMPK/ACC pathway by leptin or adiponectin in peripheral tissues. To address this issue and restore the capacity of this pathway to be activated by adipokines or pharmacological agents, it may be necessary to focus on treatment strategies that lower circulating lipid concentrations.

6.2 Study 2: Acute effects of troglitazone in skeletal muscle cells

Currently, a relatively new class of drugs termed TZDs are being utilized to treat symptoms of T2DM. These oral antidiabetic agents, such as troglitazone, pioglitazone, and rosiglitazone, improve insulin sensitivity and glucose homeostasis in both humans (55) and animals (56-58). It is widely accepted that the molecular target of TZDs is the peroxisome proliferator activated receptor-γ (PPAR-γ), a transcription factor that belongs to the nuclear receptor family and is predominantly expressed in adipose tissue (59). Activation of PPAR-γ by TZDs increases the transcription of genes involved in fatty acid synthesis and storage causing a reduction of plasma FFA levels (60, 61). This reduces the flux of fatty acids to skeletal muscle and with it fatty acid-induced AMPK activation and may liberate the AMPK/ACC pathway to respond to pharmacological stimulation.

Although a large body of evidence supports the importance of TZD-mediated PPAR-γ activation on the improvement of insulin sensitivity, it appears that TZDs also exert metabolic effects that are independent of the activation of this transcription factor.

In fact, it has recently been observed that incubating rat EDL muscles with either troglitazone or rosiglitazone for 30min increases glucose uptake and fatty acid oxidation in this tissue (64). Due to the short exposure to TZDs and also because muscle expresses very low levels of PPAR-γ (59), these acute effects were unlikely dependent on activation of this transcription factor. As a matter of fact, the increase in fatty acid oxidation and glucose uptake was attributed and coincided with an increase in the phosphorylation/activation of AMPK (64). However, the metabolic implications of TZD-induced AMPK activation in skeletal muscle, especially regarding fatty acid metabolism and substrate partitioning are still not clear.

In our experiments, treatment of L6 myotubes with troglitazone for 1h resulted in a significant increase in AMPK and ACC phosphorylation, which was also followed by an increase (~30%) in palmitate oxidation. Interestingly, inhibition of AMPK activation by compound C was accompanied by suppression of phosphorylation of ACC and abolishment of the increased fatty acid oxidation induced by troglitazone. These findings provide evidence that AMPK is a molecular target for troglitazone to induce acute LCFA oxidation in skeletal muscle cells. Since muscle cells were exposed to troglitazone for a short time period (60min), the metabolic effects observed in our studies seem to be independent of PPARγ-mediated gene transcription. Furthermore, *in vitro* studies with isolated rat muscles have also reported that 30min exposure to troglitazone concentrations similar to the ones applied in our studies (5 – 100μM) induced rapid activation of AMPK and also an increase in LCFA oxidation (64). The concentrations of troglitazone utilized in our experiments are similar to the plasma concentrations

(~100μM) that elicited anti-hyperglycemic effects in Zucker diabetic fatty rats receiving oral dosages of 500mg/kg of troglitazone (211). In humans, it has been reported that oral dosages ranging from 200 – 600mg/day of troglitazone produced plasma concentrations (measured as area under the plasma concentration-time curve) as high as 50μM (212). Therefore, it is possible that the acute effects observed in our experiments utilizing concentrations varying from 5 to 100μM may also occur under physiological conditions.

Here, we provide evidence that the mechanism by which troglitazone promoted oxidation of LCFAs involved AMPK activation and phosphorylation/inactivation of its downstream target, ACC. The latter is a critical enzyme that generates malonyl-CoA, the precursor of fatty acid synthesis and the major inhibitor of mitochondrial LCFA import and β-oxidation (103, 213). These findings confirm our original hypothesis that, by increasing LCFA oxidation troglitazone could prevent intramyocellular lipid accumulation in skeletal muscle cells independently of PPARγ activation. Additional support for this comes from other findings in our investigation in which troglitazone: **a**) inhibited basal and insulin-stimulated palmitate uptake, **b**) significantly increased (60%) CPT-1 activity, **c**) inhibited pyruvate dehydrogenase activity, and **d)** suppressed basal and insulin-stimulated incorporation of glucose into lipids.

One intriguing finding of our study was that insulin completely suppressed troglitazone-induced palmitate oxidation but the troglitazone-induced increase in CPT-1 activity was not affected by this hormone. One would expect that because insulin stimulates glucose uptake, reduces troglitazone-induced ACC phosphorylation, and accelerates the *de novo* lipid synthesis pathway, the activity of CPT-1 would be reduced.

This is particularly relevant because in all media utilized for our experiments glucose (5.5mM) was present, which could provide enough substrate for the *de novo* lipid synthesis pathway to be active and potentially inhibit CPT-1 activity. However, this was not the case in our experiments. In fact, CPT-1 activity was equally elevated (~60%) in cells exposed to troglitazone alone or when in combination with insulin. This could be explained by the fact that insulin increased glucose uptake but when combined with troglitazone glucose metabolism was diverted towards lactate production, while pyruvate decarboxylation, glucose oxidation, and *de novo* lipid synthesis were powerfully suppressed. This shift of glucose metabolism towards lactate production caused by troglitazone is compatible with a reduction in citrate production, de-activation of ACC, suppression of malonyl-CoA production, and prevention of down regulation of CPT-1 activity. This is in line with our novel findings that troglitazone powerfully suppressed pyruvate decarboxylation by inhibiting the activity of the PDC. Importantly, the oxidative effect of troglitazone on LCFAs was abolished when cells were exposed to both insulin and troglitazone. This indicates that insulin impairs LCFA oxidation via a mechanism that does not act on CPT-1, since the activity of this enzyme remained elevated when muscle cells were simultaneously exposed to troglitazone and insulin. It may also be possible that the troglitazone-induced alteration in LCFA trafficking was counteracted by a more potent insulin-induced effect that diverts LCFAs away from mitochondria preventing their oxidation.

Our findings can be partially related to the classical "glucose-fatty acid cycle" proposed by Randle et. al. (174), in which enhanced fatty acid oxidation produces an

increase in the acetyl-CoA to CoA-SH ratio and elevation of cytoplasmic citrate concentration. These, in turn, would inhibit PDC, PFK, and hexokinase activity resulting in decreased glucose uptake in muscle cells. Indeed, in our experiments we observed that troglitazone significantly increased palmitate oxidation and powerfully suppressed PDC activity in skeletal muscle cells. However, we also found that basal and insulin-stimulated glucose uptake was significantly increased, which is contrary to what was proposed for the glucose-fatty acid cycle (174). Furthermore, inhibition of PFK is expected to impair the flux of substrate through the glycolytic pathway, which again is incompatible with the significant increase we found in both basal and insulin-stimulated rates of lactate production by muscle cells exposed to troglitazone. Therefore, the acute effects of troglitazone on glucose and fatty acid metabolism reported by us in skeletal muscle cells seem to be mediated by mechanisms that are distinct from those originally proposed by Randle et. al. (174).

Currently, we do not have an explanation for the AMPK-independent mechanism(s) by which troglitazone suppresses PDC activity. It is possible that troglitazone increased the activity of PDH kinase, the enzyme responsible for phosphorylating/deactivating PDH. In this context, the increase in fatty acid oxidation in the presence of troglitazone would have likely, increased mitochondrial acetyl-CoA and NADH levels (168). The increases in the acetyl-CoA/CoA-SH and NADH/NAD^+ ratios, which are known to increase PDH kinase activation, may have been responsible for suppressing PDC activity. It may also be possible that troglitazone reduced the activity of PDH phosphatase, the enzyme that catalyses the dephosphorylation/activation of PDH

(168). However, these mechanisms are only speculative and therefore require future investigation.

Our data provide novel evidence that although troglitazone suppressed insulin-stimulated glycogen synthesis, *de novo* lipid synthesis, and glucose oxidation, it promoted basal and insulin-stimulated Akt and GSK-3α/β phosphorylation and exerted additive effects on insulin-induced glucose uptake and lactate production. Phosphorylation of GSK-3α/β deactivates this enzyme and leads to dephosphorylation and activation of glycogen synthase, which promotes glycogen synthesis (214). In our experiments, exposure of L6 myotubes to troglitazone reduced the rates of glycogen synthesis to ~30% of the control values, despite the fact that this drug significantly increased $Akt_{(Thr308/Ser473)}$ and GSK-3α/β phosphorylation either under basal or insulin stimulated conditions. As mentioned above, this may be explained by the fact that troglitazone activated the glycolytic pathway and powerfully shifted glucose metabolism towards lactate production. This metabolic shift induced by troglitazone must have limited availability of glucose for glycogen synthesis in skeletal muscle cells. Additionally, the troglitazone-induced suppression of glycogen synthesis may have been caused by activation of AMPK by this drug. In fact, we (study 3) and others (215) have demonstrated that AMPK activation may induce phosphorylation/inactivation of glycogen synthase and impair glycogen synthesis in skeletal muscle, which may occur independently of GSK-3α/β.

Interestingly, troglitazone promoted a reduction in palmitate uptake in skeletal muscle cells. Moreover, while insulin alone stimulated palmitate uptake (~20%), the

addition of troglitazone to the incubation medium completely prevented the insulin-induced increase in palmitate uptake. In fact, palmitate uptake was ~23 to 37% lower than control values in the presence of troglitazone. Notably, the suppressive effect of troglitazone on palmitate uptake was followed by an increase in oxidation of this fatty acid. One would expect that a reduction in uptake and availability of palmitate in the cell would limit its oxidation; however, in our experiments the opposite was observed. This clearly indicates that troglitazone is also shifting lipid metabolism towards oxidation despite the limited intracellular supply of LCFAs. In the present study we have not investigated the mechanisms by which troglitazone promotes an increase in fatty acid oxidation in a setting of limited availability of this substrate. However, we hypothesize that the intracellular trafficking of LCFAs may be changed in such a way that the limited intracellular pool of fatty acids is diverted towards the mitochondria for oxidation. This is compatible with the fact that lipid synthesis was suppressed and CPT-1 activity was elevated in our cells exposed to troglitazone. With respect to this, it has previously been reported that FAT/CD36, a class of plasma membrane fatty acid transporters, play an important role in fatty acid oxidation (216). There is also evidence that palmitate oxidation is reduced in skeletal muscles of mice deficient in FAT/CD36 (217). Based on these findings, we hypothesize that by altering the trafficking of FAT/CD36, and probably other fat transporters such as FATP1 and FATP4, troglitazone increases lipid oxidation despite suppressing the uptake of LCFAs in skeletal muscle cells. However, these hypotheses depart from traditional views of mechanisms involved in the regulation of CPT-1 activity and β-oxidation and warrant further investigation.

Another interesting aspect of our findings is that troglitazone powerfully suppressed glucose oxidation but significantly increased palmitate oxidation. As previously discussed, the increase in palmitate oxidation is compatible with increases in AMPK and CPT-1 activities. This is in line with previous studies demonstrating that exposing isolated rat EDL muscles to TZDs (troglitazone and pioglitazone, 5 – 250μM) for 15 – 30min increased AMPK activity and induced palmitate oxidation (64). However, other studies have demonstrated that longer exposure (25h) of isolated rat soleus muscle to troglitazone, rosiglitazone, and pioglitazone inhibited CO_2 production from glucose and palmitate (67, 162). These effects have been attributed to inhibition of mitochondrial complex I activity and respiration by TZDs (162). The results of our experiments where muscle cells were exposed to troglitazone (50μM) for 60min indicate that mitochondrial respiration is not directly inhibited by this drug, since oxidation of palmitate was actually significantly increased (~30%) by troglitazone. This is also in agreement with other studies reporting that acute (15 – 30min) exposure of rat EDL muscles to TZDs (5 – 250μM) increased palmitate oxidation (64). The reduction in glucose oxidation observed in our experiments may be at least partially explained by the potent shift of glucose metabolism towards lactate production induced by troglitazone. Additionally, we demonstrate that troglitazone suppressed the activity of the PDC, an effect that appears to be independent of AMPK activation, since it was not reversed by compound C. By regulating the generation of acetyl-CoA from pyruvate, the PDC has been demonstrated to play an important role modulating glucose oxidation and the activity of the *de novo* lipid synthesis pathway in various tissues (168). Therefore, inhibition of PDC by

troglitazone is compatible with the substantial increase in lactate production and inhibition of glucose incorporation into lipids reported by us. In addition, this shift of glucose metabolism towards lactate production caused by troglitazone must have reduced citrate production, limited the availability of substrate for activation of ACC and suppressed the production of malonyl-CoA. This is compatible with the increase (~60%) in CPT-1 activity observed in our studies. Furthermore our findings are also in line with an increase in palmitate oxidation, since this variable is not directly limited by the activity of the PDC.

In summary, we provide novel evidence that troglitazone exerts an acute insulin sensitizing effect despite a marked reduction in basal and insulin-stimulated glycogen synthesis in skeletal muscle cells. Acute troglitazone treatment also increased phosphorylation of crucial intracellular steps of insulin signaling, which was accompanied by an increase in basal and insulin-stimulated glucose uptake and by a shift of glucose metabolism towards lactate production. This metabolic shift was mediated by an inhibitory effect of troglitazone on PDC activity independently of AMPK activation, since pharmacological inhibition of this kinase did not prevent the inhibitory effect of troglitazone on pyruvate decarboxylation. Additionally, troglitazone reduced FA uptake and increased FA oxidation. These effects were partially mediated by AMPK activation and may account for potential PPAR-γ-independent anti-diabetic effects of TZDs in skeletal muscle cells.

6.3 Study 3: Effect of AICAR-induced AMPK activation on glycogen synthesis in isolated skeletal muscle

An important observation made in our experiments utilizing troglitazone was that this drug potently suppressed both the basal and insulin-stimulated rate of glycogen synthesis in L6 muscle cells. As mentioned above, this pathway is particularly important, given the fact that insulin-stimulated muscle glycogen synthesis has been demonstrated to account for the majority of whole-body glucose uptake and virtually the entire nonoxidative glucose metabolism in both normal and diabetic subjects (134). Interestingly, we observed that troglitazone-induced AMPK activation improved insulin-mediated glucose disposal in these cells independently of glycogen synthesis. This demonstrates that activation of this pathway is not necessary to maintain a high rate of glucose disposal as long as other glucose metabolism pathways such as lactate production are upregulated. However, using muscle cell lines for our investigations had advantages and disadvantages. While on one hand it was easy to manipulate these cells in vitro, on the other hand it was difficult to be certain if the phenotype of these cells was representative of muscle tissue in vivo. It has been well established that muscle tissue can be composed of different muscle fibers including fast twitch glycolytic and slow twitch oxidative fibers each having different metabolic properties (218). Whereas glycolytic fibers express low GLUT-4 and mitochondrial levels and rely primarily on the breakdown of glycogen for energy generation, oxidative fibers express higher GLUT-4 and mitochondrial content and are able to more effectively utilize fatty acids as energy substrates. This important fiber type difference is lost when using muscle cell lines and

thus, it is helpful to consider different experimental models for testing various hypotheses. Here, we used isolated soleus and epitrochlearis muscles to test whether AICAR induced-AMPK activation will have similar effects on insulin-stimulated glycogen synthesis and major intracellular insulin-signalling events as did troglitazone in L6 cells. These muscles were chosen for use in our experiments due to their different fiber type composition. While the soleus is composed of primarily oxidative fibers, the epitrochlearis is mainly composed of glycolytic fibers, and hence these two muscles are ideal for determining muscle fiber type differences.

Here we provide evidence that acute exposure of soleus muscles to AICAR, a known activator of AMPK, profoundly inhibited (~60%) the insulin-induced increase in glycogen synthesis. AICAR treatment also prevented the insulin-induced increase in glycogen content in soleus muscles. Interestingly, neither basal nor insulin-stimulated glucose uptake was affected by AICAR in soleus while epitrochlearis muscles elicited a significant increase in this variable. This differential response to AICAR in isolated soleus and epitrochlearis muscles has also been reported in previous studies (128, 129); however, no data regarding the effects of AICAR on other glucose pathways have been reported in these studies. It has been argued that the lack of a stimulatory effect of AICAR on glucose transport in slow-twitch skeletal muscles could be due to fiber type-specific differences in the expression of AMPK-subunits (128, 219). In fact, it has been demonstrated that the presence of all three AMPK subunits is required for AICAR-induced increases in glucose transport in mouse skeletal muscle (219). Here, we report clear differences in AMPK-α subunit content in slow-twitch and fast-twitch muscles.

While AMPKα2 was equally present in both muscles investigated, AMPKα1 was faintly detected in soleus, which could justify the different responses in glucose uptake to AICAR observed here.

In our system, we also observed that insulin-stimulated lactate production was increased by AICAR treatment, and since AICAR did not affect insulin-stimulated glucose uptake it indicates that AICAR-induced AMPK activation shifted insulin-stimulated glucose metabolism towards lactate production instead of accumulation as glycogen in isolated soleus muscles. However, the AICAR-induced reduction in glycogen synthesis cannot be completely accounted for by the increase in lactate production, suggesting that other pathways may also participate in this metabolic shift. Previous investigations have demonstrated that glucose oxidation increases in isolated soleus muscles exposed to AICAR (7), which may also have been the case in the present study. In addition, our data is in partial agreement with a previous *in vitro* study showing that AICAR increased lactate production in soleus muscles exposed to low concentrations of insulin (147). However, in their study neither basal nor insulin-stimulated rates of glycogen synthesis were affected by AICAR, even though an increase in glycogen phosphorylase activity was reported (147). This is intriguing, since increased glycogen phosphorylase activity is expected to decrease glycogen synthesis. In our investigation, the marked AICAR-induced decrease in insulin-stimulated glycogen synthesis as well as suppression of the increase in glycogen content in solei is compatible with the increased glycogen phosphorylase activity previously reported by Young *et al* (147). There are important methodological differences between our study and the one by Young *et al*

(147) that may justify the differences regarding the effect of AICAR on insulin-stimulated glycogen synthesis. We used intact soleus muscle (~15-20mg) from 40-60g-rats while Young *et al* (147) used muscle strips from 130-140g-rats. Splitting the muscles may have influenced the response of the tissue to AICAR and insulin treatments. Also, the differences in AICAR concentrations (2mM versus 1mM) may account for the differences in glycogen synthesis reported in these two independent studies.

Previous *in vivo* studies also have reported that glycogen content is not affected by AICAR treatment in red and white gastrocnemius muscles, even though major time-dependent fiber type differences have been reported regarding the activity of GS and glycogen phosphorylase (146). Additionally, in the same study, *in vitro* incubations of two fast twitch muscles (flexor digitorum brevis and epitrochlearis) with AICAR affected neither GS nor glycogen phosphorylase activities (146). This is in line with our *in vitro* data showing that basal glycogen content was not affected by acute AICAR treatment in isolated soleus and epitrochlearis muscles. However, in another *in vivo* study it was actually reported that glycogen synthesis was increased in white but not in red quadriceps muscles after AICAR treatment (164). The reasons for these discrepant results are not clear, but may be attributed to the utilization of different muscle groups in various studies. In fact, it has been reported that major differences in the expression of AMPK isoforms in skeletal muscles with distinct fiber type compositions exist (28, 127, 220). For instance, Ai *et al* (28) show that the epitrochlearis, composed predominantly of type II fibers, expresses more AMPKα1 subunits than type I fibers, which is in agreement with data presented in this manuscript. On the other hand, type II fibers exhibit a 5-fold

greater expression of the γ-3 subunit than type I fibers (221). Even though specific muscle groups have been classified according to fiber type composition, current data on the expression and activity of AMPK isoforms in different muscle fibers, and their respective functional implications, still lack clarity. Therefore, the hypothesis that differential expression/activity of AMPK isoforms is responsible for the dissimilar results regarding the effects of AICAR treatment on glycogen metabolism requires additional investigation.

To examine if the effects of AICAR on insulin-induced glycogen synthesis in soleus muscles are fiber type specific, we also used epitrochlearis muscles in our experiments. We found that AMPK activation does not alter either the rate of glycogen synthesis or glycogen content in fast twitch muscles under basal and insulin-stimulated conditions. Additionally, lactate production was also unaffected by AICAR, indicating that the metabolic shift towards lactate production does not seem to occur in epitrochlearis muscle. Previous investigations have shown that either intraperitoneal (146) or subcutaneous (164) injections of AICAR increase blood lactate levels in rats. However, since these were *in vivo* studies we do not know how much of this lactate was derived from muscles versus other tissues that might also have been affected by AICAR treatment.

Here, we show novel evidence that AICAR interferes with the intracellular insulin signaling steps that are crucial to regulate glycogen metabolism. As expected, after soleus muscles were exposed to insulin for 30min, GS phosphorylation was decreased relative to control, therefore increasing its activity. Interestingly, insulin-induced reduction in

phosphorylation of GS was even more accentuated after 15 and 30min of AICAR treatment, suggesting an initial increase in GS activity in soleus muscles. However, this was not accompanied by an increase in glycogen synthesis after 1h incubation with AICAR. This suggests that the AICAR-induced increase in GS phosphorylation in soleus after 45min of exposure to insulin overcame the initial reduction in phosphorylation at 15 and 30min. Furthermore, the time course incubation of soleus muscles for the purpose of insulin signaling determination was performed up to 45 minutes while the rate of glycogen synthesis and glycogen content were assessed after 1 hour incubation. This leaves an additional 15 minutes during which GS may have become even more de-activated. These data are in agreement with previous *in vitro* experiments showing that AMPK from rat liver phosphorylates GS purified from rabbit skeletal muscle (145). However, a time course analysis of the effects of AMPK on GS phosphorylation was not performed in those experiments.

Since AMPK activation has also been shown to effect insulin signaling enzymes upstream of GS (149, 222, 223), we examined whether AICAR had similar effects on GSK-3α and 3β phosphorylation. When activated (de-phosphorylated), GSK-3α and 3β phosphorylate/de-activate GS, and hence lead to decreased glycogen synthesis. As expected, insulin elicited a powerful effect on GSK-3α phosphorylation, and remarkably, treatment of the insulin-stimulated condition with AICAR led to a pronounced decrease in phosphorylation of this enzyme. Phosphorylation of GSK-3β followed a pattern similar to GSK-3α; however, the former did not appear to be affected to the same extent by insulin. The decreased phosphorylation of GSK-3α and 3β by AICAR in insulin-

stimulated soleus muscles may have been due to a direct effect of AICAR on this enzyme (222). Data from Jurkat T cells demonstrates that AICAR can have a direct inhibitory effect on GSK-3 phosphorylation, thus increasing its activity. In addition, treatment of differentiated hippocampal neurons with AICAR led to dephosphorylation/activation of GSK-3α and 3β (223). However, these findings have not been shown in skeletal muscle cells.

The suppressive effects of AICAR on GSK-3 phosphorylation could also be linked to alterations in activity of upstream kinases such as Akt. Therefore, we also examined the effects of AICAR on insulin-stimulated phosphorylation of Akt-Ser473 and Akt-Thr308. Once again, we observed a transient high degree of phosphorylation of Akt-Thr308 with insulin after 15min of incubation, which appeared to fade at 30 and 45min. However, AICAR reduced the insulin-induced phosphorylation of Akt-Thr308 at both 15 and 30min of incubation. Phosphorylation of Akt-Ser473 was not affected by AICAR at any time points. Our data is in partial agreement with a recent study (223) showing that AICAR treatment reduces phosphorylation of Akt-Thr308 and Akt-Ser473. However, it is important to point out that while we examined the effects of AICAR on insulin-stimulated muscle tissue, the investigation by King *et al* (223) tested the effects of AICAR on basal Akt phosphorylation in hippocampal cells. The use of different tissues and administration of AICAR to basal or insulin-stimulated states may account for the differences between our investigation and that by King et al (223).

Another plausible mechanism by which AICAR exerts its effects on insulin-stimulated glycogen synthesis is mediated by events that take place upstream of Akt. In

fact, it has previously been shown that AMPK directly affects early insulin-signaling events by phosphorylating the IRS-1 on the Ser789 residue (149). Even though phosphorylation of IRS-1 on Ser789 residue did not impair insulin signaling in C_2C_{12} myotubes (149), other investigations have shown that serine phosphorylation of IRS-1 is linked to reduced capacity of insulin to activate PI3-K (224, 225). Additionally, AICAR has also been shown to have a direct effect on inhibiting GSK-3 phosphorylation, thus activating it (222, 223). In turn, activated GSK-3 phosphorylates IRS-1 on serine residues, and this has also been demonstrated to attenuate insulin signaling via its phosphorylation of IRS-1 in CHO cells (224). In our system, AICAR treatment elicited a marked reduction in GSK-3α/β phosphorylation, which may have also influenced early steps of insulin signaling in isolated soleus muscle and downstream events associated with glycogen synthesis.

In conclusion, we demonstrate that acute AMPK activation by AICAR leads to suppression of insulin-stimulated glycogen synthesis in soleus but not in epitrochlearis muscles. Additionally, we provide novel evidence that AICAR-induced AMPK activation affects major steps of the insulin signaling cascade in skeletal muscle. The suppression of glycogen synthesis and decrease in glycogen content by AICAR in isolated rat soleus muscles is compatible with the transient and time-dependent reduction in Akt308 phosphorylation, activation of GSK-3 α/β, and the inactivation of GS reported here.

6.4 Study 4: Effects of chronic AICAR injections on whole-body energy homeostasis

The studies discussed thus far have focused on the effects of acute AMPK activation on various aspects of glucose and fatty acid metabolism in skeletal muscle.

The final study in this thesis is intended to explore the bigger picture and investigate the chronic effects of AICAR on whole-body AMPK activation and energy homeostasis in rats. To explore this we employed the CLAMS which allowed us to monitor and obtain data related to substrate metabolism including VO_2, RQ, EE, and activity patterns in a non-invasive manner.

Here we provide novel evidence that AICAR injection for two weeks in rats led to an initial reduction in VO_2 and EE in week 1 of the investigation after only 3 days of injections. In fact, the reduction in VO_2 in AICAR treated animals caused a 10% reduction in O_2 consumption in the 22 hours following AICAR injection. These findings are surprising given the fact that AMPK activation in many tissues is linked to an increase in fatty acid oxidation, a process that requires oxygen. One of the potential factors that may have caused the changes in O_2 utilization is food intake since either a decrease or increase in this variable can affect O_2 consumption and EE (226). In our investigation, we observed that food intake was unaltered over the course of the investigation, suggesting that AICAR, when administered intraperitoneally may not affect AMPK in the hypothalamus. If that would have been the case, food intake would be expected to increase, as is observed in investigations where this drug is administered i.c.v. (189). Interestingly, a previous investigation utilizing AICAR in a chronic 5 day treatment protocol at a dosage of 1g/kg/day has shown a tendency towards a reduction in food intake in treated animals (227). On the other hand, treatment of ZDF rats with 0.25g/kg/day for 3 days a week for periods ranging from 26 to 106 days did not diminish food intake. Animals treated with AICAR ate approximately 20% less on days receiving

the drug, but compensated by eating more on days AICAR was not administered (228). A subsequent investigation in ZDF rats utilizing daily doses of 0.5g/kg/day for 8 weeks did not show any effects on food intake in the first 2 weeks of treatment but showed a reduction in food intake in the AICAR group in the following 6 weeks (229). The reasons for these discrepant results are not fully clear but may be due to the different rat strains as well as the different dosages of AICAR utilized in the various studies. In addition, it may be possible that the presence of a threshold for the AICAR dosage beyond which food intake is reduced may dictate if this variable is affected. Although in the present investigation the dosage of 0.7g/kg/day was higher than 0.25g/kg/day or 0.5g/kg/day (228, 229), it still remained lower than the dosage of 1g/kg/day utilized by Buhl et al (227) which caused a slight reduction in food intake. Therefore, since O_2 utilization did not appear to be affected by food intake in our investigation, it may be possible that alterations in activity patterns were responsible for the observed differences. However, no differences in activity pattern were observed in our investigation leading us to conclude that the reductions in VO_2 and EE in week 1 are a direct effect of the drug, rather than secondary effects due to alteration in other variables such as activity and food intake.

An additional important finding in our investigation is that RQ was reduced for approximately 8 hours following AICAR injection in week 1, indicating that an alteration in the ratio of fatty acid to glucose oxidation took place. The drop in RQ in AICAR treated animals to ~0.77 versus 0.87 in Control animals only 3 hours following drug administration suggests that AICAR promoted a shift in substrate metabolism in favour of fatty acid oxidation. However, even though these data provide important information

regarding the relationship between glucose and fatty acid utilization in these animals, it is not evident whether AICAR treatment resulted in a greater absolute rate of fatty acid oxidation compared to saline treated controls. When the RQ was used to calculate the amount of kcal/hr fat was contributing towards total EE, it became evident that even though AICAR reduced overall EE, it increased the relative amount of fat oxidized compared to control animals. Since an increase in the utilization of fatty acids by peripheral tissues is closely linked to their availability, we considered the possibility that AICAR may be altering the release of fatty acids from adipose tissue. To test this, we performed a series of acute time-course experiments in which FFAs were measured in the plasma at various time points following a single injection of AICAR for up to 8 hours. This allowed us to gain insight into the mechanisms by which the increase in fatty acid utilization took place in AICAR treated animals. Data from these experiments show an ~2-fold increase in plasma FFAs in AICAR treated animals at 4 and 8 hours following injections (9). This increase was closely mirrored by the reduction in RQ 3 hours following injection, which may have taken place as a result of the increased delivery and utilization of fatty acids by peripheral tissues. Since RQ is a measurement of whole-body substrate utilization, it is not possible to determine from these data which tissues may have contributed the most towards lowering this variable. Previous investigations have shown that AICAR-induced AMPK activation increases fatty acid oxidation in a number of different tissues, an effect that in some cases may be dependent on the length of exposure to the drug. For instance, in isolated adipocytes, acute (1 hour) AICAR treatment reduced palmitate oxidation (8), whereas 15 hours exposure to the same drug

increased oxidation of the same fatty acid (9). Data obtained in perfused rat hindlimb skeletal muscle demonstrate that 45 minutes of AICAR exposure increases fatty acid oxidation by approximately 3-fold (99). Similarly, in isolated rat hepatocytes exposure to AICAR for 4 hours also increases fatty acid oxidation (12). Our data clearly shows that the final, whole-body response is that fatty acid oxidation is increased. In addition, a reduction in fat pad masses at the end of the second week of investigation confirms that AICAR treated animals were, in fact utilizing more lipids as an energy substrate. Since leptin is an adipose tissue derived hormone and the concentration in the plasma is positively correlated with fat content (230), then it would be expected that a reduction in fat pad size would also result in lower circulating leptin levels. In support of this, our findings show that circulating leptin concentrations were similar between the two groups at the beginning of the study but were found to be lower at the end of the first week and in the second week of the investigation in AICAR treated animals. To further support these findings, previous investigations conducted in ZDF rats have demonstrated that chronic AICAR administration leads to a reduction in ectopic lipid accumulation (228). The reduction in fat pad mass in our animals seems to be compatible with the fact that AICAR increased AMPK and ACC phosphorylation in skeletal muscle, liver, adipose tissue, and heart which would have led to an increase in CPT-1 activity ultimately resulting in an increase in LCFA import into the mitochondria for oxidation. Therefore, our observations that the RQ is reduced in AICAR treated animals shortly after injection in week 1, are compatible with the concept that the AMPK/ACC pathway is activated by this drug. Interestingly, the reduction in RQ lasted for nearly 9 hours following injection,

and the reductions in VO_2 and EE were present even longer. These alterations took place despite the fact that AICAR levels in the plasma peaked at 10 minutes and were undetectable within 4 hours following injection. This indicates that even though AICAR clearance from the plasma takes place relatively quickly, its effects at the tissue level are sustained for a longer duration. The reasons why this occurs are not clear, but we hypothesize that the tissue levels of the activated form of AICAR (ZMP), remain elevated long after this drug is cleared from the plasma. Although we did not measure tissue ZMP content, in support of this hypothesis, we observed that AMPK and ACC phosphorylation were markedly increased in tissues collected 24 hours after the last AICAR injection. This may have been an important reason why some of the effects in the AICAR group were still noticeable as long as 19 hours following drug treatment.

Aside from stimulating an increase in fatty acids oxidation in the first week of treatment, AICAR also suppressed whole-body glucose oxidation. This is at least partially compatible with the glucose-fatty acid cycle put forward by Randle et al (174). This classic hypothesis proposes that an increase in fatty acid oxidation ultimately reduces glucose utilization by inhibiting the PDC in the mitochondria and PFK-1 in the glycolytic pathway. This would ultimately lead to reduced pyruvate entry into the mitochondria as well as glucose entry into the cell. However, in light of data collected in the acute time-course experiments in our investigation, it appears that only glucose oxidation was impaired in AICAR treated animals and that glucose disposal was actually increased. A reduction in blood glucose levels coupled with the increase in plasma lactate concentrations shortly after AICAR injection (30 minute time point) indicates that the

glucose that was cleared from the plasma was diverted towards lactate production rather than oxidation. In support of these findings, our results obtained in L6 muscle cells in study 2 show that troglitazone-induced AMPK activation increases glucose uptake and shifts glucose metabolism away from glycogen synthesis in favour of lactate production. Similarly, data obtained in study 3 in isolated soleus muscles demonstrate that AICAR-induced AMPK activation also causes a shit in glucose metabolism away from glycogen synthesis and towards an increase in lactate production, an effect that appears to be fiber type specific.

Here we also describe the novel findings that AICAR treated animals underwent an adaptive response to the drug following the first week of the investigation. The initial differences in VO_2, EE, and RQ observed in week 1, completely disappeared in week 2 in the AICAR group. However, an unanticipated finding in the second week was that spontaneous physical activity increased by approximately 25% in AICAR treated animals. Thus, even though there was no apparent difference in VO_2, EE and RQ in the second week, it may be possible that the increase in spontaneous physical activity by ~25% may have masked any possible differences in these variables. Therefore, it is clear from these data that AICAR treatment for two weeks reduces whole-body oxygen consumption and EE in rats, and that these animals compensate for this by increasing physical activity. In opposition to these findings, a recent publication by Narkar et al (231) showed that four weeks of daily AICAR injections (0.5g/kg/day) in mice led to an ~10% increase in VO_2 when measured as area under the curve, rather than a reduction. Utilizing mice versus rats in combination with an additional two weeks of AICAR

treatment compared to the present study, as well as the dosage of AICAR (0.7g/kg/day in the present study vs. 0.5g/kg/day in the study by Narkar et al (231)) are all factors that may have contributed to the differing findings observed in their study compared to the present investigation. In our study it is not clear if VO_2 measurements would have eventually increased if the treatment protocol was extended for an additional two weeks and requires future investigation.

In conclusion, the experiments in this project demonstrate that VO_2 and EE are reduced in week 1 of AICAR treatment. In addition, an increase in the availability of FFAs in the circulation as well as activation of the AMPK/ACC pathway in liver, skeletal muscle, adipose tissue, and heart may have been responsible for the increase in fatty acid oxidation and reduction in RQ observed in week 1. These effects may have collectively led to the reduction in fat pad mass observed at the end of the study. In week 2 of the investigation AICAR treated animals appeared to undergo an adaptation to the drug treatment as VO_2, EE and RQ were unaffected by AICAR injections. However, an increase in spontaneous physical activity in the second week may have masked any potential differences in those variables and may have also contributed to the reduction in whole body adiposity.

7. INTEGRATED SUMMARY

7.1 Effects of AMPK activation on substrate partitioning in skeletal muscle

The experiments presented in this thesis were designed to test the effects of various physiological and pharmacological AMPK activating agents on several metabolic and insulin signalling pathways. Specifically, we demonstrated that fatty acids autoregulate their metabolic fate in skeletal muscle cells by directly regulating phosphorylation and activation of AMPK and ACC (Figure 37). These effects of fatty acids in skeletal muscle may have important physiological and pathological implications for the response of this tissue to endogenous and exogenous agonists of the AMPK/ACC pathway. This is particularly important because certain metabolic disorders, such as obesity and T2DM, are accompanied by chronically high levels of circulating lipids, which may limit the response of this pathway to further activation by AMPK agonists. Thus, it may be beneficial to treat patients suffering from T2DM with pharmacological agents that reduce the circulating levels of FFAs. In this respect, TZDs are a class of antidiabetic drugs that are currently used in the treatment of T2DM patients and address this issue by increasing the capacity of adipose tissue to store lipids. In addition, recent evidence has also shown that TZDs are capable of acutely activating AMPK in muscle; however the outcomes of this are largely unknown. To test this, we utilized the TZD troglitazone to test its effects on various aspects of glucose and fatty acid metabolism in muscle cells. We provide novel evidence that troglitazone exerts an acute insulin sensitizing effect despite a marked reduction in basal and insulin-stimulated glycogen synthesis in skeletal muscle cells (Figure 37). Acute troglitazone treatment also increased

phosphorylation of crucial intracellular steps of insulin signalling, which was accompanied by an increase in basal and insulin-stimulated glucose uptake and by a shift of glucose metabolism towards lactate production. This metabolic shift was mediated by an inhibitory effect of troglitazone on PDH activity independently of AMPK activation, since pharmacological inhibition of this kinase did not prevent the inhibitory effect of troglitazone on pyruvate decarboxylation (Figure 24). Additionally, troglitazone reduced FA uptake and increased FA oxidation. These effects were partially mediated by AMPK activation and may account for potential PPAR-γ-independent anti-diabetic effects of TZDs in skeletal muscle cells (Figure 37).

A significant observation made in our experiments utilizing troglitazone was that this drug suppressed both the basal and insulin-stimulated rate of glycogen synthesis. Due to the fact that this process is essential for the control of whole-body glucose homeostasis as it accounts for the majority of glucose disposal, we decided to test whether activation of AMPK in isolated skeletal muscle would have a similar outcome as it did in muscle cells. The advantage of using isolated skeletal muscle preparations as opposed to L6 cells was that we were able to observe the effects of AMPK activation in different fibre types. In this respect, we utilized the primarily oxidative soleus muscle and the primarily glycolytic epitrochlearis muscle for our experiments. Interestingly, we observed that acute exposure of soleus muscles to AICAR, profoundly inhibited the insulin-induced increase in glycogen synthesis and shifted glucose metabolism towards an increase in lactate production (Figure 37). More importantly, we provided novel evidence that AICAR-induced AMPK activation affects major steps of the insulin

signalling cascade in skeletal muscle. These effects appear to be fiber type specific as they did not take place in the epitrochlearis muscle.

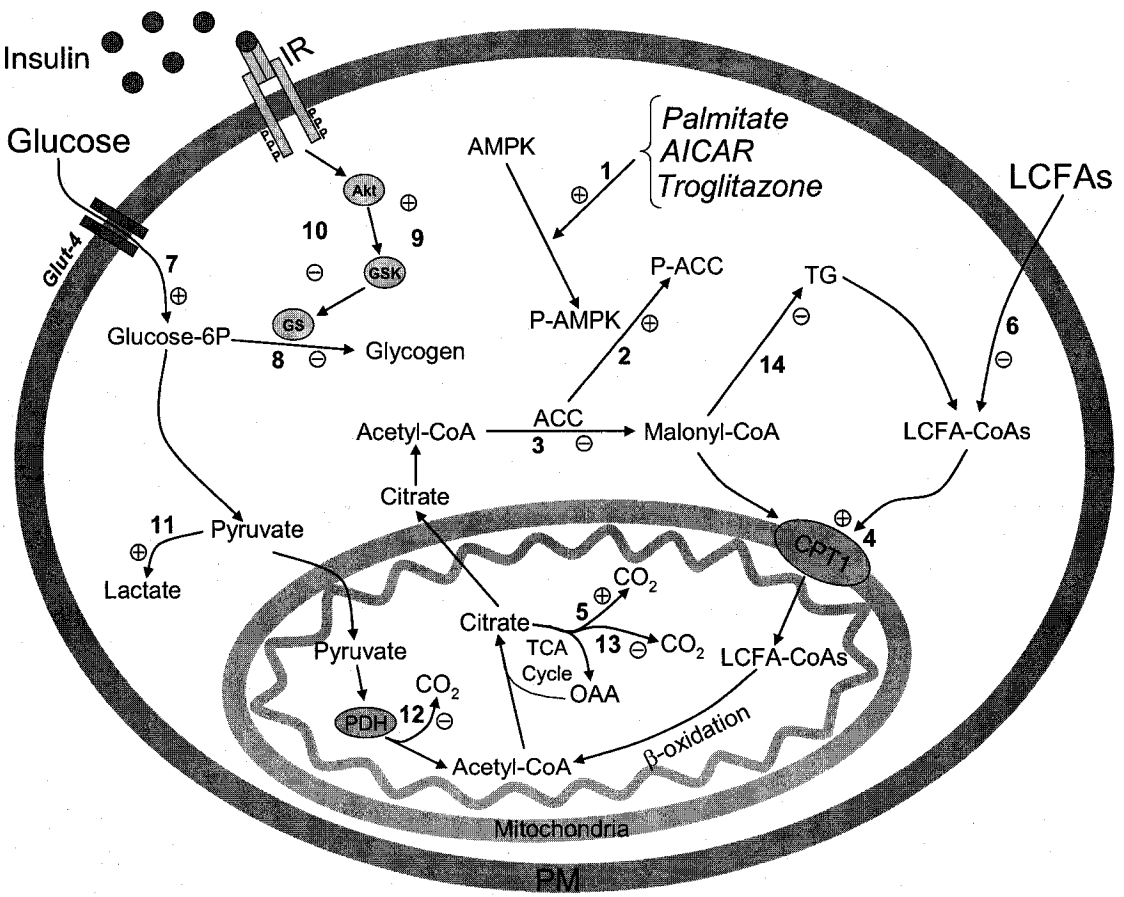

Figure 37. Schematic representation of the acute effects of palmitate, AICAR and troglitazone-induced AMPK activation on various pathways of glucose and fatty acid metabolism in skeletal muscle. Administration of palmitate, AICAR and troglitazone increases AMPK phosphorylation/activation (1) and ACC phosphorylation/de-activation (2) leading to a reduction in the conversion of acetyl-CoA into malonyl-CoA (3). As a consequence, CPT1 activity (4) and LCFA oxidation (5) were increased, even though LCFA uptake (6) was reduced when treated with troglitazone. Similar to the effect of troglitazone, palmitate also increased LCFA oxidation (5). Troglitazone also increased basal and insulin-stimulated glucose uptake (7), whereas AICAR did not affect this variable in soleus muscle but significantly increased basal glucose uptake in

epitrochlearis muscle. Both drugs also caused a reduction in insulin-stimulated glycogen synthesis (8) and a shift towards lactate production (11). Interestingly, while the reduction in glycogen synthesis was compatible with the reduced phosphorylation of AKT and GSK and increased phosphorylation of GS in response to AICAR (10), troglitazone treatment lead to the opposite effect (9). Furthermore, pyruvate decarboxylation (12), glucose oxidation (13), and the *de novo* lipid synthesis pathway (11) were powerfully suppressed by troglitazone. Upregulation or downregulation of a particular pathway is indicated by plus (+) or minus (-) signs, respectively. LCFAs = long chain fatty acids, CPT1 = carnitine palmitoyl transferase-1, GSK = Glycogen synthase kinase, GS = Glycogen synthase, IR = insulin receptor, TG = triacylglycerol, OAA = oxaloacetate, PDH = pyruvate dehydrogenase complex, TCA = tricarboxylic acid, PM = plasma membrane.

7.2 Effects of chronic whole-body AMPK activation on substrate homeostasis

Taken as a whole the data obtained in L6 cells as well as isolated skeletal muscles presents important information regarding the effects of AMPK activation on substrate partitioning in this particular tissue. However, since in *in vivo* conditions AMPK activating agents not only affect skeletal muscle but also activate AMPK in other tissues, it is important to determine the whole-body effects of such an outcome. To test this we injected rats with AICAR for two weeks and measured various metabolic parameters. We demonstrated that in the first week of treatment AICAR treated animals experienced a reduction in VO2, EE, and RQ, effects that were independent of food intake and activity patterns. Interestingly, in the second week animals injected with AICAR underwent an adaptation to the drug as VO2, EE, and RQ were similar to animals injected with vehicle. However, in the second week animals receiving AICAR showed an approximately 25% increase in spontaneous physical activity.

8. REFERENCES

1. Long, Y.C., and Zierath, J.R. 2006. AMP-activated protein kinase signaling in metabolic regulation. *J. Clin. Invest.* **116**:1776-1783.

2. Hardie, D.G. 2007. AMP-activated/SNF1 protein kinases: conserved guardians of cellular energy. *Nat. Rev. Mol. Cell Biol.* **8**:774-785.

3. Carling, D. 2005. AMP-activated protein kinase: balancing the scales. *Biochimie* **87**:87-91.

4. Cuthbertson, D.J., Babraj, J.A., Mustard, K.J., Towler, M.C., Green, K.A., Wackerhage, H., Leese, G.P., Baar, K., Thomason-Hughes, M., Sutherland, C. et al. 2007. 5-aminoimidazole-4-carboxamide 1-beta-D-ribofuranoside acutely stimulates skeletal muscle 2-deoxyglucose uptake in healthy men. *Diabetes* **56**:2078-2084.

5. Holmes, B.F., Kurth-Kraczek, E.J., and Winder, W.W. 1999. Chronic activation of 5'-AMP-activated protein kinase increases GLUT-4, hexokinase, and glycogen in muscle. *J. Appl. Physiol.* **87**:1990-1995.

6. Buhl, E.S., Jessen, N., Schmitz, O., Pedersen, S.B., Pedersen, O., Holman, G.D., and Lund, S. 2001. Chronic treatment with 5-aminoimidazole-4-carboxamide-1-beta-D-ribofuranoside increases insulin-stimulated glucose uptake and GLUT4 translocation in rat skeletal muscles in a fiber type-specific manner. *Diabetes* **50**:12-17.

7. Smith, A.C., Bruce, C.R., and Dyck, D.J. 2005. AMP kinase activation with AICAR simultaneously increases fatty acid and glucose oxidation in resting rat soleus muscle. *J. Physiol.* **565**:537-546.

8. Gaidhu, M.P., Fediuc, S., and Ceddia, R.B. 2006. 5-Aminoimidazole-4-carboxamide-1-beta-D-ribofuranoside-induced AMP-activated protein kinase phosphorylation inhibits basal and insulin-stimulated glucose uptake, lipid synthesis, and fatty acid oxidation in isolated rat adipocytes. *J. Biol. Chem.* **281**:25956-25964.

9. Gaidhu, M.P., Fediuc, S., Anthony, N.M., So, M., Mirpourian, M., Perry, R.L., and Ceddia, R.B. 2008. Prolonged aicar-induced amp-kinase activation promotes energy dissipation in white adipocytes: Novel mechanisms integrating HSL and ATGL. *J. Lipid Res.*

10. Salt, I.P., Connell, J.M., and Gould, G.W. 2000. 5-aminoimidazole-4-carboxamide ribonucleoside (AICAR) inhibits insulin-stimulated glucose transport in 3T3-L1 adipocytes. *Diabetes* **49**:1649-1656.

11. Lochhead, P.A., Salt, I.P., Walker, K.S., Hardie, D.G., and Sutherland, C. 2000. 5-aminoimidazole-4-carboxamide riboside mimics the effects of insulin on the expression of the 2 key gluconeogenic genes PEPCK and glucose-6-phosphatase. *Diabetes* **49**:896-903.

12. Zhou, G., Myers, R., Li, Y., Chen, Y., Shen, X., Fenyk-Melody, J., Wu, M., Ventre, J., Doebber, T., Fujii, N. et al. 2001. Role of AMP-activated protein kinase in mechanism of metformin action. *J. Clin. Invest.* **108**:1167-1174.

13. Habets, D.D., Coumans, W.A., Voshol, P.J., den Boer, M.A., Febbraio, M., Bonen, A., Glatz, J.F., and Luiken, J.J. 2007. AMPK-mediated increase in myocardial long-chain fatty acid uptake critically depends on sarcolemmal CD36. *Biochem. Biophys. Res. Commun.* **355**:204-210.

14. Minokoshi, Y., Alquier, T., Furukawa, N., Kim, Y.B., Lee, A., Xue, B., Mu, J., Foufelle, F., Ferre, P., Birnbaum, M.J. et al. 2004. AMP-kinase regulates food intake by responding to hormonal and nutrient signals in the hypothalamus. *Nature* **428**:569-574.

15. Minokoshi, Y., Kim, Y.B., Peroni, O.D., Fryer, L.G., Muller, C., Carling, D., and Kahn, B.B. 2002. Leptin stimulates fatty-acid oxidation by activating AMP-activated protein kinase. *Nature* **415**:339-343.

16. Misra, P., and Chakrabarti, R. 2007. The role of AMP kinase in diabetes. *Indian J. Med. Res.* **125**:389-398.

17. Shulman, G.I. 2000. Cellular mechanisms of insulin resistance. *J. Clin. Invest.* **106**:171-176.

18. Towler, M.C., and Hardie, D.G. 2007. AMP-activated protein kinase in metabolic control and insulin signaling. *Circ. Res.* **100**:328-341.

19. Carling, D., Zammit, V.A., and Hardie, D.G. 1987. A common bicyclic protein kinase cascade inactivates the regulatory enzymes of fatty acid and cholesterol biosynthesis. *FEBS Lett.* **223**:217-222.

20. Carlson, C.A., and Kim, K.H. 1973. Regulation of hepatic acetyl coenzyme A carboxylase by phosphorylation and dephosphorylation. *J. Biol. Chem.* **248**:378-380.

21. Beg, Z.H., Allmann, D.W., and Gibson, D.M. 1973. Modulation of 3-hydroxy-3-methylglutaryl coenzyme A reductase activity with cAMP and wth protein fractions of rat liver cytosol. *Biochem. Biophys. Res. Commun.* **54**:1362-1369.

22. Yeh, L.A., Lee, K.H., and Kim, K.H. 1980. Regulation of rat liver acetyl-CoA carboxylase. Regulation of phosphorylation and inactivation of acetyl-CoA carboxylase by the adenylate energy charge. *J. Biol. Chem.* **255**:2308-2314.

23. Ferrer, A., Caelles, C., Massot, N., and Hegardt, F.G. 1985. Activation of rat liver cytosolic 3-hydroxy-3-methylglutaryl coenzyme A reductase kinase by adenosine 5'-monophosphate. *Biochem. Biophys. Res. Commun.* **132**:497-504.

24. Sim, A.T., and Hardie, D.G. 1988. The low activity of acetyl-CoA carboxylase in basal and glucagon-stimulated hepatocytes is due to phosphorylation by the AMP-activated protein kinase and not cyclic AMP-dependent protein kinase. *FEBS Lett.* **233**:294-298.

25. Kemp, B.E., Oakhill, J.S., and Scott, J.W. 2007. AMPK structure and regulation from three angles. *Structure* **15**:1161-1163.

26. Kahn, B.B., Alquier, T., Carling, D., and Hardie, D.G. 2005. AMP-activated protein kinase: ancient energy gauge provides clues to modern understanding of metabolism. *Cell. Metab.* **1**:15-25.

27. Pang, T., Xiong, B., Li, J.Y., Qiu, B.Y., Jin, G.Z., Shen, J.K., and Li, J. 2007. Conserved alpha-helix acts as autoinhibitory sequence in AMP-activated protein kinase alpha subunits. *J. Biol. Chem.* **282**:495-506.

28. Ai, H., Ihlemann, J., Hellsten, Y., Lauritzen, H.P., Hardie, D.G., Galbo, H., and Ploug, T. 2002. Effect of fiber type and nutritional state on AICAR- and contraction-stimulated glucose transport in rat muscle. *Am. J. Physiol. Endocrinol. Metab.* **282**:E1291-300.

29. Salt, I., Celler, J.W., Hawley, S.A., Prescott, A., Woods, A., Carling, D., and Hardie, D.G. 1998. AMP-activated protein kinase: greater AMP dependence, and preferential nuclear localization, of complexes containing the alpha2 isoform. *Biochem. J.* **334 (Pt 1)**:177-187.

30. Turnley, A.M., Stapleton, D., Mann, R.J., Witters, L.A., Kemp, B.E., and Bartlett, P.F. 1999. Cellular distribution and developmental expression of AMP-activated protein kinase isoforms in mouse central nervous system. *J. Neurochem.* **72**:1707-1716.

31. Sakoda, H., Fujishiro, M., Fujio, J., Shojima, N., Ogihara, T., Kushiyama, A., Fukushima, Y., Anai, M., Ono, H., Kikuchi, M. et al. 2005. Glycogen debranching enzyme association with beta-subunit regulates AMP-activated protein kinase activity. *Am. J. Physiol. Endocrinol. Metab.* **289**:E474-81.

32. Bateman, A. 1997. The structure of a domain common to archaebacteria and the homocystinuria disease protein. *Trends Biochem. Sci.* **22**:12-13.

33. Jin, X., Townley, R., and Shapiro, L. 2007. Structural insight into AMPK regulation: ADP comes into play. *Structure* **15**:1285-1295.

34. Scott, J.W., Ross, F.A., Liu, J.K., and Hardie, D.G. 2007. Regulation of AMP-activated protein kinase by a pseudosubstrate sequence on the gamma subunit. *EMBO J.* **26**:806-815.

35. Hawley, S.A., Boudeau, J., Reid, J.L., Mustard, K.J., Udd, L., Makela, T.P., Alessi, D.R., and Hardie, D.G. 2003. Complexes between the LKB1 tumor suppressor, STRAD alpha/beta and MO25 alpha/beta are upstream kinases in the AMP-activated protein kinase cascade. *J. Biol.* **2**:28.

36. Long, Y.C., and Zierath, J.R. 2006. AMP-activated protein kinase signaling in metabolic regulation. *J. Clin. Invest.* **116**:1776-1783.

37. Scott, J.W., Norman, D.G., Hawley, S.A., Kontogiannis, L., and Hardie, D.G. 2002. Protein kinase substrate recognition studied using the recombinant catalytic domain of AMP-activated protein kinase and a model substrate. *J. Mol. Biol.* **317**:309-323.

38. Marks A.D., Smith C., Lieberman M. 2005. *Marks' Basic medical biochemistry: a clinical approach.* 2nd edition. Lippincott Williams & Wilkins. Philadelphia.

39. Salway, J.G. 2004. *Metabolism at a glance.* 3rd edition. Blackwell Publishing. Massachusetts.

40. Sato, R., Goldstein, J.L., and Brown, M.S. 1993. Replacement of serine-871 of hamster 3-hydroxy-3-methylglutaryl-CoA reductase prevents phosphorylation by AMP-activated kinase and blocks inhibition of sterol synthesis induced by ATP depletion. *Proc. Natl. Acad. Sci. U. S. A.* **90**:9261-9265.

41. Russell, R.,3rd. 2006. Stress signaling in the heart by AMP-activated protein kinase. *Curr. Hypertens. Rep.* **8**:446-450.

42. Woods, A., Dickerson, K., Heath, R., Hong, S.P., Momcilovic, M., Johnstone, S.R., Carlson, M., and Carling, D. 2005. Ca2+/calmodulin-dependent protein kinase kinase-beta acts upstream of AMP-activated protein kinase in mammalian cells. *Cell. Metab.* **2**:21-33.

43. Hurley, R.L., Anderson, K.A., Franzone, J.M., Kemp, B.E., Means, A.R., and Witters, L.A. 2005. The Ca2+/calmodulin-dependent protein kinase kinases are AMP-activated protein kinase kinases. *J. Biol. Chem.* **280**:29060-29066.

44. Hawley, S.A., Selbert, M.A., Goldstein, E.G., Edelman, A.M., Carling, D., and Hardie, D.G. 1995. 5'-AMP activates the AMP-activated protein kinase cascade, and Ca2+/calmodulin activates the calmodulin-dependent protein kinase I cascade, via three independent mechanisms. *J. Biol. Chem.* **270**:27186-27191.

45. Anderson, K.A., Means, R.L., Huang, Q.H., Kemp, B.E., Goldstein, E.G., Selbert, M.A., Edelman, A.M., Fremeau, R.T., and Means, A.R. 1998. Components of a calmodulin-dependent protein kinase cascade. Molecular cloning, functional characterization and cellular localization of Ca2+/calmodulin-dependent protein kinase kinase beta. *J. Biol. Chem.* **273**:31880-31889.

46. Winder, W.W. 2001. Energy-sensing and signaling by AMP-activated protein kinase in skeletal muscle. *J. Appl. Physiol.* **91**:1017-1028.

47. Rutter, G.A., Da Silva Xavier, G., and Leclerc, I. 2003. Roles of 5'-AMP-activated protein kinase (AMPK) in mammalian glucose homoeostasis. *Biochem. J.* **375**:1-16.

48. Igata, M., Motoshima, H., Tsuruzoe, K., Kojima, K., Matsumura, T., Kondo, T., Taguchi, T., Nakamaru, K., Yano, M., Kukidome, D. et al. 2005. Adenosine monophosphate-activated protein kinase suppresses vascular smooth muscle cell proliferation through the inhibition of cell cycle progression. *Circ. Res.* **97**:837-844.

49. Sabina, R.L., Kernstine, K.H., Boyd, R.L., Holmes, E.W., and Swain, J.L. 1982. Metabolism of 5-amino-4-imidazolecarboxamide riboside in cardiac and skeletal muscle. Effects on purine nucleotide synthesis. *J. Biol. Chem.* **257**:10178-10183.

50. Swain, J.L., Hines, J.J., Sabina, R.L., and Holmes, E.W. 1982. Accelerated repletion of ATP and GTP pools in postischemic canine myocardium using a precursor of purine de novo synthesis. *Circ. Res.* **51**:102-105.

51. Swain, J.L., Hines, J.J., Sabina, R.L., Harbury, O.L., and Holmes, E.W. 1984. Disruption of the purine nucleotide cycle by inhibition of adenylosuccinate lyase produces skeletal muscle dysfunction. *J. Clin. Invest.* **74**:1422-1427.

52. Pasque, M.K., and Wechsler, A.S. 1984. Metabolic intervention to affect myocardial recovery following ischemia. *Ann. Surg.* **200**:1-12.

53. Sabina, R.L., Swain, J.L., Olanow, C.W., Bradley, W.G., Fishbein, W.N., DiMauro, S., and Holmes, E.W. 1984. Myoadenylate deaminase deficiency. Functional and metabolic abnormalities associated with disruption of the purine nucleotide cycle. *J. Clin. Invest.* **73**:720-730.

54. Hardie, D.G. 2004. AMP-activated protein kinase: the guardian of cardiac energy status. *J. Clin. Invest.* **114**:465-468.

55. Inzucchi, S.E., Maggs, D.G., Spollett, G.R., Page, S.L., Rife, F.S., Walton, V., and Shulman, G.I. 1998. Efficacy and metabolic effects of metformin and troglitazone in type II diabetes mellitus. *N. Engl. J. Med.* **338**:867-872.

56. Lee, M.K., Miles, P.D., Khoursheed, M., Gao, K.M., Moossa, A.R., and Olefsky, J.M. 1994. Metabolic effects of troglitazone on fructose-induced insulin resistance in the rat. *Diabetes* **43**:1435-1439.

57. Miles, P.D., Higo, K., Romeo, O.M., Lee, M.K., Rafaat, K., and Olefsky, J.M. 1998. Troglitazone prevents hyperglycemia-induced but not glucosamine-induced insulin resistance. *Diabetes* **47**:395-400.

58. Kraegen, E.W., James, D.E., Jenkins, A.B., Chisholm, D.J., and Storlien, L.H. 1989. A potent in vivo effect of ciglitazone on muscle insulin resistance induced by high fat feeding of rats. *Metabolism* **38**:1089-1093.

59. Auboeuf, D., Rieusset, J., Fajas, L., Vallier, P., Frering, V., Riou, J.P., Staels, B., Auwerx, J., Laville, M., and Vidal, H. 1997. Tissue distribution and quantification of the expression of mRNAs of peroxisome proliferator-activated receptors and liver X receptor-alpha in humans: no alteration in adipose tissue of obese and NIDDM patients. *Diabetes* **46**:1319-1327.

60. Castelein, H., Gulick, T., Declercq, P.E., Mannaerts, G.P., Moore, D.D., and Baes, M.I. 1994. The peroxisome proliferator activated receptor regulates malic enzyme gene expression. *J. Biol. Chem.* **269**:26754-26758.

61. Guan, H.P., Li, Y., Jensen, M.V., Newgard, C.B., Steppan, C.M., and Lazar, M.A. 2002. A futile metabolic cycle activated in adipocytes by antidiabetic agents. *Nat. Med.* **8**:1122-1128.

62. Lee, M.K., and Olefsky, J.M. 1995. Acute effects of troglitazone on in vivo insulin action in normal rats. *Metabolism* **44**:1166-1169.

63. Burant, C.F., Sreenan, S., Hirano, K., Tai, T.A., Lohmiller, J., Lukens, J., Davidson, N.O., Ross, S., and Graves, R.A. 1997. Troglitazone action is independent of adipose tissue. *J. Clin. Invest.* **100**:2900-2908.

64. LeBrasseur, N.K., Kelly, M., Tsao, T.S., Farmer, S.R., Saha, A.K., Ruderman, N.B., and Tomas, E. 2006. Thiazolidinediones can rapidly activate AMP-activated protein kinase in mammalian tissues. *Am. J. Physiol. Endocrinol. Metab.* **291**:E175-81.

65. Konrad, D., Rudich, A., Bilan, P.J., Patel, N., Richardson, C., Witters, L.A., and Klip, A. 2005. Troglitazone causes acute mitochondrial membrane depolarisation and an AMPK-mediated increase in glucose phosphorylation in muscle cells. *Diabetologia* **48**:954-966.

66. Fryer, L.G., Parbu-Patel, A., and Carling, D. 2002. The Anti-diabetic drugs rosiglitazone and metformin stimulate AMP-activated protein kinase through distinct signaling pathways. *J. Biol. Chem.* **277**:25226-25232.

67. Furnsinn, C., Brunmair, B., Neschen, S., Roden, M., and Waldhausl, W. 2000. Troglitazone directly inhibits CO(2) production from glucose and palmitate in isolated rat skeletal muscle. *J. Pharmacol. Exp. Ther.* **293**:487-493.

68. Kishimoto, A., Ogura, T., and Esumi, H. 2006. A pull-down assay for 5' AMP-activated protein kinase activity using the GST-fused protein. *Mol. Biotechnol.* **32**:17-21.

69. Zoulim, F., and Trepo, C. 1994. Nucleoside analogs in the treatment of chronic viral hepatitis. Efficiency and complications. *J. Hepatol.* **21**:142-144.

70. Fiume, L., Busi, C., and Mattioli, A. 1983. Targeting of antiviral drugs by coupling with protein carriers. *FEBS Lett.* **153**:6-10.

71. Walkenbach, R.J., and Chao, W.T. 1985. Adenosine regulation of cyclic AMP in corneal endothelium. *J. Ocul. Pharmacol.* **1**:337-342.

72. Parkinson, F.E., and Geiger, J.D. 1996. Effects of iodotubercidin on adenosine kinase activity and nucleoside transport in DDT1 MF-2 smooth muscle cells. *J. Pharmacol. Exp. Ther.* **277**:1397-1401.

73. McArthur, M.J., Atshaves, B.P., Frolov, A., Foxworth, W.D., Kier, A.B., and Schroeder, F. 1999. Cellular uptake and intracellular trafficking of long chain fatty acids. *J. Lipid Res.* **40**:1371-1383.

74. Richieri, G.V., and Kleinfeld, A.M. 1995. Unbound free fatty acid levels in human serum. *J. Lipid Res.* **36**:229-240.

75. Koonen, D.P., Glatz, J.F., Bonen, A., and Luiken, J.J. 2005. Long-chain fatty acid uptake and FAT/CD36 translocation in heart and skeletal muscle. *Biochim. Biophys. Acta* **1736**:163-180.

76. Ehehalt, R., Fullekrug, J., Pohl, J., Ring, A., Herrmann, T., and Stremmel, W. 2006. Translocation of long chain fatty acids across the plasma membrane--lipid rafts and fatty acid transport proteins. *Mol. Cell. Biochem.* **284**:135-140.

77. Harmon, C.M., and Abumrad, N.A. 1993. Binding of sulfosuccinimidyl fatty acids to adipocyte membrane proteins: isolation and amino-terminal sequence of an 88-kD protein implicated in transport of long-chain fatty acids. *J. Membr. Biol.* **133**:43-49.

78. Koonen, D.P., Glatz, J.F., Bonen, A., and Luiken, J.J. 2005. Long-chain fatty acid uptake and FAT/CD36 translocation in heart and skeletal muscle. *Biochim. Biophys. Acta* **1736**:163-180.

79. Glatz, J.F., Bonen, A., and Luiken, J.J. 2002. Exercise and insulin increase muscle fatty acid uptake by recruiting putative fatty acid transporters to the sarcolemma. *Curr. Opin. Clin. Nutr. Metab. Care* **5**:365-370.

80. Luiken, J.J., Coort, S.L., Willems, J., Coumans, W.A., Bonen, A., van der Vusse, G.J., and Glatz, J.F. 2003. Contraction-induced fatty acid translocase/CD36 translocation in rat cardiac myocytes is mediated through AMP-activated protein kinase signaling. *Diabetes* **52**:1627-1634.

81. Luiken, J.J., Dyck, D.J., Han, X.X., Tandon, N.N., Arumugam, Y., Glatz, J.F., and Bonen, A. 2002. Insulin induces the translocation of the fatty acid transporter FAT/CD36 to the plasma membrane. *Am. J. Physiol. Endocrinol. Metab.* **282**:E491-5.

82. Luiken, J.J., Koonen, D.P., Willems, J., Zorzano, A., Becker, C., Fischer, Y., Tandon, N.N., Van Der Vusse, G.J., Bonen, A., and Glatz, J.F. 2002. Insulin stimulates long-chain fatty acid utilization by rat cardiac myocytes through cellular redistribution of FAT/CD36. *Diabetes* **51**:3113-3119.

83. Campbell, S.E., Tandon, N.N., Woldegiorgis, G., Luiken, J.J., Glatz, J.F., and Bonen, A. 2004. A novel function for fatty acid translocase (FAT)/CD36: involvement in long chain fatty acid transfer into the mitochondria. *J. Biol. Chem.* **279**:36235-36241.

84. Bezaire, V., Bruce, C.R., Heigenhauser, G.J., Tandon, N.N., Glatz, J.F., Luiken, J.J., Bonen, A., and Spriet, L.L. 2006. Identification of fatty acid translocase on human skeletal muscle mitochondrial membranes: essential role in fatty acid oxidation. *Am. J. Physiol. Endocrinol. Metab.* **290**:E509-15.

85. Stahl, A., Evans, J.G., Pattel, S., Hirsch, D., and Lodish, H.F. 2002. Insulin causes fatty acid transport protein translocation and enhanced fatty acid uptake in adipocytes. *Dev. Cell.* **2**:477-488.

86. Brinkmann, J.F., Abumrad, N.A., Ibrahimi, A., van der Vusse, G.J., and Glatz, J.F. 2002. New insights into long-chain fatty acid uptake by heart muscle: a crucial role for fatty acid translocase/CD36. *Biochem. J.* **367**:561-570.

87. Zhou, S.L., Stump, D., Sorrentino, D., Potter, B.J., and Berk, P.D. 1992. Adipocyte differentiation of 3T3-L1 cells involves augmented expression of a 43-kDa plasma membrane fatty acid-binding protein. *J. Biol. Chem.* **267**:14456-14461.

88. Bonen, A., Dyck, D.J., Ibrahimi, A., and Abumrad, N.A. 1999. Muscle contractile activity increases fatty acid metabolism and transport and FAT/CD36. *Am. J. Physiol.* **276**:E642-9.

89. Kiens, B., Kristiansen, S., Jensen, P., Richter, E.A., and Turcotte, L.P. 1997. Membrane associated fatty acid binding protein (FABPpm) in human skeletal muscle is increased by endurance training. *Biochem. Biophys. Res. Commun.* **231**:463-465.

90. Turcotte, L.P., Srivastava, A.K., and Chiasson, J.L. 1997. Fasting increases plasma membrane fatty acid-binding protein (FABP(PM)) in red skeletal muscle. *Mol. Cell. Biochem.* **166**:153-158.

91. Coort, S.L., Hasselbaink, D.M., Koonen, D.P., Willems, J., Coumans, W.A., Chabowski, A., van der Vusse, G.J., Bonen, A., Glatz, J.F., and Luiken, J.J. 2004. Enhanced sarcolemmal FAT/CD36 content and triacylglycerol storage in cardiac myocytes from obese zucker rats. *Diabetes* **53**:1655-1663.

92. Coort, S.L., Bonen, A., van der Vusse, G.J., Glatz, J.F., and Luiken, J.J. 2007. Cardiac substrate uptake and metabolism in obesity and type-2 diabetes: role of sarcolemmal substrate transporters. *Mol. Cell. Biochem.* **299**:5-18.

93. Simoneau, J.A., Veerkamp, J.H., Turcotte, L.P., and Kelley, D.E. 1999. Markers of capacity to utilize fatty acids in human skeletal muscle: relation to insulin resistance and obesity and effects of weight loss. *FASEB J.* **13**:2051-2060.

94. Bonen, A., Parolin, M.L., Steinberg, G.R., Calles-Escandon, J., Tandon, N.N., Glatz, J.F., Luiken, J.J., Heigenhauser, G.J., and Dyck, D.J. 2004. Triacylglycerol accumulation in human obesity and type 2 diabetes is associated with increased rates of skeletal muscle fatty acid transport and increased sarcolemmal FAT/CD36. *FASEB J.* **18**:1144-1146.

95. Bonen, A., Luiken, J.J., Arumugam, Y., Glatz, J.F., and Tandon, N.N. 2000. Acute regulation of fatty acid uptake involves the cellular redistribution of fatty acid translocase. *J. Biol. Chem.* **275**:14501-14508.

96. Stephens, F.B., Constantin-Teodosiu, D., and Greenhaff, P.L. 2007. New insights concerning the role of carnitine in the regulation of fuel metabolism in skeletal muscle. *J. Physiol.* **581**:431-444.

97. Selby, P.L., and Sherratt, H.S. 1989. Substituted 2-oxiranecarboxylic acids: a new group of candidate hypoglycaemic drugs. *Trends Pharmacol. Sci.* **10**:495-500.

98. Kelley, D.E., Goodpaster, B., Wing, R.R., and Simoneau, J.A. 1999. Skeletal muscle fatty acid metabolism in association with insulin resistance, obesity, and weight loss. *Am. J. Physiol.* **277**:E1130-41.

99. Merrill, G.F., Kurth, E.J., Hardie, D.G., and Winder, W.W. 1997. AICA riboside increases AMP-activated protein kinase, fatty acid oxidation, and glucose uptake in rat muscle. *Am. J. Physiol.* **273**:E1107-12.

100. Muoio, D.M., Seefeld, K., Witters, L.A., and Coleman, R.A. 1999. AMP-activated kinase reciprocally regulates triacylglycerol synthesis and fatty acid oxidation in liver and muscle: evidence that sn-glycerol-3-phosphate acyltransferase is a novel target. *Biochem. J.* **338 (Pt 3)**:783-791.

101. Saddik, M., Gamble, J., Witters, L.A., and Lopaschuk, G.D. 1993. Acetyl-CoA carboxylase regulation of fatty acid oxidation in the heart. *J. Biol. Chem.* **268**:25836-25845.

102. Awan, M.M., and Saggerson, E.D. 1993. Malonyl-CoA metabolism in cardiac myocytes and its relevance to the control of fatty acid oxidation. *Biochem. J.* **295 (Pt 1)**:61-66.

103. McGarry, J.D. 2002. Banting lecture 2001: dysregulation of fatty acid metabolism in the etiology of type 2 diabetes. *Diabetes* **51**:7-18.

104. Ponticos, M., Lu, Q.L., Morgan, J.E., Hardie, D.G., Partridge, T.A., and Carling, D. 1998. Dual regulation of the AMP-activated protein kinase provides a novel mechanism for the control of creatine kinase in skeletal muscle. *EMBO J.* **17**:1688-1699.

105. Ceddia, R.B., and Sweeney, G. 2004. Creatine supplementation increases glucose oxidation and AMPK phosphorylation and reduces lactate production in L6 rat skeletal muscle cells. *J. Physiol.* **555**:409-421.

106. Hudson, E.R., Pan, D.A., James, J., Lucocq, J.M., Hawley, S.A., Green, K.A., Baba, O., Terashima, T., and Hardie, D.G. 2003. A novel domain in AMP-activated protein kinase causes glycogen storage bodies similar to those seen in hereditary cardiac arrhythmias. *Curr. Biol.* **13**:861-866.

107. Wojtaszewski, J.F., Jorgensen, S.B., Hellsten, Y., Hardie, D.G., and Richter, E.A. 2002. Glycogen-dependent effects of 5-aminoimidazole-4-carboxamide (AICA)-riboside on AMP-activated protein kinase and glycogen synthase activities in rat skeletal muscle. *Diabetes* **51**:284-292.

108. Clark, H., Carling, D., and Saggerson, D. 2004. Covalent activation of heart AMP-activated protein kinase in response to physiological concentrations of long-chain fatty acids. *Eur. J. Biochem.* **271**:2215-2224.

109. Kawaguchi, T., Osatomi, K., Yamashita, H., Kabashima, T., and Uyeda, K. 2002. Mechanism for fatty acid "sparing" effect on glucose-induced transcription: regulation of carbohydrate-responsive element-binding protein by AMP-activated protein kinase. *J. Biol. Chem.* **277**:3829-3835.

110. Taylor, E.B., Ellingson, W.J., Lamb, J.D., Chesser, D.G., and Winder, W.W. 2005. Long-chain acyl-CoA esters inhibit phosphorylation of AMP-activated protein kinase at threonine-172 by LKB1/STRAD/MO25. *Am. J. Physiol. Endocrinol. Metab.* **288**:E1055-61.

111. Munday, M.R. 2002. Regulation of mammalian acetyl-CoA carboxylase. *Biochem. Soc. Trans.* **30**:1059-1064.

112. Chien, D., Dean, D., Saha, A.K., Flatt, J.P., and Ruderman, N.B. 2000. Malonyl-CoA content and fatty acid oxidation in rat muscle and liver in vivo. *Am. J. Physiol. Endocrinol. Metab.* **279**:E259-65.

113. Rosen, O.M. 1986. Insulin receptor as a tyrosine protein kinase. *Ann. N. Y. Acad. Sci.* **463**:13-19.

114. Kahn, C.R., and White, M.F. 1988. The insulin receptor and the molecular mechanism of insulin action. *J. Clin. Invest.* **82**:1151-1156.

115. Kanzaki, M. 2006. Insulin receptor signals regulating GLUT4 translocation and actin dynamics. *Endocr. J.* **53**:267-293.

116. Bjornholm, M., and Zierath, J.R. 2005. Insulin signal transduction in human skeletal muscle: identifying the defects in Type II diabetes. *Biochem. Soc. Trans.* **33**:354-357.

117. Kane, S., Sano, H., Liu, S.C., Asara, J.M., Lane, W.S., Garner, C.C., and Lienhard, G.E. 2002. A method to identify serine kinase substrates. Akt phosphorylates a novel adipocyte protein with a Rab GTPase-activating protein (GAP) domain. *J. Biol. Chem.* **277**:22115-22118.

118. Zerial, M., and McBride, H. 2001. Rab proteins as membrane organizers. *Nat. Rev. Mol. Cell Biol.* **2**:107-117.

119. Brozinick, J.T.,Jr, Berkemeier, B.A., and Elmendorf, J.S. 2007. "Actin"g on GLUT4: membrane & cytoskeletal components of insulin action. *Curr. Diabetes Rev.* **3**:111-122.

120. Kramer, H.F., Witczak, C.A., Fujii, N., Jessen, N., Taylor, E.B., Arnolds, D.E., Sakamoto, K., Hirshman, M.F., and Goodyear, L.J. 2006. Distinct signals regulate AS160 phosphorylation in response to insulin, AICAR, and contraction in mouse skeletal muscle. *Diabetes* **55**:2067-2076.

121. Huang, S., and Czech, M.P. 2007. The GLUT4 glucose transporter. *Cell. Metab.* **5**:237-252.

122. Thorens, B. 1996. Glucose transporters in the regulation of intestinal, renal, and liver glucose fluxes. *Am. J. Physiol.* **270**:G541-53.

123. Hutber, C.A., Hardie, D.G., and Winder, W.W. 1997. Electrical stimulation inactivates muscle acetyl-CoA carboxylase and increases AMP-activated protein kinase. *Am. J. Physiol.* **272**:E262-6.

124. Hayashi, T., Hirshman, M.F., Kurth, E.J., Winder, W.W., and Goodyear, L.J. 1998. Evidence for 5' AMP-activated protein kinase mediation of the effect of muscle contraction on glucose transport. *Diabetes* **47**:1369-1373.

125. Koistinen, H.A., Galuska, D., Chibalin, A.V., Yang, J., Zierath, J.R., Holman, G.D., and Wallberg-Henriksson, H. 2003. 5-amino-imidazole carboxamide riboside increases glucose transport and cell-surface GLUT4 content in skeletal muscle from subjects with type 2 diabetes. *Diabetes* **52**:1066-1072.

126. Mu, J., Brozinick, J.T.,Jr, Valladares, O., Bucan, M., and Birnbaum, M.J. 2001. A role for AMP-activated protein kinase in contraction- and hypoxia-regulated glucose transport in skeletal muscle. *Mol. Cell* **7**:1085-1094.

127. Winder, W.W., Hardie, D.G., Mustard, K.J., Greenwood, L.J., Paxton, B.E., Park, S.H., Rubink, D.S., and Taylor, E.B. 2003. Long-term regulation of AMP-activated protein kinase and acetyl-CoA carboxylase in skeletal muscle. *Biochem. Soc. Trans.* **31**:182-185.

128. Wright, D.C., Geiger, P.C., Holloszy, J.O., and Han, D.H. 2005. Contraction- and hypoxia-stimulated glucose transport is mediated by a Ca2+-dependent mechanism in slow-twitch rat soleus muscle. *Am. J. Physiol. Endocrinol. Metab.* **288**:E1062-6.

129. Wright, D.C., Hucker, K.A., Holloszy, J.O., and Han, D.H. 2004. Ca2+ and AMPK both mediate stimulation of glucose transport by muscle contractions. *Diabetes* **53**:330-335.

130. Fujii, N., Hirshman, M.F., Kane, E.M., Ho, R.C., Peter, L.E., Seifert, M.M., and Goodyear, L.J. 2005. AMP-activated protein kinase alpha2 activity is not essential for contraction- and hyperosmolarity-induced glucose transport in skeletal muscle. *J. Biol. Chem.* **280**:39033-39041.

131. Jorgensen, S.B., Viollet, B., Andreelli, F., Frosig, C., Birk, J.B., Schjerling, P., Vaulont, S., Richter, E.A., and Wojtaszewski, J.F. 2004. Knockout of the alpha2 but not alpha1 5'-AMP-activated protein kinase isoform abolishes 5-aminoimidazole-4-carboxamide-1-beta-4-ribofuranosidebut not contraction-induced glucose uptake in skeletal muscle. *J. Biol. Chem.* **279**:1070-1079.

132. Marsin, A.S., Bertrand, L., Rider, M.H., Deprez, J., Beauloye, C., Vincent, M.F., Van den Berghe, G., Carling, D., and Hue, L. 2000. Phosphorylation and activation of heart PFK-2 by AMPK has a role in the stimulation of glycolysis during ischaemia. *Curr. Biol.* **10**:1247-1255.

133. Tirone, T.A., and Brunicardi, F.C. 2001. Overview of glucose regulation. *World J. Surg.* **25**:461-467.

134. Shulman, G.I. 2000. Cellular mechanisms of insulin resistance. *J. Clin. Invest.* **106**:171-176.

135. Ferrer, J.C., Favre, C., Gomis, R.R., Fernandez-Novell, J.M., Garcia-Rocha, M., de la Iglesia, N., Cid, E., and Guinovart, J.J. 2003. Control of glycogen deposition. *FEBS Lett.* **546**:127-132.

136. Nielsen, J.N., and Richter, E.A. 2003. Regulation of glycogen synthase in skeletal muscle during exercise. *Acta Physiol. Scand.* **178**:309-319.

137. Nielsen, J.N., and Wojtaszewski, J.F. 2004. Regulation of glycogen synthase activity and phosphorylation by exercise. *Proc. Nutr. Soc.* **63**:233-237.

138. Lee, J., and Kim, M.S. 2007. The role of GSK3 in glucose homeostasis and the development of insulin resistance. *Diabetes Res. Clin. Pract.* **77 Suppl 1**:S49-57.

139. Skurat, A.V., and Roach, P.J. 1995. Phosphorylation of sites 3a and 3b (Ser640 and Ser644) in the control of rabbit muscle glycogen synthase. *J. Biol. Chem.* **270**:12491-12497.

140. Zachwieja, J.J., Costill, D.L., Pascoe, D.D., Robergs, R.A., and Fink, W.J. 1991. Influence of muscle glycogen depletion on the rate of resynthesis. *Med. Sci. Sports Exerc.* **23**:44-48.

141. Nielsen, J.N., Wojtaszewski, J.F., Haller, R.G., Hardie, D.G., Kemp, B.E., Richter, E.A., and Vissing, J. 2002. Role of 5'AMP-activated protein kinase in glycogen synthase activity and glucose utilization: insights from patients with McArdle's disease. *J. Physiol.* **541**:979-989.

142. Hiraga, A., and Cohen, P. 1986. Phosphorylation of the glycogen-binding subunit of protein phosphatase-1G by cyclic-AMP-dependent protein kinase promotes translocation of the phosphatase from glycogen to cytosol in rabbit skeletal muscle. *Eur. J. Biochem.* **161**:763-769.

143. Dent, P., Lavoinne, A., Nakielny, S., Caudwell, F.B., Watt, P., and Cohen, P. 1990. The molecular mechanism by which insulin stimulates glycogen synthesis in mammalian skeletal muscle. *Nature* **348**:302-308.

144. Wojtaszewski, J.F., Nielsen, J.N., Jorgensen, S.B., Frosig, C., Birk, J.B., and Richter, E.A. 2003. Transgenic models--a scientific tool to understand exercise-induced metabolism: the regulatory role of AMPK (5'-AMP-activated protein kinase) in glucose transport and glycogen synthase activity in skeletal muscle. *Biochem. Soc. Trans.* **31**:1290-1294.

145. Carling, D., and Hardie, D.G. 1989. The substrate and sequence specificity of the AMP-activated protein kinase. Phosphorylation of glycogen synthase and phosphorylase kinase. *Biochim. Biophys. Acta* **1012**:81-86.

146. Aschenbach, W.G., Hirshman, M.F., Fujii, N., Sakamoto, K., Howlett, K.F., and Goodyear, L.J. 2002. Effect of AICAR treatment on glycogen metabolism in skeletal muscle. *Diabetes* **51**:567-573.

147. Young, M.E., Radda, G.K., and Leighton, B. 1996. Activation of glycogen phosphorylase and glycogenolysis in rat skeletal muscle by AICAR--an activator of AMP-activated protein kinase. *FEBS Lett.* **382**:43-47.

148. Winder, W.W., Holmes, B.F., Rubink, D.S., Jensen, E.B., Chen, M., and Holloszy, J.O. 2000. Activation of AMP-activated protein kinase increases mitochondrial enzymes in skeletal muscle. *J. Appl. Physiol.* **88**:2219-2226.

149. Jakobsen, S.N., Hardie, D.G., Morrice, N., and Tornqvist, H.E. 2001. 5'-AMP-activated protein kinase phosphorylates IRS-1 on Ser-789 in mouse C2C12 myotubes in response to 5-aminoimidazole-4-carboxamide riboside. *J. Biol. Chem.* **276**:46912-46916.

150. De Fea, K., and Roth, R.A. 1997. Modulation of insulin receptor substrate-1 tyrosine phosphorylation and function by mitogen-activated protein kinase. *J. Biol. Chem.* **272**:31400-31406.

151. Gladden, L.B. 2004. Lactate metabolism: a new paradigm for the third millennium. *J. Physiol.* **558**:5-30.

152. Boon, H., Bosselaar, M., Praet, S.F., Blaak, E.E., Saris, W.H., Wagenmakers, A.J., McGee, S.L., Tack, C.J., Smits, P., Hargreaves, M. et al. 2008. Intravenous AICAR administration reduces hepatic glucose output and inhibits whole body lipolysis in type 2 diabetic patients. *Diabetologia* **51**:1893-1900.

153. Bergeron, R., Russell, R.R.,3rd, Young, L.H., Ren, J.M., Marcucci, M., Lee, A., and Shulman, G.I. 1999. Effect of AMPK activation on muscle glucose metabolism in conscious rats. *Am. J. Physiol.* **276**:E938-44.

154. Poortmans, J.R. 2004. *Principles of Exercise Biochemistry.* 3rd. revised edition edition. Karger. Basel, Switzerland.

155. Gladden, L.B. 2000. Muscle as a consumer of lactate. *Med. Sci. Sports Exerc.* **32**:764-771.

156. Gladden, L.B. 2008. A lactatic perspective on metabolism. *Med. Sci. Sports Exerc.* **40**:477-485.

157. Brooks, G.A. 2000. Intra- and extra-cellular lactate shuttles. *Med. Sci. Sports Exerc.* **32**:790-799.

158. Richter, E.A., Kiens, B., Saltin, B., Christensen, N.J., and Savard, G. 1988. Skeletal muscle glucose uptake during dynamic exercise in humans: role of muscle mass. *Am. J. Physiol.* **254**:E555-61.

159. Baldwin, K.M., Campbell, P.J., and Cooke, D.A. 1977. Glycogen, lactate, and alanine changes in muscle fiber types during graded exercise. *J. Appl. Physiol.* **43**:288-291.

160. Stanley, W.C., Gertz, E.W., Wisneski, J.A., Neese, R.A., Morris, D.L., and Brooks, G.A. 1986. Lactate extraction during net lactate release in legs of humans during exercise. *J. Appl. Physiol.* **60**:1116-1120.

161. Choi, C.S., Kim, Y.B., Lee, F.N., Zabolotny, J.M., Kahn, B.B., and Youn, J.H. 2002. Lactate induces insulin resistance in skeletal muscle by suppressing glycolysis and impairing insulin signaling. *Am. J. Physiol. Endocrinol. Metab.* **283**:E233-40.

162. Brunmair, B., Staniek, K., Gras, F., Scharf, N., Althaym, A., Clara, R., Roden, M., Gnaiger, E., Nohl, H., Waldhausl, W. et al. 2004. Thiazolidinediones, like metformin, inhibit respiratory complex I: a common mechanism contributing to their antidiabetic actions? *Diabetes* **53**:1052-1059.

163. Furnsinn, C., Brunmair, B., Meyer, M., Neschen, S., Furtmuller, R., Roden, M., Kuhnle, H.F., Nowotny, P., Schneider, B., and Waldhausl, W. 1999. Chronic and acute effects of thiazolidinediones BM13.1258 and BM15.2054 on rat skeletal muscle glucose metabolism. *Br. J. Pharmacol.* **128**:1141-1148.

164. Iglesias, M.A., Furler, S.M., Cooney, G.J., Kraegen, E.W., and Ye, J.M. 2004. AMP-activated protein kinase activation by AICAR increases both muscle fatty acid and glucose uptake in white muscle of insulin-resistant rats in vivo. *Diabetes* **53**:1649-1654.

165. Patel, M.S., and Korotchkina, L.G. 2006. Regulation of the pyruvate dehydrogenase complex. *Biochem. Soc. Trans.* **34**:217-222.

166. Nelson D.L., and Cox M.M. 2005. *Lehninger Principles of Biochemistry.* 4th edition.

167. Strumilo, S. 2005. Short-term regulation of the mammalian pyruvate dehydrogenase complex. *Acta Biochim. Pol.* **52**:759-764.

168. Sugden, M.C., and Holness, M.J. 1994. Interactive regulation of the pyruvate dehydrogenase complex and the carnitine palmitoyltransferase system. *FASEB J.* **8**:54-61.

169. Harris, R.A., Bowker-Kinley, M.M., Huang, B., and Wu, P. 2002. Regulation of the activity of the pyruvate dehydrogenase complex. *Adv. Enzyme Regul.* **42**:249-259.

170. Bao, H., Kasten, S.A., Yan, X., Hiromasa, Y., and Roche, T.E. 2004. Pyruvate dehydrogenase kinase isoform 2 activity stimulated by speeding up the rate of dissociation of ADP. *Biochemistry* **43**:13442-13451.

171. Klein, D.K., Pilegaard, H., Treebak, J.T., Jensen, T.E., Viollet, B., Schjerling, P., and Wojtaszewski, J.F. 2007. Lack of AMPKalpha2 enhances pyruvate dehydrogenase activity during exercise. *Am. J. Physiol. Endocrinol. Metab.* **293**:E1242-9.

172. Folmes, C.D., and Lopaschuk, G.D. 2007. Role of malonyl-CoA in heart disease and the hypothalamic control of obesity. *Cardiovasc. Res.* **73**:278-287.

173. van Loon, L.J., and Goodpaster, B.H. 2006. Increased intramuscular lipid storage in the insulin-resistant and endurance-trained state. *Pflugers Arch.* **451**:606-616.

174. RANDLE, P.J., GARLAND, P.B., HALES, C.N., and NEWSHOLME, E.A. 1963. The glucose fatty-acid cycle. Its role in insulin sensitivity and the metabolic disturbances of diabetes mellitus. *Lancet* **1**:785-789.

175. Ferrannini, E., Barrett, E.J., Bevilacqua, S., and DeFronzo, R.A. 1983. Effect of fatty acids on glucose production and utilization in man. *J. Clin. Invest.* **72**:1737-1747.

176. Kelley, D.E., Mokan, M., Simoneau, J.A., and Mandarino, L.J. 1993. Interaction between glucose and free fatty acid metabolism in human skeletal muscle. *J. Clin. Invest.* **92**:91-98.

177. Consoli, A. 1992. Role of liver in pathophysiology of NIDDM. *Diabetes Care* **15**:430-441.

178. Bergeron, R., Previs, S.F., Cline, G.W., Perret, P., Russell, R.R.,3rd, Young, L.H., and Shulman, G.I. 2001. Effect of 5-aminoimidazole-4-carboxamide-1-beta-D-ribofuranoside infusion on in vivo glucose and lipid metabolism in lean and obese Zucker rats. *Diabetes* **50**:1076-1082.

179. Viollet, B., Foretz, M., Guigas, B., Horman, S., Dentin, R., Bertrand, L., Hue, L., and Andreelli, F. 2006. Activation of AMP-activated protein kinase in the liver: a new strategy for the management of metabolic hepatic disorders. *J. Physiol.* **574**:41-53.

180. Pencek, R.R., Shearer, J., Camacho, R.C., James, F.D., Lacy, D.B., Fueger, P.T., Donahue, E.P., Snead, W., and Wasserman, D.H. 2005. 5-Aminoimidazole-4-carboxamide-1-beta-D-ribofuranoside causes acute hepatic insulin resistance in vivo. *Diabetes* **54**:355-360.

181. Guigas, B., Bertrand, L., Taleux, N., Foretz, M., Wiernsperger, N., Vertommen, D., Andreelli, F., Viollet, B., and Hue, L. 2006. 5-Aminoimidazole-4-carboxamide-1-beta-D-ribofuranoside and metformin inhibit hepatic glucose phosphorylation by an AMP-activated protein kinase-independent effect on glucokinase translocation. *Diabetes* **55**:865-874.

182. Grimsby, J., Sarabu, R., Corbett, W.L., Haynes, N.E., Bizzarro, F.T., Coffey, J.W., Guertin, K.R., Hilliard, D.W., Kester, R.F., Mahaney, P.E. et al. 2003. Allosteric activators of glucokinase: potential role in diabetes therapy. *Science* **301**:370-373.

183. Foretz, M., Carling, D., Guichard, C., Ferre, P., and Foufelle, F. 1998. AMP-activated protein kinase inhibits the glucose-activated expression of fatty acid synthase gene in rat hepatocytes. *J. Biol. Chem.* **273**:14767-14771.

184. Woods, A., Azzout-Marniche, D., Foretz, M., Stein, S.C., Lemarchand, P., Ferre, P., Foufelle, F., and Carling, D. 2000. Characterization of the role of AMP-activated protein kinase in the regulation of glucose-activated gene expression using constitutively active and dominant negative forms of the kinase. *Mol. Cell. Biol.* **20**:6704-6711.

185. Guilherme, A., Virbasius, J.V., Puri, V., and Czech, M.P. 2008. Adipocyte dysfunctions linking obesity to insulin resistance and type 2 diabetes. *Nat. Rev. Mol. Cell Biol.* **9**:367-377.

186. Sullivan, J.E., Brocklehurst, K.J., Marley, A.E., Carey, F., Carling, D., and Beri, R.K. 1994. Inhibition of lipolysis and lipogenesis in isolated rat adipocytes with AICAR, a cell-permeable activator of AMP-activated protein kinase. *FEBS Lett.* **353**:33-36.

187. Andersson, U., Filipsson, K., Abbott, C.R., Woods, A., Smith, K., Bloom, S.R., Carling, D., and Small, C.J. 2004. AMP-activated protein kinase plays a role in the control of food intake. *J. Biol. Chem.* **279**:12005-12008.

188. Kim, E.K., Miller, I., Aja, S., Landree, L.E., Pinn, M., McFadden, J., Kuhajda, F.P., Moran, T.H., and Ronnett, G.V. 2004. C75, a fatty acid synthase inhibitor, reduces food intake via hypothalamic AMP-activated protein kinase. *J. Biol. Chem.* **279**:19970-19976.

189. Hu, Z., Dai, Y., Prentki, M., Chohnan, S., and Lane, M.D. 2005. A role for hypothalamic malonyl-CoA in the control of food intake. *J. Biol. Chem.* **280**:39681-39683.

190. Cha, S.H., Hu, Z., Chohnan, S., and Lane, M.D. 2005. Inhibition of hypothalamic fatty acid synthase triggers rapid activation of fatty acid oxidation in skeletal muscle. *Proc. Natl. Acad. Sci. U. S. A.* **102**:14557-14562.

191. Musi, N., Hayashi, T., Fujii, N., Hirshman, M.F., Witters, L.A., and Goodyear, L.J. 2001. AMP-activated protein kinase activity and glucose uptake in rat skeletal muscle. *Am. J. Physiol. Endocrinol. Metab.* **280**:E677-84.

192. Pold, R., Jensen, L.S., Jessen, N., Buhl, E.S., Schmitz, O., Flyvbjerg, A., Fujii, N., Goodyear, L.J., Gotfredsen, C.F., Brand, C.L. et al. 2005. Long-term AICAR administration and exercise prevents diabetes in ZDF rats. *Diabetes* **54**:928-934.

193. Ceddia, R.B., William, W.N.,Jr, Lima, F.B., Flandin, P., Curi, R., and Giacobino, J.P. 2000. Leptin stimulates uncoupling protein-2 mRNA expression and Krebs cycle activity and inhibits lipid synthesis in isolated rat white adipocytes. *Eur. J. Biochem.* **267**:5952-5958.

194. Ruderman, N.B., Saha, A.K., Vavvas, D., and Witters, L.A. 1999. Malonyl-CoA, fuel sensing, and insulin resistance. *Am. J. Physiol.* **276**:E1-E18.

195. Curi, R., Newsholme, P., and Newsholme, E.A. 1988. Metabolism of pyruvate by isolated rat mesenteric lymphocytes, lymphocyte mitochondria and isolated mouse macrophages. *Biochem. J.* **250**:383-388.

196. Ceddia, R.B., William, W.N.,Jr, and Curi, R. 1999. Comparing effects of leptin and insulin on glucose metabolism in skeletal muscle: evidence for an effect of leptin on glucose uptake and decarboxylation. *Int. J. Obes. Relat. Metab. Disord.* **23**:75-82.

197. Spurway, T.D., Agius, L., Stanley, H., Sherratt, A., and Pogson, C.I. 1994. Measurement of carnitine palmitoyltransferase I in hepatocyte monolayers. *Biochem. Soc. Trans.* **22**:118S.

198. Fediuc, S., Gaidhu, M.P., and Ceddia, R.B. 2006. Inhibition of insulin-stimulated glycogen synthesis by 5-aminoimidasole-4-carboxamide-1-beta-d-ribofuranoside-induced adenosine 5'-monophosphate-activated protein kinase activation: interactions with Akt, glycogen synthase kinase 3-3alpha/beta, and glycogen synthase in isolated rat soleus muscle. *Endocrinology* **147**:5170-5177.

199. Lowry OH, Passonneau JV. 1972. *A flexible system of enzymatic analysis.* 1st edn. edition. Academic Press. New York. 1-291pp.

200. Henriksen, E.J., Bourey, R.E., Rodnick, K.J., Koranyi, L., Permutt, M.A., and Holloszy, J.O. 1990. Glucose transporter protein content and glucose transport capacity in rat skeletal muscles. *Am. J. Physiol.* **259**:E593-8.

201. Young, D.A., Uhl, J.J., Cartee, G.D., and Holloszy, J.O. 1986. Activation of glucose transport in muscle by prolonged exposure to insulin. Effects of glucose and insulin concentrations. *J. Biol. Chem.* **261**:16049-16053.

202. Fujitaki, J.M., Sandoval, T.M., Lembach, L.A., and Dixon, R. 1994. Spectrophotometric determination of acadesine (AICA-riboside) in plasma using a diazotization coupling technique with N-(1-naphthyl)ethylenediamine. *J. Biochem. Biophys. Methods* **29**:143-148.

203. Roden, M. 2004. How free fatty acids inhibit glucose utilization in human skeletal muscle. *News Physiol. Sci.* **19**:92-96.

204. Rutter, G.A., Da Silva Xavier, G., and Leclerc, I. 2003. Roles of 5'-AMP-activated protein kinase (AMPK) in mammalian glucose homoeostasis. *Biochem. J.* **375**:1-16.

205. Hardie, D.G., and Pan, D.A. 2002. Regulation of fatty acid synthesis and oxidation by the AMP-activated protein kinase. *Biochem. Soc. Trans.* **30**:1064-1070.

206. Trumble, G.E., Smith, M.A., and Winder, W.W. 1995. Purification and characterization of rat skeletal muscle acetyl-CoA carboxylase. *Eur. J. Biochem.* **231**:192-198.

207. Halestrap, A.P., and Denton, R.M. 1974. Hormonal regulation of adipose-tissue acetyl-Coenzyme A carboxylase by changes in the polymeric state of the enzyme. The role of long-chain fatty acyl-Coenzyme A thioesters and citrate. *Biochem. J.* **142**:365-377.

208. Mayes, P.A., and Topping, D.L. 1974. Regulation of hepatic lipogenesis by plasma free fatty acids: simultaneous studies on lipoprotein secretion, cholesterol synthesis, ketogenesis and gluconeogenesis. *Biochem. J.* **140**:111-114.

209. Ceddia, R.B. 2005. Direct metabolic regulation in skeletal muscle and fat tissue by leptin: implications for glucose and fatty acids homeostasis. *Int. J. Obes. (Lond)* **29**:1175-1183.

210. Kadowaki, T., and Yamauchi, T. 2005. Adiponectin and adiponectin receptors. *Endocr. Rev.* **26**:439-451.

211. Brown, K.K., Henke, B.R., Blanchard, S.G., Cobb, J.E., Mook, R., Kaldor, I., Kliewer, S.A., Lehmann, J.M., Lenhard, J.M., Harrington, W.W. et al. 1999. A novel N-aryl tyrosine activator of peroxisome proliferator-activated receptor-gamma reverses the diabetic phenotype of the Zucker diabetic fatty rat. *Diabetes* **48**:1415-1424.

212. Plosker, G.L., and Faulds, D. 1999. Troglitazone: a review of its use in the management of type 2 diabetes mellitus. *Drugs* **57**:409-438.

213. Carling, D. 2005. AMP-activated protein kinase: balancing the scales. *Biochimie* **87**:87-91.

214. Nielsen, J.N., and Wojtaszewski, J.F. 2004. Regulation of glycogen synthase activity and phosphorylation by exercise. *Proc. Nutr. Soc.* **63**:233-237.

215. Carling, D., and Hardie, D.G. 1989. The substrate and sequence specificity of the AMP-activated protein kinase. Phosphorylation of glycogen synthase and phosphorylase kinase. *Biochim. Biophys. Acta* **1012**:81-86.

216. Campbell, S.E., Tandon, N.N., Woldegiorgis, G., Luiken, J.J., Glatz, J.F., and Bonen, A. 2004. A novel function for fatty acid translocase (FAT)/CD36: involvement in long chain fatty acid transfer into the mitochondria. *J. Biol. Chem.* **279**:36235-36241.

217. Bonen, A., Han, X.X., Habets, D.D., Febbraio, M., Glatz, J.F., and Luiken, J.J. 2007. A null mutation in skeletal muscle FAT/CD36 reveals its essential role in insulin- and AICAR-stimulated fatty acid metabolism. *Am. J. Physiol. Endocrinol. Metab.* **292**:E1740-9.

218. Pette, D., and Staron, R.S. 1990. Cellular and molecular diversities of mammalian skeletal muscle fibers. *Rev. Physiol. Biochem. Pharmacol.* **116**:1-76.

219. Barnes, B.R., Marklund, S., Steiler, T.L., Walter, M., Hjalm, G., Amarger, V., Mahlapuu, M., Leng, Y., Johansson, C., Galuska, D. et al. 2004. The 5'-AMP-activated protein kinase gamma3 isoform has a key role in carbohydrate and lipid metabolism in glycolytic skeletal muscle. *J. Biol. Chem.* **279**:38441-38447.

220. Chen, Z., Heierhorst, J., Mann, R.J., Mitchelhill, K.I., Michell, B.J., Witters, L.A., Lynch, G.S., Kemp, B.E., and Stapleton, D. 1999. Expression of the AMP-activated protein kinase beta1 and beta2 subunits in skeletal muscle. *FEBS Lett.* **460**:343-348.

221. Mahlapuu, M., Johansson, C., Lindgren, K., Hjalm, G., Barnes, B.R., Krook, A., Zierath, J.R., Andersson, L., and Marklund, S. 2004. Expression profiling of the gamma-subunit isoforms of AMP-activated protein kinase suggests a major role for gamma3 in white skeletal muscle. *Am. J. Physiol. Endocrinol. Metab.* **286**:E194-200.

222. Jhun, B.S., Oh, Y.T., Lee, J.Y., Kong, Y., Yoon, K.S., Kim, S.S., Baik, H.H., Ha, J., and Kang, I. 2005. AICAR suppresses IL-2 expression through inhibition of GSK-3 phosphorylation and NF-AT activation in Jurkat T cells. *Biochem. Biophys. Res. Commun.* **332**:339-346.

223. King, T.D., Song, L., and Jope, R.S. 2006. AMP-activated protein kinase (AMPK) activating agents cause dephosphorylation of Akt and glycogen synthase kinase-3. *Biochem. Pharmacol.* **71**:1637-1647.

224. Eldar-Finkelman, H., and Krebs, E.G. 1997. Phosphorylation of insulin receptor substrate 1 by glycogen synthase kinase 3 impairs insulin action. *Proc. Natl. Acad. Sci. U. S. A.* **94**:9660-9664.

225. Ravichandran, L.V., Esposito, D.L., Chen, J., and Quon, M.J. 2001. Protein kinase C-zeta phosphorylates insulin receptor substrate-1 and impairs its ability to activate phosphatidylinositol 3-kinase in response to insulin. *J. Biol. Chem.* **276**:3543-3549.

226. Heilbronn, L.K., de Jonge, L., Frisard, M.I., DeLany, J.P., Larson-Meyer, D.E., Rood, J., Nguyen, T., Martin, C.K., Volaufova, J., Most, M.M. et al. 2006. Effect of 6-month calorie restriction on biomarkers of longevity, metabolic adaptation, and oxidative stress in overweight individuals: a randomized controlled trial. *JAMA* **295**:1539-1548.

227. Buhl, E.S., Jessen, N., Schmitz, O., Pedersen, S.B., Pedersen, O., Holman, G.D., and Lund, S. 2001. Chronic treatment with 5-aminoimidazole-4-carboxamide-1-beta-D-ribofuranoside increases insulin-stimulated glucose uptake and GLUT4 translocation in rat skeletal muscles in a fiber type-specific manner. *Diabetes* **50**:12-17.

228. Yu, X., McCorkle, S., Wang, M., Lee, Y., Li, J., Saha, A.K., Unger, R.H., and Ruderman, N.B. 2004. Leptinomimetic effects of the AMP kinase activator AICAR in leptin-resistant rats: prevention of diabetes and ectopic lipid deposition. *Diabetologia* **47**:2012-2021.

229. Pold, R., Jensen, L.S., Jessen, N., Buhl, E.S., Schmitz, O., Flyvbjerg, A., Fujii, N., Goodyear, L.J., Gotfredsen, C.F., Brand, C.L. et al. 2005. Long-term AICAR administration and exercise prevents diabetes in ZDF rats. *Diabetes* **54**:928-934.

230. Friedman, J.M., and Halaas, J.L. 1998. Leptin and the regulation of body weight in mammals. *Nature* **395**:763-770.

231. Narkar, V.A., Downes, M., Yu, R.T., Embler, E., Wang, Y.X., Banayo, E., Mihaylova, M.M., Nelson, M.C., Zou, Y., Juguilon, H. et al. 2008. AMPK and PPARdelta agonists are exercise mimetics. *Cell* **134**:405-415.

9. APPENDICES

9.1 Appendix A: Detailed Methods

Muscle incubation with D-U-^{14}C-glucose:

Preparation of KHB:

- For 24 scintilation vials, prepare 100ml of KHB buffer

1. Add 10 ml of Stock 1 to 80ml of ddH20 and gassifie with 95% O2 and 5% C02 for 45 minutes. This saturates the medium with 02 and prevents the precipitation of HCO3 (bicarbonate).

2. Add 10 ml of Stock 2 and PH to 7.4.

3. Add d-glucose (concentration in buffer either 6mM or 8mM (glucose uptake only)). This gives the muscle metabolic fuel to maintain it for the whole incubation time.

4. Add BSA (concentration in buffer 4%). This maintains the osmolality of the medium.

5. Now buffer is ready.

- Label scintillation vials:

1. label two sets of scintillation vials with the exact same conditions (one set for pre-incubation with buffer only and the second for incubation with the various conditions).

- Split KHB solution in half: 50ml for pre-incubation and 50 for the various conditions with radioactive medium. The muscles are pre-incubated in 2ml volume of buffer but are incubated in 1.5ml volume. This is done in order to save radioactive isotope. Therefore, you only need 36ml for the actual incubation. Prepare 38 ml to have an additional 2 ml to prepare insulin if necessary.

- Pipette 2ml of KHB buffer in all 24 vials for the pre-incubation.

- Pipette 1.5 ml of radioactive KHB (0.2μCi/ml of radioactivity)

- Prepare the various conditions:

1. AICAR stock is 100mM, and you need 2mM concentration in 2 ml of KHB buffer.

2. Add amount of KHB buffer needed to obtain a final volume of 2 ml in each vial. For this you need to subtract the volume of AICAR from the final volume of 2 ml. Therefore, amount of KHB buffer added should be less than 2ml.
3. For the controls, add the same amount of vehicle as was added of AICAR.

Buffers used for muscle incubation:

Krebs-Hanseleit bicarbonate buffer (KHB) or Krebs-Ringer bicarbonate buffer (KRB)

Chemicals	KHB[1]	KHB[2]	KRB[3]
NaCl (mw =58.44)	118.5 mM	116 mM	119 mM
KCl (mw = 74.55)	4.7 mM	4.6 mM	5 mM
$CaCl_2$ (mw = 147.02)	3.4 mM	2.5 mM	3 mM
KH_2PO_4 (mw = 136.09)	1.2 mM	1.16 mM	1 mM
$MgSO_4$ (mw = 120.39)	1.2 mM	1.16 mM	1 mM
$NaHCO_3$ (mw = 84.01)	25 mM	25.3 mM	25 mM

[1]Wallberg-Henriksson H. Acta Physiol Scand (Suppl.) 564:1-80, 1987.
[2]Brozinick JT Jr. Methods Mol Med. 83:163-9. Diabetes Mellitus: Methods and Protocols Edited by: S. Ozcan, Human Press Inc. Totowa, NJ. 2003.
[3]Goldberg AL, Martel SB, Kushmerick MJ. Methods Enzymol 39:82-94, 1975.

Prepare [1]KHB: (used for incubating muscles for up to 12h, for long-term incubations, the medium may be supplemented with pyrubate (1-2 mM) to enable the muscle to direct more of its glucose to glycogen.)

Stock 1 (10x):

Reagents (molarities)	**For 100ml of H_20**	**For 200ml of H_2O**
NaCl-mw=58.44 (1.185 M)	6.93 g	13.85 g
KCl-mw=74.55 (0.047 M)	0.35015 g	0.70030 g
KH_2PO_4-mw=136.09 (0.012 M)	0.16327 g	0.32654 g
$NaHCO_3$-mw=84.01 (0.25 M)	2.1025 g	4.205 g

$NaHCO_3$ needs to be gassed (95%O_2;5%CO_2) for 1h, when first prepared.

Stock 2 (10x):

Reagents (molarities)	**For 100ml of H_2O**	**For 200ml of H_2O**
$CaCl_2$-mw=110.9 (0.034 M)	0.37737 g	0.75473 g
$MgSO_4$-mw=120.39 (0.012 M)	0.14447 g	0.28894 g

- Prepare buffer by first diluting 50ml of stock 1 in 395 ml of ddH_2O and gas with 95%O_2:5%CO_2 for 20-30 min.
- Add 50ml of stock 2 and check pH, it should be close to 7.4.
- Add mannitol (mw=182.2) [32mM final] (583.04mg in 100ml). Only add mannitol for glucose uptake if you need to calculate extracellular space.
- Add D-glucose (mw=180.16) [8mM] (144.13 mg in 100ml).
- Fat-free BSA (0.1% w/v) (100mg in 100ml)
- Check pH again (should be 7.4)
- Bring volume to 500ml by adding ddH_2O.

Glycogen synthesis in Rat soleus or Epitrochlearis muscles:

Use 40-50g rats for this experiment. The size of the muscle is ideal. Fast the animals overnight to obtain a better insulin response.

1. Prepare KHB (6mM glucose).

2. Anesthetize animals with Ketamine/Xylazine cocktail (0.2ml/100g B.W.).

3. Dissect muscles in the following order, soleus, soleus, epi, epi.

4. Pre-incubate muscle in KHB for 1 hour. Use 2ml of KHB per vial for pre-incubation. Gasify the muscles with carbogen ($95\%O_2;5\%CO_2$). Keep track of time to make sure everything is per-incubated for exactly 1 hour.

5. Have a second set of vials ready with respective conditions (i.e. AICAR, Insulin etc.). This set will also have the ^{14}C-D-glucose (0.2μCi/ml). Prepare more than needed to have for totals. Use 1.5ml of medium/ vial.

6. Pre-incubate all conditions of the second set of vials at 37°C.

7. After the muscles are pre-incubated for 1h in KHB, transfer the muscle to labeled medium with the various condition. Incubate for 1 hour. Keep track of the time the incubation begins for each muscle.

8. Once incubation is complete, rinse muscles in cold PBS and weigh. Record the weight.

9. Freeze in liquid nitrogen immediately. (Have 1.5 ml eppendorf tubes ready labeled).

10. After all muscles have been removed from the radioactive medium and frozen, remove the tubes from the liquid nitrogen and add 500μl of 1M KOH to each tube and heat to 65°C for 1 hour.
11. Vortex until muscle is completely dissolved.

12. Take 400μl of dissolved muscle sample and place in a 2ml eppendorf tube. Now add 100μl of glycogen carrier (25mg/ml, Sigma, Glycogen, G-8751).

13. Perform a Bradford assay on the other 100μl to obtain protein content or perform a glycogen content assay.

14. Heat all samples at 95°C for 5 minutes (this allows the radiolabeled glycogen to form a pellet with the glycogen carrier. This also denatures any enzymes involved in glycogen metabolism).

15. To each tube add 80µl of saturated Na_2SO_4 (this forms crystals, ie precipitates with the glycogen once ethanol is added).

16. Now add 1.2ml of cold (-20 °C) Ethanol (100%). This is used to precipitate the glycogen.

17. Vortex all tubes for 1-2 seconds and gently to prevent leakage of ethanol.

18. Keep the tubes in the -20°C freezer overnight to allow the precipitation to occur.

Day 2: (This procedure gets rid of all remaining radioactive metabolic byproducts other than glycogen):

1. Centrifuge all tubes at 8000rpm for 20 min.

2. Discard supernatant by inverting the tubes and dumping it out. Dissolve the pellet in 500µl of H_2O (use the water bath/heat block if needed). Use care when vortexing all tubes to avoid leakage of radiolabeled contents. (steps 3-4 do not need to be performed. It works better if they are not performed and moved straight on to step 6.)

Optional: Results are better without performing this step.

3. **Add 1.2 ml of cold ethanol and place tubes in freezer for 10-20 minutes.**
4. **Centrifuge all tubes at 3000rpm for 10-20 minutes.**
5. **Dissolve pellet in 500µl of H_2O.**

6. Transfer 400µl of solution to scintillation vials for counting.

Glucose uptake experiment in muscle:

2-deoxy-D-glucose (2-DG) stock solution-10M

2-DG from Bioshop Canada Cat#DXG498.1 1g Can$42.00.
Dissolve 821mg of 2-DG in0.5ml of H_2O, make aliquots of 50µl, and store in the Freezer.

Muscle incubation:

1. Fast the animals overnight and anaesthetize them (ketamine/xylazine, 0.2ml/100g of body weight) immediately before the experiment. Extract intact soleus or epitrochlearis from 45-55g rats. Soleus muscle should not weigh more than 20-25mg. In fact, 15-20mg muscles (which are thinner) respond better and if the animals used are of larger size (i.e. 100-150g) cut 15-20mg strips of the muscle. Epitrochlearis is predominantly 85% fast twitch.

2. Quickly extract the muscles, remove any additional connective tissue, rinse in KHB, blot the muscle on filter paper and weigh the sample.

3. Quickly place each muscle in 2ml of pre-incubation medium (KHB with 0.1%BSA, 32mM mannitol and 8mM D-glucose) in 20ml plastic scintillation vials. The temperature of the water bath should be set between 29-35°C (for this muscle size, 35 works better). The vials should continuously be gassed with carbogen ($95\%O_2;5\%CO_2$) and shake at ~1 cycle/sec for 30-60min. Split muscle should be pre-incubated for 60min to allow for recovery.

4. Remove the pre-incubation medium and add fresh medium with the pre-prepared conditions (AICAR, insulin, etc.). You can use the same vials and simply discard the pre-incubation medium. At this point you can also perform the co-incubation with adipocytes (1ml of KHB and 1ml of fat cell suspension).

5. After the incubation period, in order to remove glucose from the extracellular space, rinse the muscle in the absence of glucose for 10min at 29°C in 2ml of gassed ($95\%O_2;5\%CO_2$) KHB containing 40mM mannitol and, if present in the incubation period, 2mU/ml of insulin. This is important for long-term incubations when maintaining the muscle viable is more difficult.

Glucose Uptake:

6. Dump out wash medium and incubate muscles for 20 min at 29°C (gassed with $95\%O_2;5\%CO_2$) in 1.5-2ml of KHB containing 8mM of 2-deoxy-glucose-[1,2-H^3]glucose (0.5µCi/ml and 32mM mannitol + [U-C^{14}]mannitol (0.1µCi/ml) in the absence or presence of insulin (2mU/ml provides a maximum response).

7. Stop the assay by removing the muscle from the vials and quickly washing them in ice cold KHB, blotting briefly on filter paper, and freezing in liquid N_2 in prelabled 1.5ml eppendorf tubes. Weigh muscle prior to freezing if desired.

8. Homogenize the muscle by heating to 65°C in 0.5ml of 1M KOH for approximately 1h. Vortex gently to dissolve the muscle. Take an aliquot of 400µl and place in scintillation vials containing 5-10ml of scintillation fluid. Count for both ^{14}C and ^{3}H.

Calculations:

The intracellular water content of the muscles is calculated by subtracting the measured extracellular space water (determined by [1-^{14}C]mannitol counting) from total muscle water. Total muscle water is assumed to be 80% of muscle weight**, which is the average value for rat epitrochlearis muscles under these experimental conditions.
** *Young DA et al. (1986). J. Biol. Chem. 261(34):16049-16053.*

Water content in epitrochlearis muscles has been reported to represent 77.5±0.6 % in muscles freeze-clamped directly after dissection and varied between 81±0.9% and 83.5±0.5% (n.s.) at different incubation times (0.5-30h).
Wallberg-Henriksson H. (1987). Acta Physiol Scand (suppl.) 564:1-80.

Glycogen Synthesis in L6 Muscle Cells (12-well paltes):

1. Cells were starved for 4 hours prior to the start of the experiment (1ml/well).
2. Prepare radiolabeled incubation medium (0.4ml/well, 0.2μCi/ml radioactivity.)
3. Prepare 2 ml microtubes with the various incubation conditions. Add 400μl of radiolabeled incubation medium/well with respective conditions. All 36 wells should receive the same length of exposure to ^{14}C (i.e. 1 hr.).
4. Prepare a set of eppendorf tubes with non-labeled incubation medium and respective agents needed for pre-incubation (only perform this step if it is necessary to preincubate the cell with certain agents before beginning the incubation).

Upon completion of the experiment:

1. After all the 60 min incubations are completed, aspirate medium.
2. Wash 3 times with cold PBS to stop the reactions.
3. Add 130μl of 1M KOH. Pipette up and down a few times in each well to ensure all the cells are lysed and detached from the bottom of the plate. Collect 100μl of cells into 2ml microtubes.
4. The remaining 30μl/well is used for protein determination and the 100μl is used for counting.
5. Add 50μl of carrier glycogen (25mg/ml, Sigma, Glycogen, G-8751) to each tube (binds to radioactive glycogen and allows it to form a pellet).
6. Heat all samples at 95°C for 5 minutes (this allows the radiolabeled glycogen to form a pellet with the glycogen carrier. This also denatures any enzymes involved in glycogen metabolism).
7. To each tube add 80μl of saturated Na_2SO_4 (this forms crystals, ie precipitates with the glycogen once ethanol is added).
8. Now add 1.2ml of cold (-20 °C) Ethanol (100%). This is used to precipitate the glycogen.
9. Vortex all tubes for 1-2 seconds gently to prevent leakage of ethanol.
10. Keep the tubes in the -20°C freezer overnight to allow the precipitation to occur.

Day 2: (This procedure gets rid of all remaining radioactive metabolic byproducts other than glycogen):

7. Centrifuge all tubes at 10 000- 13 000rpm for 20 min.
8. Discard supernatant by inverting the tubes and dumping it out. Dissolve the pellet in 500μl of H_2O (use the water bath/heat block if needed). Use care when vortexing all tubes to avoid leakage of radiolabeled contents.
9. Transfer 500μl of solution to scintillation vials for counting.

Glucose uptake in L6 Muscle cells:

Transport assay for 24 well plates:

1. After cells have been incubated with desired conditions, aspirate medium and wash cells 2x with Hepes buffered saline (HBS) at room temperature and aspirate any remaining buffer.

2. For specific uptake (glucose uptake), add 0.35ml of transport solution (T.S.) per well for 12-well dish. (0.2ml of TS for 24-well plates, and 1.0ml of TS for 6-well plates). For Non-specific uptake use TS containing 10μM Cytochalasin B in 1 or two wells.

3. Incubate for 5min at room temperature for 12 well plates. (5min for 6 well plates and 10min for 24 well plates).

4. Aspirate the TS quickly and wash **three** times with ice-cold stop solution (0.9% Saline) and aspirate to dryness.

5. Add 130μl of 1M KOH to 24-well plate, don't scrape, pipette up and down instead. This is enough to remove the cell from the bottom of the plate. Use 100μl for counting and 30μl for protein.

Solutions:

Hepes Buffer Saline (amounts for 500ml):

- 140mM NaCl (4.091 g)
- 20mM Hepes-Na, pH=7.4 (2.383 g)
- 5mM KCl (186.4 mg)
- 2.5mM $MgSO_4$ (150.5 mg or 308.1 mg hydrate)
- 1.0mM $CaCl_2$ (55.5 mg)

Stop Solution:

- 0.9% NaCl (Saline)

2-DG stock Solution:

- 10μM 2-Deoxy-D-glucose in Hepes buffer

Transport Solution (TS):

- Prepare in Hepes Buffer
- 10μM 2-Deoxy-Glucose
- 0.5 μCi/ml ^{3}H 2-Deoxy-Glucose

Cytochalasin B (CB) Transport Solution:(Non-specific uptake Solution)

- Transport Solution (above)
- Stock Solution: 10μM CB in DMSO, Sigma C-6762, Note: because CB is very powerful, very little is necessary to completely block the uptake of glucose. Use 1μl of stock per 150μl of transport solution.

Complexation of Palmitic acid with albumin:

Palmitic Acid (Sigma # P-5585) MW=256.4
12mM = 59.97mg in 10ml

Albumin (Sigma # A3803 or A6003) MW=68kDa
Albumin (12.5% w/v)
1.25g of BSA/10 ml.

1. Put 60mg of palmitic acid in an eppendorf tube and add 40µl of NaOH (10N).
2. Vortex vigorously, then dissolve in 10ml of pre-heated (50°C) 12.5% BSA solution (the BSA can be dissolved in KHB, α-MEM, or other medium for cell culture.)
3. Mix everything very well, in a beaker at 50°C. NOTE: Even overnight agitation will not result in a completely clear solution because palmitate does not dissolve completely. There is always some undissolved palmitate particles floating in the solution. The solution can be left at 50°C for 3h to improve complexation.
4. Adjust the pH to 7.4 and filter the solution.
5. Take an aliquot (100µl to measure fatty acids using the Wako kit. There is no loss of palmitate with filtration. Make aliquots of 1ml and freeze for future use.

After 3h of complexation at 50°C, the pH of the α-MEM/albumin (12.5%w/v) + 40µl of NaOH-solution was 7.22. Adjust pH to 7.4 with NaOH (1M).

The concentration of palmitic acid in the solution after filtration was ~8.87mM measured by the Wako kit. Apparently, only 75% of the total fatty acids become complexed to albumin at the end of 3h. It is important to start with a higher amount of palmitate to try to achieve the desired concentration. Consider a loss of approximately 25% of the initial concentration of fatty acids for calculation purposes.

- Prepare a similar solution with 40µl of NaOH (10N) without palmitic acid to use as a control to measure palmitic acid, and also for control experiments with cells or tissues.

Determination of FFA-Using the Wako Kit:

Adapted method using half the volume of all reagents:

Tube No		1Meq/L NEFA Std	Reagent / H_2O	Reagent A	I n c u b a ti o n	Reagent B	I n c u b a ti o n	Optical density	NEFA Conc. (Meq/L)
#1	Blank	-	25 µl	0.5 ml		1 ml		0.000	0.000
#2	Low St	12.5µl	37.5 µl	0.5 ml		1 ml		Read	0.50
#3	Mid St	25 µl	25 µl	0.5 ml		1 ml		Read	1.00
#4	High St	50 µl	-	0.5 ml		1 ml		Read	1.97
#5	Sample	25 µl	25 µl	0.5 ml		1 ml		Read	calculat e

Incubation: each incubation is 10min long at 37°C. This is a critical step. Without performing this, the values will not be accurate.

Read the optical density at 550nm in spec.

Calculation:

Absorbance of sample (A_s)
Absorbance of the NEFA mid standard solution (A_{std})
Absorbance of sample blank against reagent blank (A_{sII})

$C_s = (A_s - A_{sII})/A_{std}$ x 1.0 (mEq/l)

The unite is mEq/l = mmol/l

Gel Staining/ De-Staining and Stripping Buffers:

Staining solution currently utilized.

Methanol -225ml
H_2O- 225ml
Acetic acid – 45ml
Coomassie brilliant blue (G250)- 200mg

*SIGMA sells a premade staining solution (concentrate – Cat #B 8522 - $53 Canadian). This makes 1l of staining solution. After dilution with deionized H_2O to a final volume of 1L, solution will contain: 0.1% (w/v) brilliant blue G, 25%(v/v) methanol and 5% (v/v) acetic acid.

Coomassie brilliant blue (G250)Sigma cat#B 0770 -5g-$35.8 Canadian.

For 1l:

- 250ml of Methanol
- 50ml Acetic acid
- 700nl of H_2O
- 1g of Coomassie blue (this could be reduced to 400mg maximum)

De-Staining Solution
For 1L:

- 70ml of Acetic Acid
- 50ml of Methanol
- 875 ml of H_2O

Stripping and re-blotting membranes

Stripping buffer:

- 62.5mM Tris/HCl pH 6.8 containing 100mM 2-mercaptoethanol and 2%SDS

Wash buffer:

- 20mM Tris/HCl pH 7.5 containing 0.14 M NaCl and 0.1%(v/v) Tween 20 (NaCl/Tris)

Procedures:

1. Leave the membranes for 30 min at 50°C in stripping buffer
2. Wash three times with wash buffer
3. Block membranes for 1h
4. Wash the membranes again in wash buffer (3X). This step is not necessary
5. Re-blot with the antibody of choice

Western blotting solutions:

10X Electrophoresis/Running Buffer (pH=8.3)

30.34g (results in 25.0mM Tris)
144g (results in 192mM glycine)
10g (0.1% w/v SDS)

- Dissolve contents in 1L of ddH2O, store at room temp or in 4C fridge, if precipitation occurs, warm to room temp before use.

1X electrophoresis/running buffer (pH=8.3)

- Make 1 in 10 dilution of 10X running buffer. For example, 40ml of 10X Run Buffer in 360ml of ddH2O.

10X Transfer buffer (pH=8.3)

30.3 g Tris base
144g Glycine

- Dissolve contents in 1L of ddH20, store at RT or 4C, if precipitation occurs, warm to RT before use.

1X Transfer buffer (pH=8.3)

100ml of 10X transfer buffer
200ml methanol/ethanol
700ml ddH2O

- Store at -20C prior to use

1X TBS (Wash buffer):

- In 3L of ddH2O dissolve
- 35.1g NaCl
- 12.11g Tris-base
- pH=7.5
- 2ml Tween
- 2ml NP40
- Top up total volume to 4L

10X TBS (Wash buffer):

60.57g Tris-base
87.66 Sodium Chloride (NaCl)

- Dissolve contents in 1L of ddH2O, store at 4C

1X TBS

100ml 10X wash buffer
900ml ddH2O

- Add 1000ul (for 0.1%) to make TBS/Tween-20 add 1000ul of NP40.

Blocking Buffer:
Can be made either with Skim milk or BSA.

Skim milk

- dissolve skim milk powder in 1X TTBS (obtain a 5% milk mixture)

BSA

- 1 x TTBS and 3% BSA (w/v: 1.5g/50ml)

Antibody Buffer:
Make antibody buffer with BSA, this way you can reuse it for a few months.

- 1 part blocking buffer + 2 parts wash buffer + 0.02% NaAzide (stock in ddH_2O). Usually most antibodies can be applied in a 1:500 to 1:1000 dilution depending on how good the antibody is.

Resolving gel Tris Buffer (1.5M) (pH=8.8)
1.5M Tris, use 90.86g/500ml of ddH2O

Stacking gel Tris Buffer (0.5M) (pH=6.8)
0.5M Tris, use 30.3g/500ml of ddH2O

10% APS Solution:
10% (w/v) Ammoniumperoxide Sulfate in ddH2O, use 0.1g/ml, store at room temperature. Make fresh every time.

10% SDS Solution:
10% (w/v) Sodium dodecylsulfate in ddH2O, use 1g/10ml, store at room temp

Butanol Overlay:
Mix 18.75ml of 1.5M Tris (pH=8.8) with 0.5ml of 10% SDS, volume up to 150ml with ddH2O, mix 1:1 with butanol.

Lysis buffer for protein determination prior to Western blot

NaCl	-135 mmol/L (MW=58.44)
$MgCl_2$	-1mmol/L (MW=203.3)
KCl	-2.7mmol/l (mw=74.55)
Tris (pH 8)	-20mmol/l (mw=121.14)
Sodium vanadate (Na_3VO_4)	-0.5 mmol/l (mw= 183.9)
Sodium fluoride (NaF)	-10mmol/l (mw=41.99)
PMSF	-0.2mmol/l
Leupeptin	-10µg/ml
Triton 1%	
Glycerol 10%	

For 50ml of buffer:

NaCl	-0.394g	
$MgCl_2$	-0.0102g	
KCl	-0.01006g	
Tris(pH 8)	-0.12114g	
Na_3VO_4	-125µl	
NaF	-0.020995g	
PMSF	-100µl	
Leupeptin	-100µl	
Triton	-0.5ml	
Glycerol	-5ml	Note: Store buffer at -20

Laemmli Sample buffer (2X)-Biorad Manual

6.05 ml of ddH2O
1.25ml of 0.5M Tris-HCl, pH=6.8
2.0ml 10% (w/v)SDS
0.2ml of 0.5% (w/v) bromophenol blue

Note: Store at RT. Add 50µl of β-mercapto-2-ethanol to 950µl of buffer prior to use. Dilute the sample (1 in 2) with sample buffer and boil for 4 min/ heat to ~70°C.

Gel Recipes:
Note: the 4% gel recipe is for the stacking gel.

Gel%	ddH2O			30% Acryl			0.5M Tris			1.5M Tris			10%SDS			10%APS			TEMED		
	1X	2X	4X	1X	2X	4X	1X	2X	4X	1X	2X	4X	1X	2X	4X	1X	2X	4X	1X	2X	4X
4	3.05	6.1	12.2	0.67	1.34	2.68	1.25	2.2	5				50	100	200	12.5	25	50	15	30	60
6	7.9	15.8	31.6	3	6	12				3.8	7.6	15.2	150	300	600	150	300	600	12	24	48
7.5	4.85	9.7	19.4	2.5	5	10				2.5	5	10	100	200	400	50	100	200	10	20	40
8	5.68	11.36	22.72	2.67	5.34	10.7				2.5	5	10	100	200	400	50	100	200	15	30	60
10	4	8	16	3.33	6.66	13.3				2.5	5	10	100	200	400	50	100	200	15	30	60
12	3.35	6.7	13.4	4	8	16				2.5	5	10	100	200	400	50	100	200	15	30	60
15	3.4	6.8	13.6	7.5	15	30				3.8	7.6	15.2	150	300	600	150	300	600	15	30	60

Resolving gel:
Add APS and TEMED immediately prior to allowing the gel to set. Pipette a thin layer of water or butanol overlay to prevent the resolving gel from drying. Allow gel to set.

Stacking gel:
Once resolving gel is set, remove the water from the top of the gel and remove excess water with filter paper. Add APS and TEMED and quickly add stacking gel to the top of resolving gel. Put the combs in place without making any bubbles. Once gels have set, they can be placed in fridge overnight.

Glycogen Content Assay:

- Passoneau JV & Lauderdale VR. A comparison of three methods of glycogen measurement in tissues. Analytycal Biochemistry 60, 405-412, 1974.

- Keppler D & Decker K. Glycogen. Determination with amyloglucosidase. In Methods of Enzymatic analysis. Edited by H.U. Bergmeyer. New York: Academic, 1974, p 1196-1201.

Procedure:

1. Incubate muscles or cells with the desired compounds and treatments.
2. Wash 3 times with cold PBS. For cells, wash with PBS 1mM Ca^{++}/ 1mM Mg^{++} to avoid cell detachment.
3. Digest muscles in 1M KOH (65°C, for 60 min). For cells add 180µl of 1M KOH. Transfer cell lysates to eppendorf tubes and heat up to 95°C for 10min to cause thermal deproteinization of the sample and inactivation of glycogen decomposing enzymes. Use 10µl for protein determination.
4. If it is an experiment with D-[U-^{14}C]glucose to also determine glycogen synthesis in muscle tissue, take 100µl for glycogen content and 400µl for determination of glycogen synthesis.
5. Add 10% (v/v) of acetic acid (17.5 M) to the cell lysate or digested tissue. This is important to maintain the pH between 4 and 5 (ideal 4.8) which is the optimum condition for hydrolysis of glycogen by Amyloglucosidase. The pH of the solution after adding acetic acid is actually ~4.77 at 25°C.
6. Add 500µl of Acetate buffer (pH=4.8) + Amyloglucosidase (0.5 mg/ml should be enough).
7. Incubate on the bench (room temperature, overnight), or for 2h at 40°C with shaking.
8. Neutralize the glycogen-digested solution with 1/16 (v/v) of NaOH (5N). This should bring the pH to 7.37 at 25°C. The pH of the TRA buffer in the next step is 7.5. This is a critical step for the next step.
9. Centrifuge samples for 5 min at 3000rpm.
10. For cell lysates from a 6-well plate, collect 400µl of the digested supernatant and add 1ml of the ATP-TRA buffer. The determination of glycogen content from cell lysates requires a high amount of material compared to muscle extracts. Volumes lower than 400µl of digested cell lysates usually produce very low readings at 340nm.
11. Incubate for 30min at room temperature.
12. Read at 340nm (a plastic cuvette can be used).

Calculation:

(OD x 8.89) = µmoles of glycosil units

Buffers for Glycogen Content Assay:

Acetate buffer (0.2M, pH = 4.8)

Reagent	Volume
Acetic Acid (96%)	480µl
Sodium Acetate	975 mg
ddH_2O	100 ml

Check pH, store at 0-4°C

Triethanolamine Buffer (0.3M TRA, 4.05mM $MgSO_4$ –pH 7.5)

Reagent	Volume
TRA	5.6g
$MgSO_4$	100mg
ddH_2O	100ml

Dissolve 5.6 g of TRA + 100mg of $MgSO_4$ in 50 ml of distilled H_2O and add 12ml of 1M KOH. Check the pH and make up to 100ml with distilled water. Store at 0-4°C.

Glucose Buffer

Reagents	For 50ml of TRA buffer		For 30ml of TRA buffer	For 20ml of TRA buffer	
ATP	0.245g	100mg	0.147g	0.098g	0.098g
NADP	0.025g	6mg	0.015g	0.01g	2.4mg
HK/G6P	300µl	100µl	180µl	120µl	40µl

- **ATP (1mM)/NADP (0.9mM/HK/G6P-DH (5µg/ml) TRA-Buffer (Same as glucose buffer):**

Dissolve 6mg of ATP + 8mg of NADP in 10ml of TRA buffer and add 50µl of the HK/G6P-DG suspension. The concentration of HK and G6K-DG in the final assay mixture will be 1.25U and 0.9U, respectively. This solution is stable for approximately 1 week at 0-4°C.

- **HK/G6P-DG suspension** – 500U (Based on HK units- 125U/mg, ~4mg prot/vial)

Re-suspend the lyophilized enzyme in 2ml of 3.2M ammonium sulfate – (250U/ml)
Prepare 10ml of a 3.2M Ammonium Sulfate (MW = 132.14) solution. Dissolve 4.32 g of $(NH_4)_2SO_4$ in 10ml of ddH_2O.

- **Amyloglucosidase (AGS) [1mg/ml]**

Dissolve 20mg of enzyme protein in 20ml of acetate buffer. The amyloglucosidase solution can be stored deep-frozen without any appreciable loss of activity.

- **1M KOH (MW=56.11) for the TRA buffer.** Dissolve 5.61g of KOH in ddH_2O and make up to 100ml. The pH of this solution is above 15, off the pH meter scale.
- **For the 1mM Ca++ and 1mM Mg++ prepare a 100mM stock solution of each in ddH_2O.**

For 100 mM Ca++ use $CaCl_2$: (MW=147.02), 1.4702g in 100ml of ddH_2O.
For 100 mM Mg++ use $MgSO_4$: (MW = 120.39), 1.2039g in 100m of ddH_2O.

- **PBS**

Use PBS tablets (1tablet per 100ml of ddH_2O).

- **For PBS containing 1mM Ca++ and 1mM Mg++**

Take 1ml of Ca++ and 1ml of Mg++ stock solutions (100mM) and add to 100ml of PBS.

Sample Preparation for lactate assay:

Reagents: Triethanolamine (Sigma, T-9534, MW= 185.7)

- Samples are precipitated with 8 % perchloric acid ($HClO_4$) (PCA) in a 1:1 ratio. (i.e. 50µl of sample and 50µl of PCA). This precipitates all the proteins which can potentially break down lactate. At this point samples can be stored at -80 until ready to assay or they can be neutralized right away.
- The samples need to be neutralized with Triethanolamine (TEA 0.21M)/K_2CO_3 (1.16M). The pH of this solution should be ~6.86.
- The amount of TEA solution needed to restore the pH of 8% PCA to ~7.3-7.4 is approximately 53% of the total PCA volume.
- Thus since the samples are diluted 1:1 with 8% PCA, the [] of PCA in the sample is actually 4%. Therefore, only 26.5% of the total sample volume has to be TEA in order to restore pH to neutral.
- After adding 13.3 µl of TEA solution to 50µl of sample, a precipitate formed.
- Spin samples down and use 10µl of the supernatant for lactate determination using the lactate kit from Trinity biotech.
- Follow kit instructions for assay.

- When calculating final lactate concentration in the total sample:

1. Correct for total volume, 10 * 6.33= 63.3
2. Correct for dilution with PCA, multiply by a factor of 1.265
3. Correct for the dilution of sample with PCA, multiply by a factor of 2.
4. Now correct for the total volume of the incubation medium from which you obtained the sample.

Lactate production assay in L6 cells

1. Seed cells in 6-well plates. Make sure they are not seeded too confluent to ensure proper differentiation.
2. Wash cells daily to assure they differentiate at an optimal rate.
3. On experimental day: wash cells once with starve medium (no phenol red). Be very gentile with the cells to make sure they don't detach from the plate especially if they are very well differentiated.
4. After washing once, add 1.5ml/well of starve medium (no phenol red) and starve cells for 4hrs. Do not starve longer because cells start detaching.
5. After the cells are starved, aspirate the medium, and add 700µl/well of starve medium (no phenol red) with the respective treatments. Note: Make sure to add the conditions very slowly to ensure the cells do not detach.
6. At the end of the experimental incubation period (however long it may be), quickly remove 200µl of medium and place in 1.5ml eppendorf tubes. Place the tubes on ice right away. Subsequently, take an additional 200µl of medium and dilute 1:1 with 8% PCA. Freeze all the tubes right away for future quantification of lactate.
7. Aspirate the remaining medium and wash cell 2 times with ice cold PBS.
8. Lyse cell in 400µl of 1M KOH. Swirl each plate manually to detach all the cells of the bottom of the plate and then pipette up and down to generate a smooth lysate which can then be used to quantify protein with a Bradford assay.
9. **For measurement of lactate at a later date, use 100µl of the medium not diluted 1:1 with PCA.** The lactate kit, calls for use of 10µl only, however, these values are very low and may not be the most accurate, therefore, use 100µl/ml of lactate reagent.

Materials:

- **Alpha-Modified eagles medium without phenol red (catalogue number: 310-021-CL from Wisent)**
- **Lactate reagent: Trinity biotech (cat #: 735-10)**
- **Lactate standard: Trinity biotech (cat#: 826-10)**

Glucose incorporation into lipids in plated cells:

1. Starve cells for 4hours.
2. Incubate cells in the presence of 0.2μCi/ml of ^{14}C-D-U-glucose and your respective conditions for 1 hour.
3. After the 1hour incubation period is complete, wash cells 3 times with ice-cold PBS.
4. Lyse cells in 400μl of 1M KOH.
5. Pipette cells up and down to lyse cells well.
6. Remove 350μl of lysate and use for lipid extraction. Use the remainder for protein quantification via the Bradford method.
7. Place the 350μl of lysate in a 5ml scintillation vial.
8. Add 1.25ml of Dole's reagent. Cap and vortex.
9. Add 0.75ml of H_20 and 0.75ml of Heptane. Cap and vortex again.
10. Allow phases to separate for 10-20 minutes.
11. Uncap the vials and remove 500μl of the top (heptane) phase, and place in a regular scintillation vial. Use 4ml of scintillation liquid to count in a scintillation counter.

Dole's Reagent:
Isopropanol:Heptane:Sulfuric Acid (0.5M/1N) (Ratio 40:10:1)

Spectrophotometric determination of AICAR in plasma

Reference: *Fujitaki JM, Sandoval TM, Lembach LA, Dixon R. J. Biochem. Biophys. Methods. 29 (1994) 143-148.*

Materials:

- Sodium Nitrite (1% w/w solution), 10ml + 100mg
- Ammonium Sulfamate (3% w/w solution), 10ml + 300mg
- N-(1-naphthyl)ethylenediamine (0.75% w/w solution), 10 + 75mg

Note: These solutions have to be fresh. Prepare in ddH_2O

Generating Standard Curve:

1) Dissolve AICAR in water (6.4mg/ml). This serves as a stock solution for all standards, which range from (0.125 - 64 µg/ml)
2) Dilute the stock 1:100 to obtain 64µg/ml standard (20µl + 2ml, it is recommended to make dilutions with plasma).
3) The remaining standards are made by a series of sequential 1:1 dilutions of the 64µg/ml standard. Therefore the remaining standards are: 32, 16, 8, 4, 2, 1, 0.5, 0.25, 0.125, and 0 µg/ml.

Note: It is recommended that plasma samples must be deproteinized prior to performing measurements. Prepare the dilutions of the standard curve in 2ml tubes. Run samples directly in cuvettes.

Reaction procedure (in cuvette): (For 0.7g/kg BW ip injection, use 40µl of plasma and 460µl of H_2O:PBS (3:1).

1) Prior to use, centrifuge plasma and mix 3 : 1 (plasma : PBS (pH=7.4)) Note: dilute 40µl of plasma with 460µl H_2O:PBS (3:1)
2) Pipette 500µl of diluted plasma (or standards) into a cuvette.
3) Add 150µl of 1N HCl
4) Add 50µl of sodium nitrite solution
5) Vortex and incubate at RT for 5 min.
6) Add 50µl of ammonium sulfamate solution.
7) Vortex and incubate at RT for 10 min.
8) Add 100µl of N-(1-naphthyl)ethylenediamine solution.
9) Vortex and incubate at RT for 10 min.
10) Read at 540nm in spectrophotometer.
    - The solutions should turn a purpulish colour. The intensity of the colour is proportional to the amount of AICAR in the medium.

Reaction procedure (96-well plate):

1) Pipette 100µl of diluted plasma (or standards) into well.
2) Add 30µl of 1N HCl
3) Add 10µl of sodium nitrite.
4) Mix thoroughly by gently swirling plate and incubate at RT for 5 min.
5) Add 10µl of ammonium sulfamate solution.

6) Mix and incubate for 10 min at RT.
7) Add 20µl of N-(1-naphthyl)ethylenediamine solution.
8) Mix and incubate for 10 min at RT.
9) Read at 540nm in plate reader.

Glucose (GO) Assay Kit:
Sigma (Product Code: GAGO-20)

Standard Curve:

Tube	H2O (µl)	Sample (µl)	Glucose Standard (µl)
Blank	200	-----	-----
0 µg/ml Standard	200	-----	-----
20 µg/ml Standard	196	-----	4
40 µg/ml Standard	192	-----	8
60 µg/ml Standard	188	-----	12
80 ug/ml Standard	184	-----	16
Sample	188.9	11.1	-----

Standard Curve:
1) Pipette the glucose standards into cuvetts.
2) Add the volume of water indicated on the chart.
3) Add 400µl of Assay reagent to each cuvette and vortex (add this preferably with a repeator).
4) Incubate for 30 minutes at 37°C.
5) After the incubation add 400µl of H_2SO_4 (12N/6M) and vortex.
6) Read at 540 nm.

Samples:
1) Pipette the plasma samples into the cuvetts.
2) Add the volume of water indicated on the chart.
3) 10 minutes after incubating the standard curve, add 400µl of Assay reagent to each cuvette and vortex.
4) Incubate for 30 minutes at 37°C.
5) After incubation add 400µl of H_2SO_4 (12N/6M) and vortex.
6) Read at 540 nm.

Sample dilution:
- The samples are diluted 18X. Assuming that the samples are 6mM glucose, this dilution factor should result in a concentration of 60µg/ml of glucose.

Assay reagent preparation:

- Dissolve contents of bottle in 39.2 ml of ddH_2O. This solution can be aliquoted and frozen at -20°C for at least 6 months.
- Prior to use add o-Dianisidine reagent to the assay reagent. (20.4µl of o-Dianisidine reagent/1ml Assay reagent)

Carnitine Palmitoyltransferase 1 (CPT-1) Activity Assay in L6 Cells:

Ref: Spurway TD, Agius L, Stanley H, Sherratt A, Pogson CI. Biochemical Society Transactions 22: 118S, 1994.

Thupari JN, Landree LE, Ronnett GV, Kuhajda FP. PNAS 99:9498-9502, 2002.

The CPT-1 activity assay based on the principle of the following reaction:

$$\text{Palmitoyl-CoA} + \text{carnitine} \underset{}{\overset{\text{CPT-1}}{\rightleftharpoons}} \text{Palmitoylcarnitine} + \text{CoASH}$$

The assay measures CPT-1 by determining the rate of conversion of palmitoyl-CoA and [^{3}H]carnitine into palmitoyl[^{3}H]carnitine and CoASH.

Composition of the radioactive buffer:

50mM Imidazole (68.98mg/ml)	1mM ATP (0.605mg/ml)
70mM KCl (5.21mg/ml)	70µM Palmitoyl-CoA (0.071mg/ml)
1mM KCN (0.065mg/ml)	0.50µCi L-[^{3}H]carnitine
80mM sucrose (27.4mg/ml)	0.1% BSA-FA free
1mM EGTA (0.380mg/ml)	40µM digitonin (0.0492mg/ml, permeabilizes the cell membrane to allow Palmitoyl-CoA to cross)
2mM $MgCl_2$ (0.407 mg/ml)	1mM DTT (Dithiothreitol, 0.154mg/ml)

- The cells are treated with desired conditions before performing the CPT-1 activity assay.
- It is best to use 6-well plates for greater protein content.

Assay procedure:

1. Wash cells twice with PBS, and then add 700µl of the radioactive buffer to each well and incubate at 37°C for **5 minutes.** For non-specific wells (1 per plate), cold assay buffer is added to the well, and the reaction is immediately terminated.
2. The medium is aspirated and quickly washed 3 times with ice cold PBS to stop the reaction.
3. The reaction is terminated by adding 500µl of ice-cold PCA (4M). Plates are then scraped, and the cells are vigorously vortexed, and centrifuged at 13000rpm for 5 min at 4°C.

4. The supernatant is discarded, and the pellet is gently washed by resuspension with 500µl 2mM PCA to rid the excess radioactivity, and centrifuged again.
5. The supernatant is discarded, and the resulting pellet is re-suspended in 800µl ddH_2O and extracted with 400µl butanol.
6. The tubes are vortexed and centrifuged at 13000 rpm for 3 minutes, allowing the phases to separate.
7. 150µl of the butanol phase is counted using liquid scintillation fluid.

9.2 Appendix B: Contributions by authors and funding sources

Study 1

Sergiu Fediuc was involved with the planning and execution of all experiments, and aided in the writing of the manuscript. Mandeep Pinky Gaidhu assisted with Western blot data collection, and aided in the writing of the manuscript. Dr. Rolando Ceddia is the primary investigator and aided in the experimental design, data collection, and writing of the manuscript. The authors would like to thank Dr. David Hood for use of his laboratory to maintain cell cultures.

Study 2

All experiments were planned and conducted by Sergiu Fediuc. Dr. Aurelio Pimenta assisted with Western blot and glucose uptake experiments. Mandeep Pinky Gaidhu assisted with palmitate and glucose oxidation experiments. All data were analysed by Sergiu Fediuc. The manuscript was written by Sergiu Fediuc and Dr. Rolando Ceddia. This project was funded by the Natural Sciences and Engineering Research Council of Canada (NSERC) via a Discovery grant to Dr. Rolando Ceddia.

Study 3

All experiments were planned and conducted by Sergiu Fediuc. Mandeep Pinky Gaidhu was involved in data collection for glycogen synthesis, glycogen content, lactate production, and glucose uptake. All data were analysed by Sergiu Fediuc. The manuscript was written by Sergiu Fediuc and Dr. Rolando Ceddia. This project was funded by NSERC via a Discovery grant to Dr. Rolando Ceddia. The authors would like

to thank Dr. Michael Riddell for use of the spectrophotometer, which was required for several experiments.

Study 4

All experiments were planned, conducted, and analyzed by Sergiu Fediuc. Mandeep Pinky Gaidhu aided in the administration of daily AICAR injections, as well as the collection of plasma samples for all experiments. She also helped with the analysis of plasma NEFAs, lactate, and glucose concentrations. Mandy So aided with the analysis of plasma leptin concentrations. Nicole Anthony and Dr. Ceddia were involved with tissue extraction at the end of the two week investigation. Babak Maghdoori was involved with Western blot data collection. This project was funded by NSERC and the Canadian Diabetes Association via a grants to Dr. Rolando Ceddia.

9.3 Appendix C: Published work

9.3.1 Copyright permission

Journal of Lipid Research is part of the American Society of Biochemistry and Molecular Biology (ASMBM), which grants use without copyright permission for:
Students wanting to reproduce or republish their work for educational purposes.

Journal of Cellular Physiology is published by Wiley InterScience, which grants use without copyright permission for:
Users at institutions which have subscribed to Electronic Product and users who have access under a Society or Personal License will have access to the full text of such Electronic Product ("Authorized Users"). Authorized Users may download, view, copy and save to hard disk or diskette and store or print out single copies of individual articles or items for your own personal use, scholarly, educational or scientific research or internal business use. Authorized Users may transmit to a third-party colleague in hard copy or electronically, a single article or item from ***Wiley InterScience*** *for personal use or scholarly, educational, or scientific research or professional use but not for re-sale. In addition, Authorized Users have the right to use, with appropriate credit, figures, tables and brief excerpts from individual articles in the Electronic Product(s) in your own scientific, scholarly and educational works.*

Endocrinology is part of the Endocrine Society, which grants use without copyright permission for:
Permitted access by authorized users includes searching, downloading, printing and storing of individual articles for scholarly research, educational and personal use. Such copies may be shared with non-authorized users provided such sharing is solely for the purpose of scholarly communication or educational use, and there are no commercial benefits or purposes.

Regulation of AMP-activated protein kinase and acetyl-CoA carboxylase phosphorylation by palmitate in skeletal muscle cells

S. Fediuc, M. P. Gaidhu, and R. B. Ceddia[1]

School of Kinesiology and Health Science, York University, Toronto, Canada

Abstract **The purpose of this study was to investigate the effects of long-chain fatty acids (LCFAs) on AMP-activated protein kinase (AMPK) and acetyl-coenzyme A carboxylase (ACC) phosphorylation and β-oxidation in skeletal muscle. L6 rat skeletal muscle cells were exposed to various concentrations of palmitate (1–800 μM). Subsequently, ACC and AMPK phosphorylation and fatty acid oxidation were measured. A 2-fold increase in both AMPK and ACC phosphorylation was observed in the presence of palmitate concentrations as low as 10 μM, which was also accompanied by a significant increase in fatty acid oxidation. The effect of palmitate on AMPK and ACC phosphorylation was dose-dependent, reaching maximum increases of 3.5- and 4.5-fold, respectively. Interestingly, ACC phosphorylation was coupled with AMPK activation at palmitate concentrations ranging from 10 to 100 μM; however, at concentrations >200 μM, ACC phosphorylation and fatty acid oxidation remained high even after AMPK phosphorylation was completely prevented by the use of a selective AMPK inhibitor. This indicates that LCFAs regulate ACC activity by AMPK-dependent and -independent mechanisms, based on their abundance in skeletal muscle cells. Here, we provide novel evidence that the AMPK/ACC pathway may operate as a mechanism to sense and respond to the lipid energy charge of skeletal muscle cells.—Fediuc, S., M. P. Gaidhu, and R. B. Ceddia. Regulation of AMP-activated protein kinase and acetyl-CoA carboxylase phosphorylation by palmitate in skeletal muscle cells. *J. Lipid Res.* 2006. 47: 412–420.**

Supplementary key words acetyl-coenzyme A carboxylase • fatty acid oxidation • lipid sensing

In recent years, a large body of evidence has been published showing that in mammals, AMP-activated protein kinase (AMPK) responds to hormonal and nutrient signals in the central nervous system and peripheral tissues, modulating food intake and whole-body energy homeostasis (1). AMPK is a heterotrimeric enzyme that has been proposed to function as a "fuel gauge" that monitors changes in the energy status of cells (1–3). When activated, AMPK shuts down anabolic pathways and promotes catabolism in response to an increase in the AMP/ATP ratio by down-regulating the activity of key enzymes of intermediary metabolism (1–3). In its activated state, AMPK phosphorylates serine residues 79, 1,200, and 1,215 of acetyl-coenzyme A carboxylase (ACC), producing an 80–90% decrease in the V_{max} of the enzyme, suggesting that AMPK is the physiological ACC kinase (4). There is also evidence that long-chain fatty acids (LCFAs) act as potent feedback suppressors of lipogenesis by inhibiting ACC activity (5–7). ACC is a multifunctional enzyme that, when active (dephosphorylated form), catalyzes the conversion of acetyl-CoA to malonyl-CoA in the de novo lipid synthesis pathway (1–4). Malonyl-CoA is a potent inhibitor of carnitine palmitoyltransferase-1, a rate-limiting step for the entry of LCFAs into mitochondria for oxidation (8). When ACC is inactive (phosphorylated form), a decrease in malonyl-CoA occurs and disinhibits carnitine palmitoyltransferase-1, thereby increasing the mitochondrial import and oxidation of LCFAs (8). Therefore, the AMPK/ACC system is thought to play a central role in the regulation of cellular lipid homeostasis (2, 8, 9). In certain metabolic disorders, such as obesity and type 2 diabetes, lipid metabolism is dysfunctional, causing fatty acids to increase in the circulation and also in intracellular compartments (2, 8, 9). High levels of fatty acids are toxic to the cells and may cause deleterious metabolic abnormalities (8, 9). By increasing fatty acid oxidation in peripheral tissues, the AMPK/ACC system may play an important role by protecting the cells from these metabolic abnormalities (9). Of special interest are the mechanisms that regulate the AMPK/ACC system in skeletal muscle, because this tissue plays a major role in determining whole-body energy expenditure, accounts for 70% of total-body glucose disposal, and may modify substrate utilization toward substantially increasing fatty acid oxidation (9).

The classical view is that AMPK is activated allosterically by an increase in the intracellular AMP/ATP ratio, by phosphorylation of threonine 172 (Thr-172) within the α subunit, catalyzed by the upstream kinase LKB1 (the upstream

Manuscript received 5 October 2005 and in revised form 7 November 2005.

Published, JLR Papers in Press, November 22, 2005.
DOI 10.1194/jlr.M500438-JLR200

[1] To whom correspondence should be addressed.
e-mail: roceddia@yorku.ca

kinase of AMPK), and by inhibition of the dephosphorylation of Thr-172 by protein phosphatases (1–3). To date, a wide range of physiological stressors, pharmacological agents, and hormones associated with increases in the intracellular AMP/ATP ratio have been demonstrated to activate AMPK (10). In skeletal muscle, the activity of AMPK has also been reported to be regulated by the intracellular creatine-phosphocreatine ratio (11, 12) and glycogen content (13, 14), both directly related to the energy charge of muscle cells. Fatty acids, another major cellular energy source, may also regulate AMPK activity in skeletal muscle; however, no data for this have been published. It has been reported that in perfused rat cardiac muscle, palmitate (250 and 500 μM) and oleate (500 μM) significantly increased AMPK activity without causing any significant alteration in AMP/ATP ratio (15). Another study has reported that exposure to 150 μM acetate, octanoate, or palmitate caused a significant reduction in AMP/ATP ratio followed by a significant increase in AMPK activity in primary rat hepatocytes (16). In contrast to these observations are reports that the AMPK activity of rat liver purified LKB1/STRADMO25 (the upstream kinase of AMPK) was inhibited by long-chain acyl-CoA esters in vitro (17).

Currently, there is no consensus regarding the regulation of the AMPK/ACC system by fatty acids. To clarify this issue, we investigated the effects of different concentrations of palmitate on AMPK and ACC phosphorylation in L6 rat skeletal muscle cells. We hypothesized that LCFAs would increase AMPK and ACC phosphorylation by *1*) ATP utilization for LCFA activation (16) and 2) directly regulating ACC phosphorylation, because in the presence of exogenous fatty acids the de novo lipid synthesis pathway would be suppressed (4). In rat skeletal muscle, refeeding after a fast increases malonyl-CoA and decreases fatty acid oxidation, which has been attributed to a decrease in fatty acids that releases the allosteric inhibition of ACC2 (18). Here, we provide evidence that palmitate concentrations ranging from 1 to 800 μM significantly increase both AMPK and ACC phosphorylation and β-oxidation. Additionally, with the aid of a selective AMPK inhibitor, we describe the novel finding that ACC phosphorylation and palmitate oxidation are increased in the presence of high fatty acid concentrations by a mechanism independent of AMPK activation in L6 rat skeletal muscle cells.

METHODS

Reagents

α-Minimum Eagle's medium (α-MEM) and FBS were purchased from Wisent (Quebec, Canada). 5-Aminoimidazole-4-carboxamide-1-β-D-ribofuranoside (AICAR) was purchased from Toronto Research Chemicals, Inc. Compound C, a selective AMPK inhibitor, was provided by Merck Research Laboratories, fatty acid-free albumin, palmitic acid, and phenylethylamine were from Sigma (St. Louis, MO). [1-^{14}C]palmitic acid was purchased from American Radiolabeled Chemicals, Inc. (St. Louis, MO). Specific antibodies against P-AMPK and P-ACC were from Cell Signaling Technology (Beverly, MA) and Upstate Biotechnology (Charlottesville, VA), respectively. All other chemicals were of the highest grade available.

Cell culture and treatment

Stock cultures of rat L6 skeletal muscle cells were obtained from the American Type Culture Collection and grown in α-MEM containing 10% (v/v) FBS, 100 U/ml penicillin, 100 μg/ml streptomycin (growth medium), and antimycotic in a humidified atmosphere of 95% air and 5% CO_2 at 37°C. For experimental procedures, stocks were trypsinized and reseeded on six-well plates or 60 × 15 mm Petri dishes at a density of 4,000 cells/cm^2. After 24 h (~80% confluence), the medium was changed to α-MEM containing 2% (v/v) FBS and antibiotic/antimycotic as described above (differentiation medium) that was replaced after 2, 4, and 6 days of culture. After 7 days, myotube differentiation was complete, and experimental procedures were initiated. In all experiments, L6 myotubes were serum-starved for 4 h before exposure to fatty acids, AICAR, and/or compound C. All controls were incubated with equal amounts of the vehicles used for AICAR, compound C, and the respective concentrations of fat-free albumin as present in palmitate-treated cells.

Cell viability testing, trypan blue exclusion

Cells were treated with AICAR (2 mM), palmitate (1–800 μM), and compound C (10 and 40 μM). Subsequently, cells were rinsed with PBS, trypsinized, washed with medium, centrifuged, and resuspended in PBS. Next, cells were mixed with the same volume of 0.25% trypan blue and transferred to a slide for 3 min. A total of 300 cells were microscopically counted using a hemocytometer to determine the dead cell (stained blue) rate. The experiments were performed in triplicate. Compared with the control (cells not exposed to AICAR, palmitate, or compound C), no significant differences were detected for cell viability after exposing the cells for 1 h to all of the different treatment conditions.

Production of $^{14}CO_2$ from [1-^{14}C]palmitic acid

Palmitate was conjugated with essentially fatty acid-free BSA to generate a stock solution of 25% (w/v) BSA and 6 mM fatty acid in serum-free medium as described previously (19). After conjugation with albumin, the concentration of fatty acids in the solution was measured using a NEFA kit (Wako Chemicals, Inc.). The stock solution was diluted into the final culture medium to obtain concentrations of 1, 10, 50, 100, 200, 400, 600, and 800 μM fatty acid. Palmitate oxidation was measured by the production of $^{14}CO_2$ from [1-^{14}C]palmitic acid as described previously (11) with a few modifications. Briefly, cells were incubated for 1 h in 60 × 15 mm Petri dishes with medium containing 0.2 μCi/ml [1-^{14}C]palmitic acid and nonlabeled palmitate (1, 10, 50, 100, 200, 400, 600, and 800 μM) in the presence or absence of compound C as indicated. Each Petri dish was sealed with Parafilm, which had a piece of Whatman paper taped facing the inside of the Petri dish. After 1 h of incubation, the Whatman paper was wetted with 100 μl of phenylethylamine-methanol (1:1) to trap the CO_2 produced during the incubation period. Subsequently, 200 μl of H_2SO_4 (4 M) was added to the cells, which were then incubated for an additional 1 h at 37°C (11). Finally, the pieces of Whatman paper were carefully removed and transferred to scintillation vials for radioactivity counting.

Western blot determination of P-AMPKα and P-ACC

Cells were grown on six-well plates and incubated for 60 min in the presence or absence of palmitic acid (1, 10, 50, 100, 200, 400,

600, and 800 μM) and compound C (40 μM) as indicated. Experiments conducted using variable concentrations of ATP revealed that compound C is a potent reversible small-molecule AMPK inhibitor that is competitive with ATP (20). In in vitro assays, compound C did not exhibit significant inhibition of several structurally related kinases, including Zeta-associated Protein Kinase, Spleen Tyrosine Kinase, Protein Kinase C θ, Protein Kinase A, and Janus Kinase 3 (20). AICAR is a compound taken up by the cells and phosphorylated to the monophosphate form ZMP, which can accumulate in the cell, mimicking the effect of AMP on AMPK phosphorylation and activation (1–3). Here, AICAR (2 mM, 60 min) was used as a positive control for AMPK and ACC phosphorylation and also to test the effectiveness of compound C to inhibit AMPK phosphorylation and activation in L6 myotubes. Because ACC is a substrate for AMPK (2, 4), the determination of ACC phosphorylation also served as an indicator of AMPK activity. Immediately after all treatments, cells were lysed in buffer containing 135 mM NaCl, 1 mM $MgCl_2$, 2.7 mM KCl, 20 mM Tris, pH 8.0, 1% Triton, 10% glycerol, and protease and phosphatase inhibitors (0.5 mM Na_3VO_4, 10 mM NaF, 1 μM leupeptin, 1 μM pepstatin, 1 μM okadaic acid, and 0.2 mM PMSF), heated (65°C, 5 min), and passed through a 25 gauge syringe five times. An aliquot of the cell lysates was used to determine the protein concentration in each sample by the Bradford method. Before loading onto SDS-PAGE gels, the samples were diluted 1:1 (v/v) with 2 × Laemmli sample buffer [62.5 mM Tris-HCl, pH 6.8, 2% (w/v) SDS, 50 mM DTT, and 0.01% (w/v) bromophenol blue]. Aliquots of cell lysates containing 30 μg of

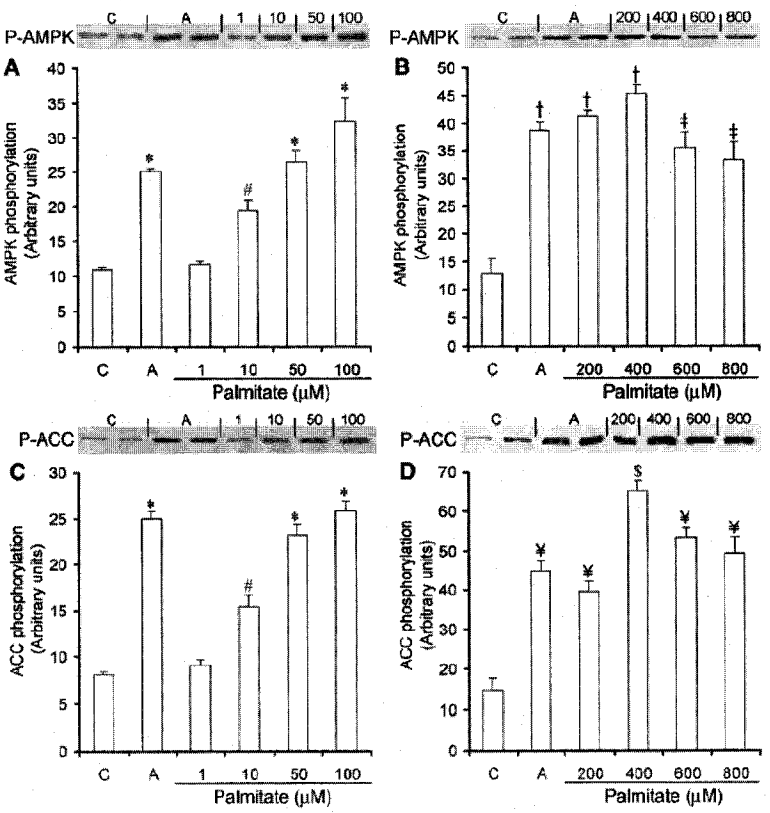

Fig. 1. Dose-response effects of palmitate on AMP-activated protein kinase (AMPK; A, B) and acetyl-coenzyme A carboxylase (ACC; C, D) phosphorylation in L6 myotubes. Densitometric analysis (graphs) and respective representative blots (upper panels) are shown for each experimental condition. Cells were exposed to different concentrations of palmitate (from 1 to 800 μM) for 1 h and then lysed as described in Methods. Control cells (C) were exposed to neither 5-aminoimidazole-4-carboxamide-1-β-D-ribofuranoside (AICAR; A) nor palmitate. AICAR was used as a positive control for AMPK and ACC phosphorylation. Data are presented as averages ± SEM. * $P < 0.05$ versus control and 1 μM palmitate. # $P < 0.05$ versus control, AICAR, and 1, 50, and 100 μM palmitate. † $P < 0.05$ versus control and 600 and 800 μM palmitate. ‡ $P < 0.05$ versus control and 400 μM palmitate. ¥ $P < 0.05$ versus control and 400 μM palmitate. $ $P < 0.05$ versus all other conditions. Data are compiled from four independent experiments with duplicates in each experiment.

protein were subjected to SDS-PAGE (12% and 7.5% resolving gels for P-AMPK and P-ACC, respectively) and then transferred to polyvinylidene difluoride membranes (Bio-Rad Laboratories, Burlington, Ontario, Canada). The phosphorylation of AMPK was determined using phospho-AMPK(Thr172) antibody (1:1,000 dilution), which detects AMPK-α only when activated by phosphorylation at Thr-172 (Cell Signaling Technology). ACC phosphorylation was detected using phospho-ACC-specific antibody (1:500 dilution; Upstate Biotechnology), which recognizes ACC when phosphorylated at serine 79 (Ser-79). Equal loading of samples was also confirmed by Coomassie blue staining of all gels.

Statistical analysis

Statistical analyses were performed by one-way or two-way ANOVA with the Tukey-Kramer multiple comparison test or Bonferroni posttest. The level of significance was set at $P < 0.05$.

RESULTS

AMPKα and ACC phosphorylation by AICAR and palmitate

As expected, AICAR elicited a 2.5- to 3.5-fold increase in AMPK and ACC phosphorylation compared with the control (Fig. 1). Interestingly, the incubation of myotubes with palmitate also caused a significant increase in AMPK and ACC phosphorylation. A significant effect (~1.9-fold) on both AMPK and ACC phosphorylation was observed in the presence of palmitate concentrations as low as 10 μM (Fig. 1A, C). A dose-response effect was found as the concentration of palmitate in the incubation medium was increased (from 1 to 800 μM). However, maximum increases of 3.5-fold for AMPK (Fig. 1B) and 4.5-fold for ACC (Fig. 1D) phosphorylation were obtained at 400 μM compared with the control; (Fig. 1C, D). Higher palmitate concentrations of 600 and 800 μM also induced the phosphorylation of AMPK (2.7- and 2.6-fold, respectively) and ACC (3.7- and 3.4-fold, respectively) compared with the control; however, the values obtained were lower than in the presence of 400 μM palmitate (Fig. 1A–D). These results indicate that either low (10 μM) or high (800 μM) fatty acid concentrations increase both AMPK and ACC phosphorylation in L6 skeletal muscle cells.

Inhibition of AICAR-induced AMPK and ACC phosphorylation by compound C

To determine whether the effects on ACC phosphorylation and fatty acid oxidation were solely attributable to the activation of AMPK by palmitate, we applied a selective AMPK inhibitor (compound C) in our experiments. To establish the efficacy of compound C to inhibit AMPK phosphorylation and activity, we treated L6 myotubes with either 10 or 40 μM of the inhibitor 30 min before exposing the cells to AICAR (2 mM). The inhibitor did not affect basal AMPK (Fig. 2A) and ACC (Fig. 2B) phosphorylation levels but significantly blocked AICAR-induced phosphorylation of AMPK and ACC. The use of 10 μM compound C significantly reduced (35% and 50%, respectively) AICAR-induced AMPK and ACC phosphorylation, whereas in the presence of 40 μM compound C, phosphorylation of both AMPK and ACC was completely abolished, reducing it to basal values (Fig. 2A, B). Therefore, 40 μM compound C was chosen to be used in all subsequent experiments.

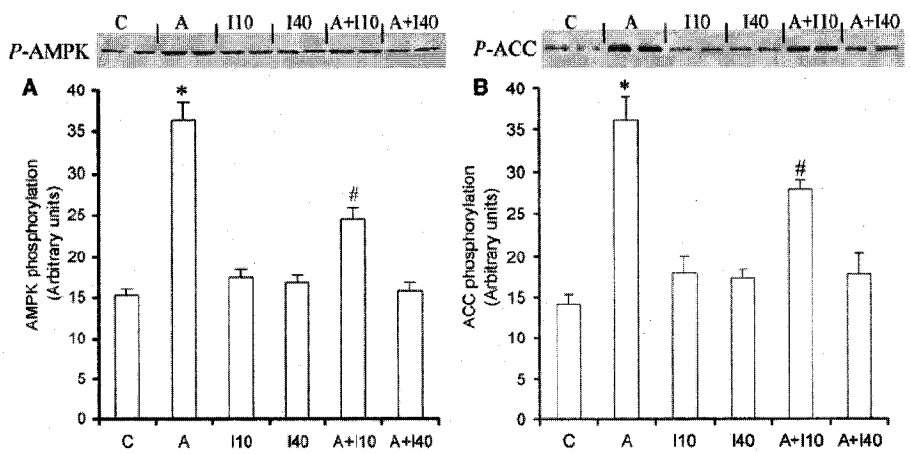

Fig. 2. Effect of compound C on basal [control (C)] and AICAR-induced (A) AMPK (A) and ACC (B) phosphorylation in L6 myotubes. Densitometric analysis (graphs) and respective representative blots (upper panels) are shown for each experimental condition. Thirty minutes before AICAR treatment, cells were exposed to either 10 μM (I10) or 40 μM (I40) compound C, an inhibitor of AMPK. Subsequently, cells were incubated for 60 min in the presence of AICAR (2 mM) as indicated. Data are presented as averages ± SEM. * $P <$ 0.05 versus control, AICAR, AICAR + 10 μM inhibitor (A+I10), and AICAR + 40 μM inhibitor (A+I40). # $P < 0.05$ versus control, AICAR, and AICAR + 40 μM inhibitor. Data are compiled from four independent experiments with duplicates in each experiment.

Effect of compound C on palmitate-induced AMPK and ACC phosphorylation

Palmitate-induced AMPK phosphorylation was blocked by compound C for all fatty acid concentrations ranging from 1 to 800 μM (**Fig. 3A, B**). Interestingly, palmitate-induced ACC phosphorylation was also prevented by compound C in the presence of palmitate concentrations ranging from 1 to 100 μM; however, this AMPK inhibitor did not prevent the palmitate-induced phosphorylation of ACC in the presence of higher concentrations (200–800 μM) of this fatty acid (Fig. 3C, D). In previous experiments, we exposed cells to various concentrations of palmitate in the presence of compound C and AICAR was used as a positive control for AMPK phosphorylation (Fig. 3). However, in those experiments, we did not have data from cells exposed to palmitate alone to serve as a control for those treated with compound C and palmitate in the same experiment. To fulfill this experimental gap, we exposed muscle cells to either 10 or 400 μM palmitate in the absence and presence of compound C. These palmitate concentrations were chosen because in previous experiments both elicited significant increases in the phosphorylation of AMPK and ACC (Fig. 1) but were differently affected by the presence of compound C (Fig. 3). As expected, AMPK phosphorylation was significantly increased in the presence of either 10 μM (1.7-fold) or 400 μM (2.4-fold) palmitate, and it was completely blocked by compound C (data not shown). Also, palmitate at 10 μM induced a significant increase (~1.6-fold) in ACC phosphorylation, which was completely prevented by compound C (**Fig. 4A**). Interestingly, in the presence of palmitate 400 μM ACC, phosphorylation increased by ~2.7-fold and remained equally phosphorylated despite the presence of compound C in the incubation medium

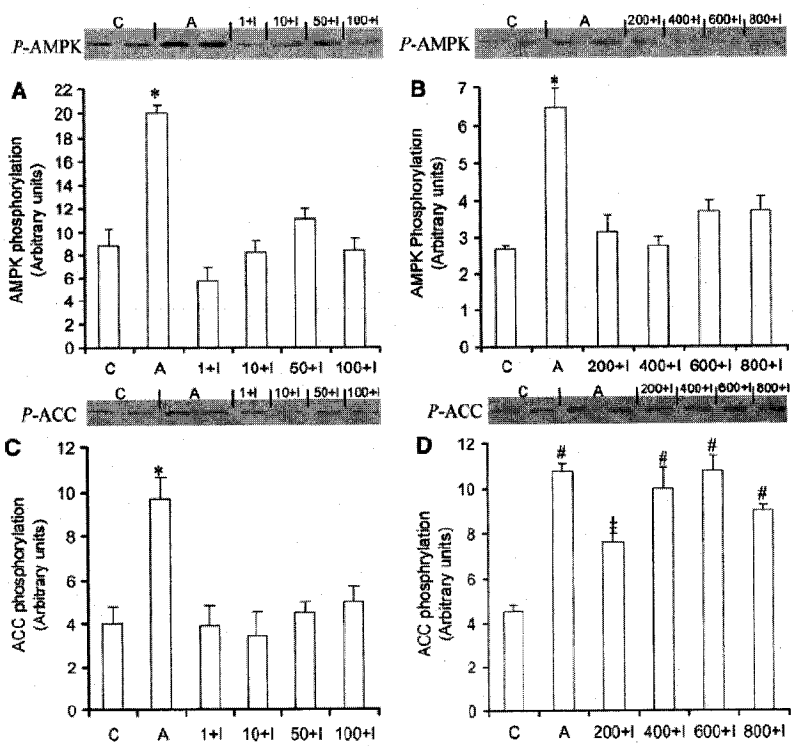

Fig. 3. Effect of compound C (40 μM) on palmitate (1–800 μM)-induced AMPK (A, B) and ACC (C, D) phosphorylation in L6 myotubes. Densitometric analysis (graphs) and respective representative blots (upper panels) are shown for each experimental condition. Compound C (I; an inhibitor of AMPK) was added to the incubation medium 30 min before palmitate treatment and was also present during the entire 1 h palmitate-incubation period. AICAR (A; 2 mM) was used as a positive control for AMPK and ACC phosphorylation. Data are presented as averages ± SEM. * $P < 0.05$ versus all conditions. # $P < 0.05$ versus control and 400 μM palmitate + inhibitor (200+I). ‡ $P < 0.05$ versus control, AICAR, 400 μM palmitate + inhibitor (400+I), and 600 μM palmitate + inhibitor (600+I). Data are compiled from four independent experiments with duplicates in each experiment.

(Fig. 4B). These results confirm and strengthen the observations that increased concentrations of palmitate exert a regulatory effect on ACC phosphorylation/activity independently of AMPK.

Effects of palmitate, AICAR, and compound C on AMPK/ACC phosphorylation and $^{14}CO_2$ production from [1-^{14}C]palmitate

AICAR and palmitate (10 and 400 μM) induced AMPK phosphorylation, and this was again prevented by compound C. Although ACC phosphorylation was also induced by AICAR and palmitate, compound C only prevented its phosphorylation at the lower concentration (10 μM) of palmitate (**Fig. 5A**). We also determined the phosphorylation state of AMPK and ACC after the cells had been exposed to a combination of AICAR and palmitate. The phosphorylation induced by AICAR and palmitate in this experiment was similar to what was observed for either AICAR or palmitate alone, with no additive effect on AMPK and ACC phosphorylation (Fig. 5A). ACC phosphorylation serves as a good indicator of AMPK activation, whereas LCFA oxidation provides an indication of ACC activity. Because AMPK and ACC phosphorylation play an important role in regulating the rate of fatty acid oxidation in skeletal muscle, we investigated the rates of $^{14}CO_2$ production from [1-^{14}C]palmitate in L6 myotubes. As palmitate concentration in the incubation medium was increased from 1 to 800 μM, the rate of oxidation of this fatty acid also increased significantly, from 12.4 pmol/h (basal; Fig. 5B, inset) to 676.86 nmol/h (800 μM; Fig. 5B). The basal condition had only labeled palmitate (0.2 μCi/ml [1-^{14}C]palmitic acid) in the incubation medium. Even though this does not reflect physiological circulating nonesterified fatty acid levels, it was technically the correct control to give us an idea of the magnitude of the increase in fatty acid oxidation by skeletal muscle cells in the presence of very low to high concentrations of palmitate.

The most accentuated increase in oxidation took place in the presence of palmitate concentrations ranging from 1 to 200 μM (from 3.9 to 487.38 nmol/h). However, as the concentration of palmitate was increased from 400 to 800 μM, the oxidation rate of this fatty acid still increased, but at a much lower rate (from 559.98 to 676.86 nmol/h, respectively) (Fig. 5B). Here, we also tested the effect of AICAR-induced AMPK activation on palmitate oxidation. As expected, in the presence of AICAR (2 mM), we observed a significant increase in $^{14}CO_2$ production either under basal conditions (~1.4-fold; Fig. 5B, inset) or in the presence of up to 100 μM palmitate (1.7-, 2-, 1.6-, and 1.7-fold vs. palmitate alone for 1, 10, 50, and 100 μM palmitate, respectively) (Fig. 5B). However, as palmitate concentration was increased from 200 to 800 μM, the AICAR-induced effect on $^{14}CO_2$ production from [1-^{14}C]palmitic acid was significantly attenuated (1.07-, 1.09-, 1.09-, and 1.08-fold for 200, 400, 600, and 800 μM palmitate, respectively) compared with palmitate alone (Fig. 5B). Interestingly, the addition of compound C significantly blocked the oxidative effect of palmitate alone and of AICAR in the presence of palmitate concentrations ranging from 1 to 100 μM. However, in the presence of higher palmitate concentrations (200, 400, 600, and 800 μM), compound C was not effective in blocking the oxidative responses induced by palmitate alone or in combination with AICAR (Fig. 5B). These results are compatible with the effects of palmitate on AMPK and ACC phosphorylation reported above (Figs. 3, 4). This suggests that under increased concentrations of fatty acids (> 200 μM), an AMPK-independent pathway

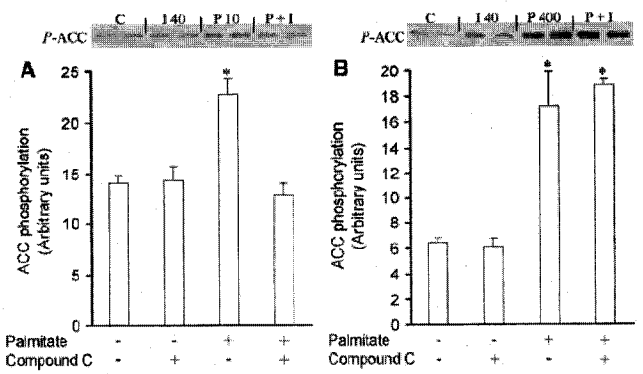

Fig. 4. Effect of compound C (40 μM) on basal [control (C), cells exposed to neither palmitate nor compound C] and palmitate-induced ACC phosphorylation in L6 myotubes. Densitometric analysis (graphs) and respective representative blots (upper panels) are shown for each experimental condition. Compound C (I; an inhibitor of AMPK) was added to the cells 30 min before palmitate treatment and was also present during the entire 1 h palmitate-incubation period. Cells were exposed to either 10 μM (A) or 400 μM (B) palmitate and then lysed for Western blotting. Data are presented as averages ± SEM. * $P < 0.05$ versus control and compound C. Data are compiled from four independent experiments with duplicates in each experiment.

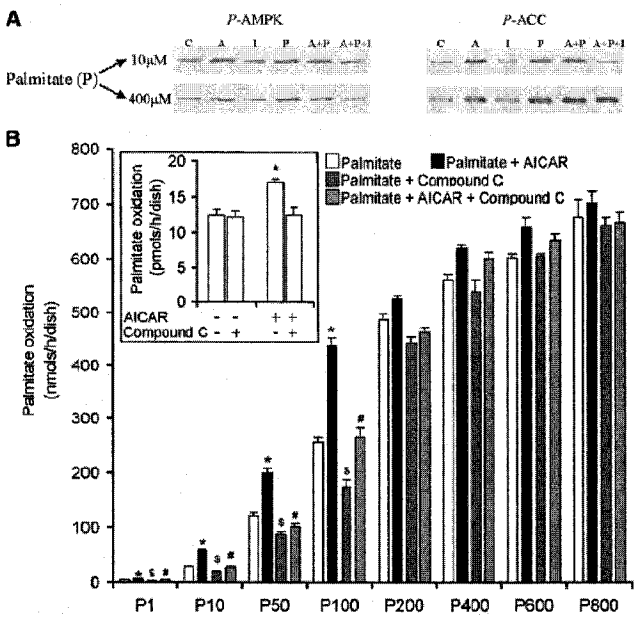

Fig. 5. A: Representative blots of the effects of palmitate (P; 10 and 400 μM), AICAR (A), compound C (I), AICAR + palmitate (A+P), and AICAR + palmitate + compound C (A+P+I) on AMPK and ACC phosphorylation. B: Effects of various palmitate concentrations (ranging from 1 to 800, μM P1 to P800), palmitate + AICAR (2 mM), palmitate + compound C (40 μM), and palmitate + AICAR + compound C on $^{14}CO_2$ production from [1-^{14}C]palmitate (palmitate oxidation; nmol/dish/h) in L6 myotubes. The inset refers to the effects of compound C on basal (in the absence of AICAR and compound C) and AICAR (2 mM)-induced $^{14}CO_2$ production from [1-^{14}C]palmitate (palmitate oxidation; pmol/dish/h). Basal values were determined in the presence of only radiolabeled palmitate (0.2 μCi/ml). Data are presented as averages ± SEM. * $P < 0.05$ versus palmitate, palmitate + compound C, and palmitate + AICAR + compound C. $ $P < 0.05$ versus palmitate and palmitate + AICAR. # $P < 0.05$ versus palmitate + AICAR. Data are compiled from four independent experiments with triplicates in each experiment.

was responsible for inducing fatty acid oxidation in skeletal muscle cells.

DISCUSSION

Here, we describe the novel finding that AMPK and ACC activity are regulated by palmitate in skeletal muscle cells in a dose-dependent manner. The concentrations of palmitate applied ranged from 1 to 800 μM, which are within the values observed either in physiological conditions such as overnight fasting (~100–500 μM) and prolonged exercise (~500–1,000 μM) or in pathological conditions such as obesity (~600–800 μM) and type 2 diabetes mellitus (~700–900 μM) (21). However, although plasma fatty acids can reach 800 μM, this is unlikely the case for the extracellular fluid to which skeletal muscle is exposed in vivo. This raises the question of whether the treatment of L6 muscle cells to high palmitate concentrations (400–800 μM) could be toxic to the cells and affect cell viability. High levels of palmitate did not alter cell viability when measured by the trypan blue exclusion method, as reported in Methods. Additionally, even though in our system the maximum phosphorylation response of AMPK and ACC was obtained in the presence of 400 μM, the effect on oxidation was increased significantly and remained high as palmitate concentrations were increased up to 800 μM in the incubation medium. This sustained functional response to high levels of palmitate (400–800 μM) indicates that the muscle cells were viable and well responsive under all experimental conditions.

ACC phosphorylation was coupled to AMPK phosphorylation and activation in the presence of palmitate concentrations ranging from 1 to 100 μM. However, at concentrations > 200 μM, ACC phosphorylation remained high, despite the total inhibition of AMPK phosphorylation by compound C, a selective AMPK inhibitor. These results indicated that palmitate regulates ACC phosphorylation/activity by AMPK-dependent and -independent mechanisms, based on its abundance in skeletal muscle cells.

It has been demonstrated previously that the cytoplasmic process of fatty acid activation (formation of fatty

acyl-CoA) consumes ATP and increases cytosolic AMP by ~30-fold, leading to AMPK activation in isolated hepatocytes (16). Also, activation of heart AMPK in response to physiological concentrations of LCFAs has been reported (15). These findings are in agreement with our results with skeletal muscle cells showing that palmitate increases AMPK phosphorylation and also the phosphorylation of its direct substrate ACC, which are also compatible with the observed increase in fatty acid oxidation. In fact, the rate of palmitate oxidation by skeletal muscle cells increased as the concentration of this fatty acid in the medium was increased up to 400 μM and practically reached a plateau thereafter. Interestingly, inhibition of AMPK phosphorylation by compound C significantly reduced (30%) basal (containing only labeled palmitate: 0.2 μCi/ml [1-^{14}C]palmitic acid) and AICAR-induced (~45%) palmitate oxidation for concentrations of this fatty acid ranging from 0 to 100 μM. However, compound C exerted no significant effect on either basal or AICAR-induced palmitate oxidation as the concentration of this fatty acid was increased from 200 to 800 μM, even though AMPK phosphorylation was prevented by compound C. Additionally, the combination of AICAR and palmitate elicited a significant additive effect on oxidation (~75%) up to 100 μM palmitate, but this effect was practically abolished (~7.5%) when palmitate concentration ranged from 200 to 800 μM. Importantly, no additive effect on AMPK and ACC phosphorylation was observed when cells were exposed to a combination of AICAR and palmitate (either 10 or 400 μM).

These findings indicate that LCFAs autoregulate their metabolism by two separate pathways: one that depends on AMPK activation, and another that directly modulates ACC phosphorylation/activity and overrides the effects of AMPK activation. The concentration of LCFAs in the cell is the major factor determining which of these pathways will prevail in the regulation of fatty acid metabolism in skeletal muscle cells. Previous studies performed with perfused heart muscle (15) and with isolated rat hepatocytes (16) have shown that not only palmitate but also acetate, octanoate, and oleate increase AMPK activity (15, 16) and fatty acid oxidation (15). In our experiments, we used only palmitate, and further studies need to be performed to test whether other fatty acids also regulate the phosphorylation/activity of the AMPK/ACC pathway and β-oxidation in skeletal muscle.

The fact that ACC remained phosphorylated even after compound C prevented palmitate-induced AMPK phosphorylation suggests that fatty acids may also regulate ACC activity by inducing the phosphorylation of this enzyme by an alternative kinase. Additionally, it may be possible that fatty acids inhibit phosphatases that might otherwise dephosphorylate and activate ACC. The inhibition by palmitate of phosphatases that target ACC would divert the metabolism of LCFAs toward oxidation instead of lipid synthesis in the presence of high levels of fatty acids. In fact, in the present study, we also observed that ACC phosphorylation was accompanied by an upregulation of palmitate oxidation in skeletal muscles cells. Further studies are necessary to precisely identify the mechanisms by which fatty acids regulate ACC phosphorylation/activity in skeletal muscle cells and, therefore, autoregulate their metabolic fate.

The AMPK-independent effect of high levels of palmitate on fatty acid oxidation may also have derived from a potent feedback inhibition of ACC by long-chain fatty acyl-CoA esters (2, 4, 22). There is compelling evidence that citrate and acetyl-CoA function as allosteric activators of ACC, whereas long-chain fatty acyl-CoA acts as an allosteric inhibitor opposing the action of citrate on purified rat hindlimb muscle ACC (23). Suppression of lipogenesis by fatty acids has also been demonstrated in extracts of rat epididymal fat pads (5) and in rat perfused livers (6), even though there is little evidence that these were through allosteric inhibition of ACC. In rat skeletal muscle, refeeding after a fast rapidly decreased fatty acid oxidation in vivo, and this has been attributed to a decrease in circulating fatty acid levels releasing allosteric inhibition of ACC in muscle (18). All of these observations are in agreement with our findings, which indicate that fatty acid abundance leads to ACC inhibition and suppression of lipogenesis. From a functional perspective, this seems logical, because it would be unnecessary and counterproductive to maintain the de novo lipid synthesis pathway active under conditions of high cellular fatty acid levels. However, it was reported recently that long-chain acyl-CoA esters inhibit the in vitro phosphorylation and activation of recombinant AMPK by liver purified LKB1/STRAD/MO25, suggesting that in the presence of LCFAs the activation of the AMPK pathway may actually be impaired (17). Even though AMPK activity was measured directly by Taylor et al. (17), the in vitro analysis performed with purified enzymes did not allow complex cellular metabolic interactions of AMPK with its allosteric regulators to take place. This is particularly important because in our experiments using muscle cells, palmitate consistently increased the phosphorylation of AMPK in a dose-dependent manner, whereas palmitate-induced ACC phosphorylation was regulated by AMPK-dependent and -independent mechanisms. From a metabolic perspective, the activity of ACC is what ultimately determines malonyl-CoA production and whether fatty acids will be produced or oxidized in the cell (2, 4). Because ACC activation does not depend exclusively on AMPK phosphorylation, the implications of AMPK regulation by fatty acids have to be analyzed in a more complex and interactive system.

The implications of our findings are that the fatty acid oxidative response that is normally triggered via AMPK activation by endogenous hormones and nutrients, and other pharmacological agonists (9, 10), may be impaired in the presence of high fatty acid concentrations in skeletal muscle. In the presence of fatty acids, the AMPK/ACC system becomes activated and the oxidative response of the muscle cell may reach its maximum capacity, preventing any potential additional effect that could be triggered by other AMPK agonists. In fact, we found that AICAR (a well-known inducer of AMPK activity) did not elicit any additive oxidative effect in L6 muscle cells in the presence

of palmitate concentrations of > 200 μM. This is particularly important because certain metabolic disorders, such as obesity and type 2 diabetes, are accompanied by chronically high levels of circulating fatty acids (~600–900 μM) (21), which may limit the response of the AMPK/ACC pathway to endogenous and exogenous AMPK agonists. Recently, it was reported that adipokines such as leptin (9, 10) and adiponectin (24) exert direct antilipotoxic effects on skeletal muscle by activating the AMPK/ACC pathway. Resistance to these adipokines could be partially attributable to high levels of fatty acids maximally activating the AMPK/ACC pathway and impairing further activation of the AMPK/ACC pathway by leptin or adiponectin in peripheral tissues. In fact, mice overexpressing leptin in liver are skinny and present increased levels of AMPK and ACC phosphorylation. However, these animals developed obesity when exposed to a high-fat diet accompanied by attenuation of AMPK and ACC phosphorylation (25). Interestingly, the levels of circulating fatty acids in these transgenic animals increased from 1.43 mEq/l on a regular diet to 2.17 mEq/l on the high-fat diet (25). It is important to note that this in vivo study did not establish any cause-and-effect relationship between fatty acids and leptin sensitivity in skeletal muscle, although it suggests a potential link between these variables.

In conclusion, our results provide evidence that fatty acids autoregulate their metabolic fate in skeletal muscle cells by directly regulating the phosphorylation and activation of AMPK and ACC. These effects of fatty acids on skeletal muscle may have important physiological and pathological implications for the response of this tissue to endogenous and exogenous agonists of the AMPK/ACC pathway.

The authors thank Merck Research Laboratories for kindly providing compound C for these experiments.

REFERENCES

1. Carling, D. 2005. AMP-activated protein kinase: balancing the scales. *Biochimie.* **87:** 87–91.
2. Ruderman, N. B., A. K. Saha, D. Vavas, and L. A. Witters. 1999. Malonyl-CoA, fuel sensing, and insulin resistance. *Am. J. Physiol.* **276:** E1–E18.
3. Winder, W. W. 2001. Roles of adenosine monophosphate-activated protein kinase in skeletal muscle: fatty acid oxidation, glucose transport, and gene regulation. *Curr. Opin. Endocrinol. Diabetes.* **8:** 180–185.
4. Munday, M. R. 2002. Regulation of mammalian acetyl-CoA carboxylase. *Biochem. Soc. Trans.* **30:** 1059–1064.
5. Halestrap, A. P., and R. M. Denton. 1974. Hormonal regulation of adipose-tissue acetyl-coenzyme A carboxylase by changes in the polymeric state of the enzyme. The role of long-chain fatty acyl-coenzyme A thioesters and citrate. *Biochem. J.* **142:** 365–377.
6. Mayes, P. A., and D. L. Topping. 1974. Regulation of hepatic lipogenesis by plasma free fatty acids: simultaneous studies on lipoprotein secretion, cholesterol synthesis, ketogenesis and gluconeogenesis. *Biochem. J.* **140:** 111–114.
7. Nikawa, J., T. Tanabe, H. Ogiwara, T. Shiba, and S. Numa. 1979. Inhibitory effects of long-chain acyl coenzyme A analogues on rat liver acetyl coenzyme A carboxylase. *FEBS Lett.* **102:** 223–226.
8. McGarry, J. D. 2002. Banting Lecture 2001. Dysregulation of fatty acid metabolism in the etiology of type 2 diabetes. *Diabetes.* **51:** 7–18.
9. Ceddia, R. B. 2005. Direct metabolic regulation in skeletal muscle and fat tissue by leptin: implications for glucose and fatty acids homeostasis. *Int. J. Obes.* **29:** 1175–1183.
10. Kahn, B. B., T. Alquier, D. Carling, and D. G. Hardie. 2005. AMP-activated protein kinase: ancient energy gauge provides clues to modern understanding of metabolism. *Cell Metab.* **1:** 15–25.
11. Ceddia, R. B., and G. Sweeney. 2004. Creatine supplementation increases glucose oxidation and AMPK phosphorylation and reduces lactate production in L6 rat skeletal muscle cells. *J. Physiol.* **555:** 409–421.
12. Ponticos, M., Q. L. Lu, J. E. Morgan, D. G. Hardie, T. A. Partridge, and D. Carling. 1998. Dual regulation of the AMP-activated protein kinase provides a novel mechanism for the control of creatine kinase in skeletal muscle. *EMBO J.* **17:** 1688–1699.
13. Hudson, E. R., D. A. Pan, J. James, J. M. Lucocq, S. A. Hawley, K. A. Green, O. Baba, T. Terashima, and D. G. Hardie. 2003. A novel domain in AMP-activated protein kinase causes glycogen storage bodies similar to those seen in hereditary cardiac arrhythmias. *Curr. Biol.* **13:** 861–866.
14. Wojtaszewski, J. F., S. B. Jorgensen, Y. Hellsten, D. G. Hardie, and E. A. Richter. 2002. Glycogen-dependent effects of 5-aminoimidazole-4-carboxamide (AICA)-riboside on AMP-activated protein kinase and glycogen synthase activities in rat skeletal muscle. *Diabetes.* **51:** 284–292.
15. Clark, H., D. Carling, and D. Saggerson. 2004. Covalent activation of heart AMP-activated protein kinase in response to physiological concentrations of long-chain fatty acids. *Eur. J. Biochem.* **271:** 2215–2224.
16. Kawaguchi, T., K. Osatomi, H. Yamashita, T. Kabashima, and K. Uyeda. 2002. Mechanism for fatty acid "sparing" effect on glucose-induced transcription: regulation of carbohydrate-responsive element-binding protein by AMP-activated protein kinase. *J. Biol. Chem.* **277:** 3829–3835.
17. Taylor, E. B., W. J. Ellingson, J. D. Lamb, D. G. Chesser, and W. W. Winder. 2005. Long-chain acyl-CoA esters inhibit phosphorylation of AMP-activated protein kinase at threonine-172 by LKB1/STRAD/MO25. *Am. J. Physiol. Endocrinol. Metab.* **288:** E1055–E1061.
18. Chien, D., D. Dean, A. K. Saha, J. P. Flatt, and N. B. Ruderman. 2000. Malonyl-CoA content and fatty acid oxidation in rat muscle and liver in vivo. *Am. J. Physiol. Endocrinol. Metab.* **279:** E259–E265.
19. Ceddia, R. B., W. N. William, Jr., F. B. Lima, P. Flandin, R. Curi, and J. P. Giacobino. 2000. Leptin stimulates uncoupling protein-2 mRNA expression and Krebs cycle activity and inhibits lipid synthesis in isolated rat white adipocytes. *Eur. J. Biochem.* **267:** 5952–5958.
20. Zhou, G., R. Myers, Y. Li, Y. Chen, X. Shen, J. Fenyk-Melody, M. Wu, J. Venture, T. Doebber, N. Fujii, et al. 2001. Role of AMP-activated protein kinase in mechanism of metformin action. *J. Clin. Invest.* **108:** 1167–1174.
21. Roden, M. 2004. How free fatty acids inhibit glucose utilization in human skeletal muscle. *News Physiol. Sci.* **19:** 92–96.
22. Hardie, D. G., and D. A. Pan. 2002. Regulation of fatty acid synthesis and oxidation by the AMP-activated protein kinase. *Biochem. Soc. Trans.* **30:** 1064–1070.
23. Trumble, G. E., M. A. Smith, and W. W. Winder. 1995. Purification and characterization of rat skeletal muscle acetyl-CoA carboxylase. *Eur. J. Biochem.* **231:** 192–198.
24. Kadowaki, T., and T. Yamauchi. 2005. Adiponectin and adiponectin receptors. *Endocr. Rev.* **26:** 439–451.
25. Tanaka, T., S. Hidaka, H. Masuzaki, S. Yasue, Y. Minokoshi, K. Ebihara, H. Chusho, Y. Ogawa, T. Toyoda, K. Sato, et al. 2005. Skeletal muscle AMP-activated protein kinase phosphorylation parallels metabolic phenotype in leptin transgenic mice under dietary modification. *Diabetes.* **54:** 2365–2374.

Journal of Cellular Physiology

Activation of AMP-Activated Protein Kinase, Inhibition of Pyruvate Dehydrogenase Activity, and Redistribution of Substrate Partitioning Mediate the Acute Insulin-Sensitizing Effects of Troglitazone in Skeletal Muscle Cells

S. FEDIUC, A.S. PIMENTA, M.P. GAIDHU, AND R.B. CEDDIA*

School of Kinesiology and Health Science, York University, Toronto, Ontario, Canada

The aim of this study was to investigate the acute effects of troglitazone on several pathways of glucose and fatty acid (FA) partitioning and the molecular mechanisms involved in these processes in skeletal muscle. Exposure of L6 myotubes to troglitazone for 1 h significantly increased phosphorylation of AMPK and ACC, which was followed by ~30% and ~60% increases in palmitate oxidation and carnitine palmitoyl transferase-1 (CPT-1) activity, respectively. Troglitazone inhibited basal (~25%) and insulin-stimulated (~35%) palmitate uptake but significantly increased basal and insulin-stimulated glucose uptake by ~2.2- and 2.7-fold, respectively. Pharmacological inhibition of AMPK completely prevented the effects of troglitazone on palmitate oxidation and glucose uptake. Interestingly, even though troglitazone exerted an insulin sensitizing effect, it reduced basal and insulin-stimulated rates of glycogen synthesis, incorporation of glucose into lipids, and glucose oxidation to values corresponding to ~30%, ~60%, and 30% of the controls, respectively. These effects were accompanied by an increase in basal and insulin-stimulated phosphorylation of Akt_{Thr308}, Akt_{Ser473}, and GSK3α/β. Troglitazone also powerfully suppressed pyruvate decarboxylation, which was followed by a significant increase in basal (~3.5-fold) and insulin-stimulated (~5.5-fold) rates of lactate production by muscle cells. In summary, we provide novel evidence that troglitazone exerts acute insulin sensitizing effects by increasing FA oxidation, reducing FA uptake, suppressing pyruvate dehydrogenase activity, and shifting glucose metabolism toward lactate production in muscle cells. These effects seem to be at least partially dependent on AMPK activation and may account for potential acute PPAR-γ-independent anti-diabetic effects of thiazolidinediones in skeletal muscle.

J. Cell. Physiol. 215: 392–400, 2008.

Thiazolidinediones (TZDs) are a common class of drugs used for treatment of type 2 diabetes mellitus. These oral anti-diabetic agents, such as troglitazone, pioglitazone, and rosiglitazone, improve insulin sensitivity and glucose homeostasis in both humans (Inzucchi et al., 1998) and animals (Kraegen et al., 1989; Lee et al., 1994; Miles et al., 1998). It is widely accepted that the molecular target of TZDs is the peroxisome proliferator activated receptor-γ (PPAR-γ), a transcription factor that belongs to the nuclear receptor family and is predominantly expressed in adipose tissue (Auboeuf et al., 1997). Activation of PPAR-γ by TZDs increases the transcription of genes involved in fatty acid (FA) synthesis and storage causing a reduction of plasma non-esterified fatty acid (NEFA) levels (Castelein et al., 1994; Guan et al., 2002).

Although a large body of evidence supports the importance of TZD-mediated PPAR-γ activation on the improvement of insulin sensitivity, it appears that TZDs also exert metabolic effects that are independent of the activation of this transcription factor. In fact, it has been reported that after 10–20 min of infusing troglitazone in rats in vivo, blood glucose levels were significantly reduced (Lee and Olefsky, 1995). However, it was not clear whether this acute in vivo glucose lowering effect was primarily due to actions of troglitazone on fat tissue or by also affecting other tissues that may contribute to glucose disposal. Interestingly, lipoatrophic (fatless) mice treated with TZDs had improved insulin sensitivity, suggesting non-adipocyte targets for these drugs (Burant et al., 1997).

More recently, it was observed that incubating rat extensor digitorum longus (EDL) muscles with either troglitazone or rosiglitazone for 30 min increased glucose uptake and FA oxidation in this tissue (LeBrasseur et al., 2006). Due to the short exposure to TZDs and also because muscle expresses very low levels of PPAR-γ (Auboeuf et al., 1997), these acute effects of TZDs were unlikely dependent on activation of this transcription factor. In fact, the authors of the study presented evidence that TZDs exert direct effects on glucose and lipid metabolism in skeletal muscle, an effect that was attributed to phosphorylation/activation of AMP-activated protein kinase (AMPK) (LeBrasseur et al., 2006).

Contract grant sponsor: Natural Science and Engineering Research Council (NSERC).

*Correspondence to: R.B. Ceddia, Department of Kinesiology and Health Science, York University, 4700 Keele St, Toronto, ON, Canada M3J 1P3. E-mail: roceddia@yorku.ca

Received 22 June 2007; Accepted 13 September 2007

DOI: 10.1002/jcp.21321

AMPK is a fuel-sensing enzyme that when activated turns on catabolic pathways that produce ATP, while turning off anabolic pathways that consume ATP to maintain cellular energy stores (Carling, 2005). In its active state, AMPK phosphorylates and deactivates its direct substrate acetyl-CoA carboxylase (ACC). When ACC is inactive, a fall in malonyl-CoA occurs, which disinhibits carnitine palmitoyl transferase-1 (CPT-1) and increases mitochondrial import and oxidation of long-chain fatty acids (LCFAs) (McGarry, 2002). Therefore, the AMPK/ACC pathway is thought to play a central role in the regulation of cellular lipid homeostasis. In this context, several studies have reported that TZDs cause rapid activation of AMPK in L6 (Konrad et al., 2005), H-2K^b muscle cells (Fryer et al., 2002), and in isolated rat EDL muscles (LeBrasseur et al., 2006). However, the metabolic implications of TZD-induced AMPK activation in skeletal muscle, especially regarding LCFA oxidation and substrate partitioning, have been controversial and not clearly established. Previous short (90 min) and long-term (up to 25 h) studies have reported that TZDs inhibit complex I respiration and suppress glucose and palmitate oxidation in isolated rat skeletal muscles (Furnsinn et al., 2000). This scenario seems clearly at odds with the hypothesis that AMPK activation by TZDs would increase LCFA oxidation and exert an anti-lipotoxic effect in skeletal muscles. It could be argued that the effects of TZDs on AMPK activation leading to oxidation of LCFAs are overridden by other more powerful direct inhibitory effects of these drugs on crucial steps of the respiratory chain. However, in opposition to this idea are the recent findings that troglitazone and pioglitazone rapidly induce phosphorylation/activation of AMPK and cause a significant increase in palmitate oxidation in isolated rat EDL muscles (LeBrasseur et al., 2006). Currently, there is no consensus regarding the regulation of the AMPK/ACC system by TZDs and its effects on lipid metabolism and substrate partitioning in skeletal muscles.

Here, we hypothesize that by promoting AMPK activity and acutely altering glucose and lipid partitioning in muscle cells, TZDs may also affect other metabolic pathways such as FA uptake and lipogenesis in muscle cells. These alterations could mediate potential insulin sensitizing effects of TZDs in skeletal muscle cells. In fact, evidence has been provided that in isolated muscle incubations ranging from 30 min to 25 h (Furnsinn et al., 2000; Konrad et al., 2005; LeBrasseur et al., 2006), TZDs improve glucose uptake in this tissue. Some of these studies indicate that AMPK activation seems to be responsible for these acute effects of TZDs in skeletal muscle (Konrad et al., 2005; LeBrasseur et al., 2006). However, it still remains to be determined whether TZDs exert acute insulin sensitizing effects exclusively by activating AMPK or by also independently affecting crucial steps of the insulin signaling pathway. In this context, a recent investigation has reported that acute treatment of L6 muscle cells with troglitazone does not alter basal PI3-kinase activity or Akt phosphorylation (Konrad et al., 2005). Surprisingly, this study did not provide data regarding the effect of combining insulin and troglitazone on insulin signaling and on glucose uptake and metabolism. This is particularly important since in in vivo conditions TZDs and insulin are simultaneously present. Therefore, analysis of potential interactions between glucose and lipid metabolism under conditions where insulin and TZDs are combined is of great physiological relevance. To clarify these issues, we have investigated the acute effects of troglitazone on AMPK activation and various aspects of glucose and LCFA metabolism either under basal or insulin-stimulated conditions in muscle cells. Here, we provide novel evidence that troglitazone exerts acute insulin sensitizing effects by reducing FA uptake, increasing FA oxidation, suppressing pyruvate dehydrogenase (PDH) activity, and shifting glucose metabolism toward lactate production in skeletal muscle cells.

Experimental Procedures

Reagents

Alpha-modified Eagle's medium (α-MEM) and FBS were purchased from Wisent (Quebec, Canada). The NEFA and lactate kits were obtained from Wako Chemicals, Inc., Richmond, VA and Trinity Biotech, St. Louis, MO, respectively. Troglitazone, etomoxir, defatted albumin, palmitic acid, phenylethylamine, and the MTT (3[-4,5-dimethylthiazol-2-yl]2,5idiphenyl tetrazolium bromide) assay kit were purchased from Sigma (St. Louis, MO). [1-^{14}C]palmitic acid, D-[U-^{14}C]glucose, 2-deoxy-D-[^{3}H]glucose, and [1-^{14}C]pyruvic acid were purchased from Amersham Biosciences (Piscataway, NJ). Compound C was kindly provided by Merck Research Laboratories, Rahway, NJ. Antibodies against *P*-AMPK, *P*-Akt, and *P*-GSK-3α/β were purchased from Cell Signaling Technology, Inc. (Beverly, MA). *P*-ACC was obtained from Upstate Biotechnology (Charlottesville, VA), and GAPDH was obtained from Abcam, Inc. (Cambridge, MA). All other reagents used in these experiments were of the highest grade available.

Cell culture and assessment of viability

L6 skeletal muscle cells were grown in α-MEM and differentiated as previously described (Fediuc et al., 2006b). Cells were serum-starved (α-MEM without FBS) for 4 h prior to exposure to troglitazone (5, 50, and 100 μM), insulin (100 nM), compound C (10 and 20 μM), etomoxir (2.5 μM), and various combinations of these drugs. All controls were incubated with equal amounts of vehicle used for the previously mentioned conditions. Cell viability was tested by using the MTT (3[-4,5-dimethylthiazol-2-yl]2,5idiphenyl tetrazolium bromide) assay kit after myotubes were exposed to all treatment conditions (Fediuc et al., 2006b). No significant differences were observed in cell viability after myotubes were exposed for 1 h to all troglitazone, compound C, and etomoxir concentrations mentioned above.

Determination of P-AMPK, P-ACC, P-Akt (Thr308 and Ser473), and P-GSK-3α/β

Cells were grown in six-well plates and incubated for 60 min in the absence or presence of either troglitazone (50 μM), insulin (100 nM), compound C (10 and 20 μM), troglitazone plus insulin, and troglitazone plus compound C. Determination of P-Akt and P-GSK were performed after cells had been exposed to insulin in the last 5, 10, and 20 min of the 60 min incubation period. Immediately after all treatments, cells were lysed in a buffer containing 135 mM NaCl, 1 mM $MgCl_2$, 2.7 mM KCl, 20 mM Tris, pH 8.0, 1% Triton, 10% glycerol, and protease and phosphatase inhibitors (0.5 mM Na_3VO_4, 10 mM NaF, 1 μM leupeptin, 1 μM pepstatin, 1 μM okadaic acid, and 0.2 mM PMSF), heated (65°C, 5 min), and passed through a 25 gauge syringe five times. Protein content was determined by the Bradford method. Aliquots (30 μg of protein) were loaded onto the gels and subjected to SDS–PAGE and then transferred to polyvinyl difluoride membranes (Bio-Rad, Hercules, CA). Equal protein loading was assessed by coomassie staining of all gels and by blotting against GAPDH. Membranes used for P-AMPK and P-ACC blotting were derived from the same samples, therefore, the same GAPDH blots are representative of loading for both proteins. Antibodies used for the determination of *P*-AMPK$_{Thr\text{-}172}$, *P*-ACC$_{Ser79}$, *P*-Akt$_{Thr308}$/*P*-Akt$_{Ser473}$, *P*-GSK3α/β, and GAPDH were applied as previously described (Fediuc et al., 2006a, b).

Production of $^{14}CO_2$ from [1-^{14}C]palmitic acid, D-[U-^{14}C]glucose, and [1-^{14}C]pyruvic acid

Palmitate, glucose, and pyruvate oxidation were measured by the production of $^{14}CO_2$ from [1-^{14}C]palmitic acid,

D-[U-^{14}C]glucose, and [1-^{14}C]pyruvic acid, respectively. Production of acetyl-CoA by the PDH complex depends on decarboxylation of pyruvate that occurs at the site of carbon 1 of the molecule; therefore determination of $^{14}CO_2$ from [1-^{14}C]pyruvic acid allows us to trace the activity of the PDH complex (Curi et al., 1988; Ceddia et al., 1999; Ceddia and Sweeney, 2004). All determinations were performed as previously described (Ceddia and Sweeney, 2004; Fediuc et al., 2006b). Briefly, cells were incubated for 1 h in 35 × 10 mm Petri dishes with α-MEM containing each specific isotope in the following concentrations: [1-^{14}C]palmitic acid (0.2 μCi/ml) plus non-labeled palmitate (20 μM), D-[U-^{14}C]glucose (0.2 μCi/ml) or [1-^{14}C]pyruvic acid (0.1 μCi/ml) plus 2 mM non-labeled pyruvic acid either in the absence or presence of troglitazone (50 μM), insulin (100 nM), compound C (10 and 20 μM), troglitazone plus insulin, troglitazone plus compound C, and troglitazone plus insulin plus compound C. The rates of $^{14}CO_2$ production from [1-^{14}C]palmitic acid, D-[U-^{14}C]glucose, and [1-^{14}C]pyruvic acid were determined in the presence of 5.5mM non-labeled D-glucose. After 1 h of incubation, produced $^{14}CO_2$ was collected for radioactivity counting (Ceddia et al., 1999; Ceddia and Sweeney, 2004; Fediuc et al., 2006b).

CPT-1 activity

L6 myotubes were exposed to insulin (100 nM), etomoxir (2.5 μM), troglitazone (50 μM), and troglitazone plus insulin for 1 h and then the activity of CPT-1 was determined by using a radiometric assay (Spurway et al., 1994). Briefly, the assay buffer contained 50 mM imidazole, 70 mM KCl, 1 mM KCN, 80 mM sucrose, 1 mM EGTA, 2 mM $MgCl_2$, 1 mM dithiothreitol (DTT), 1 mM ATP, 70 μM Palmitoyl-CoA, 0.1% fat-free BSA, 40 μM digitonin, and 0.5 μCi/ml L-[^{3}H]carnitine. Cells were exposed to the assay buffer for 5 min and the reaction was terminated by aspirating the assay buffer and adding ice-cold PCA (4M) to each well. Cells were then collected, lipid was extracted using butanol, and used for scintillation counting. Etomoxir was used as a negative control (Selby and Sherratt, 1989).

Palmitate and glucose uptake

For palmitate uptake, L6 myotubes were exposed to insulin (100 nM), troglitazone (5, 50, and 100 μM), and troglitazone plus insulin for 1 h and then incubated for 4 min in starve medium containing 0.2 μCi/ml [1-^{14}C]palmitic acid and non-labeled palmitate (20 μM) (Gaidhu et al., 2006). For glucose uptake, cells were incubated in the absence or presence of insulin (100 nM), troglitazone (50 μM), troglitazone plus insulin, compound C (20 μM), insulin plus compound C, troglitazone plus compound C, and troglitazone plus insulin plus compound C. Cells were exposed to compound C 30 min prior to receiving troglitazone while insulin was added to the medium in the last 20 min of the 1 h incubation period. Subsequently, cells were washed and incubated with Hepes-buffered saline solution containing 10 μM 2-deoxy-D-glucose (0.5 μCi/ml 2-deoxy-D-[^{3}H]glucose) as previously described (Ceddia and Sweeney, 2004). Both assays were terminated by adding ice-cold PBS and the cells were then lysed in 0.1 M KOH. An aliquot of the lysate was used for radioactivity counting and the remainder was used for protein determination by the Bradford method (Gaidhu et al., 2006).

Glycogen synthesis, glucose incorporation into lipids, and lactate production

The rate of glycogen synthesis was assessed by the incorporation of D-[U-^{14}C]glucose into glycogen (Fediuc et al., 2006a). Briefly, myotubes were incubated for 1 h in starve medium (α-MEM without FBS) containing 5.5 mM D-glucose and 0.2 μCi/ml D-[U-^{14}C]glucose either in the absence or presence of: Insulin (100 nM), troglitazone (50 μM), or troglitazone plus insulin. The reaction was terminated by adding ice-cold PBS and the cells were lysed in KOH. Glycogen was precipitated overnight and transferred to scintillation vials for radioactivity counting. Incorporation of glucose into total lipids was determined after myotubes were exposed to 0.4 μCi/ml D-[U-^{14}C]glucose for 2 h (Gaidhu et al., 2006). Lactate released into the medium was measured by a colorimetric assay using a commercially available kit (Fediuc et al., 2006a).

Statistical analysis

Statistical analysis were performed by one-way ANOVA with Tukey–Kraemer multiple comparison post-hoc tests. The level of significance was set at $P < 0.05$. All data are presented as means ± SEM and expressed relative to control.

Results

AMPK and ACC phosphorylation

Troglitazone significantly increased AMPK phosphorylation by ~2.5-fold (Fig. 1A) and insulin did not affect the phosphorylation state of this enzyme. However, the troglitazone-induced AMPK phosphorylation effect was completely suppressed by insulin (Fig. 1A). Troglitazone also significantly increased (~3.5-fold) phosphorylation of ACC (Fig. 1B), indicating that the activity of AMPK was indeed elevated by this drug. Treatment of myotubes with insulin suppressed troglitazone-induced ACC phosphorylation (Fig. 1B), which is in line with the inhibitory effect of this hormone on AMPK phosphorylation/activation.

Palmitate oxidation and CPT-1 activity

Treatment of myotubes with troglitazone led to an ~30% increase in palmitate oxidation while insulin elicited an ~40% reduction in this variable (Fig. 2A). Interestingly, even though troglitazone alone increased palmitate oxidation, exposure of myotubes to a combination of troglitazone and insulin did not fully reverse the suppressive effects of insulin on FA oxidation. In fact, the insulin plus troglitazone group elicited rates of palmitate oxidation that were ~29% lower than control but only ~14% higher than insulin alone conditions (Fig. 2A). As expected, etomoxir almost completely suppressed CPT-1 activity, which clearly demonstrates that our in vitro system was responsive to metabolic stimuli (Fig. 2B). The activity of CPT-1 in permeabilized myotubes was not affected by insulin treatment; however, troglitazone significantly increased (~60%) the activity of this enzyme (Fig. 2B). Interestingly, CPT-1 activity was also elevated (~55%) in cells exposed to both insulin and troglitazone (Fig. 2B).

Effect of compound C on troglitazone-stimulated FA oxidation

Western blot analysis of AMPK and ACC revealed that AMPK phosphorylation/activation was effectively inhibited by compound C, a selective AMPK inhibitor. As previously described, treatment of cells with troglitazone resulted in a ~2- and 2.3-fold increase in AMPK and ACC phosphorylation, respectively (Fig. 1C,D). Compound C did not affect the basal phosphorylation state of either enzyme, but completely prevented the troglitazone-induced increase in AMPK and ACC phosphorylation (Fig. 1C,D). Troglitazone increased basal FA oxidation by ~30% relative to control (Fig. 2C). Interestingly, treatment with 10 and 20 μM of compound C led to ~15% and 30% reductions in basal palmitate oxidation relative to control, respectively (Fig. 2C). Strikingly, both concentrations of compound C completely prevented troglitazone-induced increases in FA oxidation by skeletal muscle cells. In fact, the rates of troglitazone-induced palmitate oxidation in cells exposed to either 10 or 20 μM of compound

C were ~20% and ~40% lower than control values, respectively (Fig. 2C).

Palmitate uptake

Insulin elicited a ~20% increase in palmitate uptake compared to control (Fig. 3A). The incubation of myotubes with low concentrations (5 μM) of troglitazone did not affect basal palmitate uptake; however, it completely abolished the insulin-stimulated increase in this variable. Interestingly, a higher concentration (50 μM) of troglitazone reduced both basal and insulin-stimulated palmitate uptake by ~23% compared to control conditions (Fig. 3A). Further increases in troglitazone concentration from 50 to 100 μM did not affect basal palmitate uptake but the insulin-stimulated uptake was reduced by an additional ~13% (Fig. 3A).

Effect of troglitazone on basal and insulin-stimulated glucose uptake, glycogen synthesis, lactate production, glucose oxidation, and glucose incorporation into lipids

As expected, insulin elicited an ~1.7-fold increase in glucose uptake compared to control, while treatment of L6 myotubes with troglitazone resulted in ~2-fold increase in this variable (Fig. 3B). Interestingly, the combination of troglitazone and insulin elicited an additive effect leading to a ~2.8-fold increase in glucose uptake (Fig. 3B). Treatment of muscle cells with compound C did not affect basal or insulin-stimulated rates of glucose uptake; however it reduced troglitazone-induced glucose uptake by ~30% compared to control (Fig. 3B). Compound C also completely prevented the additive effect of combining troglitazone and insulin on glucose uptake. In fact, myotubes receiving insulin, troglitazone, and compound C elicited glucose uptake values that were also ~30% lower than control (Fig. 3B). Further analysis of several pathways of glucose metabolism revealed that, as expected, insulin significantly increased glucose oxidation (~1.5-fold), glycogen synthesis (~2-fold), incorporation of glucose into lipids (~1.4-fold), and lactate production (~2.5-fold) compared to control (Fig. 4A–D). Interestingly, troglitazone reduced basal and insulin-stimulated rates of glucose oxidation (Fig. 4A), glycogen synthesis (Fig. 4B), and incorporation of glucose into lipids (Fig. 4C) to values corresponding to ~30%, ~30%, and ~60%, of the controls, respectively. The inhibitory effect of troglitazone on glycogen synthesis was observed either when insulin and troglitazone were added simultaneously (Fig. 4B) or when cells were pre-treated with troglitazone for 1 h and then

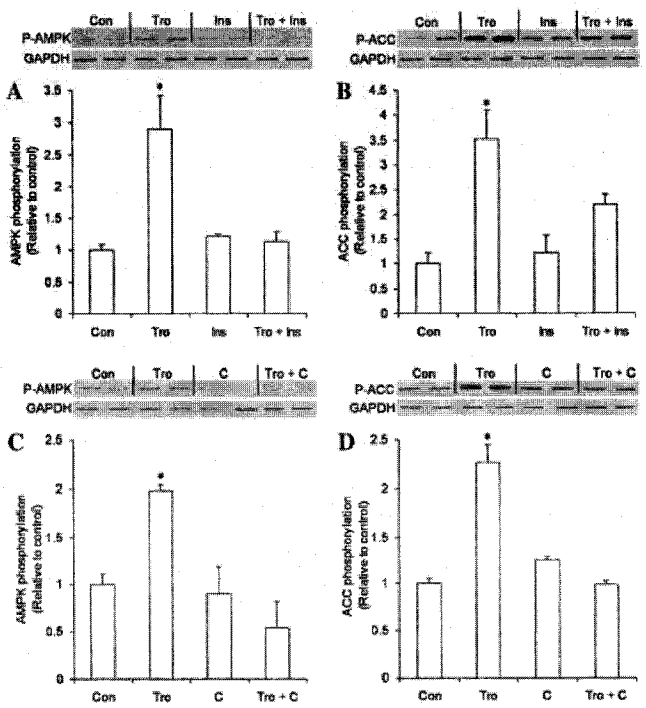

Fig. 1. Effects of troglitazone (Tro, 50 μM), insulin (Ins, 100 nM), troglitazone plus insulin (Tro + Ins), compound C (C, 10 and 20 μM), and troglitazone plus compound C (Tro + C) on AMPK (parts A and C) and ACC (parts B and D) phosphorylation in L6 myotubes. Control (Con) cells were not exposed to insulin, troglitazone, or compound C. Densitometric analysis and respective representative blots are shown for each experimental condition for AMPK (parts A and C) and ACC (parts B and D). GAPDH was used as loading control. Data were compiled from three independent experiments with duplicates in each condition and presented as means ± SEM. *$P < 0.05$ versus all groups.

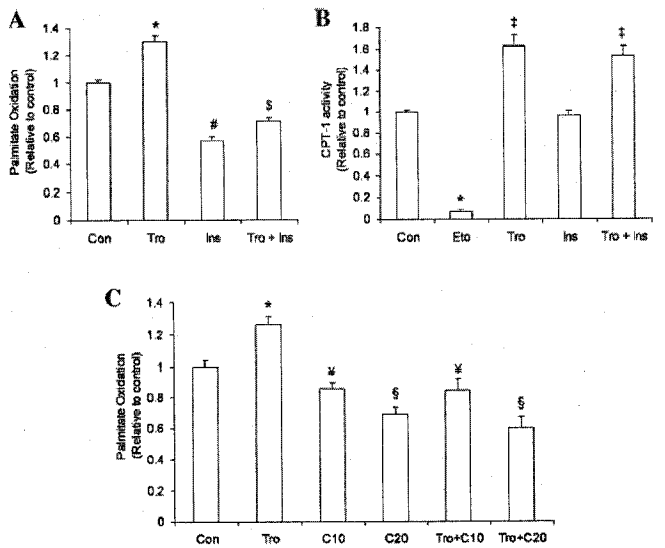

Fig. 2. Effects of troglitazone (Tro, 50 μM), insulin (Ins, 100 nM), etomoxir (Eto, 2.5 μM), troglitazone plus insulin (Tro + Ins), compound C (C, 10 and 20 μM) and troglitazone plus compound C (Tro + C) on palmitate oxidation (parts A and C) and CPT-1 activity (part B) in L6 myotubes. Control (Con) cells were not exposed to Ins, Tro, Eto, or C. Palmitate oxidation was measure by the rate of production of $^{14}CO_2$ from [1-^{14}C]palmitic acid during 1 h. CPT-1 activity was assessed by the conversion L-[^{3}H]carnitine to palmitoyl-[^{3}H]carnitine during a 5 min assay following 1 h exposure to the respective conditions mentioned above. Data were compiled from three independent experiments with triplicates in each condition and presented as means ± SEM. *$P < 0.05$ versus all groups; #$P < 0.05$ versus Con, Tro, and Tro + Ins; $P < 0.05$ versus Con, Tro, and Ins; ‡$P < 0.05$ versus Con, Eto, and Ins; ¥$P < 0.05$ versus Con, Tro, C20, and Tro + C20; §$P < 0.05$ versus Con, Tro, C10, and Tro + C10.

subsequently exposed to insulin (data not shown). On the other hand, troglitazone significantly increased basal (~3.5-fold) and insulin-stimulated (~5.5-fold) rates of lactate production (Fig. 4D). These data indicate that troglitazone promotes an insulin-sensitizing effect by increasing glucose uptake and shifting glucose metabolism toward lactate production in skeletal muscle cells.

Effect of troglitazone and compound C on [1-^{14}C]-pyruvate decarboxylation

Muscle cells exposed to troglitazone elicited a significant reduction (~97%) in the rate of $^{14}CO_2$ production from [1-^{14}C]-pyruvate in comparison to control (17.86 ± 1.26 nmol/h/dish vs. 672.75 ± 35.90 nmol/h/dish, $P < 0.05$). The addition of compound C alone to the incubation medium neither affected basal pyruvate oxidation (650.31 ± 10.99 nmol/h/dish) nor reversed the potent suppressive effect of troglitazone on this variable (27.04 ± 3.54 nmol/h/dish).

Effect of troglitazone on basal and insulin-stimulated phosphorylation of $Akt_{Thr-308}$, $Akt_{Ser-473}$, and GSK-3α/β

Cells exposed to insulin for 5 min elicited a marked (~60-fold) increase in Akt_{Thr308} phosphorylation (Fig. 5) compared to control. Troglitazone on its own led to ~4-fold increase in Akt_{Thr308} phosphorylation and when combined with insulin produced an increase in this variable that was ~50% higher than the effect of insulin alone. Also, insulin increased Akt_{Ser473} phosphorylation by ~7-fold, while troglitazone increased it by ~2.7-fold relative to control. Again, the combination of troglitazone and insulin elicited an increase in Akt_{Ser473} phosphorylation that was ~50% higher than the effect of these agents alone (Fig. 5). Under control and troglitazone treated conditions GSK-3α/β phosphorylation was undetectable; however, exposure of muscle cells to insulin for 5, 10, and 20 min resulted in ~6-, ~21-, and ~20-fold increases in GSK-3α and 1.5-, 13-, 14-fold increases in GSK-3β phosphorylation, respectively. Interestingly, exposure of muscle cells to both, troglitazone and insulin, led to an increase in phosphorylation of GSK-3α/β that was higher than insulin alone (Fig. 5). In fact, after 5 and 10 min of insulin exposure, troglitazone-treated cells elicited more than a 2-fold increase in GSK-3α/β phosphorylation when compared to insulin alone. The effect of troglitazone on insulin-stimulated GSK-3α/β phosphorylation was even more pronounced (~4-fold) after 20 min of insulin exposure (Fig. 5). All together, our data indicate that troglitazone potentiates the effects of insulin on major intracellular signaling pathways involved in glucose uptake and metabolism in L6 myotubes.

Discussion

In the present investigation, treatment of L6 myotubes with troglitazone for 1 h resulted in a significant increase in AMPK and ACC phosphorylation, which was also followed by an increase (~30%) in palmitate oxidation. Interestingly, inhibition of AMPK activation by compound C was accompanied by suppression of phosphorylation of ACC and abolishment of the increased FA oxidation induced by troglitazone. These findings provide evidence that AMPK is a molecular target for troglitazone to induce acute LCFA oxidation in skeletal muscle cells. Since muscle cells were exposed to troglitazone for a

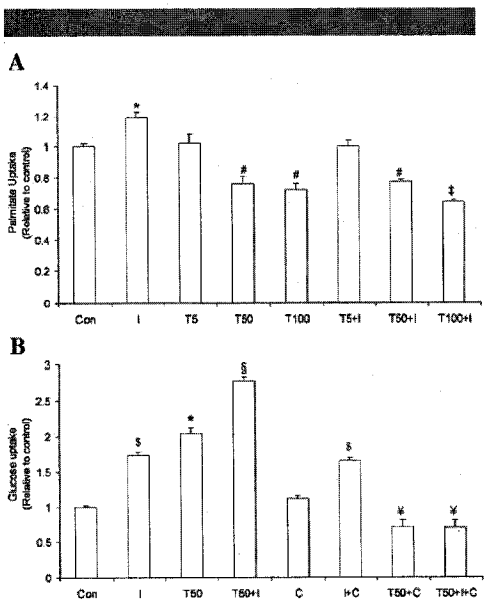

Fig. 3. Effects of insulin (I, 100 nM), troglitazone (T, 5, 50, and 100 μM), troglitazone plus insulin (T5 + I, T50 + I, and T100 + I), compound C (C, 20 μM), insulin plus compound C (I + C), troglitazone plus compound C (T50 + C), and troglitazone plus insulin plus compound C (T50 + I + C) on palmitate (part A) and glucose (part B) uptake in L6 myotubes. Control (Con) cells were not exposed to troglitazone, insulin, or compound C. All cells were exposed to the treatment conditions for a period of 1 h. The rates of palmitate and glucose uptake were assessed by the uptake of [1-^{14}C]palmitic acid and 2-deoxy-D-[^{3}H]glucose during a 4 and 5 min assay, respectively, after the 1 h incubation, as described in the methods. Data were compiled from three to four independent experiments with triplicates for each condition and presented as means ± SEM. *$P < 0.05$ versus all conditions; #$P < 0.05$ versus Con, I, T5, T5 + I, and T100 + I; ‡$P < 0.05$ versus Con, I, T5, T50, T100, T5 + I, and T50 + I; §$P < 0.05$ versus Con, T50, T50 + I, C, T50 + C, and T50 + I + C; $P < 0.05$ versus all conditions; ¥$P < 0.05$ versus Con, I, T50, T50 + I, C, and I + C.

short time period (60 min), the metabolic effects observed in our studies seem to be independent of PPARγ-mediated gene transcription. Furthermore, in vitro studies with isolated rat muscles have also reported that 30 min exposure to troglitazone concentrations similar to the ones applied in our studies (5–100 μM) induced rapid activation of AMPK and also an increase in LCFA oxidation (LeBrasseur et al., 2006). The concentrations of troglitazone utilized in our experiments are similar to the plasma concentrations (~100 μM) that elicited anti-hyperglycemic effects in Zucker diabetic fatty rats receiving oral dosages of 500 mg/kg of troglitazone (Brown et al., 1999). In humans, it has been reported that oral dosages ranging from 200 to 600 mg/day of troglitazone produced plasma concentrations (measured as area under the plasma concentration-time curve) as high as 50 μM (Plosker and Faulds, 1999). Therefore, it is possible that the acute effects observed in our experiments utilizing concentrations varying from 5 to 100 μM may also occur under physiological conditions.

Here, we provide evidence that the mechanism by which troglitazone promoted oxidation of LCFAs involved AMPK activation and phosphorylation/inactivation of its downstream target, ACC. The latter is a critical enzyme that generates malonyl-CoA, the precursor of FA synthesis and the major inhibitor of mitochondrial LCFA import and β-oxidation (McGarry, 2002; Carling, 2005). These findings confirm our original hypothesis that, by increasing LCFA oxidation troglitazone could prevent intramyocellular lipid accumulation in skeletal muscle cells independently of PPARγ activation. Additional support for this comes from other findings in our investigation in which troglitazone: (a) inhibited basal and insulin-stimulated palmitate uptake, (b) significantly increased (60%) CPT-1 activity, (c) inhibited PDH activity, and (d) suppressed basal and insulin-stimulated incorporation of glucose into lipids.

One intriguing finding of our study was that insulin completely suppressed troglitazone-induced palmitate oxidation but the troglitazone-induced increase in CPT-1 activity was not affected by this hormone. One would expect that because insulin stimulates glucose uptake, reduces troglitazone-induced ACC phosphorylation, and accelerates the de novo lipid synthesis pathway, the activity of CPT-1 would be reduced. This is particularly relevant because in all media utilized for our experiments glucose (5.5 mM) was present, which could provide enough substrate for the de novo lipid synthesis pathway to be active and potentially inhibit CPT-1 activity. However, this was not the case in our experiments. In fact, CPT-1 activity was equally elevated (~60%) in cells exposed to troglitazone alone or when in combination with insulin. This could be explained by the fact that insulin increased glucose uptake but when combined with troglitazone glucose metabolism was diverted toward lactate production, while pyruvate decarboxylation, glucose oxidation, and de novo lipid synthesis were powerfully suppressed. This shift of glucose metabolism toward lactate production caused by troglitazone is compatible with a reduction in citrate production, de-activation of ACC, suppression of malonyl-CoA production, and prevention of down regulation of CPT-1 activity. This is in line with our novel findings that troglitazone powerfully suppressed pyruvate decarboxylation by inhibiting the activity of the PDH complex. Importantly, the oxidative effect of troglitazone on LCFAs was abolished when cells were exposed to both insulin and troglitazone. This indicates that insulin impairs LCFA oxidation via a mechanism that does not act on CPT-1, since the activity of this enzyme remained elevated when muscle cells were simultaneously exposed to troglitazone and insulin. It may also be possible that the troglitazone-induced alteration in LCFA trafficking was counteracted by a more potent insulin-induced effect that diverts LCFAs away from mitochondria preventing their oxidation.

Our findings can be partially related to the classical "glucose-fatty acid cycle" proposed by Randle et al. (1963), in which enhanced FA oxidation produces an increase in the acetyl-CoA to CoA-SH ratio and elevation of cytoplasmic citrate concentration. These, in turn, would inhibit PDH, phosphofructokinase (PFK), and hexokinase activity resulting in decreased glucose uptake in muscle cells. Indeed, in our experiments we observed that troglitazone significantly increased palmitate oxidation and powerfully suppressed PDH activity in skeletal muscle cells. However, we also found that basal and insulin-stimulated glucose uptake was significantly increased, which is contrary to what was proposed for the glucose-FA cycle (Randle et al., 1963). Furthermore, inhibition of PFK is expected to impair the flux of substrate through the glycolytic pathway, which again is incompatible with the significant increase we found in both basal and insulin-stimulated rates of lactate production by muscle cells exposed to troglitazone. Therefore, the acute effects of troglitazone on glucose and FA metabolism reported by us in skeletal muscle cells seem to be mediated by mechanisms that are distinct from those originally proposed by Randle et al. (1963).

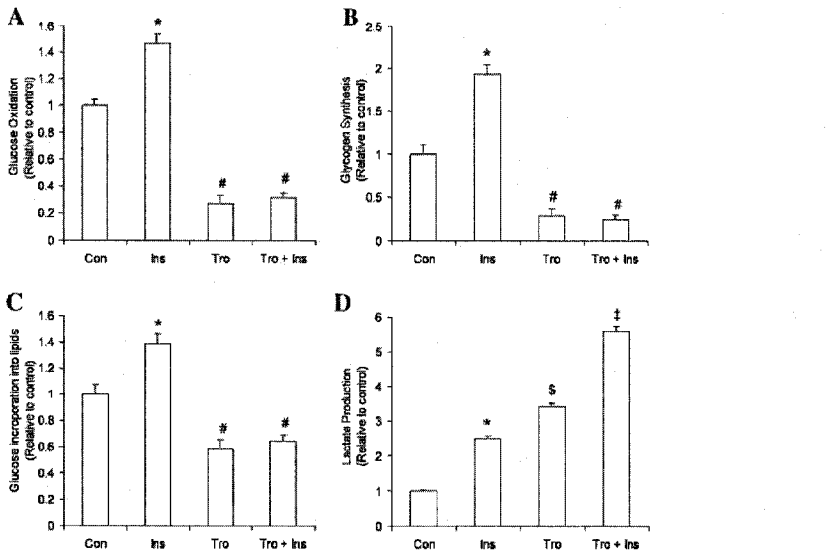

Fig. 4. Effects of insulin (Ins, 100 nM), troglitazone (Tro, 50 μM), and troglitazone plus insulin (Tro + Ins) on glucose oxidation (part A), glycogen synthesis (part B), glucose incorporation into lipids (part C), and lactate production (part D) in L6 myotubes. Control (Con) cells were treated with neither Ins nor Tro. The rates of glucose oxidation was measured by the production of $^{14}CO_2$ from D-[U-^{14}C]glucose during 1 h. The rates of glycogen synthesis, and glucose incorporation into lipids were measured by the incorporation of D-[U-^{14}C]glucose into glycogen and lipids for 1 and 2 h, respectively. Data were compiled from three independent experiments with quadruplicates in each condition and presented as means ± SEM. $^{*}P < 0.05$ versus all conditions; $^{\#}P < 0.05$ versus Con and Ins; $^{\$}P < 0.05$ versus all conditions; $^{\ddagger}P < 0.05$ versus all conditions.

Currently, we do not have an explanation for the AMPK-independent mechanism(s) by which troglitazone suppresses PDH activity. It is possible that troglitazone increased the activity of PDH kinase, the enzyme responsible for phosphorylating/deactivating PDH. In this context, the increase in FA oxidation in the presence of troglitazone would have likely increased mitochondrial acetyl-CoA and NADH levels (Sugden and Holness, 1994). The increases in the acetyl-CoA/CoA-SH and NADH/NAD$^+$ ratios, which are known to increase PDH kinase activation, may have been responsible for suppressing PDH activity. It may also be possible that troglitazone reduced the activity of PDH phosphatase, the enzyme that catalyses the dephosphorylation/activation of PDH (Sugden and Holness, 1994). However, these mechanisms are only speculative and therefore require future investigation.

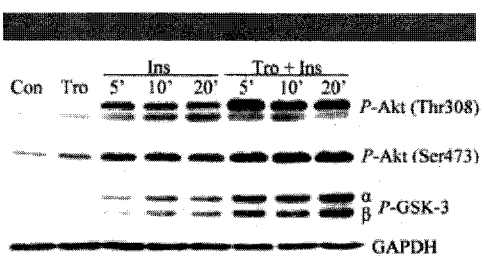

Fig. 5. Time course effects (5, 10, and 20 min) of insulin (Ins, 100 nM), troglitazone (Tro, 50 μM), and troglitazone plus insulin (Tro + Ins) on the phosphorylation of Akt-Thr308 (*P*-Akt308), Akt-Ser473 (*P*-Akt473), GSK-3α (*P*-GSK-3α), and GSK-3β (*P*-GSK-3β) in L6 myotubes. Cells were exposed to troglitazone for 1 h and insulin was added in the last 5, 10, and 20 min of the 1 h troglitazone-incubation period. Control (Con) cells were exposed to neither insulin nor troglitazone.

Our data provide novel evidence that although troglitazone suppressed insulin-stimulated glycogen synthesis, de novo lipid synthesis, and glucose oxidation, it promoted basal and insulin-stimulated Akt and GSK-3α/β phosphorylation and exerted additive effects on insulin-induced glucose uptake and lactate production. Phosphorylation of GSK-3α/β deactivates this enzyme and leads to dephosphorylation and activation of glycogen synthase, which promotes glycogen synthesis (Nielsen and Wojtaszewski, 2004). In our experiments, exposure of L6 myotubes to troglitazone reduced the rates of glycogen synthesis to ~30% of the control values, despite the fact that this drug significantly increased $Akt_{(Thr308/Ser473)}$ and GSK-3α/β phosphorylation either under basal or insulin stimulated conditions. As mentioned above, this may be explained by the fact that troglitazone activated the glycolytic pathway and powerfully shifted glucose metabolism toward lactate production. This metabolic shift induced by troglitazone must have limited availability of glucose for glycogen synthesis in skeletal muscle cells. Additionally, the troglitazone-induced suppression of glycogen synthesis may have been caused by activation of AMPK by this drug. In fact, we (Fediuc et al., 2006a) and others (Carling and Hardie, 1989) have demonstrated that AMPK activation may induce phosphorylation/inactivation of

glycogen synthase and impair glycogen synthesis in skeletal muscle, which may occur independently of GSK-3α/β (Fediuc et al., 2006a).

Interestingly, troglitazone promoted a reduction in palmitate uptake in skeletal muscle cells. Moreover, while insulin alone stimulated palmitate uptake (~20%), the addition of troglitazone to the incubation medium completely prevented the insulin-induced increase in palmitate uptake. In fact, palmitate uptake was ~23–37% lower than control values in the presence of troglitazone. Notably, the suppressive effect of troglitazone on palmitate uptake was followed by an increase in oxidation of this FA. One would expect that a reduction in uptake and availability of palmitate in the cell would limit its oxidation; however, in our experiments the opposite was observed. This clearly indicates that troglitazone is also shifting lipid metabolism toward oxidation despite the limited intracellular supply of LCFAs. In the present study we have not investigated the mechanisms by which troglitazone promotes an increase in FA oxidation in a setting of limited availability of this substrate. However, we hypothesize that the intracellular trafficking of LCFAs may be changed in such a way that the limited intracellular pool of FAs is diverted toward the mitochondria for oxidation. This is compatible with the fact that lipid synthesis was suppressed and CPT-1 activity was elevated in our cells exposed to troglitazone. With respect to this, it has previously been reported that FA translocase (FAT/CD36), a class of plasma membrane FA transporters, play an important role in FA oxidation (Campbell et al., 2004). There is also evidence that palmitate oxidation is reduced in skeletal muscles of mice deficient in FAT/CD36 (Bonen et al., 2007). Based on these findings, we hypothesize that by altering the trafficking of FAT/CD36, and probably other fat transporters such as FA transport protein 1 (FATP1) and FATP4, troglitazone increases lipid oxidation despite suppressing the uptake of LCFAs in skeletal muscle cells. However, these hypotheses depart from traditional views of mechanisms involved in the regulation of CPT-1 activity and β-oxidation and warrant further investigation.

Another interesting aspect of our findings is that troglitazone powerfully suppressed glucose oxidation but significantly increased palmitate oxidation. As previously discussed, the increase in palmitate oxidation is compatible with increases in AMPK and CPT-1 activities. This is in line with previous studies demonstrating that exposing isolated rat EDL muscles to TZDs (troglitazone and pioglitazone, 5–250 μM) for 15–30 min increased AMPK activity and induced palmitate oxidation (LeBrasseur et al., 2006). However, other studies have demonstrated that longer exposure (25 h) of isolated rat soleus muscle to troglitazone, rosiglitazone, and pioglitazone inhibited CO_2 production from glucose and palmitate (Furnsinn et al., 2000; Brunmair et al., 2004). These effects have been attributed to inhibition of mitochondrial complex I activity and respiration by TZDs (Brunmair et al., 2004). The results of our experiments where muscle cells were exposed to troglitazone (50 μM) for 60 min indicate that mitochondrial respiration is not directly inhibited by this drug, since oxidation of palmitate was actually significantly increased (~30%) by troglitazone. This is also in agreement with other studies reporting that acute (15–30 min) exposure of rat EDL muscles to TZDs (5–250 μM) increased palmitate oxidation (LeBrasseur et al., 2006). The reduction in glucose oxidation observed in our experiments may be at least partially explained by the potent shift of glucose metabolism toward lactate production induced by troglitazone. Additionally, we demonstrate that troglitazone suppressed the activity of the PDH complex, an effect that appears to be independent of AMPK activation, since it was not reversed by compound C. By regulating the generation of acetyl-CoA from pyruvate, the PDH complex has been demonstrated to play an important role modulating glucose oxidation and the activity of the de novo lipid synthesis pathway in various tissues (Sugden and Holness, 1994). Therefore, inhibition of PDH complex by troglitazone is compatible with the substantial increase in lactate production and inhibition of glucose incorporation into lipids reported by us. In addition, this shift of glucose metabolism toward lactate production caused by troglitazone must have reduced citrate production, limited the availability of substrate for activation of ACC and suppressed the production of malonyl-CoA. This is compatible with the increase (~60%) in CPT-1 activity observed in our studies. Furthermore our findings are also in line with an increase in palmitate oxidation, since this variable is not directly limited by the activity of the PDH complex.

In summary, we provide novel evidence that troglitazone exerts an acute insulin sensitizing effect despite a marked reduction in basal and insulin-stimulated glycogen synthesis in skeletal muscle cells. Acute troglitazone treatment also increased phosphorylation of crucial intracellular steps of insulin signaling, which was accompanied by an increase in basal and insulin-stimulated glucose uptake and by a shift of glucose metabolism toward lactate production. This metabolic shift was mediated by an inhibitory effect of troglitazone on PDH activity independently of AMPK activation, since pharmacological inhibition of this kinase did not prevent the inhibitory effect of troglitazone on pyruvate decarboxylation. Additionally, troglitazone reduced FA uptake and increased FA oxidation. These effects were partially mediated by AMPK activation and may account for potential PPAR-γ-independent anti-diabetic effects of TZDs in skeletal muscle cells.

Acknowledgments

The authors thank Merck Research Laboratories for kindly providing compound C for these experiments. Funding was provided by the National Science and Engineering Research Council (NSERC) via a Discovery grant to R. Ceddia. NSERC also supported S. Fediuc via a Doctoral Postgraduate Scholarship. A. Pimenta was supported by a Post-doctoral Fellowship from the Brazilian Ministry of Education (CAPES). M. Gaidhu was funded by a CIHR Canada Graduate Scholarship—Master's Award.

Literature Cited

Auboeuf D, Rieusset J, Fajas L, Vallier P, Frering V, Riou JP, Staels B, Auwerx J, Laville M, Vidal H. 1997. Tissue distribution and quantification of the expression of mRNAs of peroxisome proliferator-activated receptors and liver X receptor-alpha in humans: No alteration in adipose tissue of obese and NIDDM patients. Diabetes 46:1319–1327.

Bonen A, Han XX, Habets DD, Febbraio M, Glatz JF, Luiken JJ. 2007. A null mutation in skeletal muscle FAT/CD36 reveals its essential role in insulin- and AICAR-stimulated fatty acid metabolism. Am J Physiol Endocrinol Metab 292:E1740–E1749.

Brown KK, Henke BR, Blanchard SG, Cobb JE, Mook R, Kaldor I, Kliewer SA, Lehmann JM, Lenhard JM, Harrington WW, Novak PJ, Faison W, Binz JG, Hashim MA, Oliver WO, Brown HR, Parks DJ, Plunket KD, Tong WQ, Manius JA, Addison K, Noble SA, Willson TM. 1999. A novel N-aryl tyrosine activator of peroxisome proliferator-activated receptor-gamma reverses the diabetic phenotype of the zucker diabetic fatty rat. Diabetes 48:1415–1424.

Brunmair B, Staniek K, Gras F, Scharf N, Althaym A, Clara R, Roden M, Gnaiger E, Nohl H, Waldhäusl W, Fürnsinn C. 2004. Thiazolidinediones, like metformin, inhibit respiratory complex I: A common mechanism contributing to their antidiabetic actions? Diabetes 53:1052–1059.

Burant CF, Sreenan S, Hirano K, Tai TA, Lohmiller J, Lukens J, Davidson NO, Ross S, Graves RA. 1997. Troglitazone action is independent of adipose tissue. J Clin Invest 100:2900–2908.

Campbell SE, Tandon NN, Woldegiorgis G, Luiken JJ, Glatz JF, Bonen A. 2004. A novel function for fatty acid translocase (FAT)/C D36: Involvement in long chain fatty acid transfer into the mitochondria. J Biol Chem 279:36235–36241.

Carling D. 2005. AMP-activated protein kinase: Balancing the scales. Biochimie 87:87–91.

Carling D, Hardie DG. 1989. The substrate and sequence specificity of the AMP-activated protein kinase. Phosphorylation of glycogen synthase and phosphorylase kinase. Biochim Biophys Acta 1012:81–86.

Castelein H, Gulick T, Declercq PE, Mannaerts GP, Moore DD, Baes MI. 1994. The peroxisome proliferator activated receptor regulates malic enzyme gene expression. J Biol Chem 269:26754–26758.

Ceddia RB, Sweeney G. 2004. Creatine supplementation increases glucose oxidation and AMPK phosphorylation and reduces lactate production in L6 rat skeletal muscle cells. J Physiol 555:409–421.

Ceddia RB, William WN, Jr., Curi R. 1999. Comparing effects of leptin and insulin on glucose metabolism in skeletal muscle: Evidence for an effect of leptin on glucose uptake and decarboxylation. Int J Obes Relat Metab Disord 23:75–82.
Curi R, Newsholme P, Newsholme EA. 1988. Metabolism of pyruvate by isolated rat mesenteric lymphocytes, lymphocyte mitochondria and isolated mouse macrophages. Biochem J 250:383–388.
Fediuc S, Gaidhu MP, Ceddia RB. 2006a. Inhibition of insulin-stimulated glycogen synthesis by 5-aminoimidasole-4-carboxamide-1-beta-d-ribofuranoside-induced adenosine 5'-monophosphate-activated protein kinase activation: Interactions with akt, glycogen synthase kinase 3-3alpha/beta, and glycogen synthase in isolated rat soleus muscle. Endocrinology 147:5170–5177.
Fediuc S, Gaidhu MP, Ceddia RB. 2006b. Regulation of AMP-activated protein kinase and acetyl-CoA carboxylase phosphorylation by palmitate in skeletal muscle cells. J Lipid Res 47:412–420.
Fryer LG, Parbu-Patel A, Carling D. 2002. The anti-diabetic drugs rosiglitazone and metformin stimulate AMP-activated protein kinase through distinct signaling pathways. J Biol Chem 277:25226–25232.
Furnsinn C, Brunmair B, Neschen S, Roden M, Waldhausl W. 2000. Troglitazone directly inhibits CO(2) production from glucose and palmitate in isolated rat skeletal muscle. J Pharmacol Exp Ther 293:487–493.
Gaidhu MP, Fediuc S, Ceddia RB. 2006. 5-Aminoimidazole-4-carboxamide-1-beta-D-ribofuranoside-induced AMP-activated protein kinase phosphorylation inhibits basal and insulin-stimulated glucose uptake, lipid synthesis, and fatty acid oxidation in isolated rat adipocytes. J Biol Chem 281:25956–25964.
Guan HP, Li Y, Jensen MV, Newgard CB, Steppan CM, Lazar MA. 2002. A futile metabolic cycle activated in adipocytes by antidiabetic agents. Nat Med 8:1122–1128.
Inzucchi SE, Maggs DG, Spollett GR, Page SL, Rife FS, Walton V, Shulman GI. 1998. Efficacy and metabolic effects of metformin and troglitazone in type II diabetes mellitus. N Engl J Med 338:867–872.
Konrad D, Rudich A, Bilan PJ, Patel N, Richardson C, Witters LA, Klip A. 2005. Troglitazone causes acute mitochondrial membrane depolarisation and an AMPK-mediated increase in glucose phosphorylation in muscle cells. Diabetologia 48:954–966.
Kraegen EW, James DE, Jenkins AB, Chisholm DJ, Storlien LH. 1989. A potent in vivo effect of ciglitazone on muscle insulin resistance induced by high fat feeding of rats. Metabolism 38:1089–1093.
LeBrasseur NK, Kelly M, Tsao TS, Farmer SR, Saha AK, Ruderman NB, Tomas E. 2006. Thiazolidinediones can rapidly activate AMP-activated protein kinase in mammalian tissues. Am J Physiol Endocrinol Metab 291:E175–E181.
Lee MK, Olefsky JM. 1995. Acute effects of troglitazone on in vivo insulin action in normal rats. Metabolism 44:1166–1169.
Lee MK, Miles PD, Khoursheed M, Gao KM, Moossa AR, Olefsky JM. 1994. Metabolic effects of troglitazone on fructose-induced insulin resistance in the rat. Diabetes 43:1435–1439.
McGarry JD. 2002. Banting lecture 2001: Dysregulation of fatty acid metabolism in the etiology of type 2 diabetes. Diabetes 51:7–18.
Miles PD, Higo K, Romeo OM, Lee MK, Rafiat K, Olefsky JM. 1998. Troglitazone prevents hyperglycemia-induced but not glucosamine-induced insulin resistance. Diabetes 47:395–400.
Nielsen JN, Wojtaszewski JF. 2004. Regulation of glycogen synthase activity and phosphorylation by exercise. Proc Nutr Soc 63:233–237.
Plosker GL, Faulds D. 1999. Troglitazone: A review of its use in the management of type 2 diabetes mellitus. Drugs 57:409–438.
Randle PJ, Garland PB, Hales CN, Newsholme EA. 1963. The glucose fatty-acid cycle. Its role in insulin sensitivity and the metabolic disturbances of diabetes mellitus. Lancet 1:785–789.
Selby PL, Sherratt HS. 1989. Substituted 2-oxiranecarboxylic acids: A new group of candidate hypoglycaemic drugs. Trends Pharmacol Sci 10:495–500.
Spurway TD, Agius L, Stanley H, Sherratt A, Pogson CI. 1994. Measurement of carnitine palmitoyltransferase I in hepatocyte monolayers. Biochem Soc Trans 22:118S.
Sugden MC, Holness MJ. 1994. Interactive regulation of the pyruvate dehydrogenase complex and the carnitine palmitoyltransferase system. FASEB J 8:54–561.

0013-7227/06/$15.00/0
Printed in U.S.A.

Endocrinology 147(11):5170–5177

doi: 10.1210/en.2006-0480

Inhibition of Insulin-Stimulated Glycogen Synthesis by 5-Aminoimidasole-4-Carboxamide-1-β-D-Ribofuranoside-Induced Adenosine 5′-Monophosphate-Activated Protein Kinase Activation: Interactions with Akt, Glycogen Synthase Kinase 3-3α/β, and Glycogen Synthase in Isolated Rat Soleus Muscle

S. Fediuc, M. P. Gaidhu, and R. B. Ceddia

School of Kinesiology and Health Science, York University, Toronto, Canada N3J 1P3

The aim of this study was to investigate the effects of 5-aminoimidasole-4-carboxamide-1-β-D-ribofuranoside (AICAR)-induced AMP-activated protein kinase activation on glycogen metabolism in soleus (slow twitch, oxidative) and epitrochlearis (fast twitch, glycolytic) skeletal muscles. Isolated soleus and epitrochlearis muscles were incubated in the absence or presence of insulin (100 nM), AICAR (2 mM), and AICAR plus insulin. In soleus muscles exposed to insulin, glycogen synthesis and glycogen content increased 6.4- and 1.3-fold, respectively. AICAR treatment significantly suppressed (~60%) insulin-stimulated glycogen synthesis and completely prevented the increase in glycogen content induced by insulin. AICAR did not affect either basal or insulin-stimulated glucose uptake but significantly increased insulin-stimulated (~20%) lactate production in soleus muscles. Interestingly, basal glucose uptake was significantly increased (~1.4-fold) in the epitrochlearis muscle, even though neither basal nor insulin-stimulated rates of glycogen synthesis, glycogen content, and lactate production were affected by AICAR. We also report the novel evidence that AICAR markedly reduced insulin-induced Akt-Thr308 phosphorylation after 15 and 30 min exposure to insulin, which coincided with a marked reduction in glycogen synthase kinase 3 (GSK)-3α/β phosphorylation. Importantly, phosphorylation of glycogen synthase was increased by AICAR treatment 45 min after insulin stimulation. Our results indicate that AICAR-induced AMP-activated protein kinase activation caused a time-dependent reduction in Akt308 phosphorylation, activation of glycogen synthase kinase-3α/β, and the inactivation of glycogen synthase, which are compatible with the acute reduction in insulin-stimulated glycogen synthesis in oxidative but not glycolytic skeletal muscles. (*Endocrinology* 147: 5170–5177, 2006)

AMP-ACTIVATED PROTEIN KINASE (AMPK) is a heterotrimeric enzyme that has been proposed to function as a sensor of cellular energy status. It is comprised of a catalytic subunit (α) and two regulatory subunits (β and γ). AMPK is activated by a rise in the AMP to ATP ratio of the cell and also via phosphorylation of the α-subunit by upstream kinases. Once active, AMPK shuts down anabolic pathways and increases catabolic reactions in an attempt to restore the intracellular AMP to ATP ratio (1, 2).

A commonly used pharmacological agent to induce activation of AMPK is the compound 5-aminoimidasole-4-carboxamide-1-β-D-ribofuranoside (AICAR), which has frequently been used to characterize the effects of AMPK activation on glucose homeostasis in a variety of tissues (1, 2). AICAR is rapidly taken up by cells and phosphorylated to form 5-aminoimidazole-4-carboxamide-1-β-D-ribofuronosil-5′-monophosphate, an AMP mimetic. 5-Aminoimidazole-4-carboxamide-1-β-D-ribofuronosil-5′-monophosphate induces activation of AMPK without altering intracellular ATP and AMP levels (1). It has been repeatedly reported by *in vitro* and *in vivo* studies that AICAR-induced AMPK phosphorylation/activation causes an increase in glucose uptake in skeletal muscles (3–5), improves insulin sensitivity in obese ZDF rats (6) and human type 2 diabetics (7). To date, there seems to be a consensus that AMPK activation leads to an increase in glucose uptake in skeletal muscle. Based on these evidences, AMPK has emerged as a potential drug target for the treatment of metabolic diseases such as insulin resistance and type 2 diabetes mellitus (8). In recent years, the major research focus has been on the effects of AMPK activation on basal and insulin-stimulated glucose uptake with very little being published regarding the metabolic fate of glucose in muscle cells, especially regarding the effects of AMPK activation on muscle glycogen synthesis.

Because AMPK is activated under conditions of cellular stress to promote ATP synthesis and restore the AMP to ATP ratio, it is expected that energy consuming processes, such as glycogen synthesis, would be shut down by activation of AMPK in skeletal muscle (9). In support of this hypothesis,

First Published Online July 27, 2006

Abbreviations: ACC, Acetyl-CoA carboxylase; AICAR, 5-aminoimidazole-4-carboxamide-1-β-D-ribofuronosil; AMPK, AMP-activated protein kinase; 2-DG, 2-[1,2-^{3}H]deoxy-D-glucose; GAPDH, glyceraldehyde-3-phosphate dehydrogenase; GS, glycogen synthase; GSK, glycogen synthase kinase; IRS, insulin receptor substrate; KHB, Krebs-Hanseleit bicarbonate; p, phosphorylated; PI3-kinase, phosphatidylinositol 3-kinase.

Endocrinology is published monthly by The Endocrine Society (http://www.endo-society.org), the foremost professional society serving the endocrine community.

Carling and Hardie (10) provided evidence that AMPK phosphorylates isolated and purified glycogen synthase (GS), therefore decreasing its activity. However, subsequent *in vitro* and *in vivo* studies provide conflicting results regarding the role of AMPK activation in skeletal muscle glycogen metabolism. It has been demonstrated that incubation of isolated flexor digitorum brevis and epitrochlearis (fast twitch muscles) with AICAR did not alter either GS or glycogen phosphorylase activity (11). Glycogen phosphorylase, which catalyzes the degradation of glycogen to glucose-1-phosphate, is an important determinant of the rate of glycogenolysis. Activation of glycogen phosphorylase by AMPK is expected to lead to a reduction in glycogen content in skeletal muscle. In this context, Young *et al.* (12) demonstrated that either basal or insulin-stimulated glycogen synthesis were unaffected by AICAR treatment in soleus muscles (primarily slow twitch), even though glycogen phosphorylase activity and lactate production were increased. However, in this previous *in vitro* study reporting that acute AICAR treatment induced an increase in glycogen phosphorylase activity, glycogen content in skeletal muscle was not measured (12). To complicate this matter further, it has been demonstrated that rats chronically treated (5–28 d) with AICAR have increased (up to 2-fold) muscle glycogen content (13–15). Interestingly, white fast-twitch muscles elicit the most pronounced increases in glycogen content after chronic AICAR treatment (13, 14), suggesting important fiber type differences regarding the role of AMPK activation in muscle glycogen metabolism. Even though these *in vivo* studies provide relevant information regarding the metabolic responses to AICAR-induced AMPK activation, they do not allow for separation of direct from systemic effects of AICAR on skeletal muscle glycogen metabolism.

Another aspect that remains poorly explored is the role of AMPK activation in insulin-stimulated skeletal muscle glycogen synthesis and the impact on whole-body insulin-stimulated glucose homeostasis. This is particularly important, given the fact that insulin-stimulated muscle glycogen synthesis has been demonstrated to account for the majority of whole-body glucose uptake and virtually the entire nonoxidative glucose metabolism in both normal and diabetic subjects (16). In this context, it has been demonstrated that AICAR-induced AMPK activation causes phosphorylation of the insulin receptor substrate (IRS)-1 on Ser-789 residues in C_2C_{12} myotubes, suggesting cross talk between AMPK and early steps of insulin signaling that could have important implications for glycogen metabolism (17). Importantly, there is evidence that serine-phosphorylated forms of IRS-1 fail to associate with an active phosphatidylinositol 3-kinase (PI3-kinase), resulting in decreased translocation of glucose transporters and other associated downstream events related to glucose metabolism (18). From a glycogen synthesis perspective, it is hypothesized that AMPK activation could cause IRS-1 phosphorylation on serine residues, impair downstream insulin signaling events that depend on PI3-kinase activation, reduce phosphorylation and inactivation of glycogen synthase kinase (GSK)-3, and cause inactivation of glycogen synthase in skeletal muscle. However, no data supporting this hypothesis have been published.

The experiments outlined in this investigation are designed to elucidate the effects of AICAR-induced AMPK activation on insulin-stimulated glycogen metabolism and major intracellular insulin-signaling events relevant to the regulation of glycogen synthesis in oxidative and glycolytic skeletal muscles. Here we show that AICAR-induced AMPK activation reduces insulin-stimulated glycogen synthesis in isolated soleus muscles. Additionally, we provide novel evidences that AMPK activation caused time-dependent alterations in insulin-induced Akt-Thr308, GSK-3α/β, and GS phosphorylation, which are compatible with the acute reduction in insulin-stimulated glycogen synthesis in oxidative skeletal muscles.

Materials and Methods

Animals

Male albino rats from the Wistar strain (Charles River Laboratories, Montreal, Québec, Canada) weighing 40–60 g were used in all experiments. The animals were housed in cages with free access to water and standard rat chow, except for the night before the experiments during which they were not allowed to eat. The animals were maintained in a constant-temperature (22 C), with a fixed 12-h light, 12-h dark cycle (0700–1900 h). All animal procedures were approved and performed in accordance with the York University Animal Care Committee guidelines.

Chemicals

AICAR was purchased from Toronto Research Chemicals (Toronto, Ontario, Canada). Glycogen, fatty-acid-free albumin, amyloglucosidase, hexokinase, and glucose-6-phosphate dehydrogenase were obtained from Sigma (St. Louis, MO). Human insulin (Humulin R) was purchased from Eli Lilly Inc. (Toronto, Ontario, Canada). D-[U-^{14}C]glucose was purchased from GE Healthcare Radiochemicals (Québec City, Québec, Canada). 2-[1,2-^{3}H]deoxy-D-glucose and D-[1-^{14}C]mannitol were purchased from American Radiolabeled Chemicals, Inc. (St. Louis, MO). Lactate reagent and standards were purchased from Trinity Biotech (Berkeley Heights, NJ). ATP, nicotinamide adenine dinucleotide phosphate, mannitol, and 2-deoxy-D-glucose were obtained from BioShop Canada Inc. (Burlington, Ontario, Canada). All other reagents used for the experiments were of the highest grade available.

Muscle extraction and incubation

Before muscle extraction, all animals were anesthetized with a single ip injection of ketamine/xylazine (0.2 ml per 100 g body weight). Subsequently the soleus (15–20 mg) and epitrochlearis (10–15 mg) muscles were quickly extracted and mounted onto thin, stainless steel wire clips to maintain optimal resting length. The incubation procedures were performed as previously described (19). Briefly, immediately after extraction, the muscles were placed in plastic scintillation vials containing 2 ml of gassed [30 min with O_2:CO_2-95:5% (vol/vol)] Krebs-Hanseleit bicarbonate (KHB) buffer with 4% fat-free BSA and 6 mM glucose. The scintillation vials were then sealed with rubber stoppers, and gasification was continued for the entire 1-h preincubation period. After preincubation, the muscles were transferred to a second set of vials with 1.5 ml of KHB buffer containing D-[U-^{14}C]glucose (0.2 μCi/ml). All muscles were maintained in either the absence or presence of the following conditions: insulin (100 nM), AICAR (2 mM), and AICAR plus insulin for the entire 1-h incubation. For the AICAR plus insulin conditions, all muscles were exposed to AICAR for 30 min before the addition of insulin.

Measurement of glycogen synthesis in isolated muscle

Glycogen synthesis was assessed by measuring the incorporation of D-[U-^{14}C]glucose into glycogen as previously described (19). Briefly, upon termination of the incubation experiment as outlined above, muscles were quickly washed in ice-cold PBS, blotted on filter paper, frozen (N_2), and digested in 0.5 ml of 1 M KOH at 70 C for 1 h. Of the digested

muscle solution, aliquots were taken for protein determination (Bradford method), determination of glycogen content, and glycogen synthesis. Formation of glycogen from labeled glucose was estimated by adding 10 mg of carrier glycogen to the hydrolysates. Subsequently glycogen was precipitated overnight with 100% ethanol. The precipitate was resuspended in 0.5 ml of water and its radioactivity was determined using a scintillation counter (19).

Measurement of glycogen content and lactate production

After incubation of muscles in the presence of the various conditions outlined above, the muscles were digested in 0.5 ml of 1 M KOH. For analysis of glycogen content, the pH of muscle digest was titrated to 4.8 before the addition acetate of buffer (pH 4.8) and 0.5 mg/ml amyloglucosidase. Subsequently glycogen was hydrolyzed at 40 C for 2 h and glucose was analyzed enzymatically (20) and the absorbance read in a spectrophotometer (Ultraspec 2100 pro; Biochrom Ltd., Cambridge, UK) at 340 nm wavelength. Lactate concentration was measured in deproteinized and neutralized muscle incubation medium using a commercially available kit.

Measurement of glucose transport into muscle

Soleus and epitrochlearis muscles were extracted as described above. Subsequently they were preincubated for 1 h in KHB buffer containing 8 mM glucose, 32 mM mannitol, and 0.1% BSA. After the preincubation, all muscles were exposed for 1 h to the following conditions: insulin (100 nM), AICAR (2 mM), and AICAR plus insulin. All AICAR plus insulin conditions received AICAR for 30 min before the 1-h incubation period. After the incubation, all muscles were washed for 10 min in KHB buffer containing 40 mM mannitol at 29 C and, if present during the previous incubation period, insulin (100 nM) and AICAR (2 mM). For measurement of glucose transport, the muscles were transferred to new flasks and incubated for 20 min at 29 C in 1.5 ml KHB buffer containing 0.5 μCi/ml 2-[1,2-^{3}H]deoxy-D-glucose (2-DG, and 8 mM nonlabeled 2-DG) and 0.1 μCi/ml [U-^{14}C]mannitol as an extracellular space marker (21). To terminate the experiment, immediately after the 20-min glucose uptake period, muscles were blotted (4 C) and quickly frozen in liquid N_2. Muscles were then digested in 0.5 ml of 1 M KOH at 70 C and centrifuged (1000 × *g*). Aliquots (450 μl) of the muscle extract supernatant and the incubation medium were counted for radioactivity using a scintillation counter with channels preset for simultaneous ^{3}H and ^{14}C counting. The amounts of D-[U-^{14}C]mannitol and 2-DG present in the samples were used to calculate extracellular space and glucose transport, respectively, as previously described (22). The intracellular water content of the muscles was calculated subtracting the measured extracellular space water from total muscle water. Total water content was assumed to be 77%, which is the average value for soleus and epitrochlearis muscles after drying the tissues to a constant weight in our laboratory.

Western blot determination of phosphorylated (p)-AMPK, p-acetyl-CoA carboxylase (ACC), p-Akt (Thr308, Ser473), p-GSK-3α/β, p-GS, AMPKα1, AMPKα2, and glyceraldehyde-3-phosphate dehydrogenase (GAPDH)

Soleus muscles were incubated in the absence or presence of insulin (100 nM), AICAR (2 mM), and AICAR plus insulin. All muscles were preincubated in KHB buffer as previously described. To investigate time-dependent alterations in phosphorylation levels of Akt (Thr308 and Ser473), GSK-3α/β, and GS, we exposed the muscles to insulin for 15, 30, and 45 min. AICAR was added to the incubation medium 30 min before adding insulin and remained in the medium thereafter. Control muscles received neither AICAR nor insulin. To test the effectiveness of AICAR to induce AMPK activation, we measured the phosphorylation state of ACC, a downstream target of AMPK (23). In addition, we also examined the distribution of AMPKα1 and AMPKα2 in soleus and epitrochlearis muscles to determine the fiber type-specific distribution of the two AMPK catalytic isoform subunits. Immediately after all treatments, muscles were frozen in liquid N_2 and stored at −80 C until analysis. For preparation of muscle lysates, the solei and epitrochlearis muscles were homogenized in buffer containing 135 mM NaCl, 1 mM $MgCl_2$, 2.7 mM KCl, 20 mM Tris (pH 8.0), 1% Triton X-100, 10% glycerol, and protease and phosphatase inhibitors (0.5 mM Na_3VO_4, 10 mM NaF, 1 μM leupeptin, 1 μM pepstatin, 1 μM okadaic acid, and 0.2 mM phenylmethylsulfonyl fluoride), and heated (65 C, 5 min). An aliquot of the homogenate was used to determine the protein concentration in each sample by the Bradford method.

Before loading onto SDS-PAGE gels, the samples were diluted 1:1 (vol/vol) with 2× Laemmli sample buffer [62.5 mM Tris-HCl (pH 6.8), 2% (wt/vol) sodium dodecyl sulfate, 50 mM dithiothreitol, and 0.01% (wt/vol) bromophenol blue]. Aliquots of muscle homogenates containing 75 μg of protein were run through SDS-PAGE gels [12% for p-AMPK, 7.5% for *P*-ACC, and 10% for *P*-Akt (Thr308 and Ser473), *P*-GSK-3α/β, *P*-GS, and GAPDH] and then transferred to polyvinyl difluoride membranes (Bio-Rad Laboratories, Burlington, Ontario, Canada). The phosphorylation of AMPK was determined using a *P*-AMPK (Thr172) antibody, which detects AMPKα only when activated by phosphorylation at Thr-172. The phosphorylation of Akt was determined using *P*-Akt (Thr308) and *P*-Akt (Ser473) antibodies, which detect Akt only when phosphorylated at Thr-308 or Ser-473. The phosphorylation of GSK was determined using a *P*-GSK-3α/β (Ser21/9) antibody, which detects GSK only when phosphorylated at Ser-21 and Ser-9. GS and ACC phosphorylation was detected using *P*-GS and *P*-ACC-specific antibodies, which recognize GS and ACC when phosphorylated at serine 641 (Ser641) and serine 79 (Ser79), respectively. Equal loading of all gels was confirmed by Coomassie staining of all gels and use of GAPDH as a loading control. Specific antibodies against *P*-Akt, *P*-GSK-3α/β, *P*-GS, and *P*-AMPK were purchased Cell Signaling Technology Inc. (Beverly, MA). Specific antibodies against the α-1 and α-2 subunits of AMPK were purchased from Santa Cruz Biotechnology, Inc. (Santa Cruz, CA). *P*-ACC was obtained from Upstate Biotechnology (Charlottesville, VA), and GAPDH was from Abcam, Inc. (Cambridge, MA). All antibodies were applied in a 1:1000 dilution, except GAPDH, which was used in a 1:5000 dilution.

Statistical analyses

All statistical analyses were performed by one-way ANOVAs followed by Fisher *post hoc* tests. The level of significance was set at $P < 0.05$.

Results

Effect of AICAR on glycogen synthesis in soleus and epitrochlearis muscles

As expected, in soleus muscle, insulin elicited a 6.4-fold increase in glycogen synthesis, compared with the control condition (Fig. 1A). Interestingly, whereas treatment with AICAR alone did not alter the basal rate of glycogen synthesis, it resulted in a approximately 60% reduction of glycogen synthesis in the presence of insulin. Treatment of epitrochlearis muscles with insulin resulted in a 1.8-fold increase in glycogen synthesis relative to control (Fig. 1B). AICAR treatment did not affect either basal or insulin-stimulated conditions in epitrochlearis muscles.

Effect of AICAR on glycogen content in soleus and epitrochlearis muscles

To further characterize the effects of AICAR treatment on glycogen metabolism, glycogen content was assessed. In soleus, 1 h treatment with insulin resulted in a significant increase (~27%) in glycogen content relative to control (Fig. 2A). Interestingly, AICAR completely reversed the increase in glycogen content induced by insulin in soleus muscles. Incubation of epitrochlearis muscles (Fig. 2B) with insulin,

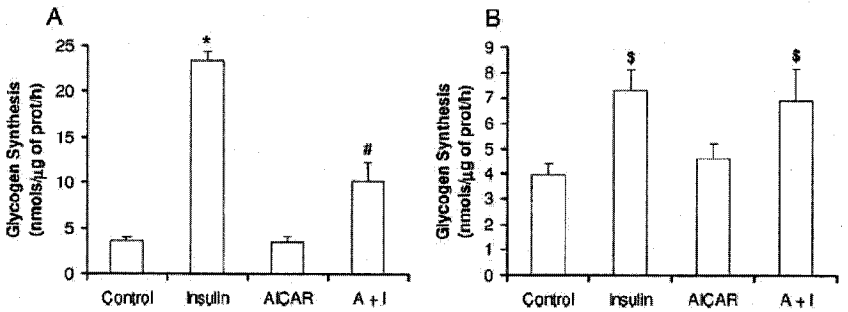

FIG. 1. Effect of insulin (100 nM), AICAR (2 mM), and AICAR plus insulin (A + I) on glycogen synthesis in isolated soleus (A) and epitrochlearis (B) muscles. Glycogen synthesis was estimated from the incorporation of D-[U-^{14}C]glucose into glycogen for 1 h in the presence of the various conditions as indicated. Control muscles were exposed to neither AICAR nor insulin. Muscles in the A + I condition were preincubated with AICAR for 30 min before insulin and D-[U-^{14}C]glucose was added to the medium. Data were compiled from three independent experiments with triplicates in each experiment and presented as means ± SEM. *, $P < 0.05$ *vs.* control, AICAR, and A + I; #, $P < 0.05$ *vs.* control, insulin, and AICAR; $, $P < 0.05$ *vs.* control and AICAR.

AICAR, and AICAR plus insulin did not have any effect on glycogen content.

Effect of AICAR on lactate production in soleus and epitrochlearis muscles

To determine whether the effects of AICAR on glycogen synthesis would also cause other metabolic changes in soleus and epitrochlearis muscles, lactate production was assessed. In soleus (Fig. 3A), incubation with insulin resulted in a significant, approximately 1.6-fold, increase in lactate production relative to control. The effect of AICAR on the basal condition showed a trend toward increased lactate production but did not reach statistical significance (Fig. 3A). However, incubation of the soleus with AICAR and insulin caused a 2-fold increase in lactate production relative to control, which was approximately 21% higher than that of insulin alone (Fig. 3A). The epitrochlearis muscles (Fig. 3B) also showed a similar increase in lactate production (~1.7-fold) when treated with insulin. However, AICAR did not affect insulin-stimulated lactate production in these muscles (Fig. 3B).

Effect of AICAR on glucose uptake in soleus and epitrochlearis muscles

In soleus muscles, treatment with insulin resulted in an approximately 3.3-fold increase in glucose uptake relative to control (Table 1). The addition of AICAR to the medium did not affect either the basal or insulin-stimulated rate of glucose transport in the soleus (Table 1). As expected, epitrochlearis muscles elicited an increase in glucose uptake (~1.7-fold) in the presence of insulin. AICAR treatment also caused a significant increase (~1.4-fold) in glucose uptake in epitrochlearis muscles (Table 1). The addition of AICAR to the insulin-stimulated epitrochlearis muscles resulted in approximately 2.0-fold increase in glucose uptake. However, this increase was not statistically different from the insulin or AICAR only conditions.

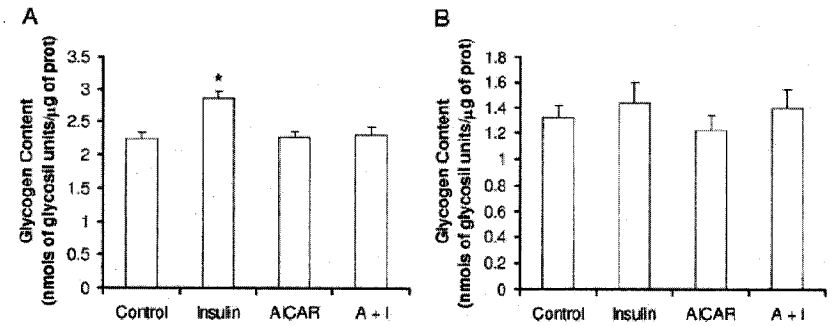

FIG. 2. Effect of insulin (100 nM), AICAR (2 mM), and AICAR plus insulin (A + I) on glycogen content in isolated soleus (A) and epitrochlearis (B) muscles. Control muscles were exposed to neither AICAR nor insulin. Muscles in the A + I condition were preincubated with AICAR for 30 min before insulin was added to the medium. Data were compiled from three independent experiments with triplicates in each experiment and presented as means ± SEM. *, $P < 0.05$ *vs.* control, AICAR, and A + I.

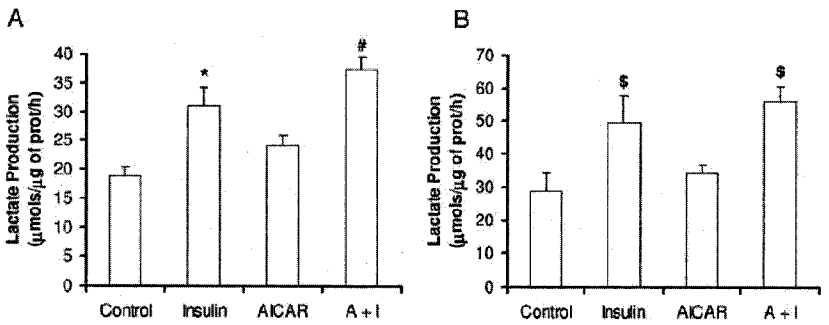

FIG. 3. Effect of insulin (100 nM), AICAR (2 mM), and AICAR plus insulin (A + I) on lactate production in isolated soleus (A) and epitrochlearis (B) muscles. Control muscles were exposed to neither AICAR nor insulin. Muscles in the A + I condition were preincubated with AICAR for 30 min before insulin and D-[U-^{14}C]glucose was added to the medium. Data were compiled from three independent experiments with triplicates in each experiment and presented as means ± SEM. *, $P < 0.05$ *vs.* control, AICAR, and A + I; #, $P < 0.05$ *vs.* control, insulin, and AICAR; $, $P < 0.05$ *vs.* control and AICAR.

Effect of AICAR on the phosphorylation of AMPK, ACC, Akt, GSK-3α/β, and GS in soleus muscles

The effectiveness of AICAR treatment to increased AMPK phosphorylation/activation was determined by Western blot. As expected, AICAR treatment led to a marked increase in AMPK and ACC phosphorylation, respectively (Fig. 4A). In addition, we also examined the differential expression of the AMPKα1 and AMPKα2 catalytic subunits in both, soleus and epitrochlearis muscles. The AMPKα1 content was markedly higher (~1.6-fold) in epitrochlearis than soleus muscles, whereas AMPKα2 appeared similar in both muscles (Fig. 4B). To determine whether the effects of AICAR-induced AMPK activation affected major intracellular pathways of insulin signaling, we examined the phosphorylation states of Akt Thr308, Akt Ser473, GSK-3α/β, and GS. As anticipated, exposure of the soleus muscle to insulin for 15 min resulted in an approximately 9-fold increase in Akt Thr308 phosphorylation, compared with control. Even though this effect decreased as exposure time to insulin increased, Akt Thr308 phosphorylation remained markedly elevated after 45 min of insulin exposure, compared with control (Fig. 4C). AICAR on its own did not cause any changes in the phosphorylation state of Akt Thr308. However, pretreatment of soleus muscles with AICAR resulted in approximately 33 and 55% reductions in Akt Thr308 phosphorylation after 15 and 30 min of insulin exposure, respectively (Fig. 4C). Insulin also increased Akt Ser473 phosphorylation (~1.6-fold), but this was unaffected by AICAR. To further investigate the effects of AICAR on enzymes involved in glycogen metabolism, we examined the phosphorylation state of GSK-3α/β (Fig. 4C).

TABLE 1. Effect of Insulin, AICAR, and AICAR plus insulin on 2-deoxy-D-glucose uptake (μmol/μl per 20 min) in soleus (Sol) and epitrochlearis (Epi) muscles

	Control	Insulin	AICAR	AICAR plus insulin
Sol	1.56 ± 0.07	5.19 ± 0.17[a]	1.92 ± 0.22	4.81 ± 0.21[a]
Epi	2.26 ± 0.09	3.81 ± 0.21[b]	3.16 ± 0.28[b]	4.43 ± 0.28[b]

Data presented as means ± SEM.
[a] $P < 0.05$ *vs.* control and AICAR.
[b] $P < 0.05$ *vs.* control.

This enzyme is a downstream target of Akt and is active when in its dephosphorylated state. Under control conditions, GSK-3α/β phosphorylation was virtually undetectable. A pronounced increase in the phosphorylation state of GSK-3α was observed in the presence of insulin (Fig. 4C). Interestingly, AICAR markedly reduced the 15-, 30-, and 45-min insulin-stimulated phosphorylation of GSK-3α. The phosphorylation of GSK-3β under insulin stimulation was not as high as GSK-3α; however, the effect of AICAR on the insulin-stimulated condition followed a similar pattern to that of GSK-3α (Fig. 4C). These data indicate that AICAR prevented the insulin-induced suppression of GSK-3α/β activity in soleus muscles.

Analysis of GS phosphorylation revealed that this enzyme was highly phosphorylated under basal conditions, and AICAR alone did not affect basal GS phosphorylation. As expected, treatment of soleus muscles with insulin elicited a time-dependent reduction in GS phosphorylation, reaching its lowest after 45 min exposure to insulin (Fig. 4C). Interestingly, AICAR treatment initially decreased the GS phosphorylation after 15 and 30 min of insulin exposure. However, GS phosphorylation markedly increased after 45 min of exposure to insulin (Fig. 4C).

Discussion

Here we provide evidence that acute exposure of soleus muscles to AICAR, a known activator of AMPK, profoundly inhibited (~60%) the insulin-induced increase in glycogen synthesis. AICAR treatment also prevented the insulin-induced increase in glycogen content in soleus muscles. Interestingly, neither basal nor insulin-stimulated glucose uptake was affected by AICAR in soleus, whereas epitrochlearis muscles elicited a significant increase in this variable. This differential response to AICAR in isolated soleus and epitrochlearis muscles has also been reported in previous studies (24, 25); however, no data regarding the effects of AICAR on other glucose pathways have been reported in these studies. It has been argued that the lack of a stimulatory effect of AICAR on glucose transport in slow-twitch skeletal muscles could be due to fiber type-specific differences in the expres-

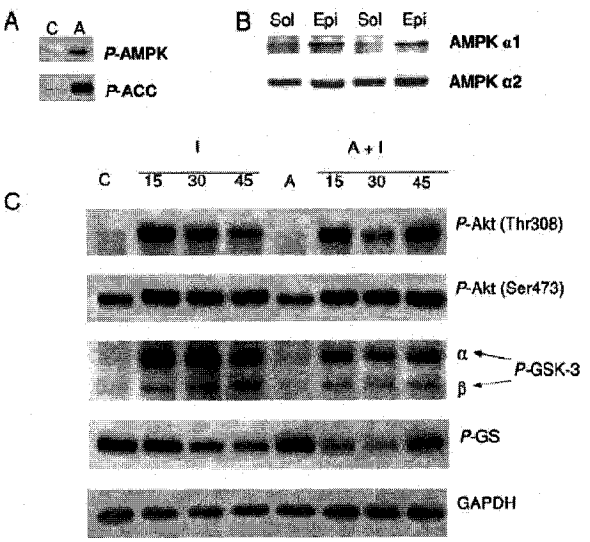

FIG. 4. A, Induction of AMPK and ACC phosphorylation by AICAR in soleus muscles. B, Expression of AMPKα1 and AMPKα2 catalytic subunits in soleus (Sol) and epitrochlearis (Epi) muscles. C, Time-course effects (15, 30, and 45 min) of insulin (I, 100 nM), AICAR (A, 2 mM), and AICAR plus insulin (A + I) on the phosphorylation of AktThr 308 (*P*-Akt308), AktSer473 (*P*-Akt473), GSK-3α (*P*-GSK-3α), GSK-3β (*P*-GSK-3β), and GS (*P*-GS) in isolated soleus muscles. Muscles were exposed to insulin for 15, 30, and 45 min. AICAR was added to the incubation medium 30 min prior to adding insulin and remained in the medium thereafter. Controls (C) represent soleus muscles not subjected to any treatment.

sion of AMPK subunits (24, 26). In fact, it has been demonstrated that the presence of all three AMPK subunits is required for AICAR-induced increases in glucose transport in mouse skeletal muscle (26). Here we report clear differences in AMPKα subunit content in slow-twitch and fast-twitch muscles (Fig. 4B). Whereas AMPKα2 was equally present in both muscles investigated, AMPKα1 was faintly detected in soleus, which could justify the different responses in glucose uptake to AICAR observed here.

In our system, we also observed that insulin-stimulated lactate production was increased by AICAR treatment, and because AICAR did not affect insulin-stimulated glucose uptake, it indicates that AICAR-induced AMPK activation shifted insulin-stimulated glucose metabolism toward lactate production instead of accumulation as glycogen in isolated soleus muscles. However, the AICAR-induced reduction in glycogen synthesis cannot be completely accounted for by the increase in lactate production, suggesting that other pathways may also participate in this metabolic shift. Previous investigations have demonstrated that glucose oxidation increases in isolated soleus muscles exposed to AICAR (27), which may also have been the case in the present study. In addition, our data are in partial agreement with a previous *in vitro* study showing that AICAR increased lactate production in soleus muscles exposed to low concentrations of insulin (12). However, in their study neither basal nor insulin-stimulated rates of glycogen synthesis were affected by AICAR, even though an increase in glycogen phosphorylase activity was reported (12). This is intriguing because increased glycogen phosphorylase activity is expected to decrease glycogen synthesis. In our investigation, the marked AICAR-induced decrease in insulin-stimulated glycogen synthesis as well as suppression of the increase in glycogen content in solei is compatible with the increased glycogen phosphorylase activity previously reported by Young *et al.* (12). There are important methodological differences between our study and the one by Young *et al.* (12) that may justify the differences regarding the effect of AICAR on insulin-stimulated glycogen synthesis. We used intact soleus muscle (~15–20 mg) from 40- to 60-g rats, whereas Young *et al.* (12) used muscle strips from 130- to 140-g rats. Splitting the muscles may have influenced the response of the tissue to AICAR and insulin treatments. Also, the differences in AICAR concentrations (2 *vs.* 1 mM) may account for the differences in glycogen synthesis reported in these two independent studies.

Previous *in vivo* studies also reported that glycogen content is not affected by AICAR treatment in red and white gastrocnemius muscles, even though major time-dependent fiber type differences have been reported regarding the activity of GS and glycogen phosphorylase (11). Additionally, in the same study, *in vitro* incubations of two fast-twitch muscles (flexor digitorum brevis and epitrochlearis) with AICAR affected neither GS nor glycogen phosphorylase activities (11). This is in line with our *in vitro* data showing that basal glycogen content was not affected by acute AICAR treatment in isolated soleus and epitrochlearis muscles. However, in another *in vivo* study, it was actually reported that glycogen synthesis was increased in white but not red quadricep muscles after AICAR treatment (5). The reasons for these discrepant results are not clear but may be attributed to the use of different muscle groups in various studies. In fact, it has been reported that major differences in the expression of AMPK isoforms in skeletal muscles with distinct fiber type compositions exist (28–30). For instance, Ai *et al.* (30) showed that the epitrochlearis, composed predominantly of type II fibers, expresses more AMPKα1 subunits than type I fibers, which is in agreement with data presented

in this manuscript (Fig. 4B). On the other hand, type II fibers exhibit a 5-fold greater expression of the γ-3 subunit than type I fibers (31). Even though specific muscle groups have been classified according to fiber type composition, current data on the expression and activity of AMPK isoforms in different muscle fibers, and their respective functional implications, still lack clarity. Therefore, the hypothesis that differential expression/activity of AMPK isoforms is responsible for the dissimilar results regarding the effects of AICAR treatment on glycogen metabolism requires additional investigation.

To examine whether the effects of AICAR on insulin-induced glycogen synthesis in soleus muscles are fiber type specific, we also used epitrochlearis muscles in our experiments. We found that AMPK activation does not alter either the rate of glycogen synthesis or glycogen content in fast-twitch muscles under basal and insulin-stimulated conditions (Figs. 1B and 2B). Additionally, lactate production was also unaffected by AICAR, indicating that the metabolic shift toward lactate production does not seem to occur in epitrochlearis muscle (Fig. 3B). Previous investigations have shown that either ip (11) or sc (5) injections of AICAR increase blood lactate levels in rats. However, because these were *in vivo* studies, we do not know how much of this lactate was derived from muscles *vs.* other tissues that might also have been affected by AICAR treatment.

Here we show novel evidence that AICAR interferes with the intracellular insulin signaling steps that are crucial to regulate glycogen metabolism. As expected, after soleus muscles were exposed to insulin for 30 min, GS phosphorylation was decreased relative to control, therefore increasing its activity. Interestingly, insulin-induced reduction in phosphorylation of GS was even more accentuated after 15 and 30 min of AICAR treatment, suggesting an initial increase in GS activity in soleus muscles. However, this was not accompanied by an increase in glycogen synthesis (Fig. 1A) after 1 h incubation with AICAR. This suggests that the AICAR-induced increase in GS phosphorylation in soleus after 45 min of exposure to insulin overcame the initial reduction in phosphorylation at 15 and 30 min. Furthermore, the time-course incubation of soleus muscles for the purpose of insulin signaling determination was performed up to 45 min, whereas the rate of glycogen synthesis and glycogen content were assessed after 1 h incubation. This leaves an additional 15 min during which GS may have become even more deactivated. These data are in agreement with previous *in vitro* experiments showing that AMPK from rat liver phosphorylates GS purified from rabbit skeletal muscle (10). However, a time-course analysis of the effects of AMPK on GS phosphorylation was not performed in those experiments.

Because AMPK activation has also been shown to effect insulin signaling enzymes upstream of GS (17, 32, 33), we examined whether AICAR had similar effects on GSK-3α and -3β phosphorylation. When activated (dephosphorylated), GSK-3α and -3β phosphorylate/deactivate GS and hence lead to decreased glycogen synthesis. As expected, insulin elicited a powerful effect on GSK-3α phosphorylation, and remarkably, treatment of the insulin-stimulated condition with AICAR led to a pronounced decrease in phosphorylation of this enzyme. Phosphorylation of GSK-3β followed a pattern similar to GSK-3α; however, the former did not appear to be affected to the same extent by insulin. The decreased phosphorylation of GSK-3α and -3β by AICAR in insulin-stimulated soleus muscles may have been due to a direct effect of AICAR on this enzyme (32). Data from Jurkat T cells demonstrates that AICAR can have a direct inhibitory effect on GSK-3 phosphorylation, thus increasing its activity. In addition, treatment of differentiated hippocampal neurons with AICAR led to dephosphorylation/activation of GSK-3α and -3β (33). However, these findings have not been shown in skeletal muscle cells.

The suppressive effects of AICAR on GSK-3 phosphorylation could also be linked to alterations in activity of upstream kinases such as Akt. Therefore, we also examined the effects of AICAR on insulin-stimulated phosphorylation of Akt-Ser473 and Akt-Thr308. Once again we observed a transient high degree of phosphorylation of Akt-Thr308 with insulin after 15 min of incubation, which appeared to fade at 30 and 45 min. However, AICAR reduced the insulin-induced phosphorylation of Akt-Thr308 at both 15 and 30 min of incubation. Phosphorylation of Akt-Ser473 was not affected by AICAR at any time points. Our data are in partial agreement with a recent study (33) showing that AICAR treatment reduces phosphorylation of Akt-Thr308 and Akt-Ser473. However, it is important to point out that whereas we examined the effects of AICAR on insulin-stimulated muscle tissue, the investigation by King *et al.* (33) tested the effects of AICAR on basal Akt phosphorylation in hippocampal cells. The use of different tissues and administration of AICAR to basal or insulin-stimulated states may account for the differences between our investigation and that by King *et al.* (33).

Another plausible mechanism by which AICAR exerts its effects on insulin-stimulated glycogen synthesis is mediated by events that take place upstream of Akt. In fact, it has previously been shown that AMPK directly affects early insulin-signaling events by phosphorylating IRS-1 on the Ser789 residue (17). Even though phosphorylation of IRS-1 on Ser789 residue did not impair insulin signaling in C_2C_{12} myotubes (17), other investigations have shown that serine phosphorylation of IRS-1 is linked to reduced capacity of insulin to activate PI3-kinase (34, 35). Additionally, AICAR has also been shown to have a direct effect on inhibiting GSK-3 phosphorylation, thus activating it (32, 33). In turn, activated GSK-3 phosphorylates IRS-1 on serine residues, and this has also been demonstrated to attenuate insulin signaling via its phosphorylation of IRS-1 in CHO cells (34). In our system, AICAR treatment elicited a marked reduction in GSK-3α/β phosphorylation, which may have also influenced early steps of insulin signaling in isolated soleus muscle and downstream events associated with glycogen synthesis.

In conclusion, we demonstrate that acute AMPK activation by AICAR leads to suppression of insulin-stimulated glycogen synthesis in soleus but not epitrochlearis muscles. Additionally, we provide novel evidence that AICAR-induced AMPK activation affects major steps of the insulin signaling cascade in skeletal muscle. The suppression of glycogen synthesis and decrease in glycogen content by AICAR in isolated rat soleus muscles is compatible with the transient and time-

dependent reduction in Akt308 phosphorylation, activation of GSK-3 α/β, and the inactivation of GS reported here.

Acknowledgments

Received April 12, 2006. Accepted July 18, 2006.

Address all correspondence and requests for reprints to: Rolando B. Ceddia, Department of Kinesiology and Health Science, York University, 4700 Keele Street, Toronto, Ontario, Canada N3J 1P3. E-mail: roceddia@yorku.ca.

This work was supported by National Science and Engineering Research Council (NSERC) via a Discovery grant (to R.B.C.). NSERC also supported S.F. via a Doctoral Postgraduate Scholarship. M.P.G. was supported by a CIHR Canada Graduate Scholarship-Master's Award.

Author disclosure summary: S.F., M.P.G., and R.B.C. have nothing to declare.

References

1. **Rutter GA, Da Silva Xavier G, Leclerc I** 2003 Roles of 5′-AMP-activated protein kinase (AMPK) in mammalian glucose homoeostasis. Biochem J 375: 1–16
2. **Carling D** 2005 AMP-activated protein kinase: balancing the scales. Biochimie (Paris) 87:87–91
3. **Merrill GF, Kurth EJ, Hardie DG, Winder WW** 1997 AICA riboside increases AMP-activated protein kinase, fatty acid oxidation, and glucose uptake in rat muscle. Am J Physiol 273:E1107–E1112
4. **Hayashi T, Hirshman MF, Kurth EJ, Winder WW, Goodyear LJ** 1998 Evidence for 5′ AMP-activated protein kinase mediation of the effect of muscle contraction on glucose transport. Diabetes 47:1369–1373
5. **Iglesias MA, Furler SM, Cooney GJ, Kraegen EW, Ye JM** 2004 AMP-activated protein kinase activation by AICAR increases both muscle fatty acid and glucose uptake in white muscle of insulin-resistant rats *in vivo*. Diabetes 53: 1649–1654
6. **Pold R, Jensen LS, Jessen N, Buhl ES, Schmitz O, Flyvbjerg A, Fujii N, Goodyear LJ, Gotfredsen CF, Brand CL, Lund S** 2005 Long-term AICAR administration and exercise prevents diabetes in ZDF rats. Diabetes 54:928–934
7. **Koistinen HA, Galuska D, Chibalin AV, Yang J, Zierath JR, Holman GD, Wallberg-Henriksson H** 2003 5-Amino-imidazole carboxamide riboside increases glucose transport and cell-surface GLUT4 content in skeletal muscle from subjects with type 2 diabetes. Diabetes 52:1066–1072
8. **Kahn BB, Alquier T, Carling D, Hardie DG** 2005 AMP-activated protein kinase: ancient energy gauge provides clues to modern understanding of metabolism. Cell Metab 1:15–25
9. **Wojtaszewski JF, Nielsen JN, Jorgensen SB, Frosig C, Birk JB, Richter EA** 2003 Transgenic models—a scientific tool to understand exercise-induced metabolism: the regulatory role of AMPK (5′-AMP-activated protein kinase) in glucose transport and glycogen synthase activity in skeletal muscle. Biochem Soc Trans 31:1290–1294
10. **Carling D, Hardie DG** 1989 The substrate and sequence specificity of the AMP-activated protein kinase. Phosphorylation of glycogen synthase and phosphorylase kinase. Biochim Biophys Acta 1012:81–86
11. **Aschenbach WG, Hirshman MF, Fujii N, Sakamoto K, Howlett KF, Goodyear LJ** 2002 Effect of AICAR treatment on glycogen metabolism in skeletal muscle. Diabetes 51:567–573
12. **Young ME, Radda GK, Leighton B** 1996 Activation of glycogen phosphorylase and glycogenolysis in rat skeletal muscle by AICAR—an activator of AMP-activated protein kinase. FEBS Lett 382:43–47
13. **Buhl ES, Jessen N, Schmitz O, Pedersen SB, Pedersen O, Holman GD, Lund S** 2001 Chronic treatment with 5-aminoimidazole-4-carboxamide-1-beta-D-ribofuranoside increases insulin-stimulated glucose uptake and GLUT4 translocation in rat skeletal muscles in a fiber type-specific manner. Diabetes 50: 12–17
14. **Winder WW, Holmes BF, Rubink DS, Jensen EB, Chen M, Holloszy JO** 2000 Activation of AMP-activated protein kinase increases mitochondrial enzymes in skeletal muscle. J Appl Physiol 88:2219–2226
15. **Holmes BF, Kurth-Kraczek EJ, Winder WW** 1999 Chronic activation of 5′-AMP-activated protein kinase increases GLUT-4, hexokinase, and glycogen in muscle. J Appl Physiol 87:1990–1995
16. **Shulman GI** 2000 Cellular mechanisms of insulin resistance. J Clin Invest 106:171–176
17. **Jakobsen SN, Hardie DG, Morrice N, Tornqvist HE** 2001 5′-AMP-activated protein kinase phosphorylates IRS-1 on Ser-789 in mouse C2C12 myotubes in response to 5-aminoimidazole-4-carboxamide riboside. J Biol Chem 276:46912–46916
18. **De Fea K, Roth RA** 1997 Modulation of insulin receptor substrate-1 tyrosine phosphorylation and function by mitogen-activated protein kinase. J Biol Chem 272:31400–31406
19. **Ceddia RB, William Jr WN, Curi R** 1999 Comparing effects of leptin and insulin on glucose metabolism in skeletal muscle: evidence for an effect of leptin on glucose uptake and decarboxylation. Int J Obes Relat Metab Disord 23:75–82
20. **Lowry OH, Passonneau JV** 1972 A flexible system of enzymatic analysis. New York: Academic Press; 1–291
21. **Henriksen EJ, Bourey RE, Rodnick KJ, Koranyi L, Permutt MA, Holloszy JO** 1990 Glucose transporter protein content and glucose transport capacity in rat skeletal muscles. Am J Physiol 259:E593–E598
22. **Young DA, Uhl JJ, Cartee GD, Holloszy JO** 1986 Activation of glucose transport in muscle by prolonged exposure to insulin. Effects of glucose and insulin concentrations. J Biol Chem 261:16049–16053
23. **Fediuc S, Gaidhu MP, Ceddia RB** 2006 Regulation of AMP-activated protein kinase and acetyl-CoA carboxylase phosphorylation by palmitate in skeletal muscle cells. J Lipid Res 47:412–420
24. **Wright DC, Geiger PC, Holloszy JO, Han DH** 2005 Contraction- and hypoxia-stimulated glucose transport is mediated by a Ca^{2+}-dependent mechanism in slow-twitch rat soleus muscle. Am J Physiol Endocrinol Metab 288:E1062–E1066
25. **Wright DC, Hucker KA, Holloszy JO, Han DH** 2004 Ca^{2+} and AMPK both mediate stimulation of glucose transport by muscle contractions. Diabetes 53:330–335
26. **Barnes BR, Marklund S, Steiler TL, Walter M, Hjalm G, Amarger V, Mahlapuu M, Leng Y, Johansson C, Galuska D, Lindgren K, Abrink M, Stapleton D, Zierath JR, Andersson L** 2004 The 5′-AMP-activated protein kinase γ3 isoform has a key role in carbohydrate and lipid metabolism in glycolytic skeletal muscle. J Biol Chem 279:38441–38447
27. **Smith AC, Bruce CR, Dyck DJ** 2005 AMP kinase activation with AICAR simultaneously increases fatty acid and glucose oxidation in resting rat soleus muscle. J Physiol 565:537–546
28. **Chen Z, Heierhorst J, Mann RJ, Mitchelhill KI, Michell BJ, Witters LA, Lynch GS, Kemp BE, Stapleton D** 1999 Expression of the AMP-activated protein kinase β1 and β2 subunits in skeletal muscle. FEBS Lett 460:343–348
29. **Winder WW, Hardie DG, Mustard KJ, Greenwood LJ, Paxton BE, Park SH, Rubink DS, Taylor EB** 2003 Long-term regulation of AMP-activated protein kinase and acetyl-CoA carboxylase in skeletal muscle. Biochem Soc Trans 31:182–185
30. **Ai H, Ihlemann J, Hellsten Y, Lauritzen HP, Hardie DG, Galbo H, Ploug T** 2002 Effect of fiber type and nutritional state on AICAR- and contraction-stimulated glucose transport in rat muscle. Am J Physiol Endocrinol Metab 282:E1291–E1300
31. **Mahlapuu M, Johansson C, Lindgren K, Hjalm G, Barnes BR, Krook A, Zierath JR, Andersson L, Marklund S** 2004 Expression profiling of the γ-subunit isoforms of AMP-activated protein kinase suggests a major role for γ3 in white skeletal muscle. Am J Physiol Endocrinol Metab 286:E194–E200
32. **Jhun BS, Oh YT, Lee JY, Kong Y, Yoon KS, Kim SS, Baik HH, Ha J, Kang I** 2005 AICAR suppresses IL-2 expression through inhibition of GSK-3 phosphorylation and NF-AT activation in Jurkat T cells. Biochem Biophys Res Commun 332:339–346
33. **King TD, Song L, Jope RS** 2006 AMP-activated protein kinase (AMPK) activating agents cause dephosphorylation of Akt and glycogen synthase kinase-3. Biochem Pharmacol 71:1637–1647
34. **Eldar-Finkelman H, Krebs EG** 1997 Phosphorylation of insulin receptor substrate 1 by glycogen synthase kinase 3 impairs insulin action. Proc Natl Acad Sci USA 94:9660–9664
35. **Ravichandran LV, Esposito DL, Chen J, Quon MJ** 2001 Protein kinase C-ζ phosphorylates insulin receptor substrate-1 and impairs its ability to activate phosphatidylinositol 3-kinase in response to insulin. J Biol Chem 276:3543–3549

Endocrinology is published monthly by The Endocrine Society (http://www.endo-society.org), the foremost professional society serving the endocrine community.